

# Theory of Light-Matter Interactions in Cascade and Diamond Type Atomic Ensembles

A Thesis  
Presented to  
The Academic Faculty

by

**Hsiang-Hua Jen**

In Partial Fulfillment  
of the Requirements for the Degree  
Doctor of Philosophy

School of Physics  
Georgia Institute of Technology  
December 2010



# Theory of Light-Matter Interactions in Cascade and Diamond Type Atomic Ensembles

Approved by:

---

Prof. T. A. Brian Kennedy, Advisor

---

Prof. Carlos Sa de Melo

---

Prof. Alex Kuzmich

---

Prof. Ken Brown

---

Prof. Michael S. Chapman

Date Approved: \_\_\_\_\_



*To grandfather,*

*who supports and believes in me unconditionally throughout the study,  
and in memory of grandmother and father.*



# ACKNOWLEDGEMENTS

I am grateful to my thesis advisor, Professor Brian Kennedy, for his instruction and support of my research. With his guidance and encouragement, I learned and gained insights along the way of study. I am thankful to Professor Alex Kuzmich for his direction in experimental perspective and to Dr. S. D. Jenkins for his helpful discussions on theoretical background. I am also thankful to the thesis committee, Professor Michael Chapman, Professor Carlos Sa de Melo, and Professor Ken Brown.

Throughout this work, I had many useful discussions with quantum optics group members, and I am thankful to them: Dr. D. N. Matsukevich, Dr. T. Chanelière, Dr. S. Y. Lan, O. A. Collins, C. Campbell, Dr. R. Zhao, and A. Radnaev. I am also appreciative to Professor Li You, Dr. P. Zhang, and Dr. D. L. Zhou for the training in my early graduate studies. A special thank you is due for the support of my friends, Shenshen Lin, Professor I-Tang Yu, Dr. S. C. Lin, Dr. Yu Tsao, Dr. Pei Lin, Dr. T. Lee, and Dr. A. Liang.





# TABLE OF CONTENTS

<b>DEDICATION</b> . . . . .	<b>v</b>
<b>ACKNOWLEDGEMENTS</b> . . . . .	<b>vii</b>
<b>LIST OF TABLES</b> . . . . .	<b>xiii</b>
<b>LIST OF FIGURES</b> . . . . .	<b>xv</b>
<b>SUMMARY</b> . . . . .	<b>xxi</b>
<b>I INTRODUCTION</b> . . . . .	<b>1</b>
1.1 DLCZ Protocol for the Quantum Repeater . . . . .	2
1.1.1 Correlated cascade emission in quantum telecommunication . . . . .	2
1.2 Quantum Memory with Light Frequency Conversion . . . . .	3
1.3 Outline . . . . .	4
<b>II REVIEW OF THEORETICAL AND NUMERICAL METHODS</b> . . . . .	<b>7</b>
2.1 Quantum and C-number Langevin Equations . . . . .	7
2.1.1 Quantum Heisenberg-Langevin equations . . . . .	9
2.1.2 C-number Langevin equation . . . . .	11
2.2 Fokker-Planck Equations and Stochastic Differential Equations . . . . .	13
2.2.1 Characteristic functions in P-representation . . . . .	13
2.2.2 A Complimentary Derivation of C-number Langevin Equations . . . . .	15
2.3 Kubo Oscillator . . . . .	17
<b>III SUPERRADIANT EMISSION FROM A CASCADE ATOMIC ENSEMBLE: ANALYTICAL METHOD</b> . . . . .	<b>21</b>
3.1 Introduction . . . . .	22
3.2 The example of two-state atoms interacting with a pump field . . . . .	22
3.3 Theory of Cascade Emission . . . . .	26
3.3.1 Probability amplitudes for signal and signal-idler emissions . . . . .	28
3.4 A Correlated Two-photon State . . . . .	32
3.5 Schmidt Decomposition . . . . .	35

<b>IV</b>	<b>SUPERRADIANT EMISSION FROM A CASCADE ATOMIC ENSEMBLE: NUMERICAL APPROACH . . . . .</b>	<b>43</b>
4.1	Introduction . . . . .	43
4.2	Theory of Cascade emission . . . . .	44
4.3	Numerical Simulation . . . . .	47
4.3.1	Shooting and secant method . . . . .	48
4.3.2	Outline of the numerical solution . . . . .	50
4.3.3	Results for signal, idler intensities, and the second-order correlation function . . . . .	52
4.4	Conclusion . . . . .	58
<b>V</b>	<b>SPECTRAL ANALYSIS FOR CASCADE-EMISSION-BASED QUANTUM COMMUNICATION . . . . .</b>	<b>61</b>
5.1	Introduction . . . . .	61
5.2	DLCZ Scheme with Cascade Emission . . . . .	61
5.3	Entanglement Swapping . . . . .	62
5.4	Polarization Maximally Entangled State (PME State) and Quantum Teleportation . . . . .	70
5.5	Conclusion . . . . .	75
<b>VI</b>	<b>EFFICIENCY OF LIGHT-FREQUENCY CONVERSION IN AN ATOMIC ENSEMBLE . . . . .</b>	<b>77</b>
6.1	Introduction . . . . .	78
6.2	Theory . . . . .	79
6.3	Optimal Conversion Efficiency . . . . .	86
6.4	Pulse Conversion: Solution of the Maxwell-Bloch Equations . . . . .	89
6.5	Discussion of Quantum Fluctuations . . . . .	92
6.6	Conclusion . . . . .	98
<b>VII</b>	<b>CONCLUSION . . . . .</b>	<b>101</b>
<b>APPENDIX A</b>	<b>— DERIVATION OF A SCHRÖDINGER WAVE EQUATION FOR SPONTANEOUS EMISSIONS FROM A CASCADE TYPE ATOMIC ENSEMBLE . . . . .</b>	<b>103</b>

APPENDIX B — DERIVATION OF A C-NUMBER LANGEVIN EQUATION FOR THE CASCADE EMISSION . . . . .	115
APPENDIX C — MULTIMODE DESCRIPTION OF CORRELATED TWO-PHOTON STATE . . . . .	147
APPENDIX D — HAMILTONIAN AND EQUATION OF MOTION FOR FREQUENCY CONVERSION IN A DIAMOND TYPE ATOMIC ENSEMBLE . . . . .	157
BIBLIOGRAPHY . . . . .	165



# LIST OF TABLES

Table 4.1	Numerical simulation parameters for different atomic densities $\rho$ . Corresponding optical depth (opd), time and space grids ( $M_t \times M_z$ ) with grid sizes ( $\Delta t, \Delta z$ ) in terms of cooperation time ( $T_c$ ) and length ( $L_c$ ), and the fitted characteristic time $T_f$ for $G_{s,i}$ (see text). . . . .	58
-----------	---	----



# LIST OF FIGURES

- Figure 2.1 The two-level atomic ensemble interacts with a classical and quantum field. (a) An elongated atomic ensemble of length  $L$  is excited by a pump field of Rabi frequency  $\Omega_a$  and emits a propagating quantized field denoted by annihilation operator  $E^+$ . (b) Two-level structure for an atomic ensemble with the ground ( $|0\rangle$ ) and excited ( $|1\rangle$ ) state. The detuning of the pump field is  $\Delta_1$ . . . . . 8
- Figure 2.2 Kubo oscillator simulation. The time evolution of  $\text{Re}\langle z(t) \rangle$  (dashed-red) averaged from an ensemble of 1024 simulations.  $z(0) = 1$ . We compare with the exact solution,  $z(0)e^{-t/2}$  (solid-black), and find good agreement. A demonstration of one stochastic realization (dashed-circle blue) shows large fluctuation around the averaged and exact results. Note that the imaginary part of the solution is almost vanishing as it should be, and is not shown here. . . . . 18
- Figure 3.1 Single- and double-excitation populations as a function of distance  $d_s$ . (a) The populations of the symmetric state for a single excitation  $P_1^s$  (dashed-red) and the sum of non-symmetric single-excitation states  $P_1^{\text{ns}}$  (dashed-dotted black). (b) The populations of the symmetric state for double excitations  $P_2^s$  (dashed-blue) and the sum of non-symmetric double-excitation states  $P_2^{\text{ns}}$  (dashed-dotted black).  $P_1^{s, \text{ns}}$  and  $P_2^{s, \text{ns}}$  are normalized respectively by the solutions of non-interacting atoms  $P_1^{(0)}$  (solid-red) and  $P_2^{(0)}$  (solid-blue).  $P_1^{(0)} = 1.58 \times 10^{-3}$  and  $P_2^{(0)} = 9.4 \times 10^{-7}$ , are the single- and double-excitation probabilities for independent atoms. . . . . 25
- Figure 3.2 Time evolution of populations for symmetric states  $P_1^s$  and  $P_2^s$ . The population of the symmetric state for a single excitation is  $P_1^s$  (dashed-red), and that for the symmetric state for double excitations is  $P_2^s$  (dashed-dotted blue). The pump condition is the same as in Figure 3.1 for  $d_s = 3\lambda$ . . . . . 27
- Figure 3.3 Four-level atomic ensemble interacting with two driving lasers (solid) with Rabi frequencies  $\Omega_a$  and  $\Omega_b$ . Signal and idler fields are labelled by  $\hat{a}_s$  and  $\hat{a}_i$ , respectively and  $\Delta_1$  and  $\Delta_2$  are one and two-photon laser detunings. . . . . 28
- Figure 3.4 The superradiance decay factor  $N\mu + 1$  ( $\mu = \bar{\mu}$ ) for a cylindrical ensemble of length  $h$  and radius  $a$  in unit of transition wavelength  $\lambda$ . The atomic density is  $8 \times 10^{10} \text{ cm}^{-3}$  and  $\lambda = 795 \text{ nm}$  corresponding to the D1 line of  $^{85}\text{Rb}$ . See the text for the explanation of the arrows. 30

Figure 3.5 (a) Absolute value of the spectrum for two-photon state probability amplitude $D_{s,i}$ and (b) the second-order correlation function $G_{s,i}^{(2)}(\Delta t_s, \Delta t_i)$ . (c) A normalized $G_{s,i}^{(2)}(\Delta t_s = 0, \Delta t_i)$ with $\Gamma_3\tau = 0.2$ . The exponential decay corresponds to the superradiant decay factor $N\bar{\mu} + 1 = 5$ . . . . .	36
Figure 3.6 Schmidt mode analysis with pulse width $\tau = 0.25$ and superradiance decay factor $N\bar{\mu} + 1 = 5$ . (a) Schmidt number and (b) signal mode functions: $\text{Re}[\psi_1]$ (solid-red) and $\text{Re}[\psi_2]$ (solid-blue). Imaginary parts are not shown, then are zero. (c) Real (solid) and imaginary (dotted) parts of first (red) and second (blue) idler mode functions, $\phi_1$ and $\phi_2$ . (d) The absolute spectrum $ f(\Delta\omega_s, \Delta\omega_i) $ . . . . .	39
Figure 3.7 Absolute spectrum of two-photon state and the eigenvalues of Schmidt decomposition. $N\bar{\mu} + 1 = 5$ for both (a) $\tau = 0.25$ (b) $\tau = 0.5$ . $N\bar{\mu} + 1 = 10$ for (c) $\tau = 0.25$ . The von Neumann entropy (S) is indicated in the plots. . . . .	41
Figure 4.1 Schematic illustration of the principle of the shooting method for two-point boundary value problems. . . . .	49
Figure 4.2 Secant method. The root is bracketed by two initial guesses of $x_1$ and $x_2$ and an updated guess $x_i$ is located at the intersection of two straight lines. . . . .	51
Figure 4.3 Time-varying pump fields and time evolution of atomic populations. (Left) The first pump field $\Omega_a$ (dotted-red) is a square pulse of duration 50 ns and $\Omega_b$ is continuous wave (dotted-blue). (Right) The time evolution of the real part of populations for three atomic levels $\sigma_{11} = \langle \tilde{\alpha}_{13} \rangle$ (dotted-red), $\sigma_{22} = \langle \tilde{\alpha}_{12} \rangle$ (dotted-blue), $\sigma_{33} = \langle \tilde{\alpha}_{11} \rangle$ (dotted-green) at $z = 0, L$ , and almost vanishing imaginary parts for all three of them. indicate convergence of the ensemble averages. Note that these atomic populations are uniform as a function of $z$ . . . . .	54
Figure 4.4 Temporal intensity profiles of counter-propagating signal and idler fields. (a) At $z = 0$ , real (dotted-red) and imaginary (diamond-red) parts of signal intensity. (b) At $z = L$ , real (dotted-blue) and imaginary (diamond-blue) parts of idler intensity. Both intensities are normalized by the peak value of signal intensity that is $7.56 \times 10^{-12} E_c^2$ . Note that the idler fluctuations and its non-vanishing imaginary part indicate a relatively slower convergence compared with the signal intensity. The ensemble size was $8 \times 10^5$ , and the atomic density $\rho = 10^{10} \text{cm}^{-3}$ . . . . .	56



- Figure 4.5 Second-order correlation function  $G_{s,i}(t_s, t_i)$ . The 2-D contour plot of the real part of  $G_{s,i}$  with a causal cut-off at  $t_s = t_i$  is shown in (a). The plot (b) gives a cross-section at  $t_s = t_m \approx 75$  ns, which is normalized to the maximum of the real part (dotted-blue) of  $G_{s,i}$ . The imaginary part (diamond-red) of  $G_{s,i}$  is nearly vanishing, and the number of realizations is  $8 \times 10^5$  for  $\rho = 10^{10} \text{ cm}^{-3}$ . . . . . 57
- Figure 4.6 Characteristic timescales,  $T_f$  and  $T_1$  vs atomic density  $\rho$  and the superradiant enhancement factor  $N\mu$  ( $\mu = \bar{\mu}$ ).  $T_f$  (dotted-blue) is the fitted characteristic timescale for  $G_{s,i}(t_s = t_m, t_i = t_m + \tau)$  where  $t_m$  is chosen at its maximum, as in Figure 4.5. The errorbars indicate the fitting uncertainties. As a comparison,  $T_1 = \gamma_{03}^{-1} / (N\mu + 1)$  (dashed-black) is plotted where  $\gamma_{03}^{-1} = 26$  ns is the natural decay time of D1 line of  $^{87}\text{Rb}$  atom, and  $\mu$  is the geometrical constant for a cylindrical atomic ensemble, as discussed in Chapter 3. The number of realizations is  $4 \times 10^5$  for  $\rho = 5 \times 10^8, 5 \times 10^9 \text{ cm}^{-3}$  and  $8 \times 10^5$  for  $\rho = 10^{10}, 2 \times 10^{10} \text{ cm}^{-3}$ . . . . . 59
- Figure 5.1 Entanglement generation in the DLCZ scheme using the cascade and Raman transitions in two different atomic ensembles. Large white arrows represent laser pump excitations corresponding to the dashed lines in either cascade or Raman level structures. Here  $\hat{a}_s^\dagger$  represents the emitted telecom photon. B.S. means beam splitter that is used to interfere the incoming photons measured by the photon detector D. The label A refers to the pair of ensembles for later reference. . . . . 63
- Figure 5.2 Entanglement swapping of DLCZ scheme using the cascade transition. The site A is described in detail in Figure 5.1 and equivalently for the site B. The telecom signal photons are sent from both sites and interfere by B.S. midway between with detectors represented by  $c_1^\dagger$  and  $c_2^\dagger$ . Synchronous single clicks of the detectors from both sites ( $m_{1,2}^\dagger, n_{1,2}^\dagger$ ) and the midway detector ( $c_{1,2}^\dagger$ ) generate the entangled state between lower atomic ensembles at sites A and B. The locally generated entanglement is swapped to distantly separated sites in this cascade-emission-based DLCZ protocol. . . . . 64
- Figure 5.3 Fidelity  $F$ , heralding  $P_H$ , and success  $P_S$  probabilities of entanglement swapping versus relative efficiency  $\eta_r$  with perfect detection efficiency  $\eta_t = 1$ . Column (a) NRPD and (b) PNRD. Solid-red, dashed-blue, and dotted-green curves correspond to the pulse width parameters  $\tau = (0.1, 0.5, 0.5)$  and superradiant factor  $N\bar{\mu} + 1 = (5, 5, 10)$  (see Chapter 3 and Appendix A). The von Neumann entropy is  $S = (0.684, 2.041, 2.886)$ , respectively. . . . . 69

Figure 5.4 Fidelity $F$ , heralding $P_H$ , and success $P_S$ probabilities of entanglement swapping versus telecom detector quantum efficiency $\eta$ for the case of (a) NRPD and (b) PNRD. Solid-red, dashed-blue, and dotted-green curves correspond to the same parameters used in Figure 5.3. . . . .	71
Figure 5.5 PME projection (a) and quantum teleportation (b) in the DLCZ scheme. Four atomic ensembles (A,B,C,D) are used to generate two DLCZ entangled states at (A,B) and (C,D). PME state is projected probabilistically conditioned on four possible detection events of ( $D_A^\dagger$ or $D_C^\dagger$ ) and ( $D_B^\dagger$ or $D_D^\dagger$ ) in (a). In the quantum teleportation protocol (b), another two ensembles ( $I_1, I_2$ ) are used to prepare a quantum state that is teleported to atomic ensembles B and D conditioned on four possible detection events of ( $\hat{D}_{I_1}$ or $\hat{D}_A$ ) and ( $\hat{D}_{I_2}$ or $\hat{D}_C$ ). . . .	72
Figure 5.6 Success probability of quantum teleportation as a function of the probability amplitude of teleported quantum state with $\eta_r = 0.5$ and a perfect detector efficiency $\eta_t = 1$ . Solid-red, dashed-blue, and dotted-green curves correspond to the same parameters used in Figure 5.3. . . . .	75
Figure 6.1 The diamond configuration of atomic system for conversion scheme. Two pump lasers (double line) with Rabi frequencies $\Omega_a, \Omega_b$ and propagated probe fields (single line) $E_s^+, E_i^+$ interact with the atomic medium. Various detunings are defined in the Appendix D, and the atomic levels used in the experiment [25] are ( $ 0\rangle,  1\rangle,  2\rangle,  3\rangle$ ) = ( $ 5S_{1/2}, F=1\rangle,  5P_{3/2}, F=2\rangle,  6S_{1/2}, F=1\rangle,  5P_{1/2}, F=2\rangle$ ). . . . .	79
Figure 6.2 Dressed-state picture from the perspective of the probe idler transition between atomic levels $ 0\rangle$ and $ 3\rangle$ . Two strong fields $\Omega_a, \Omega_b$ shift the levels with energy $\Delta E_{a,b}$ and wavy lines represent the idler field resonances. . . . .	83
Figure 6.3 Self-coupling coefficients $\beta_s, \alpha_i$ and cross-coupling coefficient $\kappa_s$ . Dimensionless quantities (a) $\beta_s L$ , (b) $\alpha_i L$ and (c) $\kappa_s L$ with real (solid blue) and imaginary (dashed red) parts are plotted as a dependence of idler detuning $\Delta\omega_i$ [same label in (b)] showing four absorption peaks to construct three parametric coupling windows. A black dashed-dot line of the constant $\pi/2$ is added in (c) to demonstrate the crossover with $\Im(\kappa_s L)$ indicating the ideal conversion efficiency condition in the left window. The parameters we use are $(\Omega_a, \Omega_b, \Delta_1, \Delta_b, \Delta\omega_i) = (33, 20, 39, 2, -21)\gamma_{03}$ for optical depth $\rho\sigma L = 150$ with $L = 6\text{mm}$ . Various natural decay rates are $\gamma_{03} = 1/27.7\text{ns}$ , $\gamma_{01} = 1/26.24\text{ns}$ , $\gamma_{12} = \gamma_{03}/2.76$ , and $\gamma_{32} = \gamma_{03}/5.38$ [97]. . . . .	85

Figure 6.4	Down conversion efficiency $\eta_d$ vs optical depth (opd) from 1 to 600. Each dotted point is the maximum for five variational parameters $\Omega_a$ , $\Omega_b$ , $\Delta_1$ , $\Delta_b$ , and $\Delta\omega_i$ .	86
Figure 6.5	Conversion efficiency $\eta_d$ , $\eta_u$ and transmission $T_d$ vs $\Delta\omega_i$ for opd=150. $\eta_d$ and $\eta_u$ are indistinguishable and shown in solid red line, and $T_d$ is in dashed blue line. High transmission efficiency corresponds to low conversion efficiency indicating the approximate conservation condition within each parametric coupling window. The maximum conversion efficiency is found in the left window at around $\Delta\omega_i = -20\gamma_{03}$ and other relevant parameters are the same as in Figure 6.3.	88
Figure 6.6	Time-varying pump fields of Rabi frequencies $\Omega_{a,b}(t)$ and down-converted signal intensity ( $ E_s^+(t, z = L) ^2$ ) from an input idler pulse ( $ E_i^+(t, z = 0) ^2$ ). Here we let $t = \tau$ that is the delayed time in co-moving frame. Pump-b (dotted green) is a continuous wave and pump-a (dashed black) is a square pulse long enough to enclose input idler pulse with (a) 100 ns and (b) 15 ns (dashed-dot blue). Output signal intensity (solid red) at the end of atomic ensemble $z = L$ is oscillatory due to the pump fields. The square pulse in rising region ( $t_r - \frac{t_s}{2} < t < t_r + \frac{t_s}{2}$ ) has the form of $\frac{1}{2}[1 + \sin(\frac{\pi(t-t_r)}{t_s})]$ that in (a) $(t_r, t_s)=(10,10)$ ns for pump-a and $(t_r, t_s)=(20,20)$ ns for input idler; (b) $(t_r, t_s)=(10,5)$ ns for pump-a and $(t_r, t_s)=(15,10)$ ns for input idler where $t_r$ is the rising time indicating the center of rising period $t_s$ . Note that the falling region of square pulse is symmetric to the rising one.	91
Figure 6.7	Three-dimensional line plots of converted signal and input idler intensities in $t$ (ns) and $L$ (mm). Here we let $t = \tau$ that is the delayed time in co-moving frame, and the parameters are the same as in Figure 6.6 (a).	93
Figure C.1	Model of quantum efficiency of detector.	148
Figure D.1	Self-coupling coefficient $\alpha_i$ . A dimensionless quantity $\alpha_i L$ is plotted with real (solid blue) and imaginery (dashed red) parts as a dependence of idler detuning $\Delta\omega_i$ showing a normal dispersion inside the EIT window.	162



# SUMMARY

In this thesis, we investigate the quantum mechanical interaction of light with matter in the form of a gas of ultracold atoms: the atomic ensemble. We present a theoretical analysis of two problems, which involve the interaction of quantized electromagnetic fields (called signal and idler) with the atomic ensemble (i) cascade two-photon emission in an atomic ladder configuration, and (ii) photon frequency conversion in an atomic diamond configuration. The motivation of these studies comes from potential applications in long-distance quantum communication where it is desirable to generate quantum correlations between telecommunication wavelength light fields and ground level atomic coherences. In the two systems of interest, the light field produced in the upper arm of an atomic Rb level scheme is chosen to lie in the telecom window. The other field, resonant on a ground level transition, is in the near-infrared region of the spectrum. Telecom light is useful as it minimizes losses in the optical fiber transmission links of any two long-distance quantum communication device.

We develop a theory of correlated signal-idler pair correlation. The analysis is complicated by the possible generation of multiple excitations in the atomic ensemble. An analytical treatment is given in the limit of a single excitation assuming adiabatic laser excitations. The analysis predicts superradiant timescales in the idler emission in agreement with experimental observation. To relax the restriction of a single excitation, we develop a different theory of cascade emission, which is solved by numerical simulation of classical stochastic differential equation using the theory of open quantum systems. The simulations are in good qualitative agreement with the analytical theory of superradiant timescales. We further analyze the feasibility

of this two-photon source to realize the DLCZ protocol of the quantum repeater communication system.

We provide a quantum theory of near-infrared to telecom wavelength conversion in the diamond configuration. The system provides a crucial part of a quantum-repeater memory element, which enables a "stored" near-infrared photon to be converted to a telecom wavelength for transmission without the destruction of light-atom quantum correlation. We calculate the theoretical conversion efficiency, analyzing the role of optical depth of the ensemble, pulse length, and quantum fluctuations on the process.

# CHAPTER I

## INTRODUCTION

A quantum communication network based on the distribution and sharing of entangled states is potentially secure to eavesdropping and is therefore of great practical interest [1, 2, 3]. A protocol for the realization of such a long distance system, known as the quantum repeater, was proposed by Briegel *et al.* [4, 5]. A quantum repeater based on the use of atomic ensembles as memory elements, distributed over the network, was subsequently suggested by Duan, Lukin, Cirac and Zoller [6]. The storage of information in the atomic ensembles involves the Raman scattering of an incident light beam from ground state atoms with the emission of a signal photon. The photon is correlated with the creation of a phased, ground-state, coherent excitation of the atomic ensemble. The information may be retrieved by a reverse Raman scattering process, sending the excitation back to the initial atomic ground state and generating an idler photon directionally correlated with the signal photon [7, 8, 9, 10, 11, 12, 13, 14, 15]. In the alkali gases, the signal and the idler field wavelengths are in the near-infrared spectral region. This presents a wavelength mismatch with telecommunication wavelength optical fiber, which has a transmission window at longer wavelengths (1.1-1.6  $\mu\text{m}$ ). It is this mismatch that motivates the search for alternative processes that can generate telecom wavelength photons correlated with atomic spin waves [16].

This motivates the research presented in this thesis where we study multi-level atomic schemes in which the transition between the excited states is resonant with a telecom wavelength light field [16]. The basic problem is to harness the absorption and the emission of telecom photons while preserving quantum correlations between

the atoms, which store information and the photons that carry along the optical fiber channel of the network. In this thesis, we theoretically study atomic cascade and diamond configurations in this context.

## ***1.1 DLCZ Protocol for the Quantum Repeater***

A long-distance quantum repeater must overcome the exponential losses in the optical fiber. To overcome this problem, the use of quantum memory was proposed [6]. For a practical system, it is essential to maximize quantum memory time, to preserve coherence during protocol operations, and connect the memory elements by light signals in the low-loss window of the optical fiber medium. The telecom wavelength range (1.1-1.6  $\mu\text{m}$ ) has a loss rate as low as 0.2 dB/km.

It is not common to have a telecom ground state transition in atomic gases except for rare earth elements [17, 18] or in an erbium-doped crystal [19]. However, a telecom wavelength (signal) can be generated from transitions between excited levels in the alkali metals [16].

### **1.1.1 Correlated cascade emission in quantum telecommunication**

The ladder configuration of atomic levels provides a source for telecom photons (signal) from the upper atomic transition. For rubidium and cesium atoms, the signal field has the range around 1.3-1.5  $\mu\text{m}$  that can be coupled to an optical fiber and transmitted to a remote location. Cascade emission may result in pairs of photons, the signal entangled with the subsequently emitted infrared photon (idler) from the lower atomic transition. Entangled signal and idler photons were generated from a phase-matched four-wave mixing configuration in a cold, optically thick  $^{85}\text{Rb}$  ensemble [16]. This correlated two-photon source is potentially useful as the signal field has telecom wavelength.

The temporal emission characteristics of the idler field, generated on the lower



arm of the cascade transition, were observed in measurements of the joint signal-idler correlation function. The idler decay time was shorter than the natural atomic decay time and dependent on optical thickness in a way reminiscent of superradiance [23, 20, 21, 22, 24].

We will develop an analytical theory of the cascade emission in an atomic ensemble in Chapter 3. The influence of electromagnetic dipole-dipole interactions between atoms is important to account for the idler field's temporal profile. By developing the theory on the assumption of weak adiabatic laser excitation, we are able to calculate the spectral characteristics of the signal and idler fields, and make a connection with the traditional theory of superradiance.

In Chapter 4, , we develop a more elaborate theory of the cascade emission under similar physical conditions to Chapter 3, but without the assumption of single atomic excitations. The theory is based on numerical solutions of stochastic differential equations derived using open-systems methods of quantum optics. We limit our analysis to the confirmation of the superradiant emission of the idler field predicted in the simple theory and observed experimentally.

In Chapter 5, we use this theory to discuss a potential application of the cascade emission process in the DLCZ protocol, and discuss the role of time-frequency entanglement.

## ***1.2 Quantum Memory with Light Frequency Conversion***

It is not sufficient to generate telecom wavelength light for quantum communication. The light field must be quantum correlated with atomic excitations stored in memory [16].

Recently there has been a breakthrough in this direction using a pair of cold, non-degenerate rubidium gas samples [25]. A correlated pair of atomic spin wave and

infrared fields are generated by conventional Raman scattering in one ensemble. The light field is directed onto a second ensemble where it is frequency converted to the telecom range by four-wave mixing using a diamond configuration of atomic levels. The experiments were designed to measure quantum correlations between the stored atomic excitation and the telecom field.

The conversion scheme exploits an efficient low-noise parametric conversion process that is facilitated by operating in the regime of high transparency [25]. This provides a basic quantum memory element for a scalable, long distance quantum network. In Chapter 6, we investigate conditions required to maximize the conversion efficiency as a function of optical thickness of the atomic ensemble. The influence of the probe pulse duration on the conversion efficiency is studied by numerical solution of the Maxwell-Bloch equations.

### ***1.3 Outline***

The remainder of this thesis is organized as follows.

In Chapter 2, we review some theoretical methods to provide background for the theories developed in Chapter 4 and 6. In particular we discuss the derivation of quantum Heisenberg-Langevin equations for the interaction of a group of atoms with a quantized propagating electromagnetic field. We illustrate the connection of these operator equations with related classical (c-number) stochastic Langevin equations. The latter have the useful property that they may be numerically simulated, under certain conditions, and we provide the Kubo oscillator as a numerical test case.

In Chapter 3, we present a theory of cascade two-photon emission in an atomic ensemble. The radiative atomic dipole-dipole coupling is shown to influence the emission of the idler photon, resulting in the appearance of superradiant time scales. The theory is developed on the basis of Schrödinger probability amplitudes assuming single atomic excitations. This approach allows a straightforward treatment of the

spectral entanglement properties of the signal-idler photons.

In Chapter 4, we relax the assumption of single atomic excitations and develop a theory based on c-number stochastic partial differential equations, derived using the methods reviewed in Chapter 2. Numerical solutions of the equations are used to compare with the superradiant timescales derived in the analytical theory.

In Chapter 5, the analysis of Chapter 3 is used to discuss the behavior of the cascade emission on the DLCZ protocol for the quantum repeater. Entanglement swapping and quantum teleportation are investigated, and the influence of time-frequency entanglement is discussed.

In Chapter 6, the use of the diamond configuration in frequency up and down conversion is analyzed using quantum-Heisenberg Langevin and Maxwell-Bloch equation methods. We present results for the optimal conversion efficiency as a function of optical thickness of the atomic ensemble. The role of pulse length and quantum fluctuations are discussed.

In Chapter 7, we present some conclusions.

In Appendixes A-D, we present a great deal of supporting information on the theoretical derivations that are quite lengthy on account of both the multimode treatment of the light fields and the complicated atomic level schemes and atomic dipole-dipole interactions.



# CHAPTER II

## REVIEW OF THEORETICAL AND NUMERICAL METHODS

In this Chapter, we review the derivations of quantum-Heisenberg equations and c-number Langevin equations for light-atom interactions. The reason for focusing on these methods is, in the first place that they are less familiar than Schrödinger picture methods (see Chapter 3 and 5) and that our applications of these methods (Chapter 4 and 6) involve rather long derivations that may obscure the basic ideas.

We provide two methods of deriving the c-number Langevin equations and their noise correlations. The equations may be found from the quantum Heisenberg-Langevin equations using a "quantum-classical" correspondence [26]. Alternatively, c-number Langevin equations are deduced by a Schrödinger-picture approach that employs characteristic equation and coherent state phase space methods. In the final step the Langevin equations are deduced from a Fokker-Planck equation for a generalized statistical distribution. Such methods were initially applied in quantum laser theory in the 1960's by Haken [27]. The independent derivations will be used to check the lengthy derivations involved in the case of cascade emission.

### ***2.1 Quantum and C-number Langevin Equations***

Langevin equations were initially derived to describe Brownian motion [28]. A fluctuating force is used to represent the random impacts of the environment on the Brownian particle. A given realization of the Langevin equation involves a trajectory perturbed by the random force. Ensemble averaging such trajectories provides a natural and direct way to investigate the dynamics of the stochastic variables.

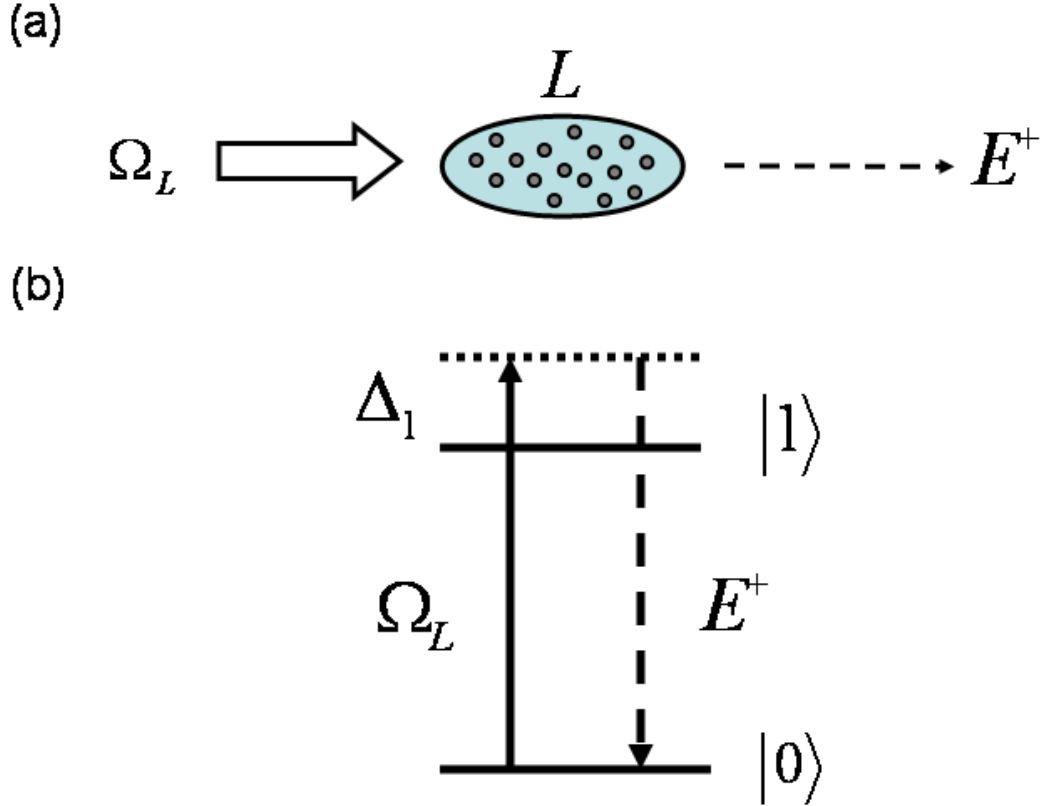


**Figure 2.1:** The two-level atomic ensemble interacts with a classical and quantum field. (a) An elongated atomic ensemble of length  $L$  is excited by a pump field of Rabi frequency  $\Omega_a$  and emits a propagating quantized field denoted by annihilation operator  $E^+$ . (b) Two-level structure for an atomic ensemble with the ground ( $|0\rangle$ ) and excited ( $|1\rangle$ ) state. The detuning of the pump field is  $\Delta_1$ .

In this section, we review quantum and c-number Langevin equation approaches for a two-level atomic ensemble interacting with a quantized electromagnetic field. As shown in Figure 2.1, the atoms are excited by a pump field of Rabi frequency  $\Omega_a$ , and a propagating quantized field  $E^+$  is considered to be emitted along the direction  $\hat{z}$  of the ensemble with length  $L$ .

### 2.1.1 Quantum Heisenberg-Langevin equations

We consider the Hamiltonian of  $N$  two-level (ground and excited states  $|0\rangle, |1\rangle$ ) atoms interacting with one pump field and a multimode quantized fields with mode annihilation operators  $\hat{a}_l$  that satisfy the commutation relation  $[\hat{a}_l, \hat{a}_{l'}^\dagger] = \delta_{ll'}$  for the  $l$ th section along the propagation direction. The propagation length  $L$  is discretized into  $2M + 1$  elements [29]. In the electric dipole approximation and rotating wave approximation, the interaction is given by  $-\vec{d} \cdot \vec{E}$ , Appendix B.1. The Hamiltonian  $H$  includes the free evolution ( $H_0$ ) of atoms with transition frequency  $\omega_1$ , the quantized field of central frequency  $\omega$ , and the dipole interaction ( $H_I$ ),

$$H = H_0 + H_I, \quad (2.1)$$

$$H_0 = \sum_{l=-M}^M \hbar\omega_1 \hat{\sigma}_{11}^l(t) + \hbar\omega \sum_{l=-M}^M \hat{a}_l^\dagger(t) \hat{a}_l(t) + \hbar \sum_{l,l'} \omega_{ll'} \hat{a}_l^\dagger(t) \hat{a}_{l'}(t), \quad (2.2)$$

$$H_I = -\hbar \sum_{l=-M}^M \left[ \Omega_L \hat{\sigma}_{01}^{l\dagger}(t) e^{ik_L z_l - i\omega_L t} + g\sqrt{2M+1} \hat{\sigma}_{01}^{l\dagger}(t) \hat{a}_l(t) e^{ik z_l} + h.c. \right] \quad (2.3)$$

where  $\hat{\sigma}_{01}^l(t) \equiv \sum_{\mu}^{N_z} |0\rangle_{\mu} \langle 1| \Big|_{r_{\mu}=z_l}$ . The Rabi frequency  $\Omega_L = d_{10}\mathcal{E}(k_L)/(2\hbar)$  is one-half the conventional definition. The dipole matrix element  $d_{10} \equiv \langle 1|\hat{d}|0\rangle$ , coupling strength  $g \equiv d_{10}\mathcal{E}(k)/\hbar$  where  $\mathcal{E}(k) = \sqrt{\hbar\omega/2\epsilon_0 V}$  is the electric field per photon, and  $z_p = \frac{pL}{2M+1}$ ,  $p = -M, \dots, M$ . The matrix  $\omega_{ll'} \equiv \sum_{n=-M}^M k_n e^{ik_n(z_l - z_{l'})}/(2M+1)$  accounts for field propagation by coupling the local mode operators.

The dynamical equations including dissipation due to spontaneous emission can be treated by introducing the reservoir field that interacts with the system [30]. After

introducing the coupling to the reservoir, we may write down by inspection the dissipation terms. We define  $\gamma_{01}$  to be the spontaneous emission rate from  $|1\rangle \rightarrow |0\rangle$ . In the co-moving frame coordinates  $z$  and  $\tau = t - z/c$ , the quantum Heisenberg-Langevin equations are

$$\frac{\partial}{\partial \tau} \tilde{\sigma}_{01} = (i\Delta_1 - \frac{\gamma_{01}}{2})\tilde{\sigma}_{01} + i\Omega_a(\tilde{\sigma}_{00} - \tilde{\sigma}_{11}) + ig(\tilde{\sigma}_{00} - \tilde{\sigma}_{11})\tilde{E}^+ + \tilde{\mathcal{F}}_{01}, \quad (2.4)$$

$$\frac{\partial}{\partial \tau} \tilde{\sigma}_{11} = -\gamma_{01}\tilde{\sigma}_{11} + i\Omega_L\tilde{\sigma}_{01}^\dagger - i\Omega_L^*\tilde{\sigma}_{01} + ig\tilde{\sigma}_{01}^\dagger\tilde{E}^+ - ig^*\tilde{\sigma}_{01}\tilde{E}^- + \tilde{\mathcal{F}}_{11}, \quad (2.5)$$

$$\frac{\partial}{\partial z} \tilde{E}^+ = \frac{iNg^*}{c}\tilde{\sigma}_{01} + \tilde{\mathcal{F}}_{E^+}, \quad (2.6)$$

where various Langevin noises  $\tilde{\mathcal{F}}$  associated with atomic operators  $\tilde{\sigma}_{01}$ ,  $\tilde{\sigma}_{11}$  and field operator  $\tilde{E}^+$  are necessary to preserve equal time commutation relations. The detuning of the pump field is  $\Delta_1 = \omega_L - \omega_1$  and the slowly-varying operators are defined as  $\tilde{\sigma}_{01} \equiv \sigma_{01}^l e^{-ik_a z_l + i\omega_a t}/N_z$ ,  $\tilde{\sigma}_{11} \equiv \sigma_{11}^l/N_z$ , and  $\tilde{E}^+(z, t) \equiv \sqrt{2M+1}\hat{a}_l e^{i\omega_a t}$  where we let  $\omega = \omega_L$ . The time evolution of atomic coherence ( $\tilde{\sigma}_{01}$ ) depends on the population difference ( $\tilde{\sigma}_{00} - \tilde{\sigma}_{11}$ ), and in turn atomic population is influenced by atomic coherence and the classical and quantized fields. The atomic coherence couples to the quantized field along the propagation direction,  $z$ .

The noise operator correlations are related to the dissipation through the fluctuation-dissipation theorem [31, 30]. If we have a quantum Langevin equation for variable  $\hat{x}$

$$\dot{\hat{x}}(t) = \hat{A}_x(t) + \hat{F}_x(t) \quad (2.7)$$

where  $\hat{A}_x$  is so-called the drift term for  $\hat{x}$ , and the corresponding Langevin noise operator is  $\hat{F}_x$ , the quantum noise correlation functions can be derived from the generalized Einstein relation,

$$\langle \hat{F}_x(t) \hat{F}_y(t) \rangle = -\langle \hat{x}(t) \hat{A}_y(t) \rangle - \langle \hat{A}_x(t) \hat{y}(t) \rangle + \frac{d}{dt} \langle \hat{x}(t) \hat{y}(t) \rangle. \quad (2.8)$$

where the bracket denotes the quantum mechanical ensemble average.



With the above recipe, we have the non-vanishing normally ordered quantum noise correlation function from Eq. (2.6),

$$\hat{D}_{11,11} = \gamma_{01} \tilde{\sigma}_{11}. \quad (2.9)$$

where  $\langle \tilde{\mathcal{F}}_{11}^\dagger(t, z) \tilde{\mathcal{F}}_{11}(t', z') \rangle = \frac{L}{N} \delta(t - t') \delta(z - z') \langle \hat{D}_{11,11} \rangle$ , and  $\hat{D}$  is also referred to as a diffusion matrix element by analogy with classical diffusion processes.

Even for this relatively simple light-matter interaction, there is no analytical solution possible. The c-number Langevin equation approach, below, provides a possible way to attack the problem numerically by stochastic simulation and to calculate normally-ordered quantities by ensemble averaging, although we will not pursue such simulations here.

### 2.1.2 C-number Langevin equation

A c-number Langevin equation approach may be suitable for stochastic simulation [32, 28], and utilizes the methods developed by Lax, Louisell, and Haken to describe the dynamics of the interaction [27, 26]. Their recipe involves a normal ordering procedure and a so-called "quantum-classical correspondence" to derive the c-number Langevin equations [26, 31, 33]. The normal ordering chosen is  $\tilde{\sigma}_{01}^\dagger, \tilde{\sigma}_{11}, \tilde{\sigma}_{01}, \tilde{E}^-, \tilde{E}^+$  where the creation operators always appear to the left of the annihilation operators. The population operator is put between the atomic coherence operators since it is self conjugate.

The c-number Langevin equations are then derived from Eq. (2.6) by making the quantum-classical correspondence that we denote as

$$\tilde{\sigma}_{01}^\dagger \rightarrow \alpha_5, \tilde{\sigma}_{11} \rightarrow \alpha_4, \tilde{\sigma}_{01} \rightarrow \alpha_3, \tilde{E}^- \rightarrow E^-, \tilde{E}^+ \rightarrow E^+. \quad (2.10)$$

Similarly for the Langevin noises,

$$\tilde{\mathcal{F}}_{01}^\dagger \rightarrow \mathcal{F}_5, \quad \tilde{\mathcal{F}}_{11} \rightarrow \mathcal{F}_4, \quad \tilde{\mathcal{F}}_{01} \rightarrow \mathcal{F}_3, \quad \tilde{\mathcal{F}}_{E^-} \rightarrow \mathcal{F}_2, \quad \tilde{\mathcal{F}}_{E^+} \rightarrow \mathcal{F}_1, \quad (2.11)$$

where the notation is chosen to facilitate the comparison with an alternative approach that we will discuss in the next Section.

The classical noise correlation functions are also derived from an Einstein relation. Consider the c-number Langevin equation for the variables  $x$  and  $y$ ,

$$\dot{x}(t) = A_x(t) + F_x(t), \quad (2.12)$$

$$\dot{y}(t) = A_y(t) + F_y(t). \quad (2.13)$$

From the requirement of equivalent time evolution of normally-ordered operators and their c-number counterparts, we have for example

$$\frac{d}{dt}\langle \hat{x}\hat{y} \rangle = \frac{d}{dt}\langle xy \rangle. \quad (2.14)$$

Classical noise correlations can be derived from the quantum ones using

$$\langle F_x F_y \rangle = \langle \hat{F}_x \hat{F}_y \rangle + \langle \hat{x} \hat{A}_y \rangle + \langle \hat{A}_x \hat{y} \rangle - \langle x A_y \rangle - \langle A_x y \rangle. \quad (2.15)$$

where the quantum and classical noise correlations are formally quite different. For non-normally-ordered operators  $\hat{x}\hat{z}$ , we may use the commutator to substitute that

$$\langle \hat{x}\hat{z} \rangle = \langle \hat{z}\hat{x} \rangle + \langle [\hat{x}, \hat{z}] \rangle. \quad (2.16)$$

The drift term of the c-number Langevin equations are closely related to the corresponding term in the quantum Heisenberg-Langevin equations. After the quantum-classical correspondence is made, we derive the coupled equations with c-number variables ( $E^+$ ,  $E^-$ ,  $\alpha_3$ ,  $\alpha_4$ ,  $\alpha_5$ ) and Langevin noises ( $\mathcal{F}_{1,2,3,4,5}$ ) that satisfy

$$\frac{\partial}{\partial \tau} \alpha_3 = (i\Delta_1 - \frac{\gamma_{01}}{2})\alpha_3 + i\Omega_a(\alpha_0 - \alpha_4) + ig(\alpha_0 - \alpha_4)E^+ + \mathcal{F}_3, \quad (2.17)$$

$$\frac{\partial}{\partial \tau} \alpha_4 = -\gamma_{01}\alpha_4 + i\Omega_a\alpha_5 - i\Omega_a^*\alpha_3 + ig\alpha_5E^+ - ig^*\alpha_3E^- + \mathcal{F}_4, \quad (2.18)$$

$$\frac{\partial}{\partial \tau} \alpha_5 = (-i\Delta_1 - \frac{\gamma_{01}}{2})\alpha_5 - i\Omega_a^*(\alpha_0 - \alpha_4) - ig^*(\alpha_0 - \alpha_4)E^- + \mathcal{F}_5, \quad (2.19)$$

$$\frac{\partial}{\partial z} E^+ = \frac{iNg^*}{c}\alpha_3 + \mathcal{F}_1, \quad \frac{\partial}{\partial z} E^- = -\frac{iNg}{c}\alpha_5 + \mathcal{F}_2, \quad (2.20)$$

The associated non-vanishing diffusion matrix elements, however look quite different to their quantum counterparts

$$\begin{aligned} D_{3,3} &= -i2\Omega_a\alpha_3 - i2g\alpha_3E^+, \\ D_{4,4} &= i\Omega_a\alpha_5 - i\Omega_a^*\alpha_3 + i\alpha_5E^+ - i\alpha_3E^- + \gamma_{01}\alpha_4. \end{aligned} \quad (2.21)$$

The diffusion matrix elements are defined as  $\langle \mathcal{F}_i(t, z) \mathcal{F}_j(t', z') \rangle = \frac{L}{N} \delta(t - t') \delta(z - z') \langle D_{ij} \rangle$  in the continuous limit. For the more complicated light-matter interactions we will encounter in Chapter 4 involving four atomic levels interacting with two propagating quantized light fields, the diffusion matrix calculation is much more intricate. It is therefore important to have an independent check of the c-number equations and the associated diffusion matrix. In the following Section we review the Fokker-Planck equation approach based on a Schrodinger picture treatment of the quantized light-atom interaction.

## ***2.2 Fokker-Planck Equations and Stochastic Differential Equations***

Here we review the alternative method, due to Haken [27], to derive the c-number Langevin equations or equivalently stochastic differential equations via Fokker-Planck equations [27, 35, 32, 34].

The Fokker-Planck equation is used to describe the fluctuations in Brownian motion [28], and its solution for probability distribution  $f(x, t)$  of Brownian particles in space  $x$  and time  $t$  is determined by the drift and diffusion properties of the particles.

### **2.2.1 Characteristic functions in P-representation**

The Characteristic function  $\chi$  is convenient for the derivation of Fokker-Planck equation, and it is the distribution function of the Fokker-Planck equation in Fourier space. We follow the same procedure of P-representation laser theory [27].

The relevant operators of our system are atomic coherences  $(\tilde{\sigma}_{01}^{l\dagger}, \tilde{\sigma}_{01}^l)$ , population  $(\tilde{\sigma}_{11}^l)$  and field operators  $(\hat{a}_l^\dagger, \hat{a}_l)$ . The normally ordered exponential operator is chosen to be

$$E(\lambda) = \prod_l E^l(\lambda),$$

$$E^l(\lambda) = e^{i\lambda_5^l \tilde{\sigma}_{01}^{l\dagger}} e^{i\lambda_4^l \tilde{\sigma}_{11}^l} e^{i\lambda_3^l \tilde{\sigma}_{01}^l} e^{i\lambda_2^l \hat{a}_l^\dagger} e^{i\lambda_1^l \hat{a}_l}, \quad (2.22)$$

where  $E(\lambda)$  the complete exponential operator and is decomposed into products of  $E^l(\lambda)$  for each section  $l$  of the propagation direction. We note that the ordering of operators is the same as we chose for the quantum-classical correspondence in the previous Section. The complex parameters  $\lambda_i^l$  are classical counterparts of operators in Fourier space, as will become clear when we derive the Fokker-Planck equation.

Then characteristic function  $\chi$  can be calculated from a density matrix  $\rho$ ,

$$\chi = \text{Tr} \{ E(\lambda) \rho \}, \quad (2.23)$$

$$\frac{\partial \chi}{\partial t} = \text{Tr} \left\{ E(\lambda) \frac{\partial \rho}{\partial t} \right\} = \sum_m \left( \frac{\partial \chi}{\partial t} \right)_m, \quad m = A, L, I, sp \quad (2.24)$$

and time evolution of  $\rho$  is

$$\frac{\partial \rho}{\partial t} = \frac{1}{i\hbar} [H, \rho] + \left( \frac{\partial \rho}{\partial t} \right)_{sp}, \quad H = H_0 + H_I,$$

$$\left( \frac{\partial \rho}{\partial t} \right)_{sp} = \sum_{l=-M}^M \sum_{\mu}^{N_z} \frac{\gamma_{01}}{2} \left[ 2\hat{\sigma}_{01}^{\mu,l} \rho \hat{\sigma}_{01}^{\mu,l\dagger} - \hat{\sigma}_{01}^{\mu,l\dagger} \hat{\sigma}_{01}^{\mu,l} \rho - \rho \hat{\sigma}_{01}^{\mu,l\dagger} \hat{\sigma}_{01}^{\mu,l} \right],$$

where  $H_0 = H_A + H_L$ .  $H_A$  is the Hamiltonian for atomic free evolution,  $H_L$  is the Hamiltonian for the pump field, and the dipole interaction Hamiltonian is  $H_I$ . The dissipation from spontaneous emission is denoted as  $sp$ .

The contribution from  $\left( \frac{\partial \rho}{\partial t} \right)_{sp}$  is calculated up to the second order in  $\lambda_i$ . The validity of truncation to second order is due to the expansion in the small parameter  $1/N_z$ . The dissipative contribution, identified by superscript (2), takes the form,

$$\begin{aligned} & \gamma_{01} \text{Tr} \left\{ E(\lambda) \left[ \hat{\sigma}_{01} \rho \hat{\sigma}_{01}^\dagger - \frac{1}{2} \hat{\sigma}_{11} \rho - \frac{1}{2} \rho \hat{\sigma}_{11} \right] \right\}^{(2)} = \\ & \gamma_{01} \left[ -\frac{i\lambda_3}{2} \frac{\partial}{\partial(i\lambda_3)} - \frac{i\lambda_5}{2} \frac{\partial}{\partial(i\lambda_5)} - i\lambda_4 \frac{\partial}{\partial(i\lambda_4)} + \frac{(i\lambda_4)^2}{2} \frac{\partial}{\partial(i\lambda_4)} \right] \chi. \end{aligned} \quad (2.25)$$

where we drop the summation over spatial slices  $l$ , which we will retrieve later. Collecting together all contributions to the characteristic function, we may proceed to write down a Fokker-Planck equation that leads to the c-number Langevin equation.

### 2.2.2 A Complimentary Derivation of C-number Langevin Equations

The time derivative of the distribution function  $f$  is found from the Fourier transform of the characteristic function  $\frac{\partial f}{\partial t} = \frac{1}{(2\pi)^n} \int \dots \int e^{-i\vec{\alpha} \cdot \vec{\lambda}} \frac{\partial \chi}{\partial t} d\lambda_1 \dots d\lambda_n$ . Separating the different contributions we may write

$$\frac{\partial f}{\partial t} = \mathcal{L}f = \sum_{l,l'} [\mathcal{L}_A \delta_{ll'} + \mathcal{L}_L + \mathcal{L}_I \delta_{ll'} + \mathcal{L}_{sp} \delta_{ll'}] f. \quad (2.26)$$

The details of the  $\mathcal{L}$  operators can be found in Appendix B. Here we show  $\mathcal{L}_I$  as an example,

$$\begin{aligned} \mathcal{L}_I = & i\Omega_a e^{ik_a z_l - i\omega_a t} \left[ -\frac{\partial^2}{\partial \alpha_3^l \partial \alpha_3^l} (\alpha_3^l) - \frac{\partial}{\partial \alpha_3^l} (-2\alpha_4^l + N_z) + e^{-\frac{\partial}{\partial \alpha_4^l}} (\alpha_5^l) \right] - i\Omega_a e^{ik_a z_l - i\omega_a t} (\alpha_5^l) \\ & + ig\sqrt{2M+1} e^{ikz_l} \left[ -\frac{\partial^2}{\partial \alpha_3^l \partial \alpha_3^l} (\alpha_3^l) - \frac{\partial}{\partial \alpha_3^l} (-2\alpha_4^l + N_z) + e^{-\frac{\partial}{\partial \alpha_4^l}} (\alpha_5^l) \right] \alpha_1^l \\ & + ig^* \sqrt{2M+1} e^{-ikz_l} (\alpha_3^l) \left( \alpha_2^l - \frac{\partial}{\partial \alpha_1^l} \right) + (C')^*, \end{aligned} \quad (2.27)$$

where  $C'$  is the correspondence that  $\alpha_3^* \leftrightarrow \alpha_5$ ,  $\alpha_4^* \leftrightarrow \alpha_4$ ,  $\alpha_1^* \leftrightarrow \alpha_2$ , and  $*$  denotes complex conjugation. The results is a Fokker-Planck equation of the form

$$\frac{\partial f}{\partial t} = -\frac{\partial}{\partial \alpha} A_\alpha f - \frac{\partial}{\partial \beta} A_\beta f + \frac{1}{2} \left( \frac{\partial^2}{\partial \alpha \partial \beta} + \frac{\partial^2}{\partial \beta \partial \alpha} \right) D_{\alpha\beta} f \quad (2.28)$$

where  $A_{\alpha,\beta}$  and  $D_{\alpha\beta}$  are drift and diffusion terms. The corresponding c-number Langevin equations may be derived rigorously when  $D$  is positive definite, and take the form

$$\frac{\partial\alpha}{\partial t} = A_\alpha + \Gamma_\alpha, \quad \frac{\partial\beta}{\partial t} = A_\beta + \Gamma_\beta \quad (2.29)$$

with a classical noise correlation  $\langle \Gamma_\alpha(t) \Gamma_\beta(t') \rangle = \delta(t - t') D_{\alpha\beta}$ . Higher order derivatives (third order and higher, from the Taylor expansions of  $e^{-\frac{\partial}{\partial\alpha^l_4}}$ ) are ignored as they involve the small parameter  $1/N_z$ . The corresponding c-number Langevin, or stochastic differential, equations are

$$\begin{aligned} \dot{\alpha}_3^l = & (-i\omega_1 - \frac{\gamma_{01}}{2})\alpha_3^l + i\Omega_a e^{ik_a z_l - i\omega_a t} (\alpha_0^l - \alpha_4^l) \\ & + ig\sqrt{2M+1}e^{ikz_l}(\alpha_0^l - \alpha_4^l)\alpha_1^l + \Gamma_3^l, \end{aligned} \quad (2.30)$$

$$\begin{aligned} \dot{\alpha}_4^l = & -\gamma_{01}\alpha_4^l + i\Omega_a e^{ik_a z_l - i\omega_a t} \alpha_5^l - i\Omega_a^* e^{-ik_a z_l + i\omega_a t} \alpha_3^l \\ & + ig\sqrt{2M+1}e^{ikz_l}\alpha_5^l\alpha_1^l - ig^*\sqrt{2M+1}e^{-ikz_l}\alpha_3^l\alpha_2^l + \Gamma_4^l, \end{aligned} \quad (2.31)$$

$$\dot{\alpha}_1^l = -i\omega\alpha_1^l - i\sum_{l'}\omega_{ll'}\alpha_1^{l'} + ig^*\sqrt{2M+1}e^{-ikz_l}\alpha_3^l + \Gamma_1^l. \quad (2.32)$$

We can retrieve the continuous limit with the slowly varying variables,  $\alpha_3(z, t) \equiv \alpha_3^l e^{-ik_a z_l + i\omega_a t}/N_z$ ,  $\alpha_4(z, t) \equiv \alpha_4^l/N_z$ ,  $E^+(z, t) \equiv \sqrt{2M+1}\alpha_1^l e^{i\omega_a t}$ , and note that

$-i\sum_{l'}\omega_{ll'}\alpha_1^{l'} = -c\frac{\partial}{\partial z_l}\alpha_1^l$  and  $\alpha_0^l = N_z - \alpha_4^l$ . Define also the slowly-varying Langevin noises,

$$\begin{aligned} \mathcal{F}_3(z, t) &= \frac{1}{N_z}\Gamma_3^l e^{-ik_a z_l + i\omega_a t}, \quad \mathcal{F}_4(z, t) = \frac{1}{N_z}\Gamma_4^l, \\ \mathcal{F}_1(z, t) &= \sqrt{2M+1}e^{i\omega t}\Gamma_1^l. \end{aligned} \quad (2.33)$$

Finally, in the co-moving frame coordinates  $z$  and  $\tau = t - z/c$ , the c-number

Langevin equation becomes

$$\frac{\partial}{\partial \tau} \alpha_3 = (i\Delta_1 - \frac{\gamma_{01}}{2})\alpha_3 + i\Omega_a(\alpha_0 - \alpha_4) + ig(\alpha_0 - \alpha_4)E^+ + \mathcal{F}_3, \quad (2.34)$$

$$\frac{\partial}{\partial \tau} \alpha_4 = -\gamma_{01}\alpha_4 + i\Omega_a\alpha_5 - i\Omega_a^*\alpha_3 + ig\alpha_5E^+ - ig^*\alpha_3E^- + \mathcal{F}_4, \quad (2.35)$$

$$\frac{\partial}{\partial \tau} \alpha_5 = (-i\Delta_1 - \frac{\gamma_{01}}{2})\alpha_5 - i\Omega_a^*(\alpha_0 - \alpha_4) - ig^*(\alpha_0 - \alpha_4)E^- + \mathcal{F}_5, \quad (2.36)$$

$$\frac{\partial}{\partial z} E^+ = \frac{iNg^*}{c}\alpha_3 + \mathcal{F}_1, \quad \frac{\partial}{\partial z} E^- = -\frac{iNg}{c}\alpha_5 + \mathcal{F}_2, \quad (2.37)$$

where  $\Delta_1 = \omega_a - \omega_1$ . The non-vanishing diffusion coefficients extracted from the Fokker-Planck equation are

$$D_{3,3} = -i2\Omega_a\tilde{\alpha}_3 - i2\tilde{\alpha}_3E_i^+; \quad D_{4,4} = i\Omega_a\tilde{\alpha}_5 - i\Omega_a^*\tilde{\alpha}_3 + i\tilde{\alpha}_5E_i^+ - i\tilde{\alpha}_3E_i^- + \gamma_{01}\tilde{\alpha}_4. \quad (2.38)$$

Comparing with the results in the previous Section and Eq. (2.21), we find complete agreement. As the c-number Langevin equations are derived from a Fokker-Planck equation, they should be interpreted as Ito-type stochastic differential equations (SDE), and this is important in the numerical solution method [32]. In numerical simulation it is common to first transform from the Ito equation to its corresponding Stratonovich form.

## 2.3 Kubo Oscillator

We present an example of the Kubo oscillator to illustrate numerical simulation of a multiplicative noise stochastic differential equation. A Kubo oscillator provides a good test case in the numerical solution of stochastic differential equations. The Langevin equation of the dimensionless Kubo oscillator with amplitude  $z(t)$  is given by the Stratonovich equation,

$$\frac{d}{dt}z(t) = i\xi(t)z(t) \quad (2.39)$$

where  $\xi(t)$  is a delta-correlated real Gaussian distributed noise with zero mean,  $\langle \xi(t) \rangle = 0$ , and  $\langle \xi(t)\xi(t') \rangle = \delta(t-t')$ . The bracket denotes an ensemble average. The

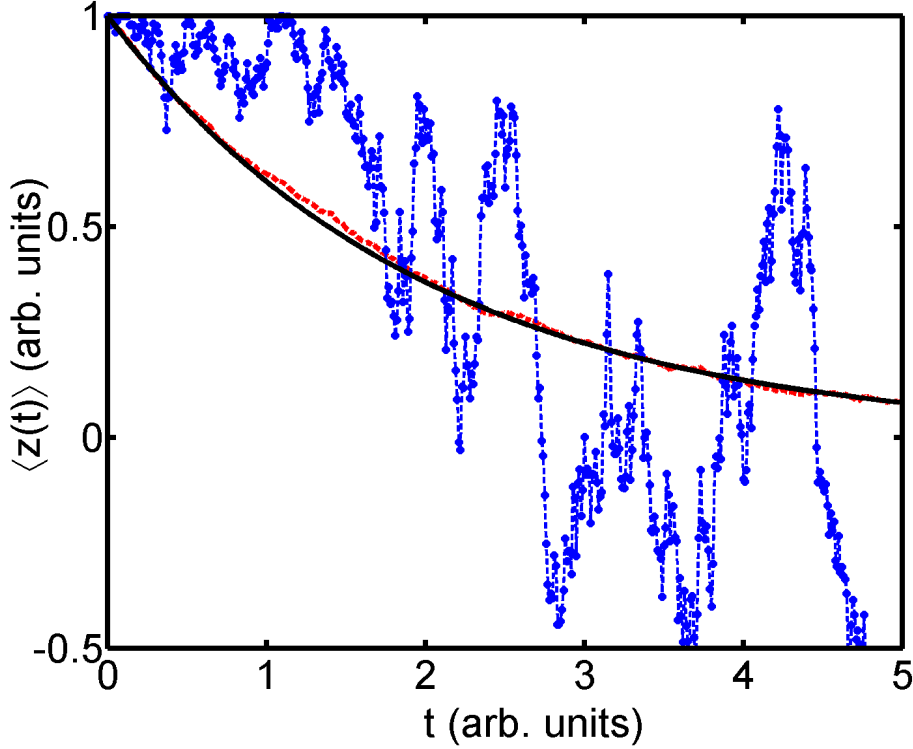


**Figure 2.2:** Kubo oscillator simulation. The time evolution of  $\text{Re}\langle z(t) \rangle$  (dashed-red) averaged from an ensemble of 1024 simulations.  $z(0) = 1$ . We compare with the exact solution,  $z(0)e^{-t/2}$  (solid-black), and find good agreement. A demonstration of one stochastic realization (dashed-circle blue) shows large fluctuation around the averaged and exact results. Note that the imaginary part of the solution is almost vanishing as it should be, and is not shown here.

exact analytical solution for the first moment is  $\langle z(t) \rangle = \langle z(t=0) \rangle e^{-t/2}$ . To numerically simulate the Stratonovich equation (2.39), we use the following discretization in time [36, 37]

$$z(t_m) = z_{n-1} + i\xi(t_{n-1})z(t_m)\frac{\Delta t}{2} \quad (2.40)$$

where  $z(t_m)$  is evaluated at the midpoint,  $t_m = (t_n + t_{n-1})/2$  and  $\Delta t = t_n - t_{n-1}$  is the time step. In this specific case where the noise is linear in  $z(t)$ , we may solve Eq. (2.40) to give  $z(t_m) = z_{n-1}/(1 - i\xi(t_{n-1})\Delta t/2)$ . Setting  $z(t_{n+1}) = 2z(t_m) - z(t_n)$ , we use  $z(t_{n+1})$  for the next time step of the integration.



The Langevin noise is numerically simulated as  $\xi(t) = \text{randn}(t)/\sqrt{\Delta t}$ , where  $\text{randn}(t)$  is a random number generated from a Gaussian distribution with zero mean and unit variance. In Figure 2.2, we compare the analytical and numerical results for the Kubo oscillator. The initial condition is set as  $z(0) = 1$ , and we use 1024 realizations for the converged numerical result  $\langle z(t) \rangle$  with  $\Delta t = 0.01$ . The numerical result is in good agreement with the exact solution,  $z(0)e^{-t/2}$ . The temporal evolution of one typical realization of the stochastic process fluctuates significantly, as shown.

We will use the approach demonstrated here to simulate the more complicated c-number Langevin noises in our investigation of cascade emission from an atomic ensemble in Chapter 4 (see also Appendix B).



# CHAPTER III

## SUPERRADIANT EMISSION FROM A CASCADE ATOMIC ENSEMBLE: ANALYTICAL METHOD

In this Chapter, we use Schrödinger's equation to investigate cascade emission from a four-level atomic ensemble. Quantum communication has opened up the possibility to transmit quantum information over long distance. Due to the transmission loss in long distance fiber-based quantum communication, telecommunication (telecom) wavelength light is important to maximize the transmission efficiency. The alkali atomic cascade transition shown in Figure 3.3 is able to generate telecom wavelength light, the signal, from the upper transition and a near-infrared field, the idler, from the lower one. The telecom light can travel through the fiber with minimal loss, while the near-infrared field is suitable for storage and retrieval in an atomic quantum memory element. Their use in a quantum information system requires quantum correlations between stored excitations and the telecom field.

We develop a quantum theory to characterize the properties of the correlated signal and idler photons and study how the laser excitation pulse modifies their spectral profile. The wave packets of this entangled source are found, and Schmidt decomposition provides the basis for engineering a pure photon source that is crucial in quantum information processing.

### 3.1 *Introduction*

The spontaneous emission from an optically dense atomic ensemble is a many-body problem due to the radiative coupling between atoms. This coupling is responsible for the phenomenon of superradiance firstly discussed by Dicke [23] in 1954.

Since then, this collective emission has been extensively studied in two atom systems indicating a dipole-dipole interaction [20, 21], in the totally inverted  $N$  atom systems [38, 39], and in the extended atomic ensemble [22]. The emission intensity has been investigated using the master equation approach [40, 41, 42] and with Maxwell-Bloch equations [43, 44]. A useful summary and review of superradiance can be found in the reference [45, 46]. Recent approaches to superradiance include the quantum trajectory method [47, 48] and the quantum correction method [49].

In the limit of single atomic excitation, superradiant emission characteristics have been discussed in the reference [50] and [51]. For a singly excited system, the basis set reduces to  $N$  rather than  $2^N$  states. Radiative phenomena have been investigated using dynamical methods [52, 53, 54] and by the numerical solution of an eigenvalue problem [55, 56, 57, 58]. A collective frequency shift [59, 60] can be significant at a high atomic density [61] and has been observed recently in an experiment where atoms are resonant with a planar cavity [62].

### 3.2 *The example of two-state atoms interacting with a pump field*

The atomic dynamics of  $N$  two-state atoms interacting with a pump field generally requires a basis of  $2^N$  orthogonal states. In this Section we investigate multiple excitations by a laser by solving numerically the master equation for few atom systems ( $N = 2, 3, 4$ ), using the quantum optics toolbox [63]. The complete orthogonal states may be chosen as 1 symmetric state and  $(C_n^N - 1)$  non-symmetric states for any excitation number  $n$  where  $C_n^N$  is the combination coefficient. It is natural to construct the

complete orthogonal states using this decomposition because the interaction Hamiltonian of the pump field,  $H_I = [-\hbar\frac{\Omega_a}{2} \sum_{\mu}^N |1\rangle\langle 0|e^{i\vec{k}\cdot\vec{r}_{\mu}} + c.c.] - \hbar\Delta_1 \sum_{\mu}^N |1\rangle\langle 1|$ , has the same form for each atom.

For the example of two two-state atoms, there are 4 orthogonal basis states: the ground state  $|00\rangle$ , the symmetric state of a single excitation  $(e^{i\vec{k}\cdot\vec{r}_1}|10\rangle + e^{i\vec{k}\cdot\vec{r}_2}|01\rangle)/\sqrt{2}$ , the associated anti-symmetric state  $(e^{i\vec{k}\cdot\vec{r}_1}|10\rangle - e^{i\vec{k}\cdot\vec{r}_2}|01\rangle)/\sqrt{2}$ , and the state of two excitations  $e^{i\vec{k}\cdot(\vec{r}_1+\vec{r}_2)}|11\rangle$ . Note that the spatial phase factor for different atomic position  $\vec{r}$  is included due to the pump field of the wavevector  $\vec{k}$  that is directed along the  $\hat{z}$  axis. If more atoms are involved, the complete states of multiple excitations can be derived by extending the results of reference [52], and here we list the states of four atoms ( $N = 4$ ),

$$\begin{aligned}
n = 0, \quad |\phi_1\rangle &= |0, 0, 0, 0\rangle, \\
n = 1 \quad \left\{ \begin{array}{l} |\phi_2\rangle = \frac{1}{\sqrt{N}} \sum_{\mu=1}^N e^{i\vec{k}\cdot\vec{r}_{\mu}} |1\rangle_{\mu} |0\rangle_{\lambda \neq \mu}; \\ |\phi_{l+2}\rangle = \sum_{j=1}^{N-1} \left( \frac{1+1/\sqrt{N}}{N-1} - \delta_{jl} \right) e^{i\vec{k}\cdot\vec{r}_j} |1\rangle_j |0\rangle_{\lambda \neq j} - \frac{e^{i\vec{k}\cdot\vec{r}_N}}{\sqrt{N}} |1\rangle_N |0\rangle_{\lambda \neq N}, \\ l = 1, 2, \dots, N-1; \end{array} \right. \\
n = 2 \quad \left\{ \begin{array}{l} |\phi_{N+2}\rangle = \frac{1}{\sqrt{N(N-1)/2}} \sum_{\mu > \nu}^N \sum_{\nu=1}^N e^{i\vec{k}\cdot(\vec{r}_{\mu}+\vec{r}_{\nu})} |1\rangle_{\mu} |1\rangle_{\nu} |0\rangle_{\lambda \neq \mu, \nu}; \\ |\phi_{m+N+2}\rangle = \sum_{l > j}^N \sum_{j=1}^{N-2} \left( \frac{1+1/\sqrt{N_2}}{N_2-1} - \delta_{m,(j,l)} \right) e^{i\vec{k}\cdot(\vec{r}_j+\vec{r}_l)} |1\rangle_j |1\rangle_l |0\rangle_{\lambda \neq j, l} \\ - \frac{e^{i\vec{k}\cdot(\vec{r}_{N-1}+\vec{r}_N)}}{\sqrt{N_2}} |1\rangle_{N-1} |1\rangle_N |0\rangle_{\lambda \neq N-1, N}, \quad m = 1, 2, \dots, N_2-1, \\ \text{where } N_2 \equiv N(N-1)/2; \end{array} \right. \\
\bullet \\
\bullet \\
\bullet \\
n = N, \quad |\phi_{2N}\rangle &= |1\rangle^{\otimes N} \prod_{j=1}^N e^{i\vec{k}\cdot\vec{r}_j}, \tag{3.1}
\end{aligned}$$

where  $(j, l)$  in the subscript of the Kronecker delta function of two excitation states

is defined so that  $(1, 2) = 1$ ,  $(1, 3) = 2$ ,  $(1, 4) = 3$ ,  $(2, 3) = 4$ , and  $(2, 4) = 5$ . Note that the  $n = 0$ ,  $|\phi_1\rangle$ , and  $n = N$ ,  $|\phi_{2N}\rangle$ , states are symmetric. For  $n \neq 0, N$  excitations, the states are constructed from one symmetric state and  $C_n^N$  non-symmetric states.

To investigate the probability of multiple atomic excitations in conditions of weak off-resonant excitation, we choose a configuration of four atoms that sit on the vertices of a square with side  $d_s$ . The atomic density matrix includes a laser excitation term in addition to the one and two-atom dissipation terms; these arise from spontaneous emission and radiative coupling due to dipole-dipole interaction [21]; see Eq. (A.15) in Appendix A. We numerically solve for the time evolution of the density matrix. The result of steady state single- and double-excitation populations are shown in Figure 3.1 as a function of  $d_s$ . We have assumed a continuous laser field with peak Rabi frequency  $\Omega_a = 0.2\gamma$  and detuning  $\Delta_1 = 5\gamma$ , where  $\gamma$  is the single-atom spontaneous decay rate for the excited state. The populations of the symmetric states are  $P_1^s \equiv \text{Tr}(\hat{\rho}|\phi_2\rangle\langle\phi_2|)$  for a single excitation and  $P_2^s \equiv \text{Tr}(\hat{\rho}|\phi_6\rangle\langle\phi_6|)$  for double excitations where  $\hat{\rho}$  is the density operator of the atomic system. The total populations of the non-symmetric excitation states are  $P_1^{\text{ns}} \equiv \text{Tr}(\hat{\rho}(\sum_{x=2}^5 |\phi_x\rangle\langle\phi_x|))$ , for a single excitation, and  $P_2^{\text{ns}} \equiv \text{Tr}(\hat{\rho}(\sum_{x=7}^{11} |\phi_x\rangle\langle\phi_x|))$ , for double excitations, respectively. The probabilities of three and four excitations are negligible under the weak excitation conditions we consider.

As  $d_s$  approaches and exceeds  $\lambda$  (the transition wavelength), the populations tend to the independent atom limit when dipole-dipole coupling is omitted. In this limit, the probability of exciting any non-symmetric states goes to zero. The single and double excitation probabilities,  $P_1^s$  and  $P_2^s$ , are normalized to their independent atom values,  $P_1^{(0)} = P_e P_g^3 C_1^4$  and  $P_2^{(0)} = P_e^2 P_g^2 C_2^4$  where  $P_e = \Omega_a^2/(4\Delta_1^2 + \gamma^2)$  [64],  $P_g = 1 - P_e$ , and  $C_i^n$  is the combination coefficient. For  $d_s \ll \lambda$ , the populations of the non-symmetric states are comparable to the symmetric ones, indicating the importance of dipole-dipole interactions. We see no evidence of a dipole blockade effect in this limit

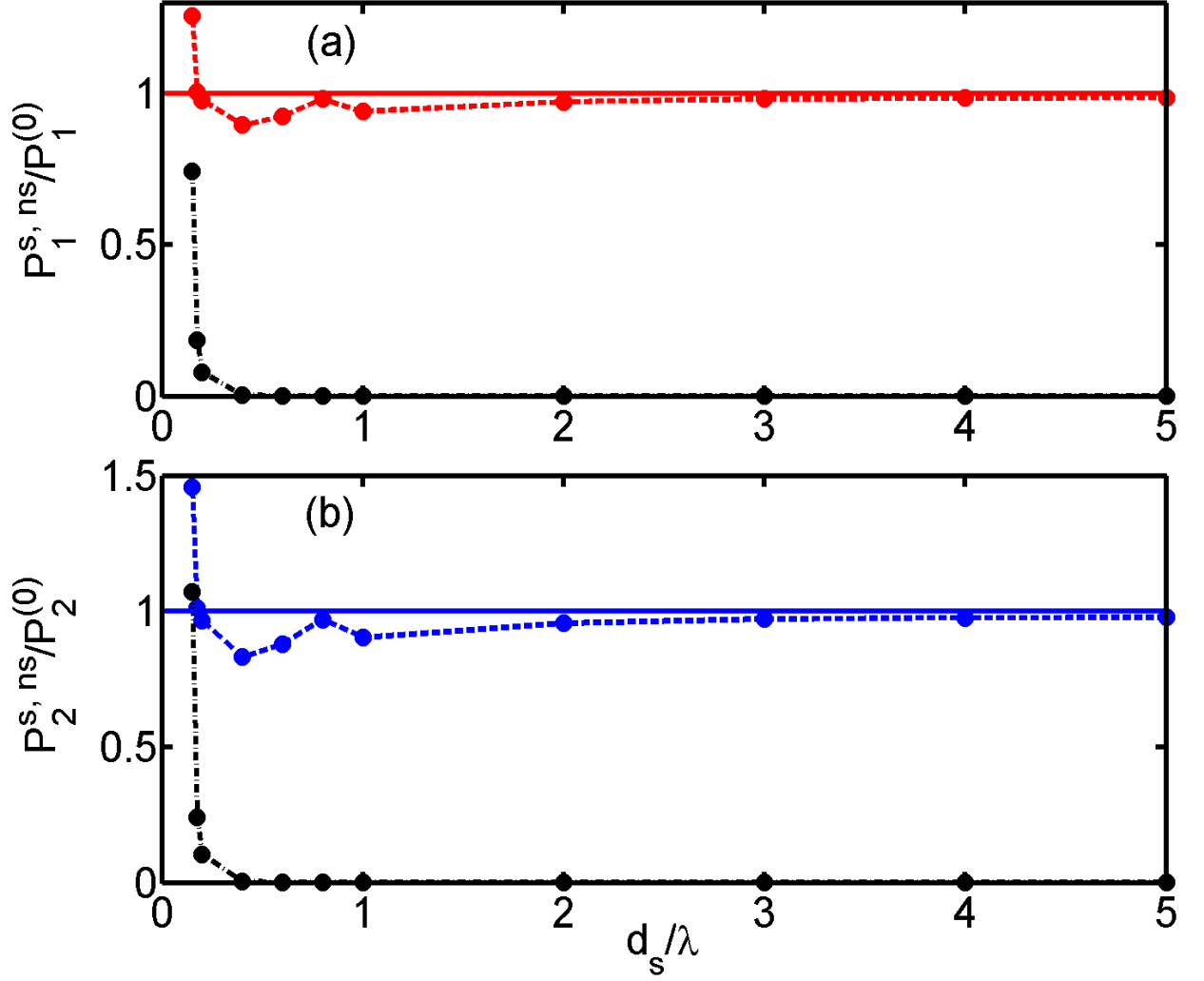


**Figure 3.1:** Single- and double-excitation populations as a function of distance  $d_s$ . (a) The populations of the symmetric state for a single excitation  $P_1^s$  (dashed-red) and the sum of non-symmetric single-excitation states  $P_1^{ns}$  (dashed-dotted black). (b) The populations of the symmetric state for double excitations  $P_2^s$  (dashed-blue) and the sum of non-symmetric double-excitation states  $P_2^{ns}$  (dashed-dotted black).  $P_1^{s, ns}$  and  $P_2^{s, ns}$  are normalized respectively by the solutions of non-interacting atoms  $P_1^{(0)}$  (solid-red) and  $P_2^{(0)}$  (solid-blue).  $P_1^{(0)} = 1.58 \times 10^{-3}$  and  $P_2^{(0)} = 9.4 \times 10^{-7}$ , are the single- and double-excitation probabilities for independent atoms.

for four atoms, but we have observed it in the case of two atoms. Dipole blockade refers to the predominance of single excitations as dipole shifts detune double and higher excitation states.

In Figure 3.2, we show the time evolution of  $P_1^s(t)$  and  $P_2^s(t)$  for  $d_s = 3\lambda$  (this corresponds to an atomic density  $8 \times 10^{10} \text{ cm}^{-3}$ ). The period of the Rabi oscillation is determined by  $2\pi/\Delta_1$ , and the asymptotic steady state value for  $P_2^s$  is about  $1.6 \times 10^{-3}$ . This coincides with the approximate result  $|\sqrt{N}\Omega_a/(2\Delta_1)|^2$  that is found when we truncate the basis to the ground state and the orthogonal states of a single atomic excitation.

We also numerically solve a line of atoms ( $N = 2, 3$ , or  $4$ ) with an equal separation from  $d_s = 1$  to  $5\lambda$ , and the results of steady state populations indicate the condition for truncation of the basis set at a single atomic excitation is valid when  $|\Delta_1| \gg \sqrt{N}\Omega_a/2$ . If the condition of a single atomic excitation  $\Delta_1 \gg \sqrt{N}\Omega_a/2$  is relaxed, we will also have dynamical couplings between symmetric and non-symmetric states (at least for  $d_s \lesssim 3\lambda$ ). It is the dipole-dipole interaction that couples the non-symmetric and symmetric states in the presence of the pump laser.

### 3.3 *Theory of Cascade Emission*

We consider  $N$  cold atoms that are initially prepared in the ground state interacting with four independent electromagnetic fields. As shown in Figure 3.3, two driving lasers (of Rabi frequencies  $\Omega_a$  and  $\Omega_b$ ) excite a ladder configuration  $|0\rangle \rightarrow |1\rangle \rightarrow |2\rangle$ . Two quantum fields, signal  $\hat{a}_s$  and idler  $\hat{a}_i$ , are generated spontaneously. The atoms adiabatically follow the two excitation pulses and decay through the cascade emission of signal and idler photons. Based on the discussion in the previous Section, we permit only single atomic excitations under the condition of large detuning,  $\Delta_1 \gg \sqrt{N}\Omega_a/2$ . The Hamiltonian and the coupled equations of the atomic dynamics are detailed in Appendix A.



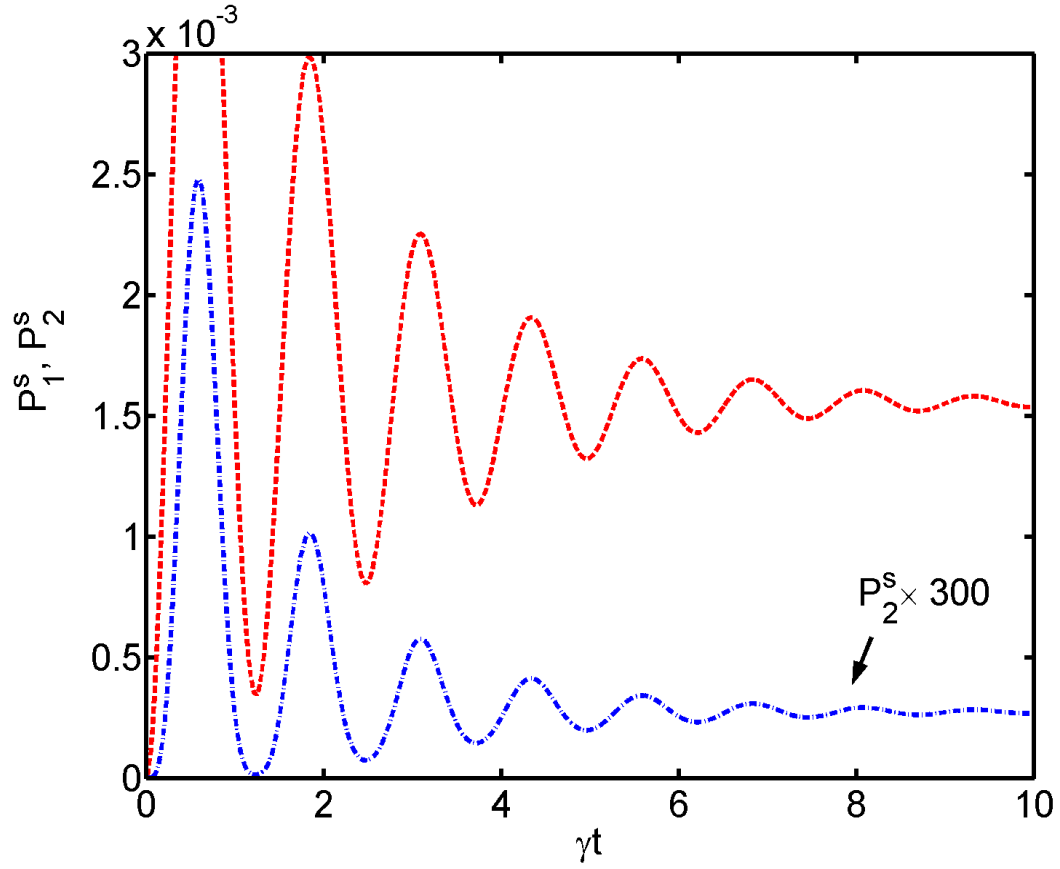


**Figure 3.2:** Time evolution of populations for symmetric states  $P_1^s$  and  $P_2^s$ . The population of the symmetric state for a single excitation is  $P_1^s$  (dashed-red), and that for the symmetric state for double excitations is  $P_2^s$  (dashed-dotted blue). The pump condition is the same as in Figure 3.1 for  $d_s = 3\lambda$ .

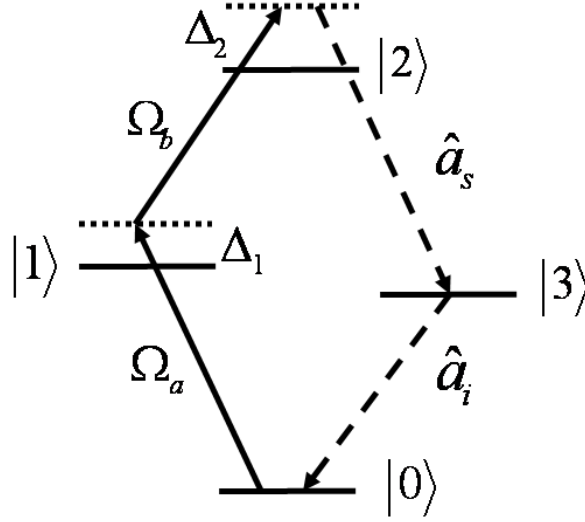


**Figure 3.3:** Four-level atomic ensemble interacting with two driving lasers (solid) with Rabi frequencies  $\Omega_a$  and  $\Omega_b$ . Signal and idler fields are labelled by  $\hat{a}_s$  and  $\hat{a}_i$ , respectively and  $\Delta_1$  and  $\Delta_2$  are one and two-photon laser detunings.

To correctly describe the frequency shifts arising from dipole-dipole interactions, we do not make the rotating wave approximation on the electric dipole interaction Hamiltonian. The frequency shift has contributions from the single atom Lamb shift and a collective frequency shift. The Lamb shift is assumed to be renormalized into the single atom transition frequency distinguishing it from the collective shift due to the atom-atom interaction.

### 3.3.1 Probability amplitudes for signal and signal-idler emissions

Writing the state-vector  $|\psi(t)\rangle$  in a basis restricted to single atomic excitations, and single pairs of signal and idler photons, we can introduce the probability amplitudes,

$$C_{s,k_i}(t) = \sum_{\mu=1}^N e^{-i\vec{k}_i \cdot \vec{r}_\mu} \langle 3_\mu, 1_{k_s, \lambda_s} | \psi(t) \rangle \quad (3.2)$$

and

$$D_{s,i}(t) = \langle 0, 1_{k_s, \lambda_s}, 1_{k_i, \lambda_i} | \psi(t) \rangle \quad (3.3)$$

defined in Appendix A. Note that  $C_{s,k_i}(t)$  is an amplitude for a phased excitation of the ensemble of atoms subsequent to signal photon emission.

After adiabatically eliminating the laser excited levels in the equations of motion, we are able to simplify and derive the amplitude  $C_{s,k_i}$  and the signal-idler (two-photon) state amplitude  $D_{s,i}$  as shown in Appendix A,

$$C_{s,k_i}(t) = g_s^* (\epsilon_{k_s, \lambda_s}^* \cdot \hat{d}_s) \sum_{\mu} e^{i\Delta\vec{k} \cdot \vec{r}_{\mu}} \int_0^t dt' e^{i(\omega_s - \omega_{23} - \Delta_2)t'} e^{(-\frac{\Gamma_3^N}{2} + i\delta\omega_i)(t-t')} b(t') \quad (3.4)$$

$$D_{s,i}(t) = g_i^* g_s^* (\epsilon_{k_i, \lambda_i}^* \cdot \hat{d}_i) (\epsilon_{k_s, \lambda_s}^* \cdot \hat{d}_s) \sum_{\mu} e^{i\Delta\vec{k} \cdot \vec{r}_{\mu}} \int_0^t \int_0^{t'} dt'' dt' e^{(-\frac{\Gamma_3^N}{2} + i\delta\omega_i)(t'-t'')} e^{i(\omega_i - \omega_3)t'} e^{i(\omega_s - \omega_{23} - \Delta_2)t''} b(t''). \quad (3.5)$$

The factor  $\sum_{\mu} e^{i\Delta\vec{k} \cdot \vec{r}_{\mu}}$  reflects phase-matching of the interaction under conditions of four-wave mixing when the wavevector mismatch  $\Delta\vec{k} = \vec{k}_a + \vec{k}_b - \vec{k}_s - \vec{k}_i \rightarrow 0$ . The radiative coupling between atoms results in the appearance of the superradiant decay constant

$$\Gamma_3^N = (N\bar{\mu} + 1)\Gamma_3 \quad (3.6)$$

where  $\Gamma_3$  is the natural decay rate of the  $|3\rangle \rightarrow |0\rangle$  transition, and  $\bar{\mu}$  is a geometrical constant depending on the shape of the atomic ensemble. An expression for the collective frequency shift  $\delta\omega_i$  is given in the Appendix A. As shown in Figure 3.4, we numerically calculate the geometrical factor  $\bar{\mu}$ , Eq.(A.12), to demonstrate how the decay factor  $N\bar{\mu} + 1$  depends on the height and radius of a cylindrical ensemble. The arrows in the figure point out the contour lines (yellow and green) of  $N\bar{\mu} + 1 \approx 4$  and 6 which are comparable to the operating conditions of the experiment [16].

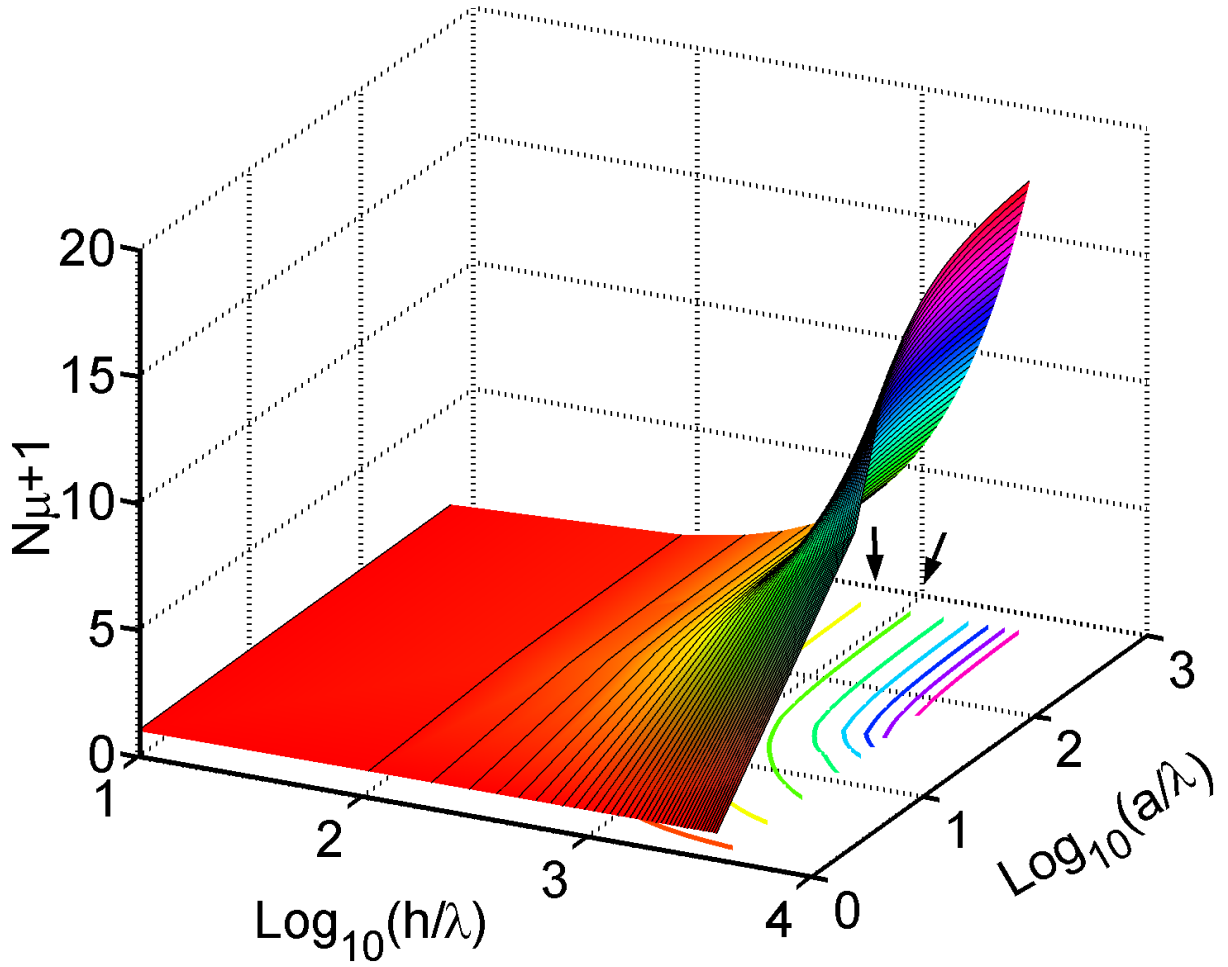


**Figure 3.4:** The superradiance decay factor  $N_{\mu}+1$  ( $\mu = \bar{\mu}$ ) for a cylindrical ensemble of length  $h$  and radius  $a$  in unit of transition wavelength  $\lambda$ . The atomic density is  $8 \times 10^{10} \text{ cm}^{-3}$  and  $\lambda = 795 \text{ nm}$  corresponding to the D1 line of  $^{85}\text{Rb}$ . See the text for the explanation of the arrows.

In the above expressions for the probability amplitudes,  $b(t) = \frac{\Omega_a(t)\Omega_b(t)}{4\Delta_1\Delta_2}$  is proportional to the product of the Rabi frequencies. We use normalized Gaussian pulses as an example where  $\Omega_a(t) = \frac{1}{\sqrt{\pi}\tau}\tilde{\Omega}_a e^{-t^2/\tau^2}$ ,  $\Omega_b(t) = \frac{1}{\sqrt{\pi}\tau}\tilde{\Omega}_b e^{-t^2/\tau^2}$ , so that the two pulses are overlapped with the same pulse width.  $\tilde{\Omega}_{a,b}$  is the pulse area, and let  $\Delta\omega_s \equiv \omega_s - \omega_{23} - \Delta_2 - \delta\omega_i$ ,  $\Delta\omega_i \equiv \omega_i - \omega_3 + \delta\omega_i$ . We have the probability amplitude for signal photon emission and atoms in a phased state,

$$\begin{aligned}
C_{s,k_i}(t, \Delta\omega_s) &= \frac{\tilde{\Omega}_a \tilde{\Omega}_b g_s^*(\epsilon_{ks,\lambda_s}^* \cdot \hat{d}_s)}{4\Delta_1\Delta_2} \sum_{\mu} e^{i\Delta\vec{k} \cdot \vec{r}_{\mu}} \frac{1}{\pi\tau^2} e^{(-\frac{\Gamma_3^N}{2} + i\delta\omega_i)t} \int_{-\infty}^t dt' e^{\frac{\Gamma_3^N}{2}t'} e^{i\Delta\omega_s t'} e^{-2t'^2/\tau^2} \\
&= \frac{\tilde{\Omega}_a \tilde{\Omega}_b g_s^*(\epsilon_{ks,\lambda_s}^* \cdot \hat{d}_s)}{4\Delta_1\Delta_2} \sum_{\mu} e^{i\Delta\vec{k} \cdot \vec{r}_{\mu}} \frac{1}{\pi\tau^2} \frac{\tau}{2} \sqrt{\frac{\pi}{2}} e^{(-\frac{\Gamma_3^N}{2} + i\delta\omega_i)t} e^{(\frac{\Gamma_3^N}{2} + i\Delta\omega_s)^2 \tau^2 / 8} \times \\
&\quad \left(1 + \operatorname{erf}\left(\frac{4t - (\frac{\Gamma_3^N}{2} + i\Delta\omega_s)\tau^2}{2\sqrt{2}\tau}\right)\right), \tag{3.7}
\end{aligned}$$

and the two-photon probability amplitude is

$$\begin{aligned}
D_{si}(t, \Delta\omega_s, \Delta\omega_i) &= \frac{\tilde{\Omega}_a \tilde{\Omega}_b g_i^* g_s^*(\epsilon_{k_i,\lambda_i}^* \cdot \hat{d}_i)(\epsilon_{ks,\lambda_s}^* \cdot \hat{d}_s)}{4\Delta_1\Delta_2} \sum_{\mu} e^{i\Delta\vec{k} \cdot \vec{r}_{\mu}} \frac{1}{\pi\tau^2} \sqrt{\frac{\pi}{2}} \frac{\tau e^{-\frac{\Gamma_3^N}{2}t}}{2(\frac{\Gamma_3^N}{2} - i\Delta\omega_i)} \left\{ \right. \\
&\quad - e^{i\Delta\omega_i t + (\frac{\Gamma_3^N}{2} + i\Delta\omega_s)^2 \tau^2 / 8} \left(1 + \operatorname{erf}\left(\frac{4t - (\frac{\Gamma_3^N}{2} + i\Delta\omega_s)\tau^2}{2\sqrt{2}\tau}\right)\right) \\
&\quad \left. + e^{-(\Delta\omega_s + \Delta\omega_i)^2 \tau^2} e^{\frac{\Gamma_3^N}{2}t} \left(1 + \operatorname{erf}\left(\frac{4t - i(\Delta\omega_s + \Delta\omega_i)\tau^2}{2\sqrt{2}\tau}\right)\right) \right\}, \tag{3.8}
\end{aligned}$$

where erf is the error function

$$\operatorname{erf}(x) = \frac{2}{\sqrt{\pi}} \int_0^x e^{-t^2} dt. \tag{3.9}$$

Asymptotically  $D_{si}$  approaches the value,

$$D_{si}(\Delta\omega_s, \Delta\omega_i) = \frac{\tilde{\Omega}_a \tilde{\Omega}_b g_i^* g_s^*(\epsilon_{k_i,\lambda_i}^* \cdot \hat{d}_i)(\epsilon_s^* \cdot \hat{d}_s)}{4\Delta_1\Delta_2} \frac{\sum_{\mu} e^{i\Delta\vec{k} \cdot \vec{r}_{\mu}}}{\sqrt{2\pi}\tau} \frac{e^{-(\Delta\omega_s + \Delta\omega_i)^2 \tau^2 / 8}}{\frac{\Gamma_3^N}{2} - i\Delta\omega_i}, \tag{3.10}$$

indicating a spectral width  $\Gamma_3^N/2$  for idler photon in a Lorentzian distribution modulating a Gaussian profile with a spectral width  $2\sqrt{2}/\tau$  for signal and idler. Energy conservation of signal and idler photons with driving fields at their central frequencies corresponds to  $\omega_s + \omega_i = \omega_a + \omega_b$ , which makes  $\Delta\omega_s + \Delta\omega_i = 0$ ; the collective frequency shifts cancel.

### 3.4 *A Correlated Two-photon State*

Using the asymptotic form of the two-photon state given in Eq. (3.10), the second-order correlation function  $G_{s,i}^{(2)}$  is calculated as [30]

$$G_{s,i}^{(2)} = \langle \psi(t \rightarrow \infty) | \hat{E}_s^-(\vec{r}_1, t_1) \hat{E}_i^-(\vec{r}_2, t_2) \hat{E}_i^+(\vec{r}_2, t_2) \hat{E}_s^+(\vec{r}_1, t_1) | \psi(t \rightarrow \infty) \rangle = |\Phi_{s,i}|^2 \quad (3.11)$$

$$\Phi_{s,i} = \langle 0 | \hat{E}_i^+(\vec{r}_2, t_2) \hat{E}_s^+(\vec{r}_1, t_1) | \psi(t \rightarrow \infty) \rangle \quad (3.12)$$

$$\hat{E}_s^+(\vec{r}_1, t_1) = \sum_{k_s, \lambda} \sqrt{\frac{\hbar\omega_s}{2\epsilon_0 V}} \hat{a}_{k_s, \lambda} \vec{\epsilon}_{k_s, \lambda_s} e^{i\vec{k}_s \cdot \vec{r}_1 - i\omega_s t_1} \quad (3.13)$$

$$\hat{E}_i^+(\vec{r}_2, t_2) = \sum_{k_i, \lambda} \sqrt{\frac{\hbar\omega_i}{2\epsilon_0 V}} \hat{a}_{k_i, \lambda} \vec{\epsilon}_{k_i, \lambda_i} e^{i\vec{k}_i \cdot \vec{r}_2 - i\omega_i t_2} \quad (3.14)$$

where  $|\psi(t \rightarrow \infty)\rangle$  denotes the state vector in the long time limit that involves the ground state and two-photon state vectors. Free electromagnetic fields, signal and idler photons, at space  $(\vec{r}_1, \vec{r}_2)$  and time  $(t_1, t_2)$  are  $\hat{E}_s^+$  and  $\hat{E}_i^+$  where  $(+)$  denotes their positive frequency part. For second order correlation function, only  $D_{si}$ , derived in the previous Section contributes to it, then we have,

$$\begin{aligned}
\Phi_{s,i} &= \sum_{k_s, \lambda_s} \sum_{k_i, \lambda_i} \frac{\omega_s}{2\epsilon_0 V} \frac{\omega_i}{2\epsilon_0 V} (\vec{d}_s \cdot \vec{\epsilon}_{k_s, \lambda_s}) \vec{\epsilon}_{k_s, \lambda_s} \times \\
& (\vec{d}_i \cdot \vec{\epsilon}_{k_i, \lambda_i}) \vec{\epsilon}_{k_i, \lambda_i} \frac{\tilde{\Omega}_a \tilde{\Omega}_b}{4\Delta_1 \Delta_2} \frac{\sum_{\mu} e^{i\Delta \vec{k} \cdot \vec{r}_{\mu}}}{\sqrt{2\pi\tau}} \frac{e^{-(\Delta\omega_s + \Delta\omega_i)^2 \tau^2 / 8}}{\frac{\Gamma_3^N}{2} - i\Delta\omega_i} e^{i\vec{k}_s \cdot \vec{r}_1 - i\omega_s t_1} e^{i\vec{k}_i \cdot \vec{r}_2 - i\omega_i t_2} \\
&= \frac{\tilde{\Omega}_a \tilde{\Omega}_b}{4\Delta_1 \Delta_2} \frac{\sum_{\mu} e^{i\Delta \vec{k} \cdot \vec{r}_{\mu}}}{\sqrt{2\pi\tau}} \frac{|\vec{d}_s| |\vec{d}_i|}{4\epsilon_0^2 c^6 (2\pi)^6} \int d\Omega_s [\hat{d}_s - \hat{k}_s (\hat{k}_s \cdot \hat{d}_s)] \\
& \int d\Omega_i [\hat{d}_i - \hat{k}_i (\hat{k}_i \cdot \hat{d}_i)] \int d\omega_i \omega_i^3 e^{-i\omega_i(t_2 - \frac{\vec{r}_2 \cdot \hat{k}_i}{c})} \frac{(\omega_{23} - \Delta\omega_i)^3}{\frac{\Gamma_3^N}{2} - i\Delta\omega_i} e^{-i(\omega_{23} + \Delta_2)(t_1 - \frac{\vec{r}_1 \cdot \hat{k}_s}{c})} \\
& e^{i(\Delta\omega_i - \delta\omega_i)(t_1 - \frac{\vec{r}_1 \cdot \hat{k}_s}{c})} \int d\Delta\omega_s e^{-i\Delta\omega_s(t_1 - \frac{\vec{r}_1 \cdot \hat{k}_s}{c})} e^{-\Delta\omega_s^2 \tau^2 / 8} \tag{3.15}
\end{aligned}$$

where we have used the change of variables in the first step, replaced  $\omega_s = \omega_{23} + \Delta_2 + \Delta\omega_s + \delta\omega_i$ , and changed the variable  $\Delta\omega_s \rightarrow \Delta\omega_s - \Delta\omega_i$ . Solid angle integration is denoted as  $d\Omega_{s,i}$  for signal (idler) photon. The divergent part of  $\omega_s^3$  (which varies relatively slowly) has been moved out from the integral of  $d\Delta\omega_s$ , and we replace  $\omega_s$  with the signal transition frequency  $\omega_{23}$ . We then have

$$\begin{aligned}
\Phi_{s,i} &= \frac{\tilde{\Omega}_a \tilde{\Omega}_b}{4\Delta_1 \Delta_2} \frac{\sum_{\mu} e^{i\Delta \vec{k} \cdot \vec{r}_{\mu}}}{\sqrt{2\pi\tau}} \frac{|\vec{d}_s| |\vec{d}_i| \omega_3^3 \omega_{23}^3}{4\epsilon_0^2 c^6 (2\pi)^6} \int d\Omega_s d\Omega_i [\hat{d}_s - \hat{k}_s (\hat{k}_s \cdot \hat{d}_s)] [\hat{d}_i - \hat{k}_i (\hat{k}_i \cdot \hat{d}_i)] \\
& \frac{2\sqrt{2\pi}}{\tau} \int d\Delta\omega_i \frac{e^{-i\Delta\omega_i(t_2 - \frac{\vec{r}_2 \cdot \hat{k}_i}{c} - t_1 + \frac{\vec{r}_1 \cdot \hat{k}_s}{c})}}{(\frac{\Gamma_3^N}{2} - i\Delta\omega_i - i\delta\omega_i)} e^{-i(\omega_{23} + \Delta_2)(t_1 - \frac{\vec{r}_1 \cdot \hat{k}_s}{c})} e^{-i\omega_3(t_2 - \frac{\vec{r}_2 \cdot \hat{k}_i}{c})} e^{-2(t_1 - \frac{\vec{r}_1 \cdot \hat{k}_s}{c})^2 / \tau^2} \tag{3.16}
\end{aligned}$$

where we replace  $\omega_i = \omega_3 + \Delta\omega_i - \delta\omega_i$  and change the variable  $\Delta\omega_i \rightarrow \Delta\omega_i + \delta\omega_i$ . The divergent part of  $\omega_i^3$  is again moved out from the integral of  $d\Delta\omega_i$  and replace  $\omega_i$  with the signal transition frequency  $\omega_3$ . Finally we have

$$\begin{aligned}
\Phi_{s,i} &= \frac{\tilde{\Omega}_a \tilde{\Omega}_b}{4\Delta_1 \Delta_2} \frac{|\vec{d}_s| |\vec{d}_i| \omega_3^3 \omega_{23}^3}{2\epsilon_0^2 c^6 \tau^2 (2\pi)^6} \sum_{\mu} e^{i\Delta \vec{k} \cdot \vec{r}_{\mu}} \int d\Omega_s d\Omega_i [\hat{d}_s - \hat{k}_s (\hat{k}_s \cdot \hat{d}_s)] [\hat{d}_i - \hat{k}_i (\hat{k}_i \cdot \hat{d}_i)] \\
&e^{-2(t_1 - \frac{\vec{r}_1 \cdot \hat{k}_s}{c})^2 / \tau^2} e^{-i(\omega_{23} + \Delta_2)(t_1 - \frac{\vec{r}_1 \cdot \hat{k}_s}{c})} e^{-i\omega_3(t_2 - \frac{\vec{r}_2 \cdot \hat{k}_i}{c})} e^{(-\frac{\Gamma_3^N}{2} + i\delta\omega_i)(t_2 - \frac{\vec{r}_2 \cdot \hat{k}_i}{c} - t_1 + \frac{\vec{r}_1 \cdot \hat{k}_s}{c})} \\
&\Theta(t_2 - \frac{\vec{r}_2 \cdot \hat{k}_i}{c} - t_1 + \frac{\vec{r}_1 \cdot \hat{k}_s}{c})
\end{aligned} \tag{3.17}$$

where the complex integral with the pole at  $\Delta\omega_i = -i\frac{\Gamma_3^N}{2} - \delta\omega_i$  in the lower half plane leads to a step function  $\Theta$  that shows the causal connection between signal and idler emission. The emission time for the signal field ( $t_1 - \frac{\vec{r}_1 \cdot \hat{k}_s}{c}$ ) is within the pulse envelope of width  $\tau$ , and the idler photon decays with a superradiant constant  $\Gamma_3^N/2$ . Note that the collective frequency shift  $\delta\omega_i$  appears in the signal ( $\omega_{23} + \Delta_2 + \delta\omega_i$ ) and idler ( $\omega_3 - \delta\omega_i$ ) frequency consistent with energy conservation. Let  $\Delta t_s \equiv t_1 - \frac{\vec{r}_1 \cdot \hat{k}_s}{c}$  and  $\Delta t_i \equiv t_2 - \frac{\vec{r}_2 \cdot \hat{k}_i}{c}$ , we then have

$$\begin{aligned}
&|\Phi_{s,i}(\Delta t_s, \Delta t_i)| \\
&= \frac{\tilde{\Omega}_a \tilde{\Omega}_b}{4\Delta_1 \Delta_2} \frac{|\vec{d}_s| |\vec{d}_i| \omega_3^3 \omega_{23}^3}{2\epsilon_0^2 c^6 \tau^2 (2\pi)^6} \sum_{\mu} e^{i\Delta \vec{k} \cdot \vec{r}_{\mu}} \int d\Omega_s d\Omega_i [\hat{d}_s - \hat{k}_s (\hat{k}_s \cdot \hat{d}_s)] [\hat{d}_i - \hat{k}_i (\hat{k}_i \cdot \hat{d}_i)] \\
&e^{-2(\Delta t_s)^2 / \tau^2} e^{-\frac{\Gamma_3^N}{2}(\Delta t_i - \Delta t_s)} \Theta(\Delta t_i - \Delta t_s).
\end{aligned} \tag{3.18}$$

If we let  $\Delta t \equiv \Delta t_i - \Delta t_s$  and choose  $\Delta t_s = 0$  as the origin in time (idler gating time), then we have the second-order correlation function

$$G_{s,i}^{(2)}(\Delta t) = |\Phi_{s,i}(\Delta t)|^2 \propto e^{-\Gamma_3^N \Delta t} \text{ where } \Delta t \geq 0. \tag{3.19}$$

It resembles the result for the second-order correlation function in the case of single atom, whereas here we have an enhanced decay rate due to the atomic dipole-dipole interaction.



In Figure 3.5, we plot out the absolute value of spectrum  $D_{si}(\Delta\omega_s, \Delta\omega_i)$  and the second-order correlation function  $G_{s,i}^{(2)}(\Delta t_s, \Delta t_i)$ . In (c), we show for  $\Gamma_3 \Delta t_i = 0.2$ . The width of  $1/\Delta t_i = 5\Gamma_3$  corresponds to  $\Gamma_3^N = (N\bar{\mu} + 1)\Gamma_3 = 5\Gamma_3$ .

### 3.5 *Schmidt Decomposition*

Correlated photon pairs may be generated by parametric down conversion (PDC) [65, 66, 67]. The degree of entanglement can be quantified by Schmidt mode decomposition [68, 69], allowing the influence of group-velocity matching [70] to be assessed. A pure single photon source is a basis element for quantum computation by linear optics (LOQC) [71], and it can be conditionally generated by measurement [72]. A similar approach can be applied to the study of the transverse degrees of freedom in type-II PDC [73] and PDC in a distributed microcavity [74]. In photonic-crystal fiber (PCF), a factorizable photon pair can be generated by spectral engineering [75]. The spectral effect has been discussed in relation to a quantum teleportation protocol [76] as a first step toward quantum communication.

We would like to perform an analysis of entanglement properties of our cascade emission source. In addition to polarization entanglement, a characterization of frequency space entanglement is required to clarify its suitability in, for example, the DLCZ protocol [6].

In the long time limit, the state function is given by, Eq. (3.10),

$$|\psi\rangle = |0, \text{vac}\rangle + \sum_{s,i} D_{s,i} |0, 1_{\vec{k}_s, \lambda_s}, 1_{\vec{k}_i, \lambda_i}\rangle \quad (3.20)$$

where  $s = (k_s, \lambda_s)$ ,  $i = (k_i, \lambda_i)$ , and  $|0, \text{vac}\rangle$  is the joint atomic ground and photon vacuum state.

The spatial correlation of two-photon state in FWM condition can be eliminated by pinholes or by coupling to single mode fiber so we consider only the continuous frequency space. For some specific polarizations  $\lambda_s$  and  $\lambda_i$ , we have the state vector

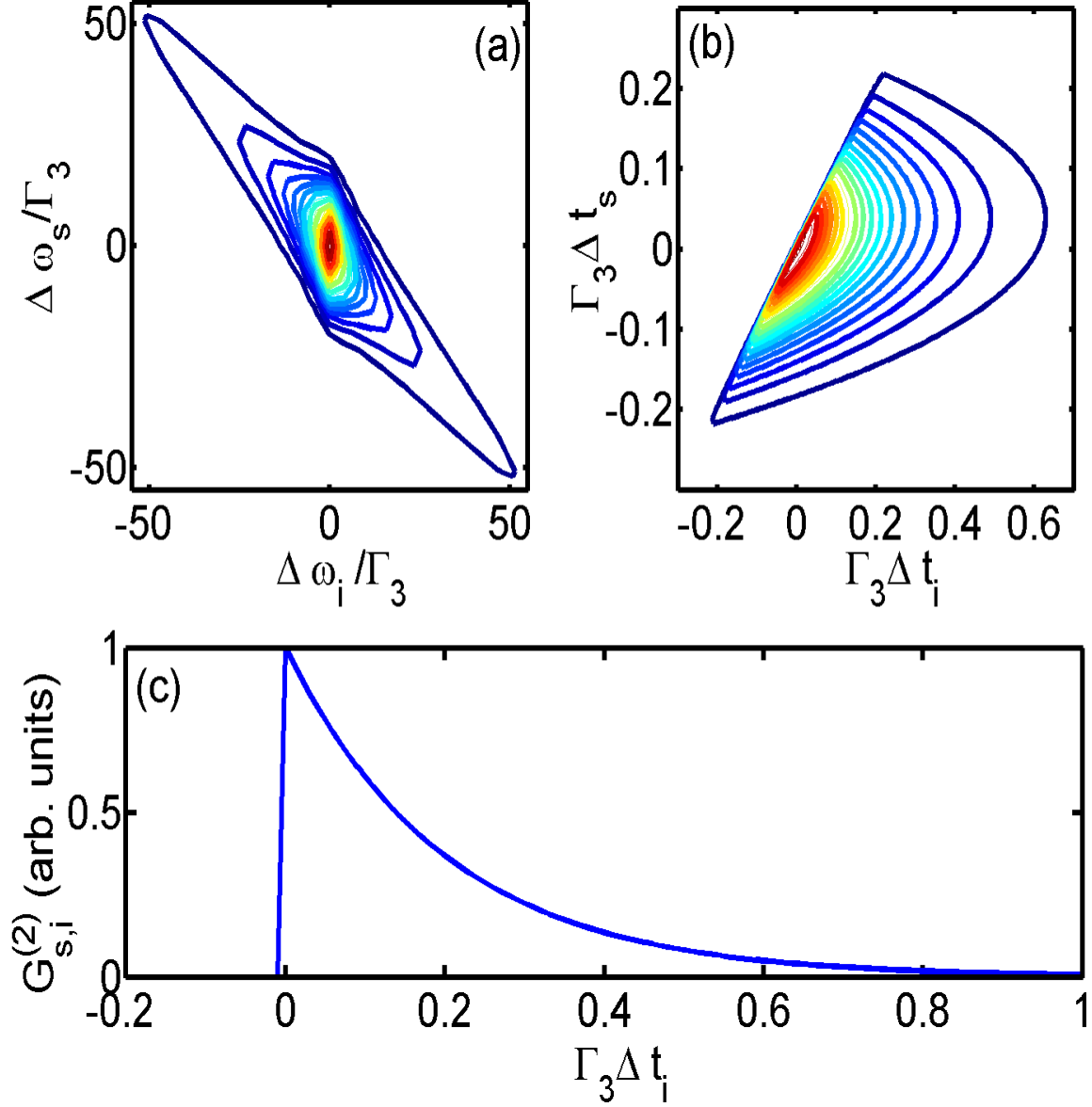


**Figure 3.5:** (a) Absolute value of the spectrum for two-photon state probability amplitude  $D_{s,i}$  and (b) the second-order correlation function  $G_{s,i}^{(2)}(\Delta t_s, \Delta t_i)$ . (c) A normalized  $G_{s,i}^{(2)}(\Delta t_s = 0, \Delta t_i)$  with  $\Gamma_3 \tau = 0.2$ . The exponential decay corresponds to the superradiant decay factor  $N\bar{\mu} + 1 = 5$ .

$|\Psi\rangle$ ,

$$|\Psi\rangle = \int f(\omega_s, \omega_i) \hat{a}_{\lambda_s}^\dagger(\omega_s) \hat{a}_{\lambda_i}^\dagger(\omega_i) |0\rangle d\omega_s d\omega_i, \quad (3.21)$$

where

$$f(\omega_s, \omega_i) = \frac{e^{-(\Delta\omega_s + \Delta\omega_i)^2 \tau^2 / 8}}{\frac{\Gamma_3^N}{2} - i\Delta\omega_i}. \quad (3.22)$$

The quantification of entanglement can be determined in the Schmidt basis where the state vector is expressed as

$$|\Psi\rangle = \sum_n \sqrt{\lambda_n} \hat{b}_n^\dagger \hat{c}_n^\dagger |0\rangle, \quad (3.23)$$

$$\hat{b}_n^\dagger \equiv \int \psi_n(\omega_s) \hat{a}_{\lambda_s}^\dagger(\omega_s) d\omega_s, \quad (3.24)$$

$$\hat{c}_n^\dagger \equiv \int \phi_n(\omega_i) \hat{a}_{\lambda_i}^\dagger(\omega_i) d\omega_i, \quad (3.25)$$

where  $\hat{b}_n^\dagger, \hat{c}_n^\dagger$  are effective creation operators. Eigenvalues  $\lambda_n$ , and eigenfunctions  $\psi_n$  and  $\phi_n$ , are the solutions of the eigenvalue equations,

$$\int K_1(\omega, \omega') \psi_n(\omega') d\omega' = \lambda_n \psi_n(\omega), \quad (3.26)$$

$$\int K_2(\omega, \omega') \phi_n(\omega') d\omega' = \lambda_n \phi_n(\omega), \quad (3.27)$$

where  $K_1(\omega, \omega') \equiv \int f(\omega, \omega_1) f^*(\omega', \omega_1) d\omega_1$  and  $K_2(\omega, \omega') \equiv \int f(\omega_2, \omega) f^*(\omega_2, \omega') d\omega_2$  are the kernels for the one-photon spectral correlations [68, 69]. Orthogonality of eigenfunctions is  $\int \psi_i(\omega) \psi_j(\omega) d\omega = \delta_{ij}$ ,  $\int \phi_i(\omega) \phi_j(\omega) d\omega = \delta_{ij}$ , and the normalization of quantum state requires  $\sum_n \lambda_n = 1$ .

In the Schmidt basis, the von Neumann entropy may be written

$$S = - \sum_{n=1}^{\infty} \lambda_n \ln \lambda_n. \quad (3.28)$$

If there is only one non-zero Schmidt number  $\lambda_1 = 1$ , the entropy is zero, which means no entanglement and a factorizable state. For more than one non-zero Schmidt number, the entropy is larger than zero and bipartite entanglement is present.

The kernel in Eq. (3.22) has all the frequency entanglement information, entanglement means  $f(\omega_s, \omega_i)$  cannot be factorized in the form  $g(\omega_s)h(\omega_i)$ , a multiplication of two separate spectral functions. By inspection the Gaussian profile of signal and idler emission is a source of correlation. The joint spectrum  $\Delta\omega_s + \Delta\omega_i$  is confined within the width of order of  $1/\tau$ . The Lorentzian factor associated with the idler emission has a width governed by the superradiant decay rate.

In Figure 3.6, we show the Schmidt decomposition of the spectrum. We use a moderate superradiant decay constant  $N\bar{\mu} + 1 = 5$ , comparable to the reference [16], and a nanosecond pulse duration  $\tau = 0.25$  ( $\approx 26/4$  ns), and  $\Gamma_3/2\pi = 6$  MHz. Due to slow convergence associated with the Lorentzian profile, we use a frequency range up to  $\pm 1200$  (in unit of  $\Gamma_3$ ) with  $2000 \times 2000$  grid. The numerical error in the eigenvalue calculation is estimated to be about 1% error. In this case, the largest Schmidt number is 0.8 and corresponding signal mode function has a FWHM Gaussian profile  $4\sqrt{2 \ln(2)}/\tau \approx 19\Gamma_3$ . The idler mode function  $\phi_1$  reflects the Lorentzian profile in the spectrum at the signal peak frequency ( $\Delta\omega_s = 0$ ),

$$f(\Delta\omega_s = 0, \Delta\omega_i) = \frac{e^{-\Delta\omega_i^2 \tau^2 / 8}}{(N\bar{\mu} + 1)\Gamma_3/2 - i\Delta\omega_i} \quad (3.29)$$

where a relatively broad Gaussian distribution is overlapped with a narrow spread of superradiant decay rate  $[\text{FWHM} > (N\bar{\mu} + 1)\Gamma_3/2]$ .

Figure 3.7 shows that the cascade emission source is more entangled if the superradiant decay constant, or the pulse duration increases. We note that the Gaussian profile aligns the spectrum along the axis  $\Delta\omega_s = -\Delta\omega_i$  and the spectral width for signal photon at the center of the idler frequency distribution ( $\Delta\omega_i = 0$ ) is determined by pulse duration  $\tau$ . For a shorter pulse  $\tau^{-1} > (N\bar{\mu} + 1)\Gamma_3/2$ , the joint Gaussian profile

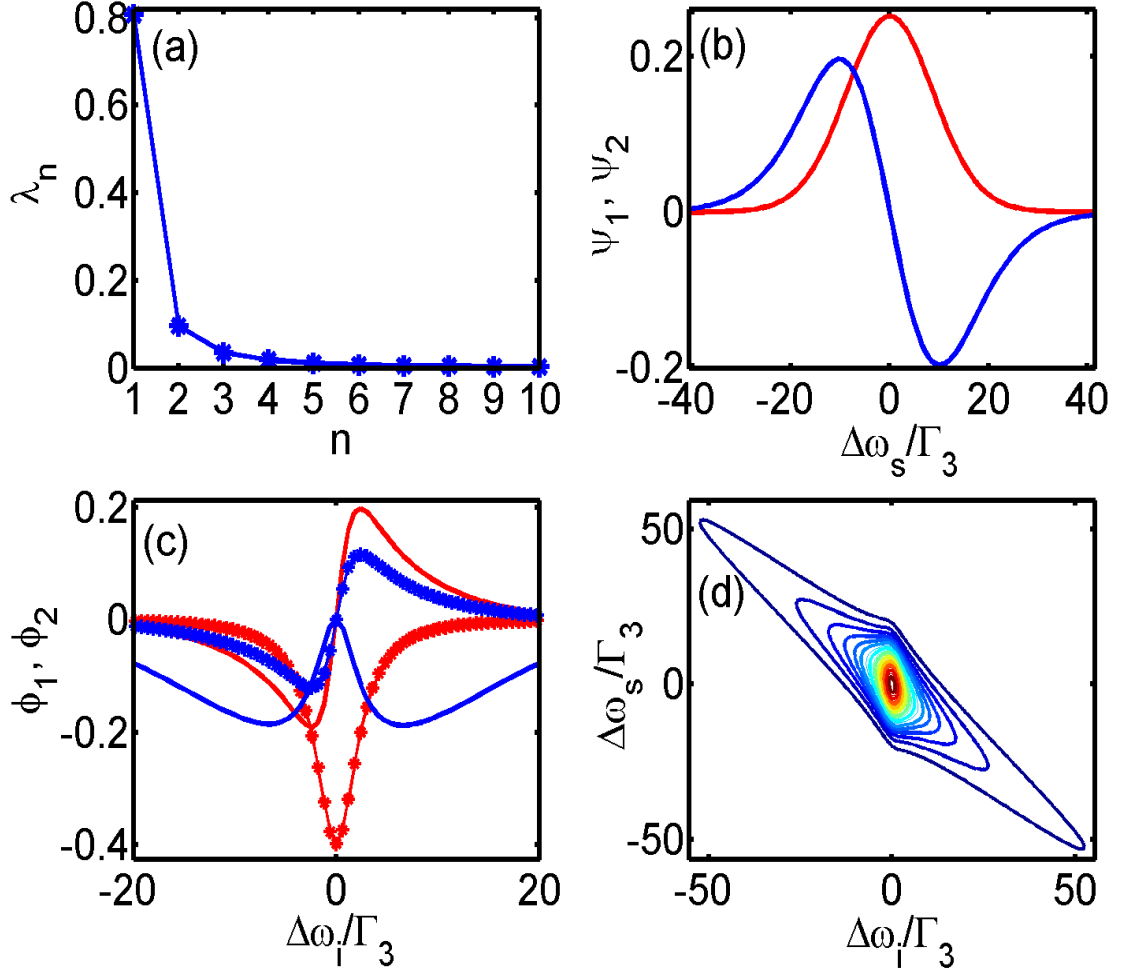


**Figure 3.6:** Schmidt mode analysis with pulse width  $\tau = 0.25$  and superradiance decay factor  $N\bar{\mu} + 1 = 5$ . (a) Schmidt number and (b) signal mode functions:  $\text{Re}[\psi_1]$  (solid-red) and  $\text{Re}[\psi_2]$  (solid-blue). Imaginary parts are not shown, then are zero. (c) Real (solid) and imaginary (dotted) parts of first (red) and second (blue) idler mode functions,  $\phi_1$  and  $\phi_2$ . (d) The absolute spectrum  $|f(\Delta\omega_s, \Delta\omega_i)|$ .

has a larger width, and the spectrum is cut off by the Lorentzian idler distribution. A larger width leads to a less entangled source and distributes the spectral weight mainly along the crossed axes  $\Delta\omega_s = 0$  and  $\Delta\omega_i = 0$ . A narrow Lorentzian profile cuts off the entanglement source term  $e^{-(\Delta\omega_s + \Delta\omega_i)^2 \tau^2 / 8}$  tilting the spectrum along the line  $\Delta\omega_s + \Delta\omega_i = 0$ . In the opposite limit,  $\tau^{-1} < (N\bar{\mu} + 1)\Gamma_3/2$ , the spectrum is highly entangled corresponding to tight alignment along the axis  $\Delta\omega_s = -\Delta\omega_i$  (Figure 3.7 (c)).

Note that the short pulse duration ( $\tau \geq 0.25$  (6.5 ns)) should not violate the assumption of adiabaticity  $\tau \gtrsim 1/\Delta_1$  or  $1/\Delta_2$ .

The Schmidt analysis and calculation of von Neumann entropy shows that signal-idler fields are more entangled if the ensemble is more optically dense, corresponding to stronger superradiance. For the DLCZ protocol, we wish to avoid frequency entanglement. The superradiance may be reduced with smaller atomic densities but good qubit storage and retrieval efficiency require a moderate optical thickness [16]. A better approach involves using short pulse excitation  $\tau^{-1} > (N\bar{\mu} + 1)\Gamma_3$ . We will investigate the spectral properties in more details for the DLCZ scheme in Chapter 5.

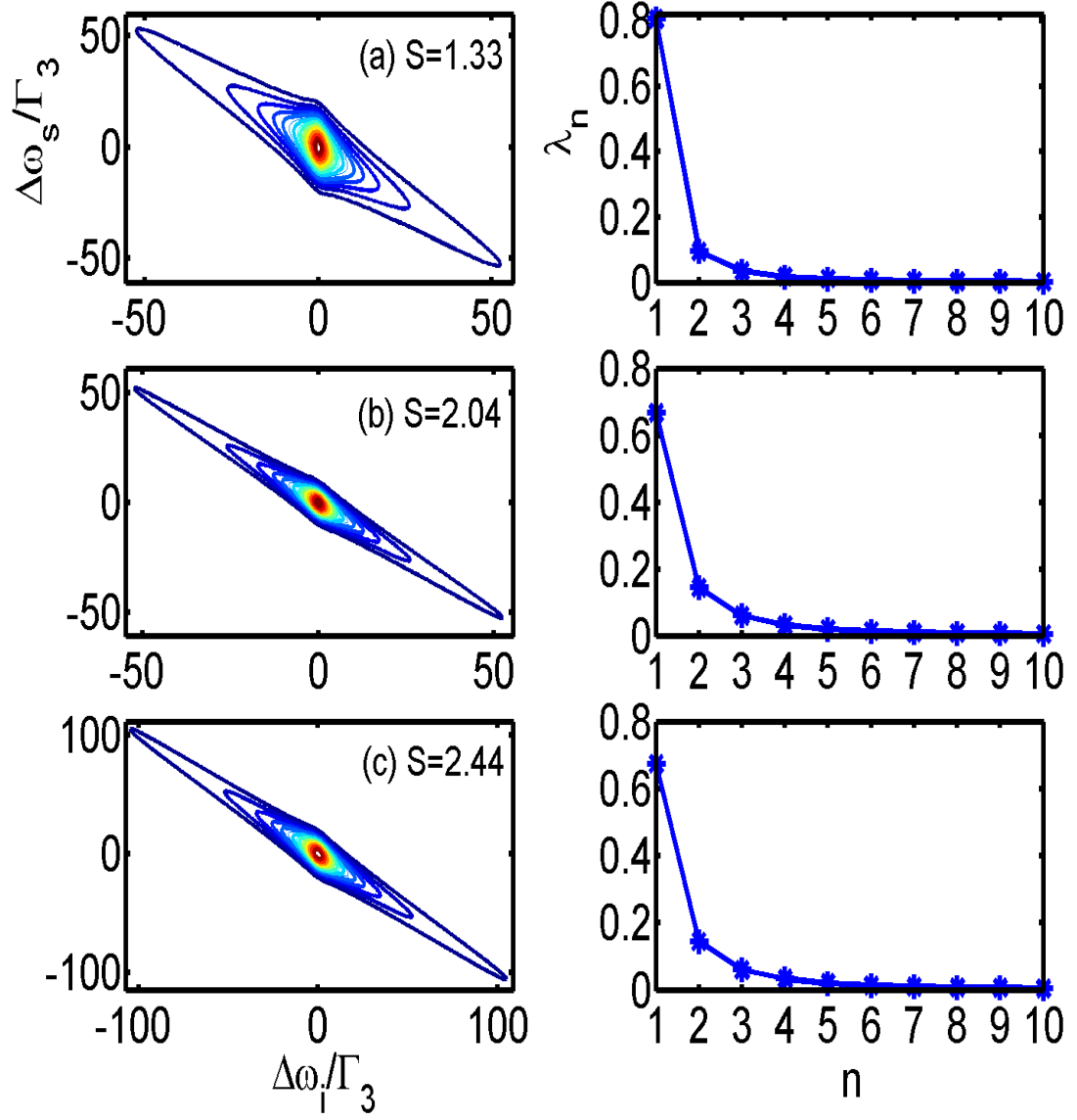


**Figure 3.7:** Absolute spectrum of two-photon state and the eigenvalues of Schmidt decomposition.  $N\bar{\mu} + 1 = 5$  for both (a)  $\tau = 0.25$  (b)  $\tau = 0.5$ .  $N\bar{\mu} + 1 = 10$  for (c)  $\tau = 0.25$ . The von Neumann entropy ( $S$ ) is indicated in the plots.





# CHAPTER IV

## SUPERRADIANT EMISSION FROM A CASCADE ATOMIC ENSEMBLE: NUMERICAL APPROACH

In this Chapter, we investigate the cascade emission (signal and idler) from an atomic ensemble using a numerical approach. In Chapter 3, we studied the correlated emission using Schrödinger's equation assuming single atomic excitations. To relax the assumption of single atomic excitations, we derive a set of c-number stochastic differential equations derived using the quantum statistical methods reviewed in Chapter 2. We solve numerically for the dynamics of the atoms and counter-propagating signal and idler fields. The signal and idler field intensities are calculated, and the signal-idler correlation function is studied for different optical depths of the atomic ensemble, and compared with the analytical results of Chapter 3.

### ***4.1 Introduction***

To account for multiple atomic excitations in the signal-idler emission from a cascade atomic ensemble, the Schrödinger's equation approach becomes cumbersome. An alternative theory based on c-number Langevin equations as discussed in Chapter 2, is suitable for solution by stochastic simulations. An essential element in the stochastic simulations is a proper characterization of the Langevin noises. These represent the quantum fluctuations responsible for the initiation of the spontaneous emission from the inverted [44, 77, 78, 79], or pumped atomic system [81, 80] as in our case.

The positive-P phase space method [32, 29, 83, 85, 84, 82, 86] is employed to derive the Fokker-Planck equations that lead directly to the c-number Langevin equations. The classical noise correlation functions, equivalently diffusion coefficients, are alternatively confirmed by use of the Einstein relations reviewed in Chapter 2. The c-number Langevin equations correspond to Ito-type stochastic differential equations that may be simulated numerically. The noise correlations can be represented either by using a square [87] or a non-square "square root" diffusion matrix [84]. The approach enables us to calculate normally-ordered quantities, signal-idler field intensities, and the second-order correlation function. The numerical approach involves a semi-implicit difference algorithm and shooting method [88] to integrate the stochastic "Maxwell-Bloch" equations.

Recently a new positive-P phase space method involving a stochastic gauge function [89] has been developed. This approach has an improved treatment of sampling errors and boundary errors in the treatment of quantum anharmonic oscillators [90, 91]. It has also been applied to a many-body system of bosons [92] and fermions [93]. In this Chapter, we follow the traditional positive-P representation method [94].

## 4.2 *Theory of Cascade emission*

The complete derivation of the c-number Langevin equations for cascade emission from the four-level atomic ensemble is described in detail in Appendix B. After setting up the Hamiltonian, we follow the standard procedure to construct the characteristic functions [27] in Appendix B.2 using the positive-P representation [32]. In Appendix B.3.1, the Fokker-Planck equation is found by directly Fourier transforming the characteristic functions, and making a  $1/N_z$  expansion.

Finally the Ito stochastic differential equations are written down from inspection of the first-order derivative (drift term) and second-order derivative (diffusion term) in

the Fokker-Planck equation. The equations are then written in dimensionless form by introducing the Arecchi-Courtens cooperation units [115] in Appendix B.3.2. From Eq. (B.73) and the field equations that follow, these c-number Langevin equations in a co-moving frame are,

$$\begin{aligned}
\frac{\partial}{\partial \tau} \pi_{01} &= (i\Delta_1 - \frac{\gamma_{01}}{2})\pi_{01} + i\Omega_a(\pi_{00} - \pi_{11}) + i\Omega_b^* \pi_{02} - i\pi_{13}^\dagger E_i^+ + \mathcal{F}_{01} \text{ (I)}, \\
\frac{\partial}{\partial \tau} \pi_{12} &= i(\Delta_2 - \Delta_1 + i\frac{\gamma_{01} + \gamma_2}{2})\pi_{12} - i\Omega_a^* \pi_{02} + i\Omega_b(\pi_{11} - \pi_{22}) + i\pi_{13} E_s^+ e^{-i\Delta k z} \\
&\quad + \mathcal{F}_{12}, \\
\frac{\partial}{\partial \tau} \pi_{02} &= (i\Delta_2 - \frac{\gamma_2}{2})\pi_{02} - i\Omega_a \pi_{12} + i\Omega_b \pi_{01} + i\pi_{03} E_s^+ e^{-i\Delta k z} - i\pi_{32} E_i^+ + \mathcal{F}_{02}, \\
\frac{\partial}{\partial \tau} \pi_{11} &= -\gamma_{01} \pi_{11} + \gamma_{12} \pi_{22} + i\Omega_a \pi_{01}^\dagger - i\Omega_a^* \pi_{01} - i\Omega_b \pi_{12}^\dagger + i\Omega_b^* \pi_{12} + \mathcal{F}_{11}, \\
\frac{\partial}{\partial \tau} \pi_{22} &= -\gamma_2 \pi_{22} + i\Omega_b \pi_{12}^\dagger - i\Omega_b^* \pi_{12} + i\pi_{32}^\dagger E_s^+ e^{-i\Delta k z} - i\pi_{32} E_s^- e^{i\Delta k z} + \mathcal{F}_{22}, \\
\frac{\partial}{\partial \tau} \pi_{33} &= -\gamma_{03} \pi_{33} + \gamma_{32} \pi_{22} - i\pi_{32}^\dagger E_s^+ e^{-i\Delta k z} + i\pi_{32} E_s^- e^{i\Delta k z} + i\pi_{03}^\dagger E_i^+ - i\pi_{03} E_i^- \\
&\quad + \mathcal{F}_{33}, \\
\frac{\partial}{\partial \tau} \pi_{13} &= -(i\Delta_1 + \frac{\gamma_{01} + \gamma_{03}}{2})\pi_{13} - i\Omega_a^* \pi_{03} - i\Omega_b \pi_{32}^\dagger + i\pi_{12} E_s^- e^{i\Delta k z} + i\pi_{01}^\dagger E_i^+ \\
&\quad + \mathcal{F}_{13}, \\
\frac{\partial}{\partial \tau} \pi_{03} &= -\frac{\gamma_{03}}{2} \pi_{03} - i\Omega_a \pi_{13} + i\pi_{02} E_s^- e^{i\Delta k z} + i(\pi_{00} - \pi_{33}) E_i^+ + \mathcal{F}_{03}, \\
\frac{\partial}{\partial \tau} \pi_{32} &= i\Delta_2 - \frac{\gamma_{03} + \gamma_2}{2} \pi_{32} + i\Omega_b \pi_{13}^\dagger - i(\pi_{22} - \pi_{33}) E_s^+ e^{-i\Delta k z} - i\pi_{02} E_i^- + \mathcal{F}_{32}, \\
\frac{\partial}{\partial z} E_s^+ &= -i\pi_{32} e^{i\Delta k z} \frac{|g_s|^2}{|g_i|^2} - \mathcal{F}_s, \quad \frac{\partial}{\partial z} E_i^+ = i\pi_{03} + \mathcal{F}_i,
\end{aligned} \tag{4.1}$$

where (I) stands for Ito type SDE.  $\pi_{ij}$  is the stochastic variable that corresponds to the atomic populations of state  $|i\rangle$  when  $i = j$  and to atomic coherence when  $i \neq j$ , and  $\mathcal{F}_{ij}$  are c-number Langevin noises. The remaining equations of motion, which close the set, can be found by replacing the above classical variables,  $\pi_{jk}^* \rightarrow \pi_{jk}^\dagger$ ,  $(\pi_{jk}^\dagger)^* \rightarrow \pi_{jk}$ ,  $(E_{s,i}^+)^* \rightarrow E_{s,i}^-$ ,  $(E_{s,i}^-)^* \rightarrow E_{s,i}^+$ , and  $\mathcal{F}_{jk}^* \rightarrow \mathcal{F}_{jk}^\dagger$ . Note that the atomic

populations satisfy  $\pi_{jj}^* = \pi_{jj}$ . The superscripts, dagger ( $\dagger$ ) for atomic variables and ( $-$ ) for field variables, denote the independent variables, which is a feature of the positive-P representation: there are double dimension spaces for each variable. These variables are complex conjugate to each other when ensemble averages are taken, for example  $\langle \pi_{jk} \rangle = \langle \pi_{jk}^\dagger \rangle^*$  and  $\langle E_{s,i}^+ \rangle = \langle E_{s,i}^- \rangle^*$ . The doubled spaces allow the variables to explore trajectories outside the classical phase space.

Before going further to discuss the numerical solution of the SDE, we point out that the diffusion matrix elements have been computed using Fokker-Planck equations and by the Einstein relations described in Appendix B.3.3. This provides the important check on the lengthy derivations of the diffusion matrix elements we need for the simulations.

The next step is to find expressions for the Langevin noises, and the details are given in Appendix B.3.4 in terms of a non-square matrix  $B$  [35, 84]. The matrix  $B$  is used to construct the symmetric diffusion matrix  $D(\alpha) = B(\alpha)B^T(\alpha)$  for a Ito SDE,

$$dx_t^i = A_i(t, \vec{x}_t)dt + \sum_j B_{ij}(t, \vec{x}_t)dW_t^j(t) \quad (\text{I}) \quad (4.2)$$

where  $\xi_i dt = dW_t^i(t)$  (Wiener process) and  $\langle \xi_i(t)\xi_j(t') \rangle = \delta_{ij}\delta(t-t')$ . Note that  $B \rightarrow BS$ , where  $S$  is an orthogonal matrix ( $SS^T = I$ ), leaves  $D$  unchanged, so  $B$  is not unique. We could also construct a square matrix representation  $B$  [32, 28, 87]. This involves a procedure of matrix decomposition into a product of lower and upper triangular matrix factors. A Cholesky decomposition can be used to determine the  $B$  matrix elements successively row by row. The downside of this procedure is that the  $B$  matrix elements must be differentiated in converting the Ito SDE to its equivalent Stratonovich form for numerical solution.

The Stratonovich SDE is necessary for the stability and the convergence of semi-implicit methods. Because of the analytic difficulties in transforming to the Stratonovich

form, we use instead the non-square form of  $B$  [84] that is shown explicitly in Appendix B.3.4.

In this case a typical  $B$  matrix element is a sum of terms, each one of which is a product of the square root of a diffusion matrix element with a unit strength real (if the diffusion matrix element is diagonal) or complex (if the diffusion matrix element is off-diagonal) Gaussian unit white noise. It is straightforward to check that a  $B$  matrix constructed in this way reproduces the required diffusion matrix  $D = BB^T$ .

As pointed out in the reference [86], the transverse dipole-dipole interaction can be neglected and nonparaxial spontaneous decay rate can be accounted for by a single atom decay rate one if the atomic density is not too high. We are interested here in conditions where the ensemble length  $L$  is significant and propagation effects are non-negligible, and the average distance between atoms  $d = \sqrt[3]{V/N}$  is larger than the transition wavelength  $\lambda$ . The length scales satisfy  $\lambda \lesssim d \ll L$ , and we consider a pencil-like cylindrical atomic ensemble. The paraxial or one-dimensional assumption for field propagation is then valid, and the transverse dipole-dipole interaction is not important for the atomic density we focus here.

### 4.3 Numerical Simulation

In this Section, we discuss the numerical integration of the atomic and field equations derived given in the last Section.

There are several possible ways to integrate the differential equation numerically. Three main categories of algorithm used are forward (explicit), backward (implicit), and mid-point (semi-implicit) methods [88]. The midpoint method is in a sense between the explicit and implicit methods, and we will use an algorithm of this type in the following. Let  $t_m = t_n + \frac{\Delta t}{2}$  for  $n$ th segment and iterate (m denotes mid point)

$$x(t_m) = x(t_n) + f[t_m, x(t_m)] \frac{\Delta t}{2} \quad (4.3)$$

until convergence is reached. Then step forward with  $x(t_{n+1}) = 2x(t_m) - x(t_n)$ .

The forward difference method, which Euler or Runge-Kutta methods utilizes, is not guaranteed to converge in stochastic integrations [37]. There it is shown that the semi-implicit method [95] is more robust in Stratonovich type SDE simulations [36]. More extensive studies of the stability and convergence of SDE can be found in the reference [96]. The Stratonovich type SDE equivalent to the Ito type equation (4.2), is

$$\begin{aligned} dx_t^i = & [A_i(t, \vec{x}_t) - \frac{1}{2} \sum_j \sum_k B_{jk}(t, \vec{x}_t) \frac{\partial}{\partial x^j} B_{ik}(t, \vec{x}_t)] dt \\ & + \sum_j B_{ij}(t, \vec{x}_t) dW_t^j \quad (\text{Stratonovich}), \end{aligned} \quad (4.4)$$

which has the same diffusion terms  $B_{ij}$ , but with modified drift terms. This "correction" term arises from the different definitions of stochastic integral in the Ito and Stratonovich calculus.

At the end of Appendix B 3.3, we derive the Stratonovich SDE with the (underlined) "correction" terms noted above. We then have 19 classical variables including atomic populations, coherences, and two counter-propagating cascade fields. With 64 diffusion matrix elements and an associated 117 random numbers required to represent the instantaneous Langevin noises, we are ready to solve the equations numerically using the robust midpoint difference method.

#### 4.3.1 Shooting and secant method

The problem we encounter here involves counter-propagating field equations in the space dimension and initial value type atomic equations in the time dimension. The initial value problem is addressed by the difference method discussed in the previous Section.

The counter-propagating field equations have a boundary condition specified at each end of the medium. This is a two-point boundary value problem, and a numerical

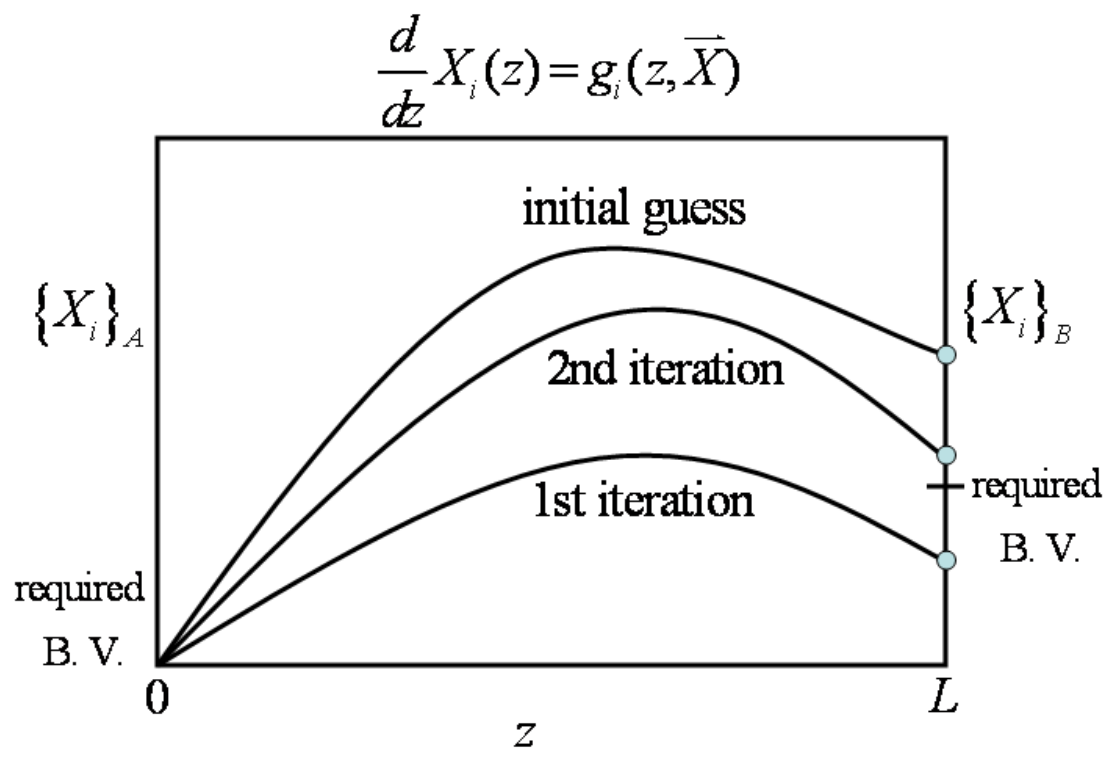


**Figure 4.1:** Schematic illustration of the principle of the shooting method for two-point boundary value problems.

approach to its solution, the shooting method [88], is illustrated in Figure 4.1.

Consider the set of differential equations  $dX_i(z)/dz = g_i(z, \vec{X})$ . A subset  $A$  of  $\{X_i\}$  satisfy boundary conditions at  $z = 0$ , and the complementary subset  $B$  satisfy boundary conditions at  $z = L$ .

The shooting method augments the set  $A$  with a set of "guesses"  $A'$ , so that  $A \cup A'$  enable the differential equations to be integrated as an initial value problem (from  $z = 0$  to  $z = L$ ). The idea is that  $A'$  is the correct choice when the integrated values at  $z = L$  reproduce the true boundary conditions, set  $B$ , within a permissible tolerance. The set  $A'$  is updated to enable convergence of the output at  $z = L$  to the set  $B$ .

The secant method that is used to update each element of  $A'$  takes two guesses  $x_1$  and  $x_2$  for each variable of  $A'$  and returns an updated value  $x_i$ ,

$$x_i = x_2 - f_2 \frac{f_2 - f_1}{x_2 - x_1}. \quad (4.5)$$

where  $f_1$  and  $f_2$  are the differences between the required values of that variable in set  $B$  and the numerically computed values assuming  $x_1$  and  $x_2$  values at  $z = 0$ . This method is iterated until convergence to all values in  $B$  is obtained. The secant method is illustrated in Figure 4.2.

### 4.3.2 Outline of the numerical solution

We use Matlab to perform the numerical integrations. For simplicity, we label the atomic and field variables as  $a_i$  and  $e_i$ . The counter-propagating field ( $-z$  direction) variables are  $e_1$  and  $e_2$  (signal fields) and  $e_3$  and  $e_4$  (idler fields) propagate in the  $+z$  direction. We set the local time  $\tau \rightarrow t$  in the following description of the algorithm.

We initialize 15  $a_i(z, t)$ , 4  $e_i(z, t)$  in time  $t \in (0, T)$  and space  $z \in (0, L)$ , and select 19 Gaussian random numbers  $n_i(z, t)$ . Set time and space grids with spacings  $\Delta t, \Delta z$  respectively. For each realization among  $R$  statistical ensemble averages, we



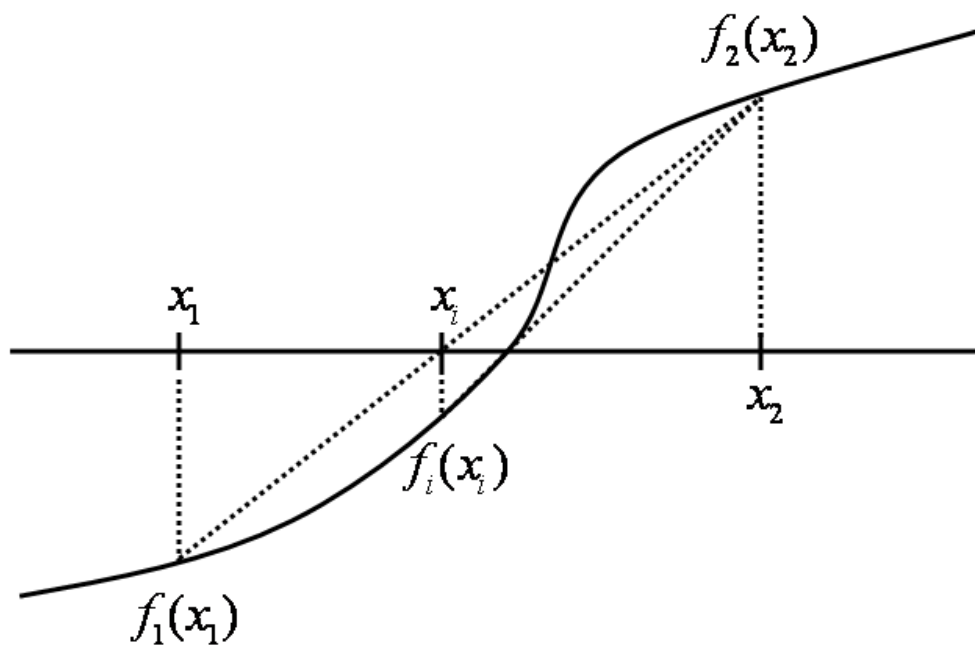


**Figure 4.2:** Secant method. The root is bracketed by two initial guesses of  $x_1$  and  $x_2$  and an updated guess  $x_i$  is located at the intersection of two straight lines.

update the variables governed by the symbolic equations of motion,

$$\frac{\partial}{\partial z} e_i = P_i(\vec{e}, \vec{a}, n_{e_i}), \quad (4.6)$$

$$\frac{\partial}{\partial t} a_i = A_i(\vec{e}, \vec{a}, n_{a_i}), \quad (4.7)$$

where  $P_i$  and  $A_i$  are in general the functions of variables that are denoted as vectors  $\vec{e}$  and  $\vec{a}$ . Each variable has its own stochastic source term as  $n_{e_i}$  or  $n_{a_i}$ .

The algorithm proceeds by using the midpoint difference method for the evolutions in space and time and the shooting method for  $e_i$ ,

$$\begin{aligned} e_i(z_m, t) &= e_i(z, t) + \frac{\Delta z}{2} P_i[\vec{e}(z_m, t), \vec{a}(z, t), n_{e_i}(z, t)], \\ a_i(z, t_m) &= a_i(z, t) + \frac{\Delta t}{2} A_i[\vec{e}(z, t), \vec{a}(z, t_m), n_{a_i}(z, t)], \end{aligned}$$

where  $z_m = z + \Delta z/2$  and  $t_m = t + \Delta t/2$ . The two guesses required in the secant method used in the shooting method are chosen as  $x_1 = \{e_1(0, t), e_2(0, t)\}$  and  $x_2 = \{e_3(L, t), e_4(L, t)\}$ .

Any normally-ordered quantity  $\langle Q \rangle$  can be derived by ensemble averages that  $\langle Q \rangle = \sum_{i=1}^R Q_i / R$  where  $Q_i$  is the result for each realization. Note that the update for field variables in space precedes the update for atomic variables, which takes into account that field variables evolve faster than atomic variables. The order should not matter when finer grids are used.

### 4.3.3 Results for signal, idler intensities, and the second-order correlation function

In this subsection, we present the second-order correlation function of signal-idler fields, and their intensity profiles. We define the intensities of signal and idler fields by

$$I_s(t) = \langle E_s^-(t)E_s^+(t) \rangle, \quad I_i(t) = \langle E_i^-(t)E_i^+(t) \rangle, \quad (4.8)$$

respectively, and the second-order signal-idler correlation function

$$G_{s,i}(t, \tau) = \langle E_s^-(t)E_i^-(t + \tau)E_i^+(t + \tau)E_s^+(t) \rangle \quad (4.9)$$

where  $\tau$  is the delay time of the idler field with respect a reference time  $t$  of the signal field. Since the correlation function is not stationary [64], we choose  $t$  as the time when  $G_{s,i}$  is at its maximum.

We consider a cigar shaped  $^{85}\text{Rb}$  ensemble of radius 0.25 mm and  $L = 3$  mm. The operating conditions of the pump lasers are  $(\Omega_a, \Omega_b, \Delta_1, \Delta_2) = (0.4, 1, 1, 0)\gamma_{03}$  where  $\Omega_a$  is the peak value of a 50 ns square pulse, and  $\Omega_b$  is the Rabi frequency of a continuous wave laser. The four atomic levels are chosen as  $(|0\rangle, |1\rangle, |2\rangle, |3\rangle) = (|5S_{1/2}, F=3\rangle, |5P_{3/2}, F=4\rangle, |5P_{3/2}, F=4\rangle, |4D_{5/2}, F=5\rangle)$ . The natural decay rate for atomic transition  $|1\rangle \rightarrow |0\rangle$  or  $|3\rangle \rightarrow |0\rangle$  is  $\gamma_{01} = \gamma_{03} = 1/26$  ns and they have a wavelength 780 nm. For atomic transition  $|2\rangle \rightarrow |1\rangle$  or  $|2\rangle \rightarrow |3\rangle$  is  $\gamma_{12} = \gamma_{32} = 0.156\gamma_{03}$  [97] with a telecom wavelength  $1.53\mu\text{m}$ . The scale factor of the coupling constants for signal and idler transitions is  $g_s/g_i = 0.775$ .

We have investigated four different atomic densities from a dilute ensemble with an optical density (opd) of 0.11 to a opd = 4.35. In Figure 4.3, 4.4, and 4.5, we take the atomic density  $\rho = 10^{10} \text{ cm}^{-3}$  (opd = 2.18) for example, and the grid sizes for dimensionless time  $\Delta t = 4$  and space  $\Delta z = 0.0007$  are chosen. The convergence of the grid spacings is fixed in practice by convergence to the signal intensity profile with an estimated relative error less than 0.5%.

The temporal profiles of the exciting lasers are shown in the left panel of Figure 4.3. The atomic density is chosen as  $\rho = 10^{10} \text{ cm}^{-3}$ , and the cooperation time  $T_c$  is 0.35 ns. The right panel shows time evolution of atomic populations for levels  $|1\rangle$ ,  $|2\rangle$ , and  $|3\rangle$  at  $z = 0, L$ , that are spatially uniform. The populations are found by

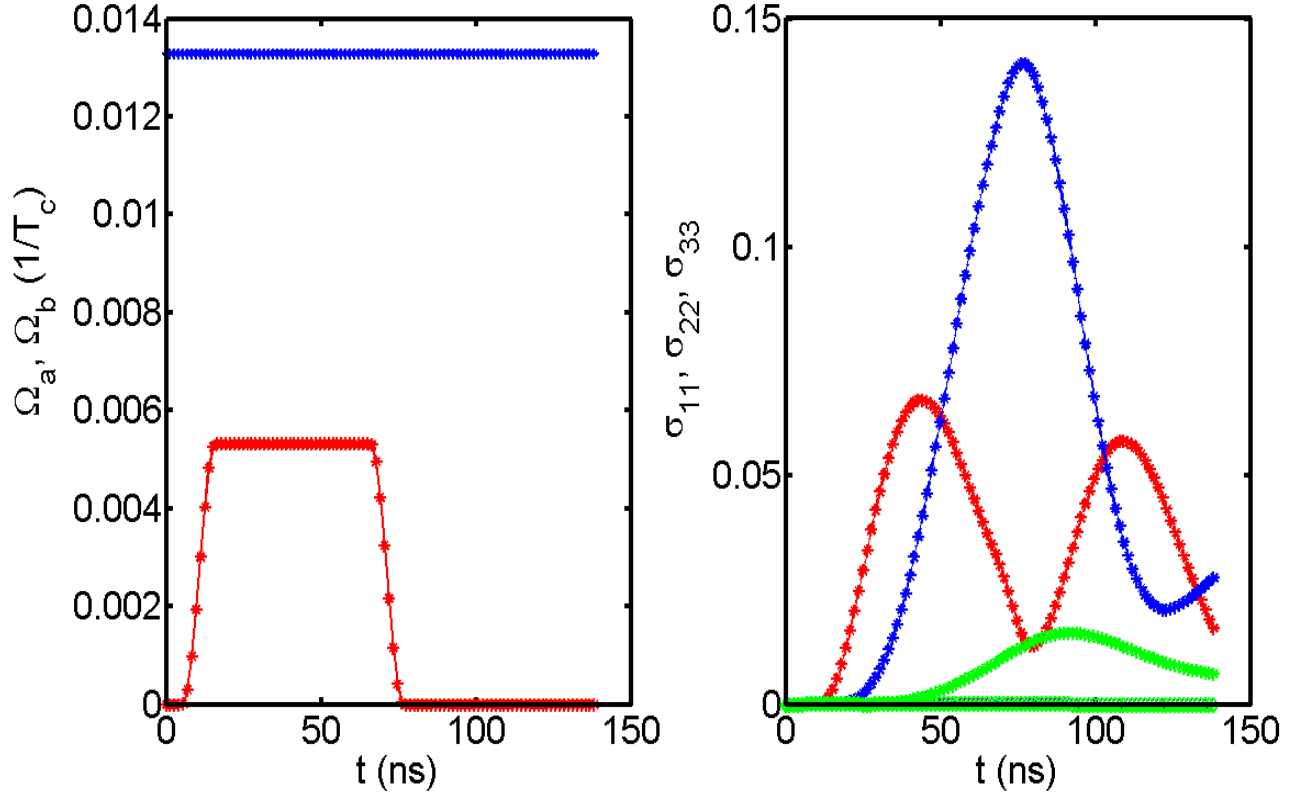


**Figure 4.3:** Time-varying pump fields and time evolution of atomic populations. (Left) The first pump field  $\Omega_a$  (dotted-red) is a square pulse of duration 50 ns and  $\Omega_b$  is continuous wave (dotted-blue). (Right) The time evolution of the real part of populations for three atomic levels  $\sigma_{11} = \langle \tilde{\alpha}_{13} \rangle$  (dotted-red),  $\sigma_{22} = \langle \tilde{\alpha}_{12} \rangle$  (dotted-blue),  $\sigma_{33} = \langle \tilde{\alpha}_{11} \rangle$  (dotted-green) at  $z = 0, L$ , and almost vanishing imaginary parts for all three of them. indicate convergence of the ensemble averages. Note that these atomic populations are uniform as a function of  $z$ .

ensemble averaging the complex stochastic population variables. The imaginary parts of the ensemble averages tend to zero as the ensemble size is increased, and this is a useful indicator of convergence, see Appendix B.2 for a discussion. In this example, the ensemble size was  $8 \times 10^5$ . The small rise after the pump pulse  $\Omega_a$  is turned off is due to the modulation caused by the pump pulse  $\Omega_b$ , which has a generalized Rabi frequency  $\sqrt{\Delta_2^2 + 4\Omega_b^2}$ . This influences also the intensity profiles and the correlation functions.

In Figure 4.4, we show that counter-propagating signal ( $-\hat{z}$ ) and idler ( $+\hat{z}$ ) fields at the respective ends of the atomic ensemble. The plots show the real and imaginary parts of the observables, and both are normalized to the peak value of signal intensity. Note that the characteristic field strength in terms of natural decay rate of the idler transition ( $\gamma_{03}$ ) and dipole moment ( $d_i$ ) is  $(d_i/\hbar)E_c \approx 36.3\gamma_{03}$ . The fluctuation in the real idler field intensity at  $z = L$  and non-vanishing imaginary part indicates a slower convergence compared to the signal field that has an almost vanishing imaginary part. The slow convergence is a practical limitation of the method.

In Figure 4.5 (a), we show a contour plot of the second-order correlation function  $G_{s,i}(t_s, t_i)$  where  $t_i \geq t_s$ . In Figure 4.5 (b), a section is shown through  $t_s \approx 75$  ns where  $G_{s,i}$  is at its maximum. The approximately exponential decay of  $G_{s,i}$  is clearly superradiant consistent with the theory of Chapter 3 and the reference [16]. The non-vanishing imaginary part of  $G_{s,i}$  calculated by ensemble averaging is also shown in (b) and indicates a reasonable convergence after  $8 \times 10^5$  realizations. In Table 4.1, we display numerical parameters of our simulations for four different atomic densities. The number of dimensions in space and time is  $M_t \times M_z$  with grid sizes  $(\Delta t, \Delta z)$  in terms of cooperation time ( $T_c$ ), length ( $L_c$ ). The superradiant time scale ( $T_f$ ) is found by fitting  $G_{s,i}$  to an exponential function ( $e^{-t/T_f}$ ), with 95% confidence range.

In Figure 4.6, the characteristic time scale is plotted as a function of atomic density and the factor  $N\bar{\mu}$ , and shows faster decay for optically denser atomic ensembles.

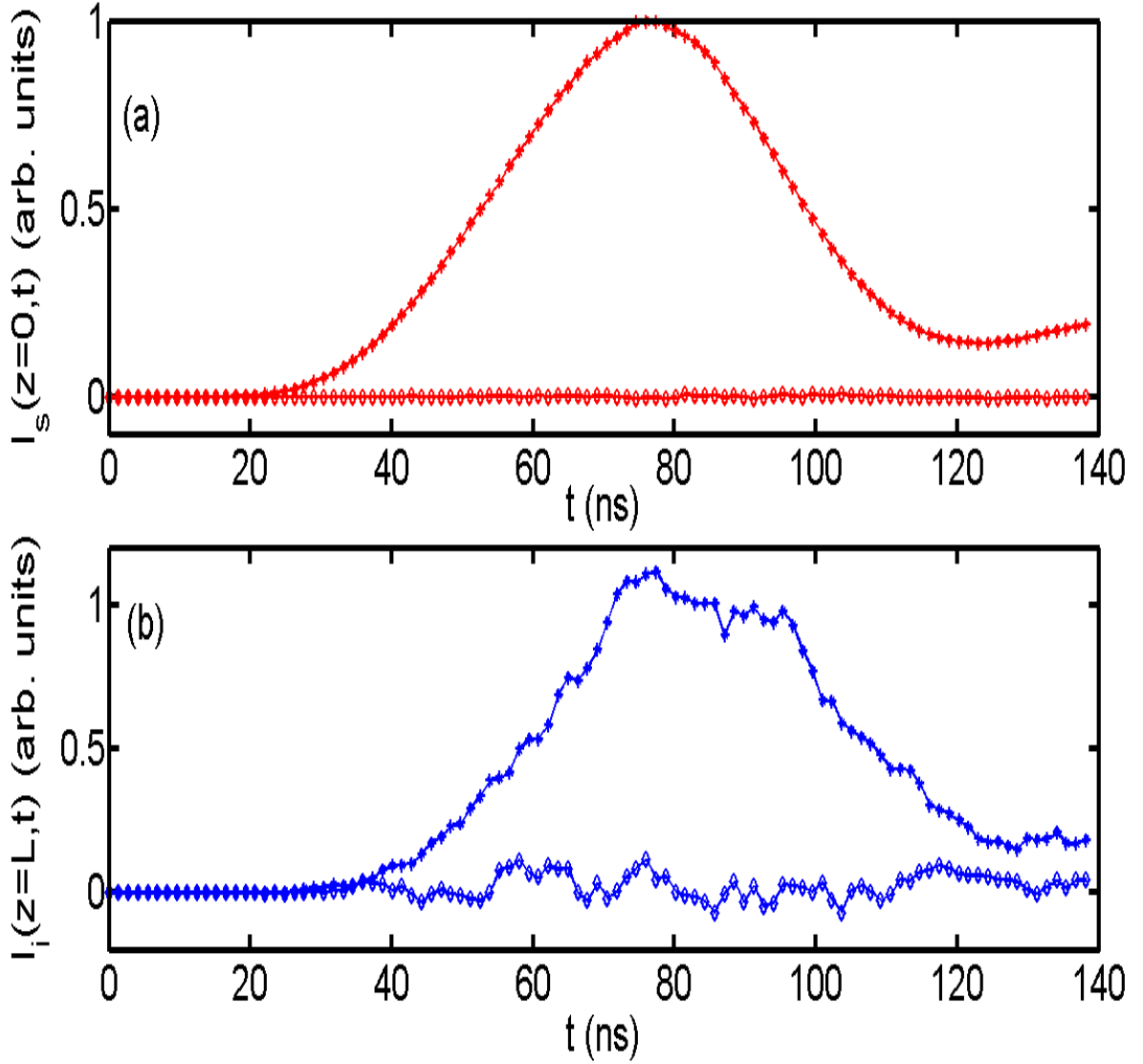


**Figure 4.4:** Temporal intensity profiles of counter-propagating signal and idler fields. (a) At  $z = 0$ , real (dotted-red) and imaginary (diamond-red) parts of signal intensity. (b) At  $z = L$ , real (dotted-blue) and imaginary (diamond-blue) parts of idler intensity. Both intensities are normalized by the peak value of signal intensity that is  $7.56 \times 10^{-12} E_c^2$ . Note that the idler fluctuations and its non-vanishing imaginary part indicate a relatively slower convergence compared with the signal intensity. The ensemble size was  $8 \times 10^5$ , and the atomic density  $\rho = 10^{10} \text{cm}^{-3}$ .

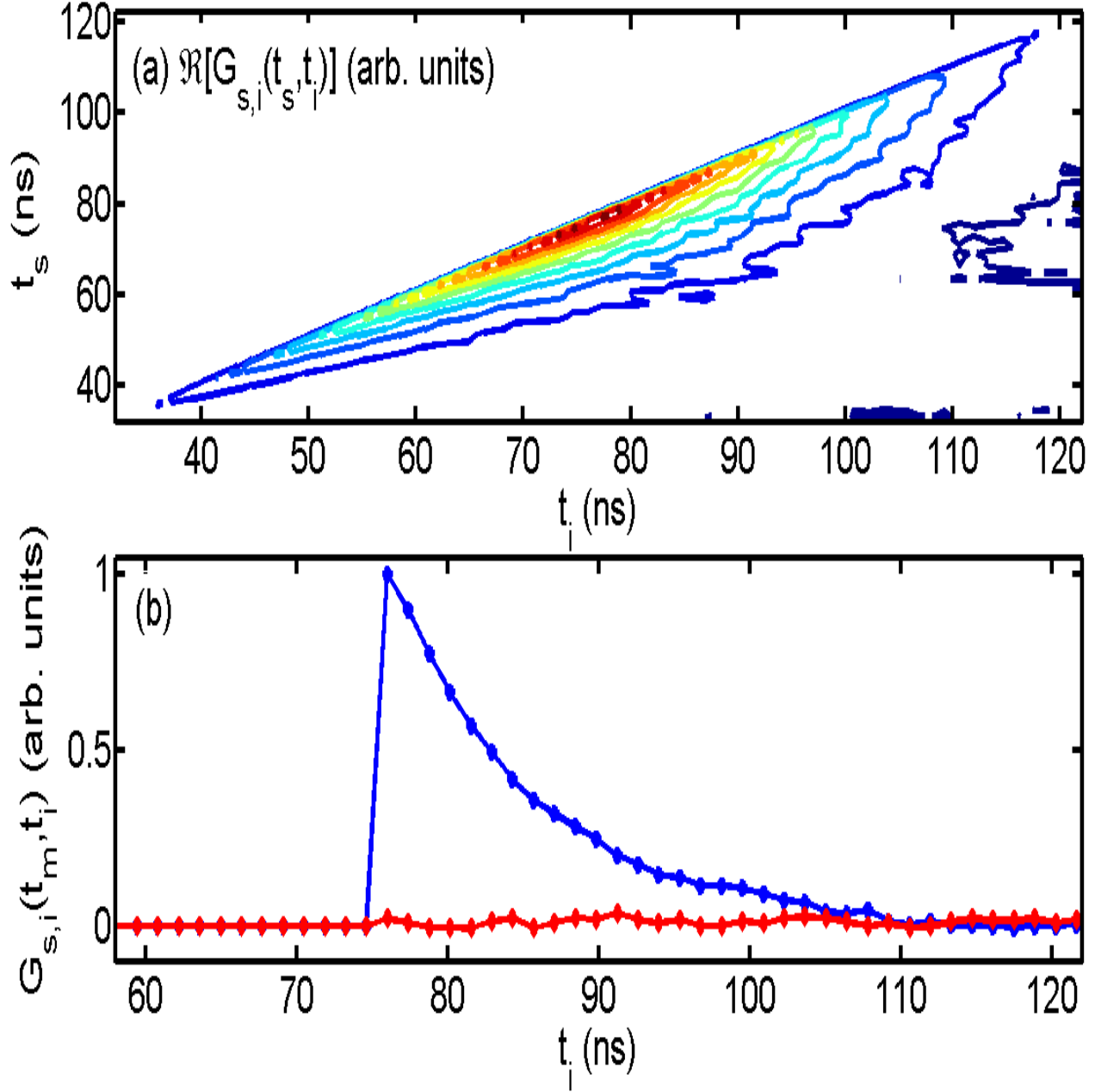


**Figure 4.5:** Second-order correlation function  $G_{s,i}(t_s, t_i)$ . The 2-D contour plot of the real part of  $G_{s,i}$  with a causal cut-off at  $t_s = t_i$  is shown in (a). The plot (b) gives a cross-section at  $t_s = t_m \approx 75$  ns, which is normalized to the maximum of the real part (dotted-blue) of  $G_{s,i}$ . The imaginary part (diamond-red) of  $G_{s,i}$  is nearly vanishing, and the number of realizations is  $8 \times 10^5$  for  $\rho = 10^{10} \text{cm}^{-3}$ .

**Table 4.1:** Numerical simulation parameters for different atomic densities  $\rho$ . Corresponding optical depth (opd), time and space grids ( $M_t \times M_z$ ) with grid sizes ( $\Delta t, \Delta z$ ) in terms of cooperation time ( $T_c$ ) and length ( $L_c$ ), and the fitted characteristic time  $T_f$  for  $G_{s,i}$  (see text).

$\rho(\text{cm}^{-3})$	opd	$M_t \times M_z$	$\Delta t(T_c),$ $\Delta z(L_c)$	$T_c(\text{ns}),$ $L_c(\text{m})$	fitted $T_f(\text{ns})$ [95% confidence range]
$5 \times 10^8$	0.11	$101 \times 44$	$0.9, 1.5 \times 10^{-4}$	1.55, 0.46	24.6 [24.2, 25.0]
$5 \times 10^9$	1.09	$101 \times 42$	$2.8, 4.5 \times 10^{-4}$	0.49, 0.15	14.8 [14.4, 15.3]
$1 \times 10^{10}$	2.18	$101 \times 42$	$4, 7 \times 10^{-4}$	0.35, 0.10	9.4 [9.2, 9.7]
$2 \times 10^{10}$	4.35	$101 \times 42$	$5.5, 1 \times 10^{-3}$	0.24, 0.07	5.0 [4.6, 5.5]

We also plot the timescale  $T_1 = \gamma_{03}^{-1}/(N\mu + 1)$  (ns) that is derived from the theory of Chapter 3, in which  $\bar{\mu}$  is the geometrical constant for a cylindrical ensemble, Eq. (A.12). The natural decay time  $\gamma_{03}^{-1} = 26$  ns corresponds to the D2 line of  $^{87}\text{Rb}$ . The error bar indicates the deviation due to the fitting range from the peak of  $G_{s,i}$  to approximately 25% and 5% of the peak value. The theory and simulations are in good qualitative agreement, approaching independent atom behavior at lower densities. For larger opd atomic ensembles, larger statistical ensembles are necessary for numerical simulations to converge. The integration of  $8 \times 10^5$  realizations used in the case of  $\rho = 10^{10} \text{ cm}^{-3}$  consumes about 14 days with Matlab's parallel computing toolbox (function "*parfor*") with a Dell precision workstation T7400 (64-bit Quad-Core Intel Xeon processors).

## 4.4 Conclusion

We have derived c-number Langevin equations in the positive-P representation for the cascade signal-idler emission process in an atomic ensemble. The complete c-number Langevin noise correlations are derived and confirmed by an alternative theoretical method. The equations are solved numerically by a stable and convergent semi-implicit difference method, while the counter-propagating spatial evolution is solved by implementing the shooting method.



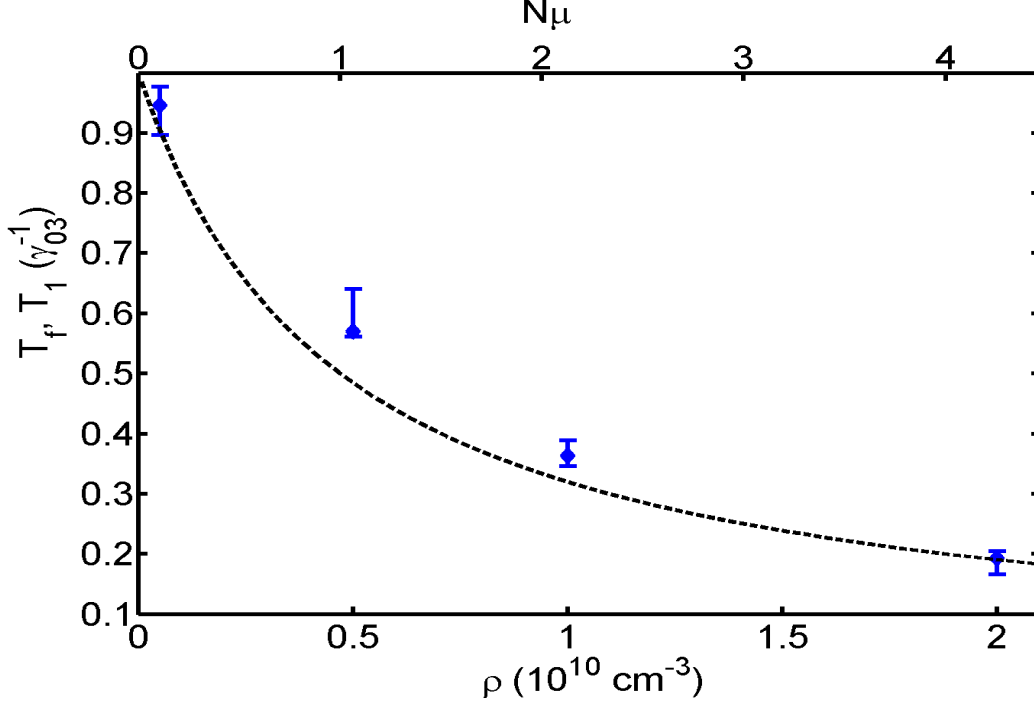


**Figure 4.6:** Characteristic timescales,  $T_f$  and  $T_1$  vs atomic density  $\rho$  and the super-radiant enhancement factor  $N\mu$  ( $\mu = \bar{\mu}$ ).  $T_f$  (dotted-blue) is the fitted characteristic timescale for  $G_{s,i}(t_s = t_m, t_i = t_m + \tau)$  where  $t_m$  is chosen at its maximum, as in Figure 4.5. The errorbars indicate the fitting uncertainties. As a comparison,  $T_1 = \gamma_{03}^{-1}/(N\mu + 1)$  (dashed-black) is plotted where  $\gamma_{03}^{-1} = 26$  ns is the natural decay time of D1 line of  $^{87}\text{Rb}$  atom, and  $\mu$  is the geometrical constant for a cylindrical atomic ensemble, as discussed in Chapter 3. The number of realizations is  $4 \times 10^5$  for  $\rho = 5 \times 10^8, 5 \times 10^9 \text{ cm}^{-3}$  and  $8 \times 10^5$  for  $\rho = 10^{10}, 2 \times 10^{10} \text{ cm}^{-3}$ .

We investigate four different atomic densities readily obtainable in a magneto-optical trap experiment. Signal and idler field intensities and their correlation function are calculated by ensemble averages. Vanishing of the unphysical imaginary parts within some tolerance is used as a guide to convergence. We find an enhanced characteristic time scale for idler emission in the second-order correlation functions from a dense atomic ensemble, consistent with the superradiance timescales predicted by the analytical method in Chapter 3, and observed experimentally [16].

# CHAPTER V

## SPECTRAL ANALYSIS FOR CASCADE-EMISSION-BASED QUANTUM COMMUNICATION

Cascade emission in alkali atoms is a source of telecommunication photons. In this Chapter, we investigate the DLCZ [6] scheme using the cascade emission from an atomic ensemble.

### ***5.1 Introduction***

Long distance quantum communication based on atomic ensembles was proposed by Duan, Lukin, Cirac, and Zoller [6]. This scheme involves Raman scattering of light by the atoms. The cascade transitions investigated in Chapter 3 and 4 provide a source of telecommunication wavelength photons. It is interesting to assess the cascade scheme in the DLCZ protocol given that it could potentially reduce transmission losses in a quantum telecommunication system. The DLCZ scheme is based on entanglement generation and swapping and quantum state transfer.

In this Chapter, we first discuss entanglement generation and then investigate how frequency entanglement of the cascade photon pair influences entanglement swapping.

### ***5.2 DLCZ Scheme with Cascade Emission***

In the DLCZ protocol, a weak pump laser Raman scatters a single photon generating a quantum correlated spin excitation in the ensemble. By interfering the Raman photons generated from two separate atomic ensembles on a beam splitter (B.S.), the

DLCZ entangled state  $(|01\rangle + |10\rangle)/\sqrt{2}$  [98] is prepared conditioned on one and only one click of the detectors after the B.S. Hence  $|0\rangle$  and  $|1\rangle$  represent the state of zero or one collective spin excitations stored in the hyperfine ground state coherences. This state originates from an indistinguishable photon paths. The error from multiple excitations can be made negligible if the pump laser is weak enough.

As shown in Figure 5.1, we consider instead that one of the ensembles employ cascade emission. The idea is for cascade emission to generate a telecom photon ( $\hat{a}_s^\dagger$ ) for transmission in the optical fiber, and an infrared photon that interferes locally with the Raman photon generated in the  $\Lambda$ -type atomic ensemble. In this way interference of the infrared photons generate the entangled state,

$$|\Psi\rangle = \frac{1}{\sqrt{2}}(|01\rangle_{a,s} + |10\rangle_{a,s}), \quad (5.1)$$

similar to the conventional DLCZ entanglement generation scheme. Now, however, instead of a stored spin excitation, we generate a telecom photon.

The entanglement swapping with the cascade emission may be implemented as shown in Figure 5.2, and will be discussed in detail in the next Section. The initial state is a tensor product of two state vectors generated locally at the sites A and B.

$$|\Psi\rangle = (\sqrt{1-\eta_{1A}}|0\rangle + \sqrt{\eta_{1A}}|1\rangle_i^A|1\rangle_s^A) \otimes (\sqrt{1-\eta_{2A}}|0\rangle + \sqrt{\eta_{2A}}|1\rangle_r^A|1\rangle_a^A) \otimes (\sqrt{1-\eta_{1B}}|0\rangle + \sqrt{\eta_{1B}}|1\rangle_i^B|1\rangle_s^B) \otimes (\sqrt{1-\eta_{2B}}|0\rangle + \sqrt{\eta_{2B}}|1\rangle_r^B|1\rangle_a^B), \quad (5.2)$$

where (s, i) represent the signal and idler photons from the cascade emission, and (r, a) are Raman scattered photon and the collective spin excitation. Here  $\eta_1$  and  $\eta_2$  are efficiencies to generate cascade and Raman emission. Since  $\eta_1$  and  $\eta_2 \ll 1$ , multiple atomic excitations or multi-photon generation can be excluded.

### 5.3 Entanglement Swapping

Consider the product state generated from A and B, Figure 5.2,

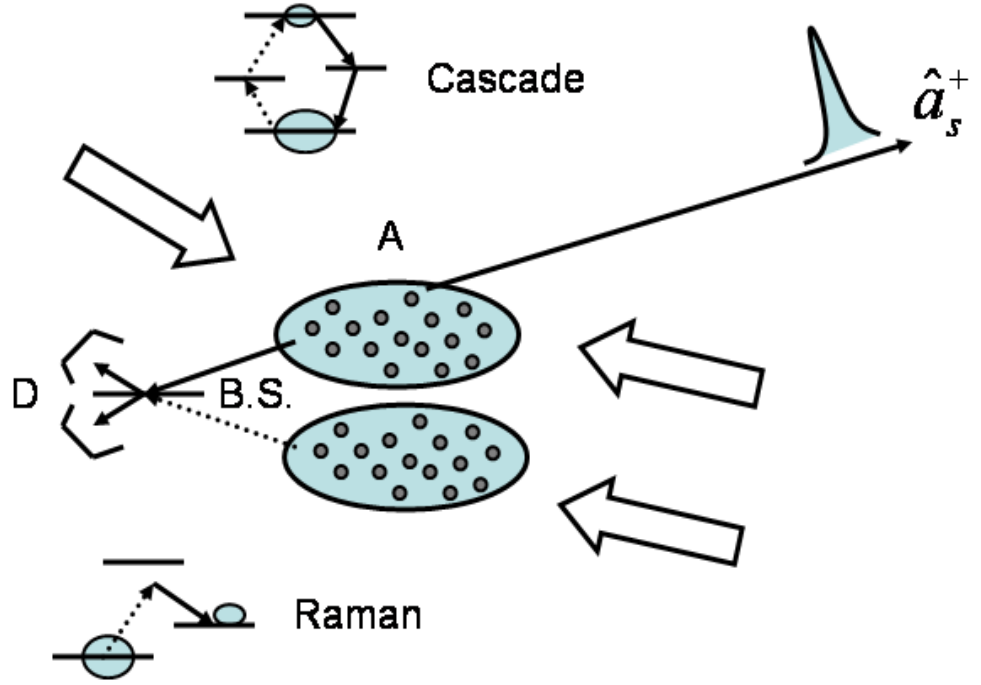


**Figure 5.1:** Entanglement generation in the DLCZ scheme using the cascade and Raman transitions in two different atomic ensembles. Large white arrows represent laser pump excitations corresponding to the dashed lines in either cascade or Raman level structures. Here  $\hat{a}_s^+$  represents the emitted telecom photon. B.S. means beam splitter that is used to interfere the incoming photons measured by the photon detector D. The label A refers to the pair of ensembles for later reference.

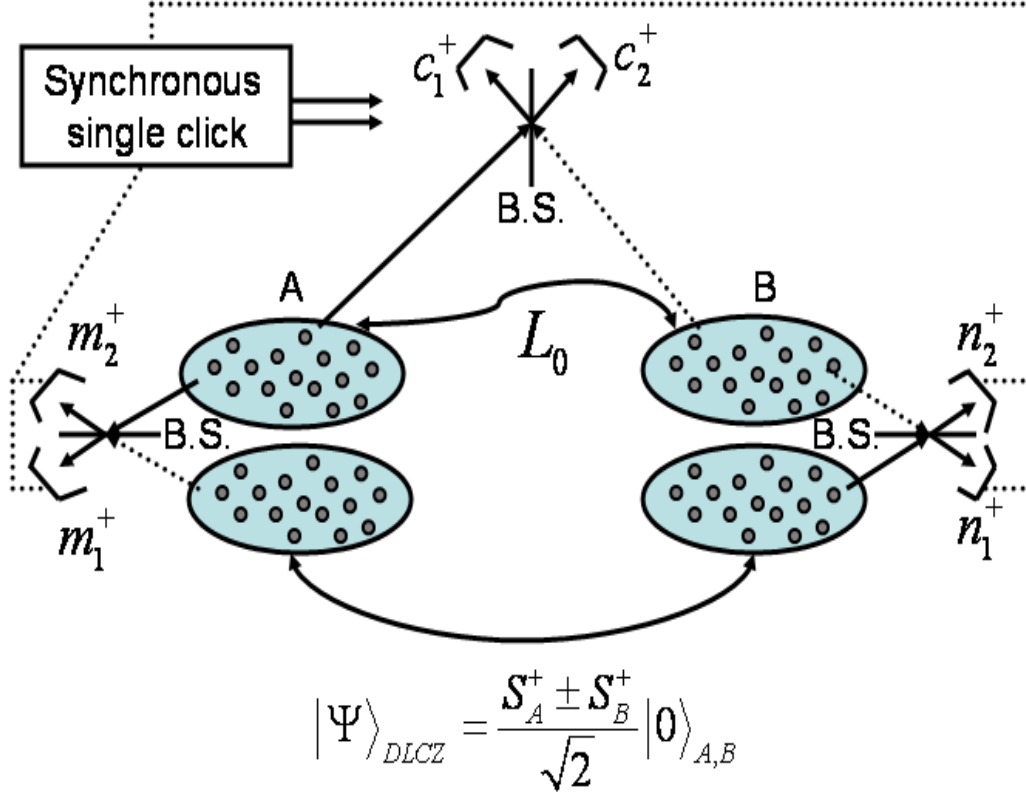


**Figure 5.2:** Entanglement swapping of DLCZ scheme using the cascade transition. The site A is described in detail in Figure 5.1 and equivalently for the site B. The telecom signal photons are sent from both sites and interfere by B.S. midway between with detectors represented by  $c_1^\dagger$  and  $c_2^\dagger$ . Synchronous single clicks of the detectors from both sites ( $m_{1,2}^\dagger, n_{1,2}^\dagger$ ) and the midway detector ( $c_{1,2}^\dagger$ ) generate the entangled state between lower atomic ensembles at sites A and B. The locally generated entanglement is swapped to distantly separated sites in this cascade-emission-based DLCZ protocol.

$$\begin{aligned}
|\Psi\rangle &= \left(\frac{|10\rangle_{as} + |01\rangle_{as}}{\sqrt{2}}\right)_A \otimes \left(\frac{|10\rangle_{as} + |01\rangle_{as}}{\sqrt{2}}\right)_B \\
&= \frac{1}{2}(|1010\rangle_{asas} + |1001\rangle_{asas} + |0110\rangle_{asas} + |0101\rangle_{asas}), \tag{5.3}
\end{aligned}$$

where the subscript (a) represents a stored local atomic excitation, and (s) means a telecom photon propagating toward the B.S. in the middle. We can tell from this effective state that the first component ( $|1010\rangle_{asas}$ ) contributes no telecom photons at all (two local excitations) and can be ruled out by measuring a "click" at one of the middle detectors. The second and the third components have components of the entangled state of quantum swapping, and the fourth one is the source of error if the photodetector cannot resolve one from two photons. The error could be corrected by using a photon number resolving detector (PNRD) if other drawbacks like dark counts, photon losses during propagation, and detector inefficiency are not considered.

Now we will formulate the entanglement swapping including the spectral effects discussed in Chapter 3. We ignore pump-phase offsets, assuming 50/50 B.S. and a symmetric set-up ( $\eta_{1A} = \eta_{1B} = \eta_1$ ,  $\eta_{2A} = \eta_{2B} = \eta_2$ ) for simplicity. Expand the previous joint state, Eq. (5.2) and keep the terms up to the second order of  $\eta_{1,2}$  that can contribute to detection events ( $\hat{m}_{1,2}^\dagger, \hat{n}_{1,2}^\dagger$ ),

$$\begin{aligned}
|\Psi\rangle_{eff} &= \eta_1(1 - \eta_2)|1\rangle_i^A|1\rangle_s^A|1\rangle_i^B|1\rangle_s^B + \eta_2(1 - \eta_1)|1\rangle_r^A|1\rangle_{cs}^A|1\rangle_r^B|1\rangle_{cs}^B + \\
&\sqrt{\eta_1\eta_2(1 - \eta_1)(1 - \eta_2)}|1\rangle_i^A|1\rangle_s^A|1\rangle_r^B|1\rangle_{cs}^B + \sqrt{\eta_1\eta_2(1 - \eta_1)(1 - \eta_2)}|1\rangle_r^A|1\rangle_{cs}^A|1\rangle_i^B|1\rangle_s^B, \tag{5.4}
\end{aligned}$$

where the cascade emission state  $|1\rangle_s|1\rangle_i \equiv \int f(\omega_s, \omega_i) \hat{a}_{\lambda_s}^\dagger(\omega_s) \hat{a}_{\lambda_i}^\dagger(\omega_i) |0\rangle d\omega_s d\omega_i$  has the spectral distribution  $f(\omega_s, \omega_i)$  as derived in Chapter 3.

As shown in Figure 5.2, entanglement swapping protocol is fulfilled by measuring three clicks from the three pairs of the detectors respectively ( $\hat{m}_{1,2}^\dagger, \hat{n}_{1,2}^\dagger, \hat{c}_{1,2}^\dagger$ ). The

quantum efficiency of the detector is considered in the protocol, and we describe a model for quantum efficiency in Appendix C.1. We then use this model to describe photodetection events registered by non-resolving photon detectors (NRPD). Starting with the input density operator  $\hat{\rho}_{in} = |\Psi\rangle_{eff}\langle\Psi|$ , we derive the projected density operator, Eq. (C.16), conditioned on the three clicks of  $\hat{m}_1^\dagger, \hat{n}_1^\dagger$ , and  $\hat{c}_1^\dagger$  in Appendix C.2. We use the Schmidt decomposition of the projected density operator and assume a single mode for the Raman scattered photon. We find the un-normalized density operator  $\hat{\rho}_{out}^{(2)}$  given in Eq. (C.16),

$$\begin{aligned} \hat{\rho}_{out}^{(2)} = & \frac{\eta_1^2(1-\eta_2)^2}{16}(2-\eta_t)\eta_t\eta_{eff}^2\left(1+\sum_j\lambda_j^2\right)|0\rangle\langle 0| + \frac{\eta_1\eta_2(1-\eta_1)(1-\eta_2)}{8}\eta_t\eta_{eff}^2 \\ & \left\{ \left( \hat{S}_B^\dagger|0\rangle\langle 0|\hat{S}_B + \hat{S}_A^\dagger|0\rangle\langle 0|\hat{S}_A \right) + \sum_j\lambda_j \int \phi_j(\omega_i)\phi_j^*(\omega'_i)\Phi^*(\omega_i)\Phi^*(\omega'_i)d\omega_id\omega'_i \right. \\ & \left. \left( \hat{S}_B^\dagger|0\rangle\langle 0|\hat{S}_A + \hat{S}_A^\dagger|0\rangle\langle 0|\hat{S}_B \right) \right\}, \end{aligned} \quad (5.5)$$

where  $\eta_t$  and  $\eta_{eff}$  are quantum efficiencies of the detectors at the telecom and infrared wavelengths respectively. The first term in Eq. (5.5) is the atomic vacuum state at sites A and B and contributes an error to the output density operator. The second term contains the components of the DLCZ entangled state.

We can define the fidelity  $F$ , the success probability  $P_S$  of entanglement swapping of the entangled state  $|\Psi\rangle_{DLCZ} = (S_A^\dagger + S_B^\dagger)|0\rangle/\sqrt{2}$ , and the heralding probability  $P_H$  for the third click as

$$F \equiv \frac{\text{Tr}(\hat{\rho}_{out}^{(2)}|\Psi\rangle_{DLCZ}\langle\Psi|)}{\text{Tr}(\hat{\rho}_{out}^{(2)})}, \quad (5.6)$$

$$P_H = P_1 + P_2, \quad P_1 = P_2 = \frac{\text{Tr}(\hat{\rho}_{out}^{(2)})}{\mathcal{N}}, \quad (5.7)$$

$$P_S = P_1 \times F_1 + P_2 \times F_2, \quad F_1 = F_2 = F, \quad (5.8)$$



where  $P_{1,2}$  is the heralding probability of the single click from the midway detector ( $\hat{c}_{1,2}^\dagger$ ) as shown in Figure 5.2, and a trace (Tr) is taken over atomic degrees of freedom.

The normalization factor  $\mathcal{N}$  is calculated in Eq. (C.9) and is given by

$$\mathcal{N} = \frac{\eta_1^2(1-\eta_2)^2}{4}\eta_{eff}^2 + \frac{\eta_1\eta_2(1-\eta_1)(1-\eta_2)}{2}\eta_{eff}^2 + \frac{\eta_2^2(1-\eta_1)^2}{4}\eta_{eff}^2. \quad (5.9)$$

We have used the following properties for the calculation of  $\hat{\rho}_{out}^{(2)}$  and  $\mathcal{N}$ ,

$$\int d\omega_s d\omega_i |f(\omega_s, \omega_i)|^2 = 1, \quad (5.10)$$

where orthonormal relations in the mode functions are used, and

$$\int d\omega_s d\omega'_s d\omega_i d\omega'_i f(\omega'_s, \omega'_i) f^*(\omega'_s, \omega_i) f(\omega_s, \omega_i) f^*(\omega_s, \omega'_i) = \sum_j \lambda_j^2. \quad (5.11)$$

Note that the single mode spectral function for the Raman photon satisfies  $\int d\omega |\Phi(\omega)|^2 = 1$ .

The fidelity, heralding, and success probability become

$$F = \frac{1 + \sum_j \lambda_j \int \phi_j(\omega_i) \phi_j^*(\omega'_i) \Phi^*(\omega_i) \Phi^*(\omega'_i) d\omega_i d\omega'_i}{\eta_r(2 - \eta_t)(1 + \sum_j \lambda_j^2)/2 + 2}, \quad (5.12)$$

$$P_H = \frac{\eta_r \eta_t (2 - \eta_t)(1 + \sum_j \lambda_j^2)/2 + 2\eta_t}{(\sqrt{\eta_r} + 1/\sqrt{\eta_r})^2}, \quad (5.13)$$

$$P_S = \eta_t \frac{1 + \sum_j \lambda_j \int \phi_j(\omega_i) \phi_j^*(\omega'_i) \Phi^*(\omega_i) \Phi^*(\omega'_i) d\omega_i d\omega'_i}{(\sqrt{\eta_r} + 1/\sqrt{\eta_r})^2}, \quad (5.14)$$

where  $\frac{1-\eta_2}{1-\eta_1} \approx 1$  and  $\eta_r = \eta_1/\eta_2$ .

The fidelity depends on a sum of square of Schmidt numbers in the denominator and the mode mismatch between the idler and Raman photons in the numerator. Let us assume that the Raman photon mode is engineered to be matched with the idler photon mode of the largest Schmidt number ( $\phi_1(\omega_i)$  in our case), which is required to have a larger fidelity (so is the success probability) compared to other modes. We may also compare the NRPD with the performance of PNRD in the midway detectors, then we have the fidelity, heralding, and success probability,

$$F = \begin{cases} \frac{1+\lambda_1}{\eta_r(2-\eta_t)(1+\sum_j \lambda_j^2)/2+2}, & \text{NRPD} \\ \frac{1+\lambda_1}{\eta_r(1-\eta_t)(1+\sum_j \lambda_j^2)+2}, & \text{PRND} \end{cases} \quad (5.15)$$

$$P_H = \begin{cases} \frac{\eta_r \eta_t (2-\eta_t)(1+\sum_j \lambda_j^2)/2+2\eta_t}{(\sqrt{\eta_r}+1/\sqrt{\eta_r})^2}, & \text{NRPD} \\ \frac{\eta_r \eta_t (1-\eta_t)(1+\sum_j \lambda_j^2)+2\eta_t}{(\sqrt{\eta_r}+1/\sqrt{\eta_r})^2}, & \text{PRND} \end{cases} \quad (5.16)$$

$$P_S = \begin{cases} \frac{\eta_t(1+\lambda_1)}{(\sqrt{\eta_r}+1/\sqrt{\eta_r})^2}, & \text{NRPD} \\ \frac{\eta_t(1+\lambda_1)}{(\sqrt{\eta_r}+1/\sqrt{\eta_r})^2}, & \text{PRND} \end{cases}. \quad (5.17)$$

When the relative efficiency is made arbitrarily small, the fidelity approaches  $(1+\lambda_1)/2$  for both types of detectors. It reaches one if a pure cascade emission source is generated (von Neumann entropy  $E = 0$  and  $\lambda_1 = 1$ ). When  $\eta_r = 1$  with a pure source using NRPD with a perfect quantum efficiency,  $F = 2/3$ ,  $P_H = 3/4$ ,  $P_S = 1/2$ , which coincide with the results of the reference [99] (with perfect quantum efficiency).

We discuss the frequency entanglement for various pulse widths and superradiant decay rates in Chapter 3.4. We find that for shorter driving pulses and smaller superradiant decay rates, the cascade emission source is less spectrally entangled. That means when  $\eta_r$  is fixed, a shorter driving pulse heralds a higher fidelity DLCZ entangled state.

In Figure 5.3, we numerically calculate the entropy and plot out the fidelity from Eq. (5.15), the heralding probability from Eq. (5.16), and the success probability from Eq. (5.17) as a function of the relative efficiency  $\eta_r$ . With a perfect detection efficiency ( $\eta = 1$ ), we find that at a smaller  $\eta_r$ , the less entangled source gives us a higher fidelity DLCZ entangled state but with a smaller success probability. Small generation probability for cascade emission ( $\eta_r < 1$ ) reduces the error of NRPD from two telecom photons interference, but it reduces the successful entanglement swapping at the same time.

The optimal success probability occurs by using the same excitation efficiency for both cascade and Raman configurations. For PNRD, the fidelity is higher than

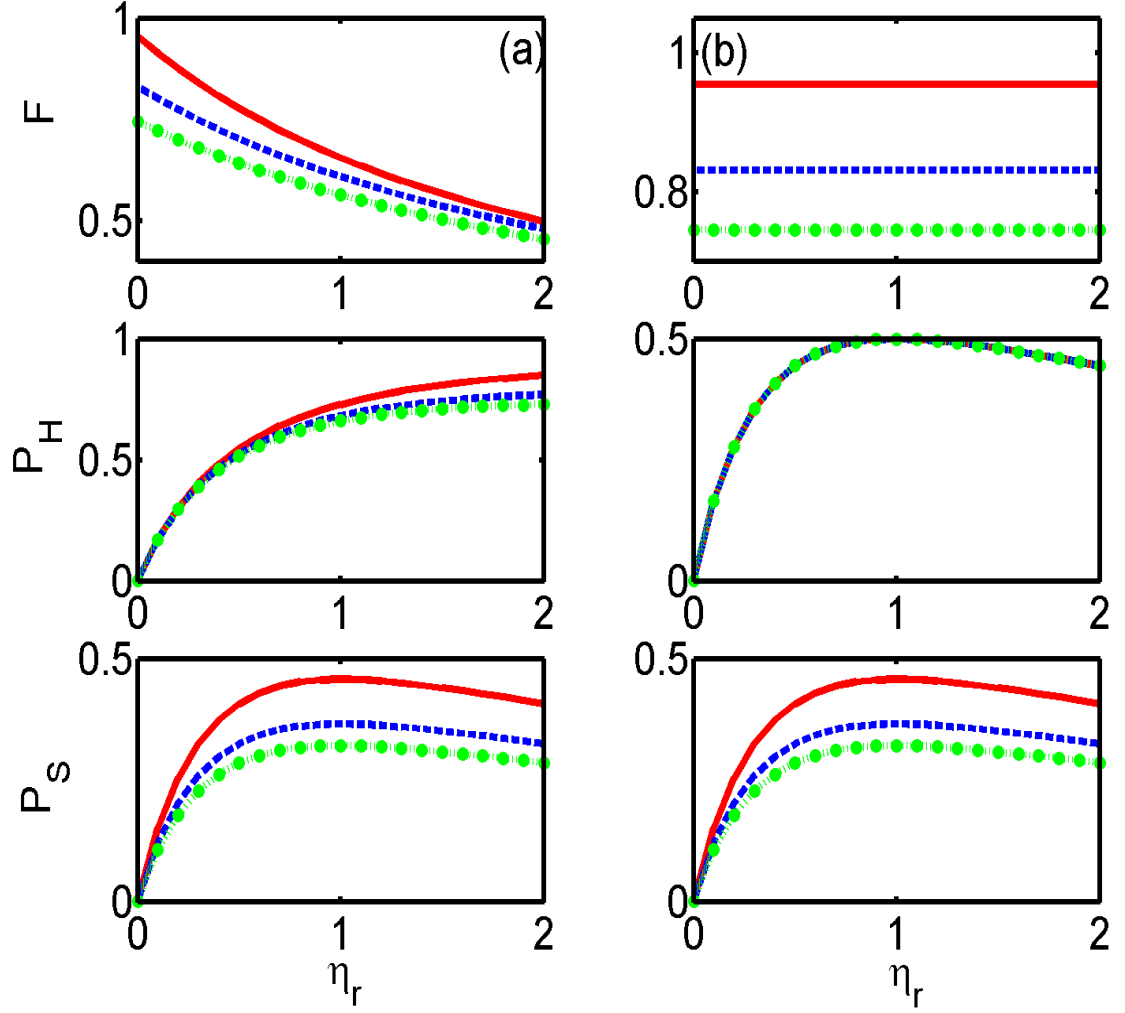


**Figure 5.3:** Fidelity  $F$ , heralding  $P_H$ , and success  $P_S$  probabilities of entanglement swapping versus relative efficiency  $\eta_r$  with perfect detection efficiency  $\eta_t = 1$ . Column (a) NRPD and (b) PNRD. Solid-red, dashed-blue, and dotted-green curves correspond to the pulse width parameters  $\tau = (0.1, 0.5, 0.5)$  and superradiant factor  $N\bar{\mu} + 1 = (5, 5, 10)$  (see Chapter 3 and Appendix A). The von Neumann entropy is  $S = (0.684, 2.041, 2.886)$ , respectively.

NRPD, and the heralding probability is the same independent of the degree of frequency space entanglement. The success probabilities for both types of detectors are equal. The advantage of PNRD shows up in the fidelity of quantum swapping.

In Figure 5.4, we show that the measures improve monotonically with the quantum efficiency ( $\eta = \eta_t$ ) of the detector at telecom wavelength, with  $\eta_r = 0.5$ . The success probabilities for both types of detectors are the same and again the advantage of PNRD shows up in the fidelity.

## 5.4 *Polarization Maximally Entangled State (PME State) and Quantum Teleportation*

In Figure 5.5, we illustrate schematically a scheme for probabilistic PME state preparation and quantum teleportation. Four ensembles (ABCD) are used to generate two entangled pairs of DLCZ entangled states, and another two ensembles ( $I_1, I_2$ ) are used to prepare a quantum state to be teleported.

With the conditional output density matrix from Eq. (C.16), we proceed to construct the PME state  $|\Psi\rangle_{PME} = \frac{1}{\sqrt{2}}(\hat{S}_A^\dagger \hat{S}_D^\dagger + \hat{S}_B^\dagger \hat{S}_C^\dagger)|0\rangle$  where ( $C, D$ ) represents another parallel entanglement connection setup, Figure 5.5 (a). This PME state is useful in entanglement-based communication schemes [6], and we will here calculate its success probability. The normalized density matrix for the AB system is from Eq. (5.5) (let  $\eta_t = \eta$ ),

$$\begin{aligned} \hat{\rho}_{out,n}^{(2),AB} = & \frac{a}{a+4}|0\rangle\langle 0| + \frac{2}{a+4}\left(\hat{S}_B^\dagger|0\rangle\langle 0|\hat{S}_B + \hat{S}_A^\dagger|0\rangle\langle 0|\hat{S}_A \right. \\ & \left. + \lambda_1\hat{S}_B^\dagger|0\rangle\langle 0|\hat{S}_A + \lambda_1\hat{S}_A^\dagger|0\rangle\langle 0|\hat{S}_B\right), \end{aligned} \quad (5.18)$$

where the largest Schmidt number ( $\lambda_1$ ) of mode overlap is chosen and  $a \equiv \eta_r(2 - \eta)\left(1 + \sum_j \lambda_j^2\right)$ .

A parallel pair of entangled ensembles (C,D) is introduced, and the joint density

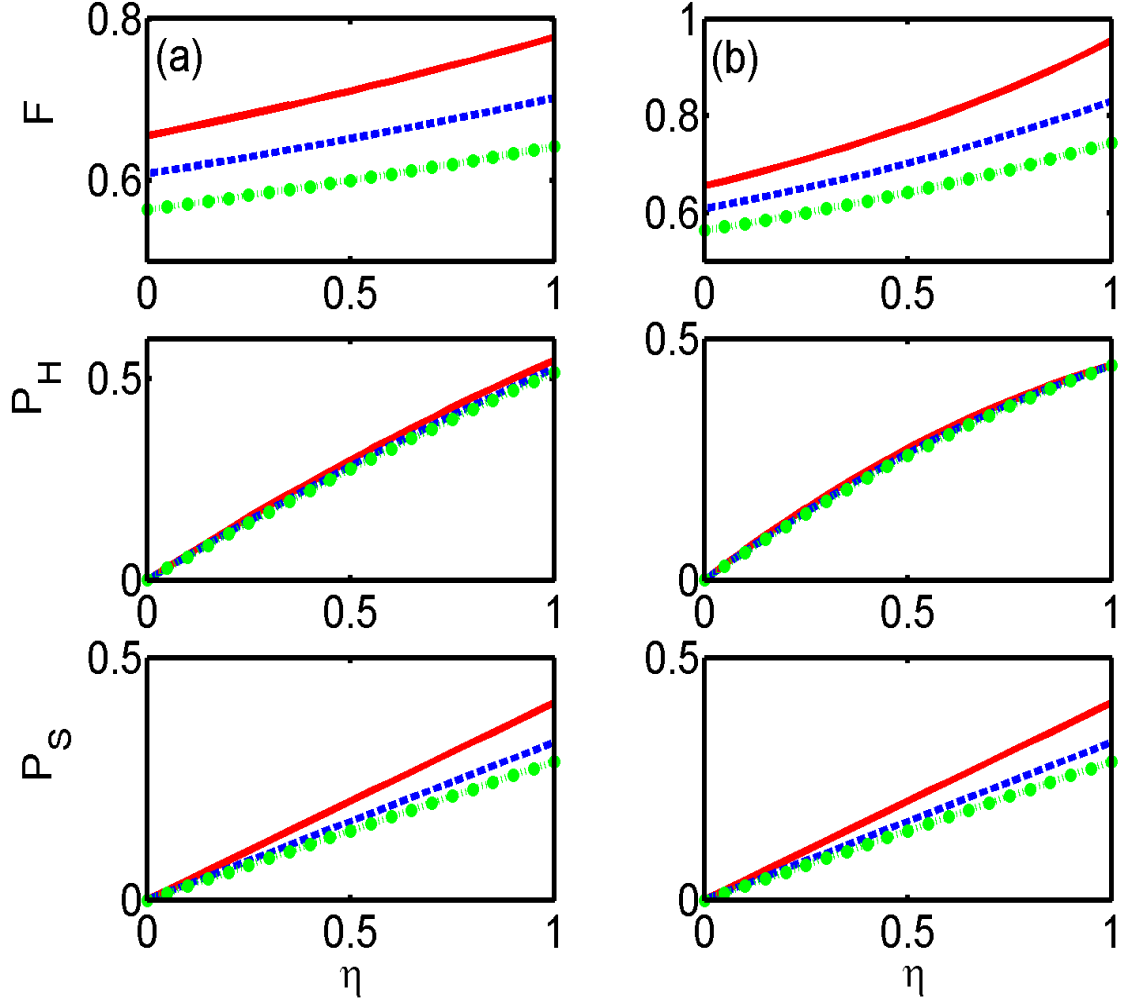


**Figure 5.4:** Fidelity  $F$ , heralding  $P_H$ , and success  $P_S$  probabilities of entanglement swapping versus telecom detector quantum efficiency  $\eta$  for the case of (a) NRPD and (b) PNRD. Solid-red, dashed-blue, and dotted-green curves correspond to the same parameters used in Figure 5.3.

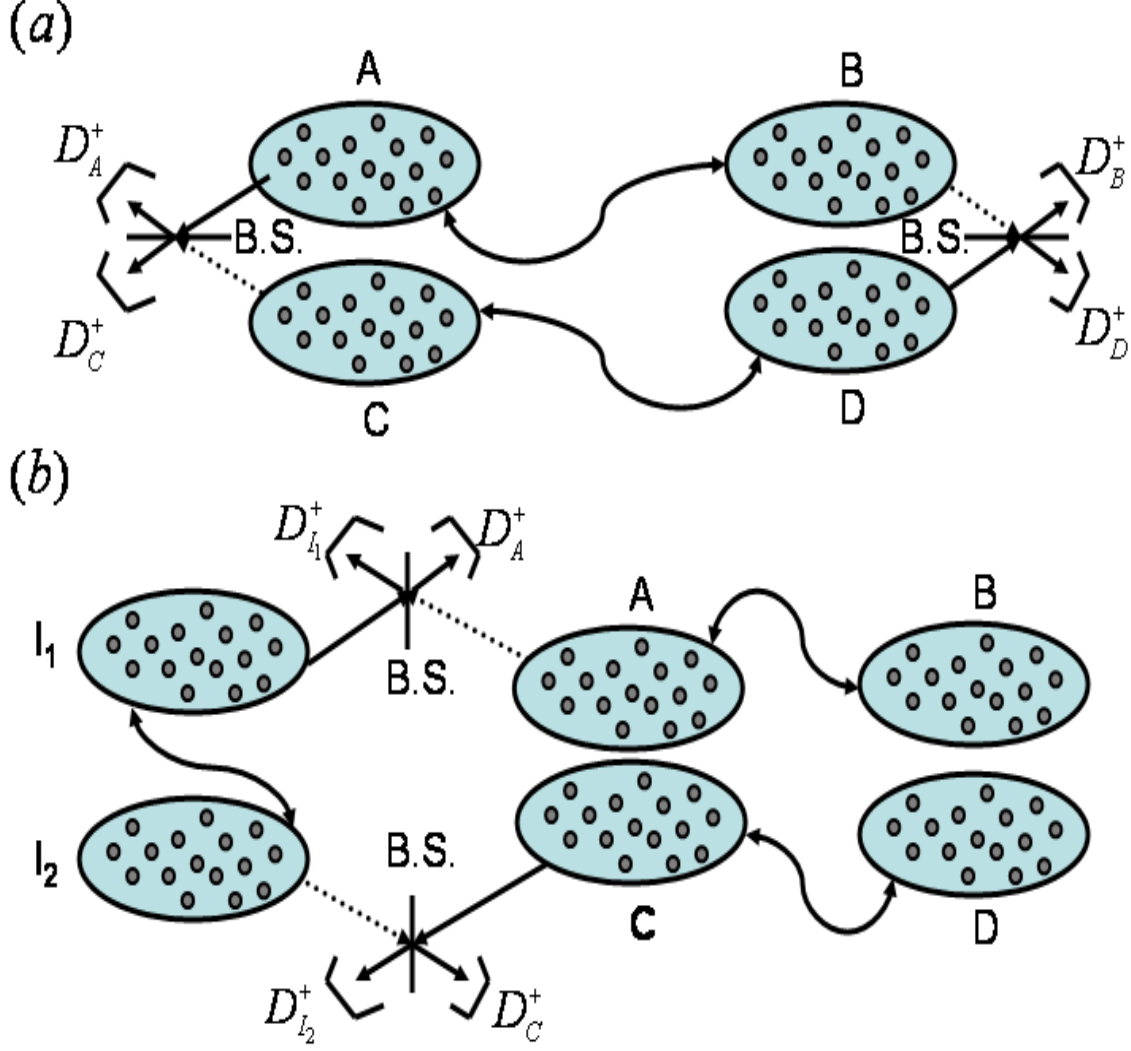


**Figure 5.5:** PME projection (a) and quantum teleportation (b) in the DLCZ scheme. Four atomic ensembles (A,B,C,D) are used to generate two DLCZ entangled states at (A,B) and (C,D). PME state is projected probabilistically conditioned on four possible detection events of ( $D_A^\dagger$  or  $D_C^\dagger$ ) and ( $D_B^\dagger$  or  $D_D^\dagger$ ) in (a). In the quantum teleportation protocol (b), another two ensembles ( $I_1, I_2$ ) are used to prepare a quantum state that is teleported to atomic ensembles B and D conditioned on four possible detection events of ( $\hat{D}_{I_1}$  or  $\hat{D}_A$ ) and ( $\hat{D}_{I_2}$  or  $\hat{D}_C$ ).

operator is  $\hat{\rho}_{out,n}^{(2),AB} \otimes \hat{\rho}_{out,n}^{(2),CD}$ . The latter expression is developed mathematically in Appendix C.3.

With projection of the PME state, we have the post measurement success probability [a click from each side; the side of (A or C) and (B or D)],

$$\begin{aligned} P_{S,PME} &= \langle \Psi | \hat{\rho}_{out,n}^{(2),AB} \otimes \hat{\rho}_{out,n}^{(2),CD} | \Psi \rangle_{PME}, \\ &= \frac{4(1 + \lambda_1^2)}{[\eta_r(2 - \eta_t)(1 + \sum_j \lambda_j^2) + 4]^2}. \end{aligned} \quad (5.19)$$

For  $\eta_r \ll 1$ ,  $P_{S,PME}$  reaches the maximum of 1/2 when a pure source ( $\lambda_1 = 1$ ) is used.

For an arbitrary quantum state transfer to long distance, quantum teleportation scheme may be used. Another two ensembles ( $I_1, I_2$ ) are introduced [6], and the quantum state can be described by  $|\Psi\rangle = (d_0 \hat{S}_{I_1}^\dagger + d_1 \hat{S}_{I_2}^\dagger)|0\rangle$  with  $|d_0|^2 + |d_1|^2 = 1$ . The joint density matrix for quantum teleportation is

$$\hat{\rho}_{QT} = (d_0 \hat{S}_{I_1}^\dagger + d_1 \hat{S}_{I_2}^\dagger)|0\rangle\langle 0| (d_0^* \hat{S}_{I_1} + d_1^* \hat{S}_{I_2}) \otimes \hat{\rho}_{out,n}^{(2),AB} \otimes \hat{\rho}_{out,n}^{(2),CD}. \quad (5.20)$$

Atomic ensembles (A,B) in parallel with (C,D) provide a scheme for PME state preparation. Retrieve the quantum state [ensemble ( $I_1, I_2$ )] into photons and interfere them at B.S., respectively, with photons from A and C. We have the teleported quantum state at B and D conditioned on the single click of ( $\hat{D}_{I_1}$  or  $\hat{D}_A$ ) and ( $\hat{D}_{I_2}$  or  $\hat{D}_C$ ).

Consider single detection events at  $\hat{D}_{I_1}$  and  $\hat{D}_{I_2}$  as an example. With the NRPD measurement operators  $\hat{M}_{I_1, I_2} \equiv (\hat{I}_{D_1}^\dagger - |0\rangle_{D_1}\langle 0|) \otimes |0\rangle_{D_A}\langle 0| \otimes (\hat{I}_{D_2}^\dagger - |0\rangle_{D_2}\langle 0|) \otimes |0\rangle_{D_C}\langle 0|$  (we use  $D_1, D_2$  for  $D_{I_1}, D_{I_2}$ ), the density matrix after the measurement becomes

$$\begin{aligned}
\hat{\rho}_1 \equiv \text{Tr}(\hat{\rho}_{QT,eff} \hat{M}_{I_1, I_2}) = \\
\frac{a+2}{2(a+4)^2} |0\rangle_{ABCD} \langle 0| + \frac{4}{(a+4)^2} \left( \frac{|d_0|^2}{4} \hat{S}_B^\dagger |0\rangle \langle 0| \hat{S}_B + \frac{|d_1|^2}{4} \hat{S}_D^\dagger |0\rangle \langle 0| \hat{S}_D + \right. \\
\left. \frac{\lambda_1^2 d_0 d_1^*}{4} \hat{S}_B^\dagger |0\rangle \langle 0| \hat{S}_D + \frac{\lambda_1^2 d_0^* d_1}{4} \hat{S}_D^\dagger |0\rangle \langle 0| \hat{S}_B \right), \tag{5.21}
\end{aligned}$$

where  $\hat{\rho}_{QT,eff}$  is calculated in Eq. (C.18), and the trace is taken over the electromagnetic field degrees of freedom.

For a successful transfer of the quantum state  $|\Phi\rangle = (d_0 \hat{S}_B^\dagger + d_1 \hat{S}_D^\dagger) |0\rangle$ , the fidelity  $F_1 = \langle \Phi | \hat{\rho}_1 | \Phi \rangle / \text{Tr}(\hat{\rho}_1)$ , and the heralding probability is  $P_1 = \text{Tr}(\hat{\rho}_1)$ , with the trace over all atomic degrees of freedom. Except for the detection event we consider here, there are three other detection events including  $(D_A, D_C)$ ,  $(D_{I_1}, D_C)$  and  $(D_A, D_{I_2})$ . The teleported state from the detection events  $(D_{I_1}, D_C)$  and  $(D_{I_2}, D_A)$  requires a  $\pi$  rotation correction on the relative phase ( $d_0 \rightarrow d_0, d_1 \rightarrow -d_1$ ).

The fidelity and heralding probabilities conditioned on the other three pairs of clicks are the same as  $F_1$  and  $P_1$  respectively, so the success probability is

$$\begin{aligned}
P_{S,QT} &= \sum_i^4 P_i F_i = 4P_1 F_1, \\
&= \frac{F^2}{(1+\lambda_1)^2} [1 + (2\lambda_1^2 - 2)|d_0|^2 |d_1|^2], \tag{5.22}
\end{aligned}$$

where  $F$  is the fidelity of entanglement swapping for NRPD, Eq. (5.15). For PNRD, the success probability for quantum teleportation is unchanged.

The success probability for quantum teleportation depends on the probability amplitude of the quantum state and the fidelity  $F$  of the entanglement swapping. In Figure 5.6, for  $\eta_r = 0.5$  and  $\eta_t = 1$ , we can see in the region  $|d_0| \approx 0.3 \sim 0.9$ , higher success probability requires a less entangled cascade emission source. Outside this region, it prefers a more entangled source. When a pure source is used ( $\lambda_1 = 1$ ) and let  $\eta_r \ll 1, \eta_t = 1$ , we can achieve the maximum of the success probability  $P_{S,QT} = \frac{1}{4}$



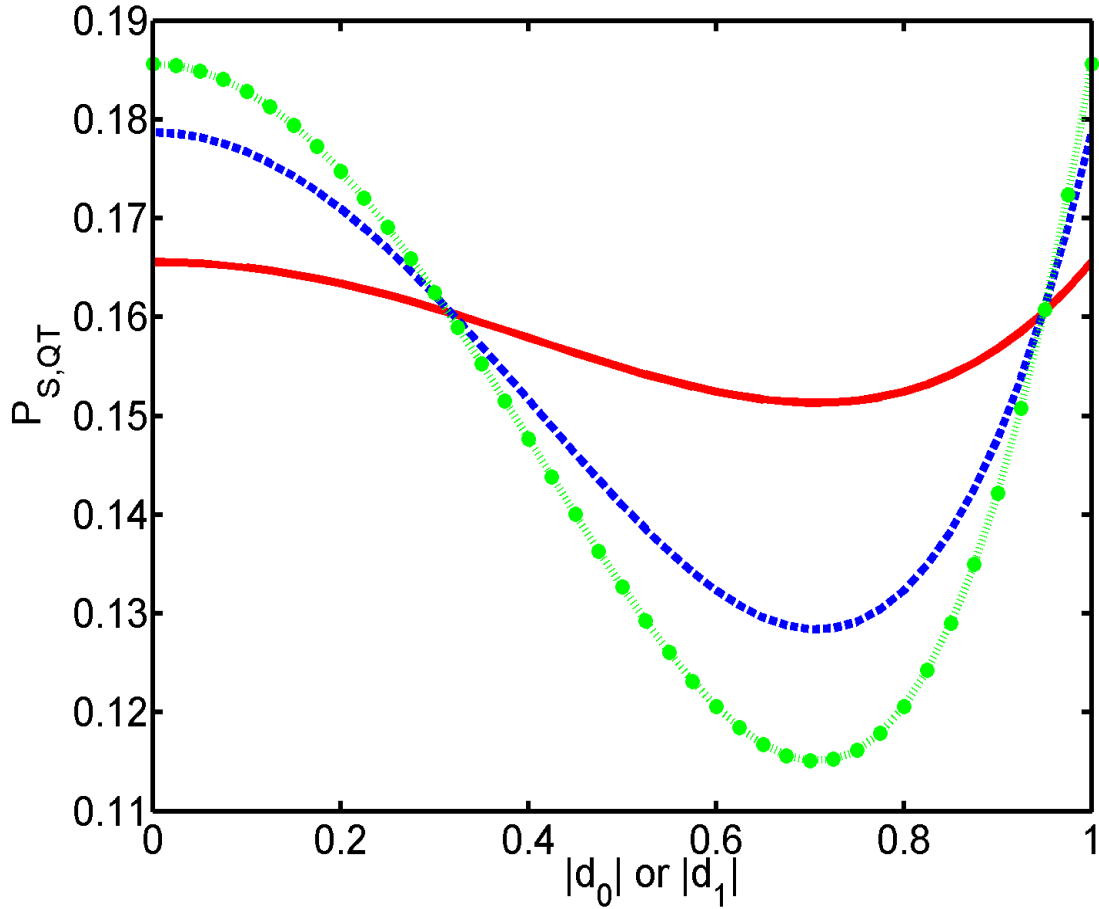


**Figure 5.6:** Success probability of quantum teleportation as a function of the probability amplitude of teleported quantum state with  $\eta_r = 0.5$  and a perfect detector efficiency  $\eta_t = 1$ . Solid-red, dashed-blue, and dotted-green curves correspond to the same parameters used in Figure 5.3.

when  $F = 1$ , which is also achieved in the traditional DLCZ scheme with perfect quantum efficiencies [99].

## 5.5 Conclusion

We have described probabilistic protocols for the DLCZ scheme implementing the cascade emission source. We characterize the spectral properties of the cascade emission by Schmidt mode analysis and investigate the fidelity and success probability of the protocols using photon resolving and non-resolving photon detectors. The

success probability is independent of the detector type, but photon number resolving detection improves the fidelity.

The performance of the protocol also depends on the ratio of efficiencies in generating the cascade and Raman photons. The success probability is optimized for equal efficiencies while the fidelity is higher when the ratio is smaller than one for non-resolving photon detectors.

The frequency space entanglement of telecom photons produced in cascade emission deteriorates the performance of DLCZ protocols. The harmful effect can be diminished by using shorter pump pulses to generate the cascade emission. A state dependent success probability of quantum teleportation was calculated, and in some cases a more highly frequency entangled cascade emission source teleports more successfully. An improved performance could be achieved if the error source (vacuum part) were removed. This could be done by entanglement purification [3] at the stage of entanglement swapping and then using the purified source to teleport the quantum state.

# CHAPTER VI

## EFFICIENCY OF LIGHT-FREQUENCY CONVERSION IN AN ATOMIC ENSEMBLE

In this Chapter <sup>1</sup>, the efficiency of frequency up and down conversion of light in an atomic ensemble, with a diamond level configuration, is analyzed theoretically. The conditions of pump field intensities and detunings required to maximize the conversion as a function of optical thickness of the ensemble are determined. The influence of the probe pulse duration on the conversion efficiency is investigated by the numeric solution of the Maxwell-Bloch equations. The set of equations are similar to those in Chapter 4, but a c-number version of the interaction is considered here. The properties of absorption and dispersion of fields are extracted from the steady state solutions to demonstrate the parametric coupling between the fields. We will show that, in calculating conversion efficiency, a quantum version of the equation including Langevin noises is equivalent to the c-number one. Frequency conversion provides the bridge for transmitted qubit (telecommunication wavelength) and local quantum memory (near-infrared light), in which a large scale quantum communication can be fulfilled.

In Section II, we discuss the four-wave mixing process and present solutions for the up- and down- converted fields. The dressed state picture is used as a guide to understand the characteristic features of the absorption and signal-idler field coupling. In Section III, we present the results of an optimization in conversion efficiency as a function of the optical depth of the atomic ensemble. In Section IV, we investigate

---

<sup>1</sup>This Chapter is based on reference [100].

the effects of a finite pulse duration by numerically integrating the Maxwell-Bloch equations. Section V demonstrates the results of Langevin noise correlations and we conclude in Section VI. The derivations of the Maxwell-Bloch and parametric equations are relegated to the Appendix D.

## 6.1 *Introduction*

The frequency conversion of light fields has been an important theme in optical physics for around half a century. In quantum information physics the conversion of single photons to and from the telecom wavelength band is a topic of more recent vintage, and is motivated by the desire to minimize optical fiber transmission losses when distributing entangled states over distant quantum memory elements in a quantum repeater [4].

An associated technical problem is that telecom light is not readily stored in ground level atomic memory coherences. Retrieval processes in atomic ensembles, for example using electromagnetically induced transparency [101], or more specifically the dark-polariton mechanism [102, 103], generate shorter wavelength radiation correlated to the stored atomic excitation by Raman scattering. Such radiation, optically resonant to the ground level of typical atoms and ions, has been retrieved in numerous experiments [7, 8, 10, 9, 11, 13, 14, 15, 104, 105]. An important advance would involve generation of atomic memory coherences quantum-correlated with telecom wavelength radiation, thereby minimizing transmission losses over long distances. Recently there has been a breakthrough in this direction using a pair of cold, non-degenerate rubidium gas samples [25]. The stored excitation is correlated with an infra-red field (idler) in one gas sample, and the idler is then frequency converted to a telecom wavelength signal field in the other ensemble. The frequency conversion mechanism involves the diamond configuration of atomic levels shown in Figure 6.1.

In a probabilistic protocol it is important to maximize all efficiencies, e.g., fiber

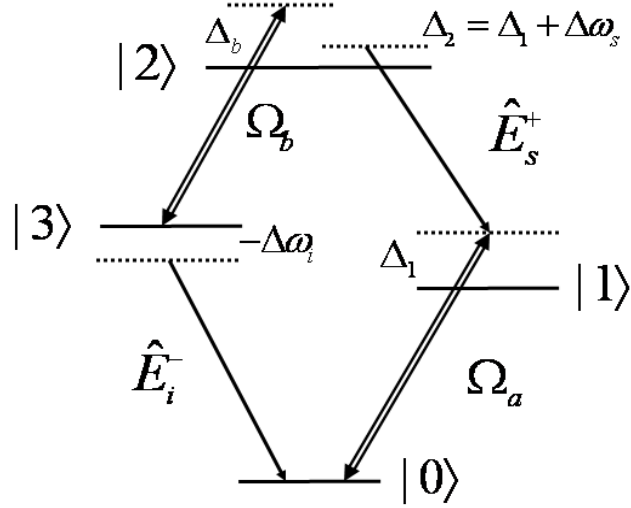


**Figure 6.1:** The diamond configuration of atomic system for conversion scheme. Two pump lasers (double line) with Rabi frequencies  $\Omega_a, \Omega_b$  and propagated probe fields (single line)  $E_s^+, E_i^+$  interact with the atomic medium. Various detunings are defined in the Appendix D, and the atomic levels used in the experiment [25] are  $(|0\rangle, |1\rangle, |2\rangle, |3\rangle) = (|5S_{1/2}, F = 1\rangle, |5P_{3/2}, F = 2\rangle, |6S_{1/2}, F = 1\rangle, |5P_{1/2}, F = 2\rangle)$ .

transmission, single-photon detection, and quantum memory lifetime [106]. In the present work we investigate the efficiency of frequency up- and down- conversion in the diamond atomic configuration [16, 107], as a function of the ensemble's optical thickness, and the intensity and detuning of the pump fields involved in the near-resonant, four-wave mixing process.

## 6.2 Theory

We consider a cold and cigar-shaped  $^{87}\text{Rb}$  atomic ensemble with co-propagating light fields similar to the experimental setup in the reference [25].

The conversion scheme shown in Figure 6.1 involves two pump lasers with frequencies  $\omega_a$  and  $\omega_b$ , respectively; their Rabi frequencies are given by  $\Omega_a$  and  $\Omega_b$ . Two

weak probe fields, signal and idler, with frequency  $\omega_s$  and  $\omega_i$ , respectively, propagate through the optically thick atomic medium. Unlike the cascade driving scheme, where two-photon excitation generates a photon pair spontaneously [16], pump laser b experiences a transparent medium if both the signal and idler fields are in the vacuum state. With an incident signal field, four-wave mixing with the pumps generates an up-converted idler field, while an incident idler field generates a down-converted signal.

The Maxwell-Bloch equations for the interacting system of light and four light fields is derived in the Appendix D. By linearizing the equations with respect to the signal and idler field amplitudes, and adiabatically eliminating the atoms, one arrives at coupled parametric equations for the signal and idler fields. We discuss their solution in this section, and leave numerical solutions of the Maxwell Bloch equations to Section IV.

The calculation of conversion efficiencies can also be carried out with the quantized Heisenberg-Langevin version of the coupled parametric equations, which we will show in Section V. The resulting conversion efficiencies are identical to the semiclassical treatment; the additional quantum noise contributions vanish as the  $|2\rangle \rightarrow |3\rangle$  transition driven by pump laser b has vanishing populations and atomic coherence. A similar simplification occurs in the calculation of the storage efficiency of spin waves in a system of atoms in the  $\Lambda$  configuration [108, 109].

The co-moving propagation equation for c-number signal and idler fields (respectively,  $E_s^+$  and  $E_i^+$ ) under energy conservation ( $\Delta\omega = \omega_a + \omega_s - \omega_b - \omega_i = 0$ ) and four-wave mixing conditions ( $\Delta k = k_a - k_s + k_b - k_i = 0$ ) are

$$\begin{aligned}\frac{\partial}{\partial z} E_s^+ &= \beta_s E_s^+ + \kappa_s E_i^+ \\ \frac{\partial}{\partial z} E_i^+ &= \kappa_i E_s^+ + \alpha_i E_i^+.\end{aligned}\tag{6.1}$$

The coupled equations are similar to those found for the double  $\Lambda$  system [110, 111]. The self-coupling coefficients  $\beta_s, \alpha_i$  and parametric coefficients  $\kappa_s, \kappa_i$  are defined in Appendix D. The set of equations can be simplified as

$$\frac{\partial}{\partial z}x(z) = Ax \quad (6.2)$$

where

$$x = \begin{pmatrix} E_s^+ \\ E_i^+ \end{pmatrix}, A = \begin{pmatrix} \beta_s & \kappa_s \\ \kappa_i & \alpha_i \end{pmatrix}. \quad (6.3)$$

The equations are solved by considering a similarity transformation  $S$  that  $\Lambda = S^{-1}AS$  is diagonalized and  $y = S^{-1}x$  such that

$$\frac{\partial}{\partial z}y = \Lambda y \quad (6.4)$$

$$y(z) = e^{\Lambda(z-z_0)}y(z_0) \quad (6.5)$$

where  $y(z_0)$  is the boundary condition. With the known boundary condition  $x_1(0)$  and  $x_2(0)$  where we choose the input face of propagation as  $z_0 = 0$ , we have

$$x(z) = Se^{\Lambda z}S^{-1}x(0). \quad (6.6)$$

And the diagonalized and transformation matrix are

$$\Lambda = \begin{pmatrix} (\alpha_i + \beta_s)/2 + w & 0 \\ 0 & (\alpha_i + \beta_s)/2 - w \end{pmatrix}, \quad (6.7)$$

$$S = \begin{pmatrix} q + w & \kappa_s \\ \kappa_i & -q - w \end{pmatrix}, \quad (6.8)$$

$$S^{-1} = \frac{1}{2w(w+q)} \begin{pmatrix} q + w & \kappa_s \\ \kappa_i & -q - w \end{pmatrix} \quad (6.9)$$

where  $w \equiv \sqrt{q^2 + \kappa_s \kappa_i}$ , and  $q \equiv (-\alpha_i + \beta_s)/2$ .

The solution of fields from down conversion is

$$\begin{bmatrix} E_s^+(L) \\ E_i^+(L) \end{bmatrix} = S e^{\Lambda L} S^{-1} \begin{bmatrix} 0 \\ E_i^+(0) \end{bmatrix} = \frac{E_i^+(0) e^{(\alpha_i + \beta_s)L/2}}{2w} \begin{bmatrix} \kappa_s (e^{wL} - e^{-wL}) \\ \frac{1}{(w+q)} [\kappa_s \kappa_i e^{wL} + (q+w)^2 e^{-wL}] \end{bmatrix}. \quad (6.10)$$

Similarly, the solution of fields from up conversion is

$$\begin{bmatrix} E_s^+(L) \\ E_i^+(L) \end{bmatrix} = S e^{\Lambda L} S^{-1} \begin{bmatrix} E_s^+(0) \\ 0 \end{bmatrix} = \frac{E_s^+(0) e^{(\alpha_i + \beta_s)L/2}}{2w} \begin{bmatrix} \frac{1}{(w+q)} [(q+w)^2 e^{wL} + \kappa_s \kappa_i e^{-wL}] \\ \kappa_i (e^{wL} - e^{-wL}) \end{bmatrix}. \quad (6.11)$$

We define the down conversion efficiency  $\eta_d$  and transmission of input idler field  $T_d$  as

$$\eta_d = \left| \frac{E_s^+(L)}{E_i^+(0)} \right|^2 = \left| \frac{\kappa_s}{2w} e^{(\alpha_i + \beta_s)L/2} (e^{wL} - e^{-wL}) \right|^2 \quad (6.12)$$

$$T_d = \left| \frac{E_i^+(L)}{E_i^+(0)} \right|^2 = \left| \frac{e^{(\alpha_i + \beta_s)L/2}}{2w(w+q)} [\kappa_s \kappa_i e^{wL} + (q+w)^2 e^{-wL}] \right|^2. \quad (6.13)$$

Similarly the up conversion efficiency  $\eta_u$  and transmission of input signal field  $T_u$  is

$$\eta_u = \left| \frac{E_i^+(L)}{E_s^+(0)} \right|^2 = \left| \frac{\kappa_i}{2w} e^{(\alpha_i + \beta_s)L/2} (e^{wL} - e^{-wL}) \right|^2 \quad (6.14)$$

$$T_u = \left| \frac{E_s^+(L)}{E_s^+(0)} \right|^2 = \left| \frac{e^{(\alpha_i + \beta_s)L/2}}{2w(w+q)} [(q+w)^2 e^{wL} + \kappa_s \kappa_i e^{-wL}] \right|^2. \quad (6.15)$$

The above is the central result of this section. The up and down conversion efficiencies differ only in the parametric coupling coefficients  $\kappa_i$  and  $\kappa_s$ . In the strong parametric coupling regime where  $|\kappa_i|, |\kappa_s| \gg |\alpha_i|, |\beta_s|$ , the coefficients can be simplified to  $\eta_u \simeq \sqrt{\frac{\kappa_i}{\kappa_s}} \sinh(\sqrt{\kappa_s \kappa_i} L)$ ,  $\eta_d \simeq \sqrt{\frac{\kappa_s}{\kappa_i}} \sinh(\sqrt{\kappa_s \kappa_i} L)$  and  $T_u = T_d \simeq$



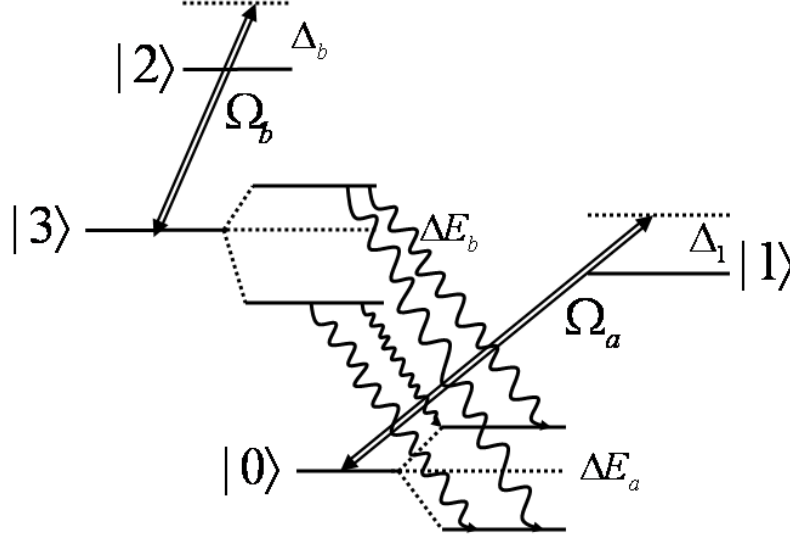


**Figure 6.2:** Dressed-state picture from the perspective of the probe idler transition between atomic levels  $|0\rangle$  and  $|3\rangle$ . Two strong fields  $\Omega_a, \Omega_b$  shift the levels with energy  $\Delta E_{a,b}$  and wavy lines represent the idler field resonances.

$\cosh(\sqrt{\kappa_s \kappa_i} L)$ . Under the further assumptions  $\alpha_i = \beta_s = 0$  and  $\kappa_i, \kappa_s$  are pure imaginary, we find  $\eta_u = \eta_d = \sin^2[\text{Im}(\kappa_s L)]$  and  $T_u = T_d = \cos^2[\text{Im}(\kappa_s L)]$ . This result was recently derived by Gogyan using a dressed state approach [112], in the case of resonant pump fields  $\Delta_1 = \Delta_b = 0$  [113]. In this ideal limit there is a conservation condition  $\eta_u + T_u = \eta_d + T_d = 1$ . The parametric coupling coefficients are not identical, but in the regime of strong coupling they approach each other. As noted by Gogyan, when the pump-a intensity is large ( $\Omega_a \gg |\Delta_1|, \gamma_{03}$ ) the  $|0\rangle \leftrightarrow |1\rangle$  is saturated, the atomic coherence is negligible and  $\kappa_s \approx \kappa_i \propto \tilde{\sigma}_{00,s}(\frac{\Omega_a^* \Omega_b}{T_{02}} + \frac{\Omega_a^* \Omega_b}{T_{13}})$ . Alternatively, in the limit  $\Omega_b \gg \Omega_a, \gamma_{32}$  and  $|\Delta_1| \gg \gamma_{01}$  the atomic coherence of  $|0\rangle \leftrightarrow |1\rangle$  dominates and once again  $\kappa_s \approx \kappa_i \propto \frac{i\Omega_b |\Omega_b|^2 \tilde{\sigma}_{01,s}^\dagger}{T_{13} T_{02}}$ . Note that this scheme is also similar to the frequency conversion in nonlinear materials [114].

The ac-Stark splitting induced by the pump lasers shifts the resonant absorption condition for the idler and signal fields. The idler and signal experience resonant absorption at the transition frequency of the dressed atom. The corresponding transitions for the idler are shown in Figure 6.2. The bare states are shifted by  $\Delta E_a = \left| \Delta_1 \pm \sqrt{\Delta_1^2 + 4\Omega_a^2} \right| / 2$  and  $\Delta E_b = \left| \Delta_b \pm \sqrt{\Delta_b^2 + 4\Omega_b^2} \right| / 2$ , respectively. Note that our Rabi frequencies are smaller by a factor 2 than the standard definitions to avoid a plethora of prefactors in the equations of the Appendix.

For resonant pump fields,  $\Delta E_{a,b} = \pm\Omega_{a,b}$ . The idler transition resonances are at  $\Delta\omega_i = -(\Omega_a + \Omega_b)$ ,  $-|\Omega_a - \Omega_b|$ ,  $|\Omega_a - \Omega_b|$ ,  $(\Omega_a + \Omega_b)$  and these delineate three windows separated by these four absorption peaks. For  $\Omega_a > \Omega_b$  the centers of these windows are at  $-\Omega_a$ , 0, and  $\Omega_a$ , respectively. Choosing the idler detuning  $\Delta\omega_i = \pm\Omega_a$  as in Ref. [113], the idler interacts with the atomic medium at the center of the left or right window.

As an example of the strong coupling windows created by intense pump lasers, we show in Figure 6.3 the self and cross coupling coefficients for the signal and idler fields as a function of the idler frequency. Note that the corresponding frequency of signal field is determined by  $\Delta\omega_s = \Delta\omega_i - \Delta_1 + \Delta_b$ . The dimensionless quantities  $\alpha_i L$ ,  $\beta_s L$  and  $\kappa_s L$  are shown under the conditions of maximum conversion efficiency to be discussed in the next section. We choose the optical depth (opd)  $\rho\sigma L = 150$  where  $\rho$  is the number density,  $\sigma \equiv 3\lambda^2/(4\pi)$  the resonant absorption cross-section, and  $L$  the atomic ensemble length in the propagation direction. Three parametric coupling windows are separated by two strong absorption peaks on the left and two relatively weak ones on the right. The imaginary part of the self-coupling coefficients are seen to vanish in each window at a certain point, while the real parts are small away from resonances. At the same time the cross-coupling coefficients have a large imaginary part. The positive gradient of  $\Im(\beta_s L)$  and  $\Im(\alpha_i L)$  inside the windows is indicative of normal dispersion.

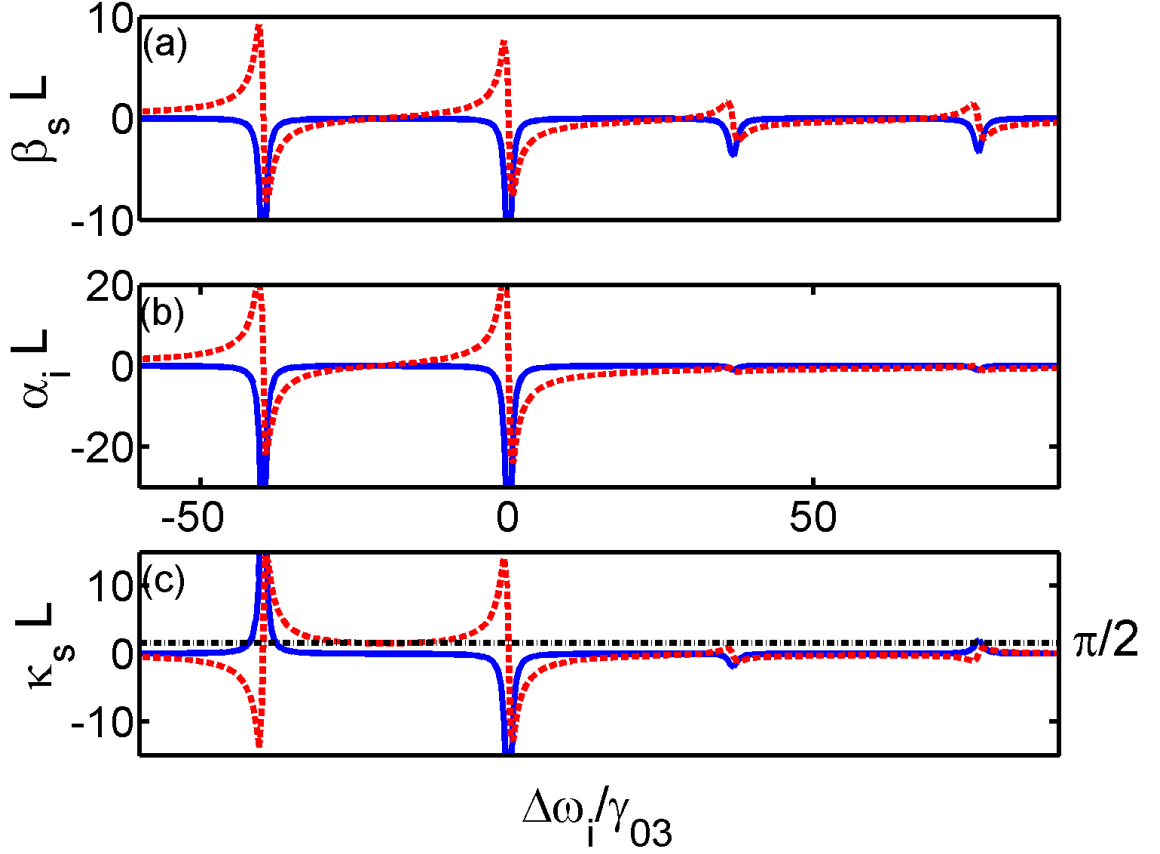


**Figure 6.3:** Self-coupling coefficients  $\beta_s, \alpha_i$  and cross-coupling coefficient  $\kappa_s$ . Dimensionless quantities (a)  $\beta_s L$ , (b)  $\alpha_i L$  and (c)  $\kappa_s L$  with real (solid blue) and imaginary (dashed red) parts are plotted as a dependence of idler detuning  $\Delta\omega_i$  [same label in (b)] showing four absorption peaks to construct three parametric coupling windows. A black dashed-dot line of the constant  $\pi/2$  is added in (c) to demonstrate the crossover with  $\Im(\kappa_s L)$  indicating the ideal conversion efficiency condition in the left window. The parameters we use are  $(\Omega_a, \Omega_b, \Delta_1, \Delta_b, \Delta\omega_i) = (33, 20, 39, 2, -21)\gamma_{03}$  for optical depth  $\rho\sigma L = 150$  with  $L = 6\text{mm}$ . Various natural decay rates are  $\gamma_{03} = 1/27.7\text{ns}$ ,  $\gamma_{01} = 1/26.24\text{ns}$ ,  $\gamma_{12} = \gamma_{03}/2.76$ , and  $\gamma_{32} = \gamma_{03}/5.38$  [97].

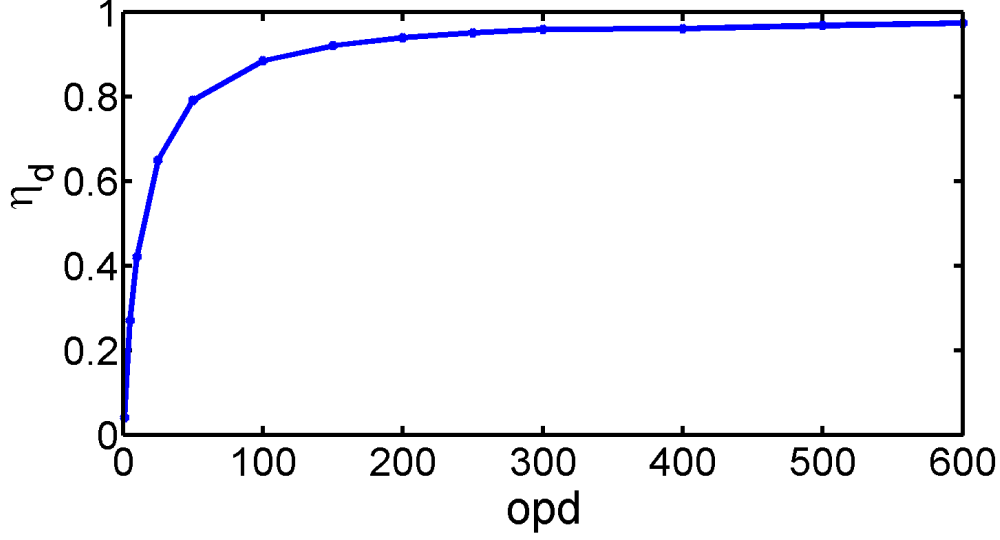


**Figure 6.4:** Down conversion efficiency  $\eta_d$  vs optical depth (opd) from 1 to 600. Each dotted point is the maximum for five variational parameters  $\Omega_a$ ,  $\Omega_b$ ,  $\Delta_1$ ,  $\Delta_b$ , and  $\Delta\omega_i$ .

### 6.3 Optimal Conversion Efficiency

It is important to ascertain the parameters that allow maximum efficiency of conversion due its potential in practical quantum information processing. In principle we need to search the three parametric coupling windows to find the optimum conditions for an atomic ensemble of a given optical thickness.

In the previous section we have discussed how three parametric coupling windows appear for some particular values of pump laser parameters. In the search for the maximal conversion efficiency, five parameters  $\Omega_a$ ,  $\Omega_b$ ,  $\Delta_1$ ,  $\Delta_b$ , and  $\Delta\omega_i$  are varied to maximize the conversion efficiency for a fixed optical depth of atomic ensemble, using functional optimization.

The optical depth  $\rho\sigma L$  appears through the dependence on atomic number  $N$  in the Arecchi-Courtens cooperation time  $T_c$  [115]

$$T_c^{-2} \equiv N|g_i|^2 = \frac{\gamma_{03}c}{2L} \rho\sigma L.$$

In Figure 6.4, we show the maximum of down conversion efficiency using Eq. (6.12) for different optical depths from 1 to 600. The maximum is found by varying five parameters mentioned above and the conversion efficiency reaches 100% asymptotically when the optical depth becomes larger. In the strong parametric coupling regime as we discussed in the previous section,  $\eta_d \simeq \sin^2[\text{Im}(\kappa_s L)]$  and it has a maximum when  $\text{Im}(\kappa_s L) = \frac{\pi}{2}$ , see Figure 6.3. Since  $\text{Im}(\kappa_s L)$  is proportional to optical depth and inversely proportional to the Rabi frequencies of the driving lasers, an order of magnitude estimate of the optical depth necessary for near unit conversion efficiency is  $\text{opd} \simeq \frac{\pi}{2} \Omega_{a,b} / \gamma_{03} \gg 1$ .

The behavior of the cross-coupling coefficient  $\text{Im}(\kappa_s L)$  as a function of idler detuning indicates where large conversion is to be found, as a comparison with Figure 6.5 shows. The maximum efficiency of about 0.92 is located in the left parametric coupling window at the intersection of  $\text{Im}(\kappa_s L)$  and  $\frac{\pi}{2}$ . Inside the windows the trade-off between conversion and transmission is clear. In the region where absorption is large, on the sides of the window (especially for the left window), the efficiency and the transmission are both low although the valley in conversion efficiency corresponds to a peak in transmission as expected in parametric coupling. The transmission approaches unity when the incident idler field is far off-resonance.

We note that the symmetry  $(\Delta_1, \Delta_b, \Delta\omega_i) \rightarrow -(\Delta_1, \Delta_b, \Delta\omega_i)$  gives degenerate optimal conversion conditions.

Moreover, for the region where absorption is large on the sides of the window (especially for the left window), the efficiency and the transmission are both low but the valley of efficiency corresponds to a peak for transmission indicating the feature of parametric coupling. The plateau for efficiency in absorption region can

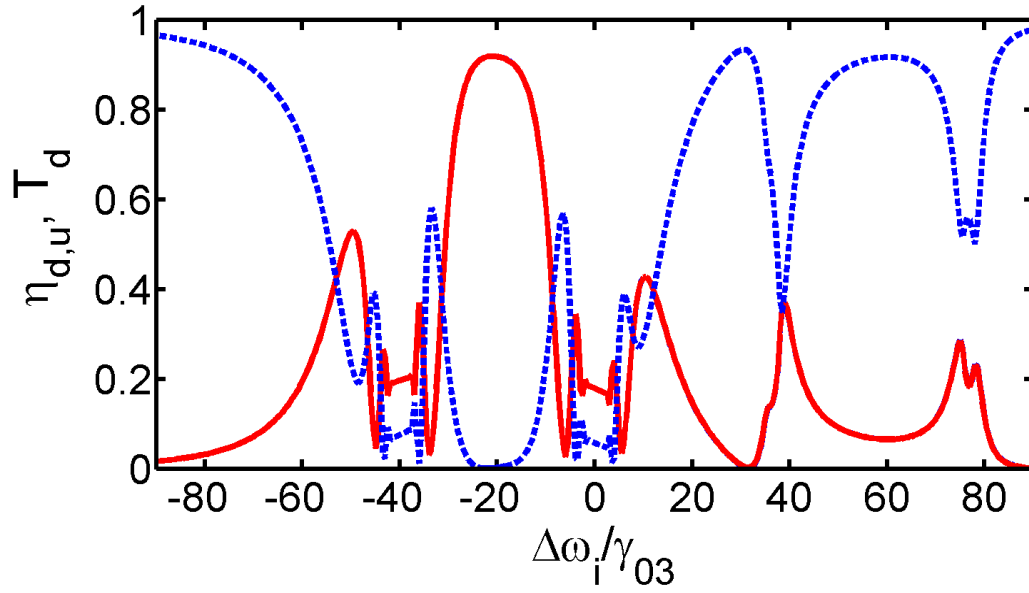


**Figure 6.5:** Conversion efficiency  $\eta_d$ ,  $\eta_u$  and transmission  $T_d$  vs  $\Delta\omega_i$  for  $\text{opd}=150$ .  $\eta_d$  and  $\eta_u$  are indistinguishable and shown in solid red line, and  $T_d$  is in dashed blue line. High transmission efficiency corresponds to low conversion efficiency indicating the approximate conservation condition within each parametric coupling window. The maximum conversion efficiency is found in the left window at around  $\Delta\omega_i = -20\gamma_{03}$  and other relevant parameters are the same as in Figure 6.3.

be estimated as  $\eta_d \approx \left| \frac{\kappa_s}{2w} \right|^2$  where  $\alpha_i \beta_s \approx \kappa_s \kappa_i$ . Based on the study of finding the maximum efficiency for frequency conversion, we will investigate the situation when the input is a pulse and numerical integration of full equation of motion is required in the next section.

## ***6.4 Pulse Conversion: Solution of the Maxwell-Bloch Equations***

The effect of finite-duration input probe pulses, which are often employed in practice, can be assessed by numerically solving the Maxwell-Bloch equations for the coupled atoms-fields system. The characteristic scales of time and length are given by the Arecchi-Courtens time  $T_c$  and  $L_c = cT_c$ , respectively, which are inversely proportional to the square root of the opd. The cooperative electric field is the product of the atomic number and the idler electric field per photon, i.e.,  $E_c = \sqrt{\rho \hbar \omega_i / (2\epsilon_0)}$ .

Scaling the space, time, electric field amplitude, various detunings, and natural decay rates accordingly, indicated by tildes, the Maxwell-Bloch equations of Eqs. (D.4,D.6,D.7) under energy conservation ( $\Delta\omega = \omega_a + \omega_s - \omega_b - \omega_i = 0$ ) and four-wave

mixing conditions ( $\Delta k = k_a - k_s + k_b - k_i = 0$ ) become

$$\begin{aligned}
\frac{\partial}{\partial \tilde{\tau}} \tilde{\sigma}_{01} &= (i\tilde{\Delta}_1 - \frac{\tilde{\gamma}_{01}}{2})\tilde{\sigma}_{01} + i\tilde{\Omega}_a(\tilde{\sigma}_{00} - \tilde{\sigma}_{11}) + i\tilde{\sigma}_{02}\tilde{E}_s^- - i\tilde{\sigma}_{13}^\dagger\tilde{E}_i^+, \\
\frac{\partial}{\partial \tilde{\tau}} \tilde{\sigma}_{12} &= (i\Delta\tilde{\omega}_s - \frac{\tilde{\gamma}_{01} + \tilde{\gamma}_2}{2})\tilde{\sigma}_{12} - i\tilde{\Omega}_a^*\tilde{\sigma}_{02} + i(\tilde{\sigma}_{11} - \tilde{\sigma}_{22})\tilde{E}_s^+ + i\tilde{\Omega}_b\tilde{\sigma}_{13}, \\
\frac{\partial}{\partial \tilde{\tau}} \tilde{\sigma}_{02} &= (i\tilde{\Delta}_2 - \frac{\tilde{\gamma}_2}{2})\tilde{\sigma}_{02} - i\tilde{\sigma}_{12}\tilde{\Omega}_a + i\tilde{\sigma}_{01}\tilde{E}_s^+ + i\tilde{\sigma}_{03}\tilde{\Omega}_b - i\tilde{\sigma}_{32}\tilde{E}_i^+, \\
\frac{\partial}{\partial \tilde{\tau}} \tilde{\sigma}_{11} &= -\tilde{\gamma}_{01}\tilde{\sigma}_{11} + \tilde{\gamma}_{12}\tilde{\sigma}_{22} + i\tilde{\Omega}_a\tilde{\sigma}_{01}^\dagger - i\tilde{\Omega}_a^*\tilde{\sigma}_{01} - i\tilde{\sigma}_{12}^\dagger\tilde{E}_s^+ + i\tilde{\sigma}_{12}\tilde{E}_s^-, \\
\frac{\partial}{\partial \tilde{\tau}} \tilde{\sigma}_{22} &= -\tilde{\gamma}_2\tilde{\sigma}_{22} + i\tilde{\sigma}_{12}^\dagger\tilde{E}_s^+ - i\tilde{\sigma}_{12}\tilde{E}_s^- + i\tilde{\Omega}_b\tilde{\sigma}_{32}^\dagger - i\tilde{\Omega}_b^*\tilde{\sigma}_{32}, \\
\frac{\partial}{\partial \tilde{\tau}} \tilde{\sigma}_{33} &= -\tilde{\gamma}_{03}\tilde{\sigma}_{33} + \tilde{\gamma}_{32}\tilde{\sigma}_{22} - i\tilde{\Omega}_b\tilde{\sigma}_{32}^\dagger + i\tilde{\Omega}_b^*\tilde{\sigma}_{32} + i\tilde{\sigma}_{03}^\dagger\tilde{E}_i^+ - i\tilde{\sigma}_{03}\tilde{E}_i^-, \\
\frac{\partial}{\partial \tilde{\tau}} \tilde{\sigma}_{13} &= (i\Delta\tilde{\omega}_i - i\tilde{\Delta}_1 - \frac{\tilde{\gamma}_{01} + \tilde{\gamma}_{03}}{2})\tilde{\sigma}_{13} - i\tilde{\Omega}_a^*\tilde{\sigma}_{03} - i\tilde{\sigma}_{32}^\dagger\tilde{E}_s^+ + i\tilde{\Omega}_b^*\tilde{\sigma}_{12} + i\tilde{\sigma}_{01}^\dagger\tilde{E}_i^+, \\
\frac{\partial}{\partial \tilde{\tau}} \tilde{\sigma}_{03} &= (i\Delta\tilde{\omega}_i - \frac{\tilde{\gamma}_{03}}{2})\tilde{\sigma}_{03} - i\tilde{\Omega}_a\tilde{\sigma}_{13} + i\tilde{\Omega}_b^*\tilde{\sigma}_{02} + i(\tilde{\sigma}_{00} - \tilde{\sigma}_{33})\tilde{E}_i^+, \\
\frac{\partial}{\partial \tilde{\tau}} \tilde{\sigma}_{32}^\dagger &= (-i\tilde{\Delta}_b - \frac{\tilde{\gamma}_{03} + \tilde{\gamma}_2}{2})\tilde{\sigma}_{32}^\dagger - i\tilde{\sigma}_{13}\tilde{E}_s^- + i\tilde{\Omega}_b^*(\tilde{\sigma}_{22} - \tilde{\sigma}_{33}) + i\tilde{\sigma}_{02}^\dagger\tilde{E}_i^+, \tag{6.16}
\end{aligned}$$

and

$$\frac{\partial}{\partial \tilde{z}} \tilde{E}_s^+ = i\tilde{\sigma}_{12} \frac{|g_s|^2}{|g_i|^2}, \quad \frac{\partial}{\partial \tilde{z}} \tilde{E}_i^+ = i\tilde{\sigma}_{03} \tag{6.17}$$

where  $\tilde{z} = z/L_c$ ,  $\tilde{\tau} = \tau/T_c$ ,  $\tilde{\Omega}_{a,b} = \Omega_{a,b}T_c$ ,  $\tilde{E}_{s,i}^+ = E_{s,i}^+/E_c$ , and  $|g_s|^2/|g_i|^2$  is a factor of unit transformation from signal to idler field strength. Natural life time [97] for signal and idler transitions is used to calculate the ratio of coupling strength  $g_s/g_i = 1.035$ . The above equations were integrated with a semi-implicit finite difference method [95]. The midpoint integration method is stable and has high accuracy without sacrificing memory for finer grids [88]. The algorithm has been tested by comparing with the parametric equations' solutions in appropriate limits, and these solutions are recovered when fine enough grids are employed.

To illustrate the influence of finite pump pulse duration, we compute the down conversion efficiency

$$\eta_d = \frac{\int |E_s^+(z=L, \tau)|^2 d\tau}{\int |E_i^+(z=0, \tau)|^2 d\tau}. \tag{6.18}$$

In Figure 6.6, we show the computed values of  $\eta_d$  for two different input idler pulse durations. We fix the  $\text{opd}=150$  and use the near optimum parameters ( $\Omega_a$ ,



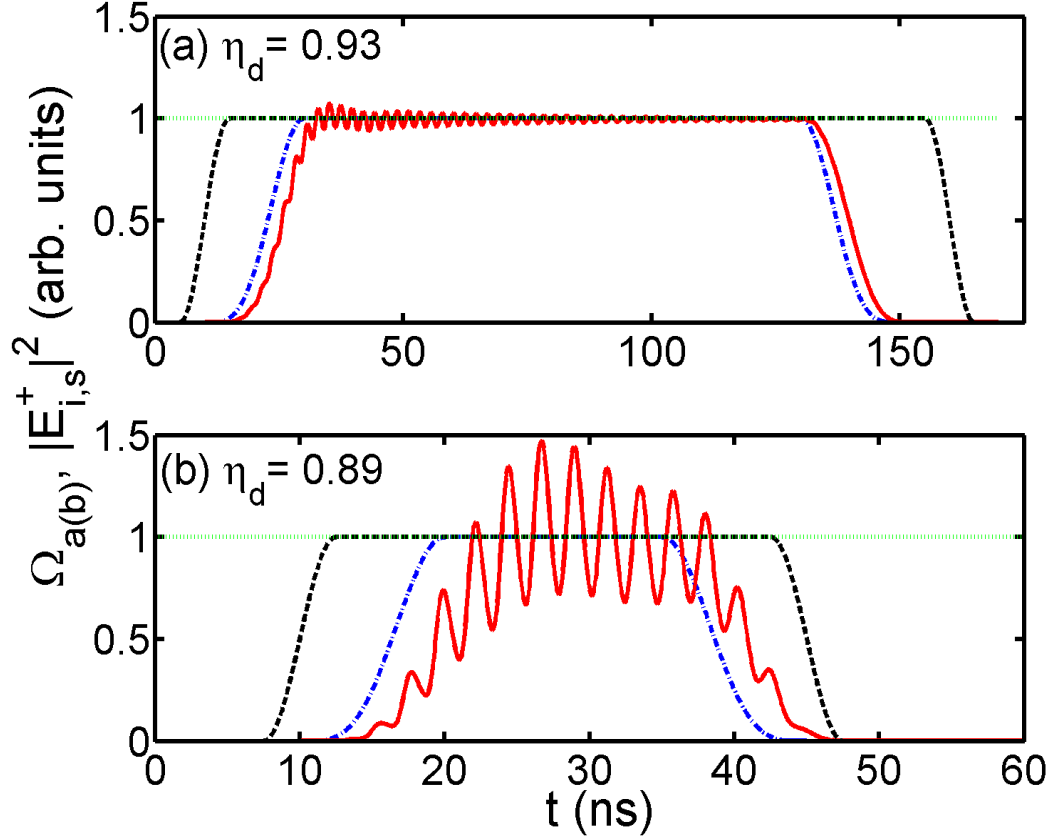


**Figure 6.6:** Time-varying pump fields of Rabi frequencies  $\Omega_{a,b}(t)$  and down-converted signal intensity ( $|E_s^+(t, z = L)|^2$ ) from an input idler pulse ( $|E_i^+(t, z = 0)|^2$ ). Here we let  $t = \tau$  that is the delayed time in co-moving frame. Pump-b (dotted green) is a continuous wave and pump-a (dashed black) is a square pulse long enough to enclose input idler pulse with (a) 100 ns and (b) 15 ns (dashed-dot blue). Output signal intensity (solid red) at the end of atomic ensemble  $z = L$  is oscillatory due to the pump fields. The square pulse in rising region ( $t_r - \frac{t_s}{2} < t < t_r + \frac{t_s}{2}$ ) has the form of  $\frac{1}{2}[1 + \sin(\frac{\pi(t-t_r)}{t_s})]$  that in (a)  $(t_r, t_s) = (10, 10)$  ns for pump-a and  $(t_r, t_s) = (20, 20)$  ns for input idler; (b)  $(t_r, t_s) = (10, 5)$  ns for pump-a and  $(t_r, t_s) = (15, 10)$  ns for input idler where  $t_r$  is the rising time indicating the center of rising period  $t_s$ . Note that the falling region of square pulse is symmetric to the rising one.

$\Omega_b, \Delta_1, \Delta_b, \Delta\omega_i) = (33, 20, 39, 2, -21)\gamma_{03}$  determined from the coupled parametric equations. The temporal shape of the pump laser intensities is also shown. Pump laser b is taken to be continuous wave, while pump a is a square pulse with duration large enough to completely overlap the input idler pulse. To compare with the steady state solutions, we choose the Rabi frequency of idler as  $0.1\gamma_{03}$ , which is small compared to those of the pumps. We find that the conversion efficiency is reduced for shorter idler pulse inputs. A 100 ns idler pulse is long enough that it has **a** almost the same maximum conversion efficiency of 0.92 as in Figure 6.4 for  $\text{opd}=150$ . While for the shorter idler pulse of 15 ns, the signal develops significant temporal modulation, and this reduces the conversion efficiency, although it is still quite appreciable. The modulation frequency is at the generalized Rabi frequency of pump-a  $\sqrt{\Delta_1^2 + 4\Omega_a^2}$ . We note the characteristic time and space scales of the calculations are  $T_c = 0.086$  ns and  $L_c = 26$  mm for a moderate atomic density  $\rho = 1.7 \times 10^{11} \text{cm}^{-3}$  and  $L = 6$  mm. The grid size for dimensionless time  $\Delta\tilde{t} = 0.5$  and space  $\Delta\tilde{z} = 0.001$  were chosen for both 100 and 15 ns idler pulse durations, and the convergence is reached with an estimated relative error less than 1%.

Moreover, we show in Figure 6.7 of three dimensional plots of signal  $|E_s^+(z, t)|^2$  and idler intensities  $|E_i^+(z, t)|^2$ . A 100 ns input idler pulse is demonstrated in time-space propagation which is converted to signal pulse at the output surface of the ensemble.

## 6.5 Discussion of Quantum Fluctuations

In this Section, we derive quantized Heisenberg-Langevin equations by adding corresponding Langevin noises to the coupled equations. Similar to the results of Appendix D, we have

$$\frac{\partial}{\partial z} E_s^+ = \beta_s E_s^+ + \kappa_s E_i^+ + \hat{f}_s, \quad (6.19)$$

$$\frac{\partial}{\partial z} E_i^+ = \kappa_i E_s^+ + \alpha_i E_i^+ + \hat{f}_i \quad (6.20)$$

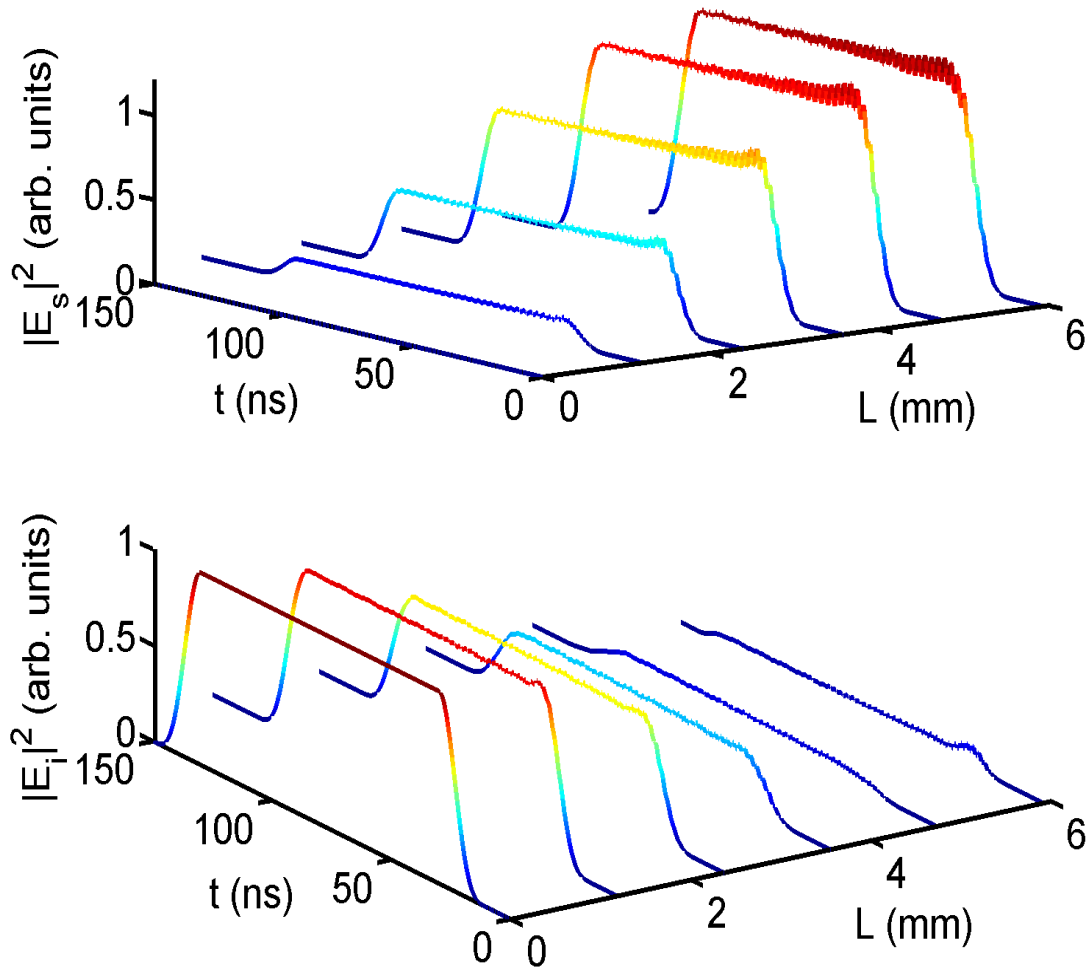


**Figure 6.7:** Three-dimensional line plots of converted signal and input idler intensities in  $t$  (ns) and  $L$  (mm). Here we let  $t = \tau$  that is the delayed time in co-moving frame, and the parameters are the same as in Figure 6.6 (a).

where signal and idler fields (respectively,  $E_s^+$  and  $E_i^+$ ) are now quantized, and Langevin noises ( $\hat{f}_s$  and  $\hat{f}_i$ ) in linearized equations are

$$\begin{aligned}\hat{f}_s = & \frac{iNg_s^*}{cD}[(T_{03} + \frac{|\Omega_a|^2}{T_{13}} + \frac{|\Omega_b|^2}{T_{02}})\tilde{\mathcal{F}}_{12} + (\frac{\Omega_a^*\Omega_b}{T_{02}} + \frac{\Omega_a^*\Omega_b}{T_{13}})\tilde{\mathcal{F}}_{03} \\ & + \frac{i\Omega_b}{T_{13}}(T_{03} + \frac{|\Omega_b|^2 - |\Omega_a|^2}{T_{02}})\tilde{\mathcal{F}}_{13} + \frac{i\Omega_a^*}{T_{02}}(-T_{03} + \frac{|\Omega_b|^2 - |\Omega_a|^2}{T_{13}})\tilde{\mathcal{F}}_{02}] + \tilde{\mathcal{F}}_s,\end{aligned}\tag{6.21}$$

$$\begin{aligned}\hat{f}_i = & \frac{iNg_i^*}{cD}[(\frac{\Omega_a\Omega_b^*}{T_{02}} + \frac{\Omega_a\Omega_b^*}{T_{13}})\tilde{\mathcal{F}}_{12} + (T_{12} + \frac{|\Omega_a|^2}{T_{02}} + \frac{|\Omega_b|^2}{T_{13}})\tilde{\mathcal{F}}_{03} \\ & + \frac{i\Omega_a}{T_{13}}(-T_{12} + \frac{|\Omega_b|^2 - |\Omega_a|^2}{T_{02}})\tilde{\mathcal{F}}_{13} + \frac{i\Omega_a^*}{T_{02}}(T_{12} + \frac{|\Omega_b|^2 - |\Omega_a|^2}{T_{13}})\tilde{\mathcal{F}}_{02}] + \tilde{\mathcal{F}}_i\end{aligned}\tag{6.22}$$

where various atomic and field Langevin noises  $\tilde{\mathcal{F}}_y$  are associated with coupled equations of atomic operators  $\hat{\sigma}_y$  and field operators  $E_{s,i}^+$  when  $y = s, i$ .

Note that various normal correlation functions of quantum Langevin noises have  $\langle \tilde{\mathcal{F}}_i^\dagger(t, z)\tilde{\mathcal{F}}_j(t', z') \rangle = \frac{L}{N}\delta(t-t')\delta(z-z')\hat{D}_{ij}$  in continuous limit. If ensemble average is taken over the above field equations, with the property of Langevin noises that  $\langle \tilde{\mathcal{F}}_i^\dagger(t, z) \rangle = \langle \tilde{\mathcal{F}}_i(t', z') \rangle = 0$ , the field equations are reduced to c-number ones where fluctuations due to Langevin noises do not matter. For calculation of normally-ordered operators, semi-classical approximation is valid even in quantum regime. We demonstrate in the following and include Langevin noises in derivation of solutions of field operators.

The set of equations can be written as

$$\frac{\partial}{\partial z}x(z) = Ax + f\tag{6.23}$$

where  $x(z) = \begin{bmatrix} E_s^+(z) \\ E_i^+(z) \end{bmatrix}$  and  $f = \begin{bmatrix} \hat{f}_s(z) \\ \hat{f}_i(z) \end{bmatrix}$ .

Consider a similarity transformation  $S$  that  $S^{-1}AS = \Lambda$  and  $y = S^{-1}x$ , then we

have

$$\frac{\partial}{\partial z}y = \Lambda y + S^{-1}f, \quad (6.24)$$

$$y(z) = e^{\Lambda(z-z_0)}y(z_0) + \int_{z_0}^z dz' e^{\Lambda(z-z')}S^{-1}f(z'). \quad (6.25)$$

With the boundary condition  $x_1(0)$  and  $x_2(0)$ , we have

$$x(z) = Se^{\Lambda z}S^{-1}x(0) + \int_0^z dz' Se^{\Lambda(z-z')}S^{-1}f(z'). \quad (6.26)$$

So we have correspondingly

$$\begin{aligned} A &= \begin{pmatrix} \beta_s & \kappa_s \\ \kappa_i & \alpha_i \end{pmatrix}, \quad \Lambda = \begin{pmatrix} (\alpha_i + \beta_s)/2 + w & 0 \\ 0 & (\alpha_i + \beta_s)/2 - w \end{pmatrix} \\ S &= \begin{pmatrix} q + w & \kappa_s \\ \kappa_i & -q - w \end{pmatrix}, \quad S^{-1} = \frac{1}{2w(w+q)} \begin{pmatrix} q + w & \kappa_s \\ \kappa_i & -q - w \end{pmatrix} \end{aligned} \quad (6.27)$$

where  $w \equiv \sqrt{q^2 + \kappa_s \kappa_i}$ , and  $q \equiv (-\alpha_i + \beta_s)/2$ .

The solutions of fields from down conversion for example are

$$\begin{aligned}
\begin{bmatrix} E_s^+(L) \\ E_i^+(L) \end{bmatrix} &= \begin{bmatrix} q+w & \kappa_s \\ \kappa_i & -q-w \end{bmatrix} \begin{bmatrix} e^{[(\alpha_i+\beta_s)/2+w]L} & 0 \\ 0 & e^{[(\alpha_i+\beta_s)/2-w]L} \end{bmatrix} \frac{1}{2w(w+q)} \times \\
&\quad \begin{bmatrix} q+w & \kappa_s \\ \kappa_i & -q-w \end{bmatrix} \begin{bmatrix} 0 \\ E_i^+(0) \end{bmatrix} \\
&+ \int_0^L dz' S \begin{bmatrix} e^{[(\alpha_i+\beta_s)/2+w](L-z')} & 0 \\ 0 & e^{[(\alpha_i+\beta_s)/2-w](L-z')} \end{bmatrix} S^{-1} f(z'), \\
&= \begin{bmatrix} \frac{\kappa_s}{2w} (e^{[(\alpha_i+\beta_s)/2+w]L} - e^{[(\alpha_i+\beta_s)/2-w]L}) \\ \frac{1}{2w(w+q)} [\kappa_s \kappa_i e^{[(\alpha_i+\beta_s)/2+w]L} + (q+w)^2 e^{[(\alpha_i+\beta_s)/2-w]L}] \end{bmatrix} E_i^+(0) \\
&+ \int_0^L dz' S \begin{bmatrix} e^{[(\alpha_i+\beta_s)/2+w](L-z')} & 0 \\ 0 & e^{[(\alpha_i+\beta_s)/2-w](L-z')} \end{bmatrix} S^{-1} f(z'), \\
&= \begin{bmatrix} \sqrt{\eta_d} e^{i \arg(\sqrt{\eta_d})} \\ \sqrt{T_d} e^{i \arg(\sqrt{T_d})} \end{bmatrix} E_i^+(0) + \int_0^L dz' \begin{bmatrix} \xi_s(z') \hat{f}_s(z') + \xi_i(z') \hat{f}_i(z') \\ \zeta_s(z') \hat{f}_s(z') + \zeta_i(z') \hat{f}_i(z') \end{bmatrix} \quad (6.28)
\end{aligned}$$

where  $\eta_d$  and  $T_d$  are conversion efficiency and transmission for down conversion as derived in Section II,  $\arg$  represents the argument for complex numbers, and we see that extra terms involve Langevin noises.  $\xi_{s,i}$  and  $\zeta_{s,i}$  are defined in the below,

$$\xi_s = \frac{1}{2w(w+q)} [(w+q)^2 e^{[(\alpha_i+\beta_s)/2+w](L-z')} + \kappa_s \kappa_i e^{[(\alpha_i+\beta_s)/2-w](L-z')}], \quad (6.29)$$

$$\xi_i = \frac{\kappa_s}{2w} [e^{[(\alpha_i+\beta_s)/2+w](L-z')} - e^{[(\alpha_i+\beta_s)/2-w](L-z')}], \quad (6.30)$$

$$\zeta_s = \frac{\kappa_i}{2w} [e^{[(\alpha_i+\beta_s)/2+w](L-z')} - e^{[(\alpha_i+\beta_s)/2-w](L-z')}], \quad (6.31)$$

$$\zeta_i = \frac{1}{2w(w+q)} [\kappa_s \kappa_i e^{[(\alpha_i+\beta_s)/2+w](L-z')} + (w+q)^2 e^{[(\alpha_i+\beta_s)/2-w](L-z')}]. \quad (6.32)$$

The down conversion efficiency  $\eta_{\text{down}}$  is defined as

$$\begin{aligned}
\eta_{\text{down}} &= \frac{\langle E_s^-(L) E_s^+(L) \rangle}{\langle E_i^-(0) E_i^+(0) \rangle} \\
&= \eta_d + \frac{1}{\langle E_i^-(0) E_i^+(0) \rangle} \times \\
&\quad \left\langle \int_0^L dz' [\xi_s^*(z') \hat{f}_s^\dagger(z') + \xi_i(z') \hat{f}_i^\dagger(z')] \int_0^L dz'' [\xi_s(z'') \hat{f}_s(z'') + \xi_i(z'') \hat{f}_i(z'')] \right\rangle
\end{aligned} \tag{6.33}$$

in which expectation value of normally-ordered operators involves contributions from semi-classical treatment and normally-ordered noise correlation functions. The relevant normally-ordered quantum diffusion coefficients  $\hat{D}_{ij}$  from Einstein's relation are (note that  $\hat{D}_{ij} = \hat{D}_{ji}^\dagger$ )

$$\begin{aligned}
\text{(i)} \quad \hat{D}_{12,12} &= \gamma_{01} \langle \tilde{\sigma}_{22} \rangle \approx \gamma_{01} \tilde{\sigma}_{22,s} = 0; \\
\hat{D}_{12,03} &= \hat{D}_{12,02} = 0; \\
\hat{D}_{12,13} &= \gamma_{01} \langle \tilde{\sigma}_{23} \rangle \approx \gamma_{01} \tilde{\sigma}_{23,s} = 0; \\
\hat{D}_{12,s} &= \hat{D}_{12,i} = 0;
\end{aligned} \tag{6.34}$$

$$\begin{aligned}
\text{(ii)} \quad \hat{D}_{03,03} &= \gamma_{32} \langle \tilde{\sigma}_{22} \rangle \approx \gamma_{32} \tilde{\sigma}_{22,s} = 0; \\
\hat{D}_{03,02} &= \hat{D}_{03,13} = 0; \\
\hat{D}_{03,s} &= \hat{D}_{03,i} = 0;
\end{aligned} \tag{6.35}$$

$$\begin{aligned}
\text{(iii)} \quad \hat{D}_{02,02} &= \hat{D}_{02,13} = 0; \\
\hat{D}_{02,s} &= \hat{D}_{02,i} = 0;
\end{aligned} \tag{6.36}$$

$$\begin{aligned}
\text{(iV)} \quad \hat{D}_{13,13} &= \gamma_{01} \langle \tilde{\sigma}_{33} \rangle + \gamma_{32} \langle \tilde{\sigma}_{22} \rangle \approx \gamma_{01} \tilde{\sigma}_{33,s} + \gamma_{32} \tilde{\sigma}_{22,s} = 0; \\
\hat{D}_{13,s} &= \hat{D}_{13,i} = 0;
\end{aligned} \tag{6.37}$$

$$\text{(V)} \quad \hat{D}_{s,s} = \hat{D}_{s,i} = 0; \tag{6.38}$$

$$\text{(Vi)} \quad \hat{D}_{i,i} = 0; \tag{6.39}$$

where we have approximated various nonvanishing quantum diffusion coefficients by zeroth order properties of atomic operators (the steady state solutions). The above normally-ordered correlation functions give zero contributions in the linearized equations of motion, so c-number Langevin equation is sufficient to derive the conversion efficiency. The normally-ordered noise correlations are zero because the population ( $\tilde{\sigma}_{22,s}, \tilde{\sigma}_{33,s}$ ) and coherence ( $\tilde{\sigma}_{23,s}$ ) properties are zero for the atomic level driven by pump-b. The linearized field equations in diamond structure have similar noise properties to  $\Lambda$  system in which most atoms are on the ground state, and Langevin noise can be neglected if normally-ordered quantities, say storage efficiency, are considered [108, 109].

## 6.6 Conclusion

We have studied light frequency conversion in an atomic ensemble with a diamond configuration of atomic levels such as  $^{87}\text{Rb}$ . The motivation stems from the need to efficiently convert light resonant with ground state transitions (storable in the sense of quantum memories) to and from the telecom wavelength band for low-loss quantum network communication. The optically thick atomic sample is driven by two strong co-propagating pump fields, and a probe idler or signal field depending on whether we consider down- or up-conversion. Parametric equations for the probe fields are derived and used to compute conversion efficiencies. They can be understood by dressed-state picture where we can visualize four absorption lines due to two strong pump lasers and thus three parametric coupling windows are created. There are two major contributions to the conversion efficiency, which are related to atomic populations and coherences in the lower arm of the diamond level driven by laser pump-a. When this transition is saturated by a large pump Rabi frequency or when the coherence dominates due to a large pump-b Rabi frequency in the upper transition, the cross-coupling coefficients and hence the conversion efficiencies are equal.



By performing a global parameter search we find conditions of pump Rabi frequencies, detunings, and signal/idler input frequency to maximize the conversion efficiency as a function of optical depth of the ensemble. Only in the limit of very large optical depth does the maximum efficiency approach the ideal strong coupling result [113]. Under conditions routinely obtained in cold, non-degenerate rubidium gas, with  $\text{opd} \simeq 100 - 200$ , optimal conversion efficiencies of the order 80% to 90% are predicted. Numerical solution of the Maxwell-Bloch equations confirms the solution of the parametric equations in the limit of long pulse duration, and indicates that for shorter pulses, pump pulse induced modulation may reduce the conversion efficiency.



# CHAPTER VII

## CONCLUSION

We provide a theoretical study of light-matter interactions in cascade and diamond type atomic ensembles. A correlated two-photon (telecom signal-infrared idler) state vector is derived in the long time limit within the adiabatic approximation. The second-order correlation function is calculated, and shows a superradiant time scale in the infrared idler emission. The entanglement in frequency space for such a two-photon state is analyzed by Schmidt decomposition. We are able to derive the mode functions and investigate the influence of pump pulse duration and superradiant decay rate that depends on optical density and ensemble geometry.

To investigate multiple atomic excitations on the correlated emission from the atomic cascade transitions, we use the coherent state positive-P representation and derive an equivalent Ito type stochastic differential equation (SDE). The equations are solved numerically by a stable and convergent semi-implicit difference method, while the counter-propagating spatial evolution is solved by implementing the shooting method. We find an enhanced characteristic time scale for idler emission in the second-order correlation functions, consistent with the superradiance timescales predicted by the analytical method in Chapter 3, and observed experimentally.

In Chapter 5, the correlated two-photon state derived in Chapter 3 is used to investigate the spectral effects on DLCZ protocols involving entanglement generation, swapping, and quantum teleportation. We analyze the performance of the protocol using, photon-number resolving and non-resolving photon detectors. We find that a more genuine and high fidelity protocol requires a source with reduced frequency space entanglement.

In Chapter 6, we present the analytical results on the efficiency of light-frequency conversion in a diamond atomic configuration. We find the optimum efficiency as a function of optical density. We find the maximum conversion efficiency by studying parametric coupling windows that are created by strong pump fields, and provide numerical solutions for the pulse conversion.

## APPENDIX A

# DERIVATION OF A SCHRÖDINGER WAVE EQUATION FOR SPONTANEOUS EMISSIONS FROM A CASCADE TYPE ATOMIC ENSEMBLE

In this appendix, we derive the Hamiltonian for the cascade emission (signal-idler) from a four-level atomic ensemble. We use Schrödinger's equation to study the correlated two-photon state from a two-photon laser excitation. Apart from the rotating wave approximation, non-rotating wave probability amplitudes are introduced to take into account the proper frequency shift. The adiabatic approximation on laser-excited states is used to simplify the atomic dynamics and solve for the signal-idler probability amplitude.

### ***A.1 Hamiltonian and Equation of Motion***

Consider an ensemble of  $N$  four-level atoms interacting with two classical fields and spontaneously emitted signal and idler photons as shown in Figure 3.3. These identical atoms distribute randomly with a uniform density. Use dipole approximation of light-matter interactions,  $-\vec{d} \cdot \vec{E}$  where  $\vec{E}$  is classical or quantum electric field, and include non-rotating wave approximation (RWA) terms in the interaction of quantum fields, the Hamiltonian in interaction picture is

$$\begin{aligned}
V_I(t) = & -\hbar\Delta_1 \sum_{\mu=1}^N |1\rangle_\mu \langle 1| - \hbar\Delta_2 \sum_{\mu=1}^N |2\rangle_\mu \langle 2| - \frac{\hbar}{2} \sum_{\mu=1}^N \left[ \Omega_a |1\rangle_\mu \langle 0| e^{i\vec{k}_a \cdot \vec{r}_\mu} + \Omega_b |2\rangle_\mu \langle 1| e^{i\vec{k}_b \cdot \vec{r}_\mu} \right. \\
& \left. + h.c. \right] - i\hbar \sum_{k_s, \lambda_s} g_{k_s} \left[ \vec{\epsilon}_{k_s, \lambda_s} \hat{a}_{k_s, \lambda_s} e^{-i\omega_{k_s} t + i\vec{k}_s \cdot \vec{r}_\mu} - \vec{\epsilon}_{k_s, \lambda_s}^* \hat{a}_{k_s, \lambda_s}^\dagger e^{i\omega_{k_s} t - i\vec{k}_s \cdot \vec{r}_\mu} \right] \cdot \hat{d}_s \sum_{\mu=1}^N \\
& \left[ |2\rangle_\mu \langle 3| e^{i(\omega_{23} + \Delta_2)t} + |3\rangle_\mu \langle 2| e^{-i(\omega_{23} + \Delta_2)t} \right] - i\hbar \sum_{k_i, \lambda_i} g_{k_i} \left[ \vec{\epsilon}_{k_i, \lambda_i} \hat{a}_{k_i, \lambda_i} e^{-i\omega_{k_i} t + i\vec{k}_i \cdot \vec{r}_\mu} - \right. \\
& \left. \vec{\epsilon}_{k_i, \lambda_i}^* \hat{a}_{k_i, \lambda_i}^\dagger e^{i\omega_{k_i} t - i\vec{k}_i \cdot \vec{r}_\mu} \right] \cdot \hat{d}_i \sum_{\mu=1}^N \left[ |3\rangle_\mu \langle 0| e^{i\omega_3 t} + |0\rangle_\mu \langle 3| e^{-i\omega_3 t} \right], \tag{A.1}
\end{aligned}$$

where the time dependence of laser frequency is absorbed into interaction terms of signal and idler fields. Single photon detuning  $\Delta_1 = \omega_a - \omega_1$ , two-photon detuning  $\Delta_2 = \omega_a + \omega_b - \omega_2$ , and  $\omega_{23} = \omega_2 - \omega_3$ . Rabi frequencies are  $\Omega_a \equiv (1|\hat{d}|0)\mathcal{E}(k_a)/\hbar$ ,  $\Omega_b \equiv (2|\hat{d}|1)\mathcal{E}(k_b)/\hbar$ , and coupling coefficients are  $g_{k_s} \equiv (3|\hat{d}|2)\mathcal{E}(k_s)/\hbar$ ,  $g_{k_i} \equiv (0|\hat{d}|3)\mathcal{E}(k_i)/\hbar$ . The double matrix element of the dipole moment is independent of the hyperfine structure, and  $\mathcal{E}(k) = \sqrt{\frac{\hbar k c}{2\epsilon_0 V}}$ . Polarizations of signal and idler fields are  $\vec{\epsilon}_{k_s, \lambda_s}$ ,  $\vec{\epsilon}_{k_i, \lambda_i}$ , and the unit direction of dipole operators are  $\hat{d}_s$ ,  $\hat{d}_i$ .

In the limit of large detuned and weak driving fields,  $\Delta_1 \gg \frac{\sqrt{N}\Omega_a}{2}$ , that is discussed in Chapter 3.2, we consider only single excitations and ignore the spontaneous decay during the excitation process. The state function can be written as

$$\begin{aligned}
|\psi(t)\rangle = & \mathcal{E}(t)|0, \text{vac}\rangle + \sum_{\mu=1}^N A_{\mu}(t)|1_{\mu}, \text{vac}\rangle + \sum_{\mu=1}^N B_{\mu}(t)|2_{\mu}, \text{vac}\rangle + \sum_{\mu=1}^N \sum_{k_s, \lambda_s} C_s^{\mu}(t)|3_{\mu}, 1_{\vec{k}_s, \lambda_s}\rangle \\
& + \sum_{\substack{k_s, \lambda_s \\ k_i, \lambda_i}} D_{s,i}(t)|0, 1_{\vec{k}_s, \lambda_s}, 1_{\vec{k}_i, \lambda_i}\rangle + \underbrace{\sum_{\mu=1}^N \sum_{k_i, \lambda_i} C_i^{\mu}(t)|3_{\mu}, 1_{\vec{k}_i, \lambda_i}\rangle + \sum_{\mu=1}^N C^{\mu}(t)|3_{\mu}\rangle}_{\text{}} \\
& + \underbrace{\sum_{\mu=1}^N \sum_{k_s, \lambda_s} B_s^{\mu}(t)|2_{\mu}, 1_{\vec{k}_s, \lambda_s}\rangle + \sum_{\nu < \mu}^N \sum_{\mu=1}^N \sum_{\substack{k_s, \lambda_s \\ k_i, \lambda_i}} C_{s,i}^{\mu\nu}(t)|3_{\mu}, 3_{\nu}, 1_{\vec{k}_s, \lambda_s}, 1_{\vec{k}_i, \lambda_i}\rangle}_{\text{}} \quad (\text{A.2})
\end{aligned}$$

where  $|\text{vac}\rangle$  is the photon vacuum state,  $s \equiv (k_s, \lambda_s)$ ,  $i \equiv (k_i, \lambda_i)$ ,  $|m_{\mu}\rangle \equiv |m_{\mu}\rangle|0\rangle_{\nu \neq \mu}^{N-1}$ ,  $m = 1, 2, 3$  and  $|3_{\mu}, 3_{\nu}\rangle \equiv |3_{\mu}\rangle|3_{\nu}\rangle|0\rangle_{\lambda \neq \mu, \nu}^{N-2}$ . The probability amplitudes coupled from rotating wave terms in the Hamiltonian are  $\mathcal{E}(t)$ ,  $A_{\mu}(t)$ ,  $B_{\mu}(t)$ ,  $C_s^{\mu}(t)$ ,  $D_{s,i}(t)$ , which indicate the complete cycle of single excitation process from the ground state, intermediate, upper excited state, intermediate excited state with emission of a signal photon, and the ground state with the signal-idler emission. Note that the states underlined are coupled through non-RWA terms that describe a transition from upper excited state to intermediate one by absorbing a photon for  $B_s^{\mu}(t)$  and  $C^{\mu}(t)$  and a transition from the ground state to the intermediate one by emitting a photon for  $C_i^{\mu}(t)$  and  $\mathcal{E}(t)$  or  $C_s^{\mu}(t)$  and  $C_{s,i}^{\mu\nu}(t)$ . Apply the Schrödinger equation  $i\hbar \frac{\partial}{\partial t} |\psi(t)\rangle = V_I(t) |\psi(t)\rangle$ , and we have the coupled equations of motion,

$$\begin{aligned}
i\dot{\mathcal{E}} &= -\frac{\Omega_a^*}{2} \sum_{\mu} e^{-i\vec{k}_a \cdot \vec{r}_{\mu}} A_{\mu} - i \underbrace{\sum_{i,\mu} g_i(\vec{\epsilon}_i \cdot \hat{d}_i^*) e^{i\vec{k}_i \cdot \vec{r}_{\mu}} e^{-i(\omega_{ki} + \omega_3)t} C_i^{\mu}}_{}, \\
i\dot{C}_i^{\mu} &= i \underbrace{g_i^*(\vec{\epsilon}_i^* \cdot \hat{d}_i) e^{-i\vec{k}_i \cdot \vec{r}_{\mu}} e^{i(\omega_i + \omega_3)t} \mathcal{E}}_{}, \\
i\dot{A}_{\mu} &= -\Delta_1 A_{\mu} - \frac{\Omega_a}{2} e^{i\vec{k}_a \cdot \vec{r}_{\mu}} \mathcal{E} - \frac{\Omega_b^*}{2} e^{-i\vec{k}_b \cdot \vec{r}_{\mu}} B_{\mu}, \\
i\dot{B}_{\mu} &= -\Delta_2 B_{\mu} - \frac{\Omega_b}{2} e^{i\vec{k}_b \cdot \vec{r}_{\mu}} A_{\mu} - i \sum_s g_s(\vec{\epsilon}_s \cdot \hat{d}_s^*) e^{i\vec{k}_s \cdot \vec{r}_{\mu}} e^{-i(\omega_s - \omega_{23} - \Delta_2)t} C_s^{\mu}, \\
i\dot{C}_s^{\mu} &= i g_s^*(\vec{\epsilon}_s^* \cdot \hat{d}_s) e^{-i\vec{k}_s \cdot \vec{r}_{\mu}} e^{i(\omega_{ks} - \omega_{23} - \Delta_2)t} B_{\mu} - i \sum_i g_i(\vec{\epsilon}_i \cdot \hat{d}_i^*) e^{i\vec{k}_i \cdot \vec{r}_{\mu}} e^{-i(\omega_i - \omega_3)t} D_{s,i} \\
&\quad - i \underbrace{\sum_i g_i(\vec{\epsilon}_i \cdot \hat{d}_i^*) e^{i(\omega_i + \omega_3)t} \left[ \sum_{\nu < \mu} C_{s,i}^{\mu\nu} e^{i\vec{k}_i \cdot \vec{r}_{\nu}} + \sum_{\nu > \mu} e^{i\vec{k}_i \cdot \vec{r}_{\nu}} C_{s,i}^{\nu\mu} \right]}_{}, \\
i\dot{C}_{s,i}^{\mu\nu} &= i \underbrace{g_i^*(\vec{\epsilon}_i^* \cdot \hat{d}_i) e^{i(\omega_i + \omega_3)t} \left[ e^{-i\vec{k}_i \cdot \vec{r}_{\nu}} C_s^{\mu} + C_s^{\nu} e^{-i\vec{k}_i \cdot \vec{r}_{\mu}} \right]}_{\Big|_{\nu < \mu}}, \\
i\dot{D}_{s,i} &= i g_i^*(\vec{\epsilon}_i^* \cdot \hat{d}_i) \sum_{\mu} e^{-i\vec{k}_i \cdot \vec{r}_{\mu}} e^{i(\omega_{ki} - \omega_3)t} C_s^{\mu}, \\
i\dot{C}_{\mu} &= -i \underbrace{\sum_s g_s(\vec{\epsilon}_s \cdot \hat{d}_s^*) e^{i\vec{k}_s \cdot \vec{r}_{\mu}} e^{-i(\omega_s + \omega_{23} + \Delta_2)t} B_s^{\mu}}_{}, \\
i\dot{B}_s^{\mu} &= i \underbrace{g_s^*(\vec{\epsilon}_s^* \cdot \hat{d}_s) e^{-i\vec{k}_s \cdot \vec{r}_{\mu}} e^{i(\omega_{ks} + \omega_{23} + \Delta_2)t} C_{\mu}}_{}. \tag{A.3}
\end{aligned}$$

The Lamb shift for the atomic transition  $|3\rangle \rightarrow |0\rangle$  with the optical frequency  $\omega_3$  and spontaneous decay rate  $\Gamma$  is  $\int_0^{\infty} d\omega \frac{\Gamma}{2\pi} [\text{P.V.}(\omega - \omega_3)^{-1} - \text{P.V.}(\omega + \omega_3)^{-1}]$  that can be identified partly within the substitution of these non-RWA terms. We substitute  $C_i^{\mu}$  into  $\mathcal{E}$ ,  $C_{s,i}^{\mu\nu}$  into  $C_s^{\mu}$ , and  $B_s^{\mu}$  into  $C_{\mu}$ , and they are



$$\begin{aligned}
\dot{\mathcal{E}} &= \frac{i\Omega_a^*}{2} \sum_{\mu} e^{-i\vec{k}_a \cdot \vec{r}_{\mu}} A_{\mu} - N \sum_i |g_i|^2 |(\vec{\epsilon}_i \cdot \hat{d}_i^*)|^2 \int_0^t dt' e^{i(\omega_i + \omega_3)(t' - t)} \mathcal{E}(t') \\
&= \frac{i\Omega_a^*}{2} \sum_{\mu} e^{-i\vec{k}_a \cdot \vec{r}_{\mu}} A_{\mu} - N \mathcal{E} \oint d\Omega_i [1 - (\hat{k}_i \cdot \hat{d}_i)^2] \frac{V}{(2\pi)^3} \int_0^{\infty} dk_i k_i^2 \frac{\hbar \omega_i}{2\epsilon_0 V} \frac{|d_i|^2}{\hbar^2} \\
&\times [\pi \delta(\omega_i + \omega_3) - i \text{P.V.}(\omega_i + \omega_3)^{-1}] \\
&= \frac{i\Omega_a^*}{2} \sum_{\mu} e^{-i\vec{k}_a \cdot \vec{r}_{\mu}} A_{\mu} + iN \mathcal{E} \int_0^{\infty} d\omega_i \frac{\Gamma_i}{2\pi} \text{P.V.}(\omega_i + \omega_3)^{-1}, \tag{A.4}
\end{aligned}$$

$$\begin{aligned}
\dot{C}_s^{\mu} &= g_s^*(\epsilon_s^* \cdot \hat{d}_s) e^{-i\vec{k}_s \cdot \vec{r}_{\mu}} e^{i(\omega_{ks} - \omega_{23} - \Delta_2)t} B_{\mu} - \sum_i g_i(\vec{\epsilon}_i \cdot \hat{d}_i^*) e^{i\vec{k}_i \cdot \vec{r}_{\mu}} e^{-i(\omega_i - \omega_3)t} D_{s,i} \\
&- \sum_i |g_i|^2 |(\vec{\epsilon}_i \cdot \hat{d}_i^*)|^2 \int_0^t dt' e^{i(\omega_i + \omega_3)(t' - t)} \mathcal{E}(t') \left\{ \sum_{\nu < \mu} \left[ C_s^{\mu}(t') + e^{i\vec{k}_i \cdot (\vec{r}_{\nu} - \vec{r}_{\mu})} C_s^{\nu}(t') \right] \right. \\
&+ \left. \sum_{\nu > \mu} \left[ e^{i\vec{k}_i \cdot (\vec{r}_{\nu} - \vec{r}_{\mu})} C_s^{\nu}(t') + C_s^{\mu}(t') \right] \right\} \\
&= g_s^*(\epsilon_s^* \cdot \hat{d}_s) e^{-i\vec{k}_s \cdot \vec{r}_{\mu}} e^{i(\omega_{ks} - \omega_{23} - \Delta_2)t} B_{\mu} - \sum_i g_i(\vec{\epsilon}_i \cdot \hat{d}_i^*) e^{i\vec{k}_i \cdot \vec{r}_{\mu}} e^{-i(\omega_i - \omega_3)t} D_{s,i} \\
&+ i(N - 1) C_s^{\mu} \int_0^{\infty} d\omega_i \frac{\Gamma_i}{2\pi} \text{P.V.}(\omega_i + \omega_3)^{-1} - \sum_i |g_i|^2 |(\vec{\epsilon}_i \cdot \hat{d}_i^*)|^2 \times \\
&\int_0^t dt' e^{i(\omega_i + \omega_3)(t' - t)} \sum_{\nu \neq \mu} e^{i\vec{k}_i \cdot (\vec{r}_{\mu} - \vec{r}_{\nu})} C_s^{\nu}(t'), \tag{A.5}
\end{aligned}$$

where we have used the symmetric property of  $\Omega_{\nu\mu}^+(\xi) = \Omega_{\mu\nu}^+(\xi) \equiv \sum_i |g_i|^2 |(\vec{\epsilon}_i \cdot \hat{d}_i^*)|^2 \int_0^t dt' e^{i(\omega_i + \omega_3)(t' - t)} e^{i\vec{k}_i \cdot (\vec{r}_{\nu} - \vec{r}_{\mu})}$  [21]. The spontaneous decay rate for the idler transition is  $\Gamma_i \equiv \frac{|d_i|^2 \omega_i^3}{3\pi \hbar \epsilon_0 c^3}$  [116, 30], and the same thing for signal transition  $\Gamma_s \equiv \frac{|d_s|^2 \omega_s^3}{3\pi \hbar \epsilon_0 c^3}$  that

$$\dot{C}_{\mu} = iC_{\mu} \int_0^{\infty} d\omega_s \frac{\Gamma_s}{2\pi} \text{P.V.}(\omega_s + \omega_{23} + \Delta_2)^{-1}. \tag{A.6}$$

It is now clear the contribution from non-RWA terms to the Lamb shift of the idler transition resides in  $\dot{\mathcal{E}}$  and  $\dot{C}_s^{\mu}$ , which are proportional to  $N$  and  $N - 1$ . The difference of the level shifts then gives rise to  $-\int_0^{\infty} d\omega \frac{\Gamma}{2\pi} \text{P.V.}(\omega + \omega_3)^{-1}$ , and the other

part can be derived from substitutions of RWA terms. The signal transition has the same effect as shown in  $\dot{C}_\mu$ . The frequency shift due to dipole-dipole interaction also appeared in  $\dot{C}_s^\mu$  that has the contribution of interactions from other atoms. There also will be contributions from RWA terms, and we will show the complete expression for collective decay rate and frequency shift.

Define  $C_{s,q_i} = \sum_\mu C_s^\mu e^{-i\vec{q}_i \cdot \vec{r}_\mu}$ , substitute  $D_{s,i}$  into  $C_s^\mu$ , and we have

$$\begin{aligned}
\dot{C}_{s,q_i} &= g_s^* (\epsilon_s^* \cdot \hat{d}_s) \sum_\mu e^{-i(\vec{k}_s + \vec{q}_i) \cdot \vec{r}_\mu} e^{i(\omega_{ks} - \omega_{23} - \Delta_2)t} B_\mu - \sum_i |g_i|^2 |(\vec{\epsilon}_i \cdot \hat{d}_i^*)|^2 \times \\
&\quad \sum_\mu e^{i(\vec{k}_i - \vec{q}_i) \cdot \vec{r}_\mu} \int_0^t dt' e^{i(\omega_i - \omega_3)(t' - t)} C_{s,ki}(t') - \sum_i |g_i|^2 |(\vec{\epsilon}_i \cdot \hat{d}_i^*)|^2 \times \\
&\quad \int_0^t dt' e^{i(\omega_i + \omega_3)(t' - t)} \left[ \sum_\mu e^{i(\vec{k}_i - \vec{q}_i) \cdot \vec{r}_\mu} C_{s,ki} - C_{s,q_i} \right] \\
&\quad + i(N-1)C_{s,q_i} \int_0^\infty d\omega_i \frac{\Gamma_i}{2\pi} \text{P.V.}(\omega_i + \omega_3)^{-1} \\
&= g_s^* (\epsilon_s^* \cdot \hat{d}_s) \sum_\mu e^{-i(\vec{k}_s + \vec{q}_i) \cdot \vec{r}_\mu} e^{i(\omega_{ks} - \omega_{23} - \Delta_2)t} B_\mu - \frac{3}{8\pi} \oint d\Omega_i [1 - (\hat{k}_i \cdot \hat{d}_i)^2] \frac{\Gamma_3}{2} \\
&\quad \times \sum_\mu e^{i(\vec{k}_i - \vec{q}_i) \cdot \vec{r}_\mu} \Big|_{|\vec{k}_i|=k_3} C_{s,k_3 \hat{k}_i} + i \frac{3}{8\pi} \oint d\Omega_i [1 - (\hat{k}_i \cdot \hat{d}_i)^2] \int_0^\infty d\omega_i \frac{\Gamma_i}{2\pi} \\
&\quad \left[ \text{P.V.}(\omega_i - \omega_3)^{-1} + \text{P.V.}(\omega_i + \omega_3)^{-1} \right] \left[ \sum_\mu e^{i(\vec{k}_i - \vec{q}_i) \cdot \vec{r}_\mu} C_{s,ki} - C_{s,q_i} \right] \\
&\quad + iC_{s,q_i} \int_0^\infty d\omega_i \frac{\Gamma_i}{2\pi} \text{P.V.}(\omega_i - \omega_3)^{-1} \\
&\quad + i(N-1)C_{s,q_i} \int_0^\infty d\omega_i \frac{\Gamma_i}{2\pi} \text{P.V.}(\omega_i + \omega_3)^{-1}. \tag{A.7}
\end{aligned}$$

Renormalize the Lamb shift (last two lines in the above) and use  $\sum_{q_i} C_{s,q_i} e^{i\vec{q}_i \cdot \vec{r}_\nu} = NC_s^\nu$  then we have

$$\begin{aligned}
\dot{C}_{s,q_i} &= g_s^*(\epsilon_s^* \cdot \hat{d}_s) \sum_{\mu} e^{-i(\vec{k}_s + \vec{q}_i) \cdot \vec{r}_{\mu}} e^{i(\omega_{ks} - \omega_{23} - \Delta_2)t} B_{\mu} - \frac{3}{8\pi} \oint d\Omega_i [1 - (\hat{k}_i \cdot \hat{d}_i)^2] \frac{\Gamma_3}{2} \times \\
&\quad \sum_{\mu} e^{i(\vec{k}_i - \vec{q}_i) \cdot \vec{r}_{\mu}} \sum_{\nu} e^{-i\vec{k}_i \cdot \vec{r}_{\nu}} \frac{1}{N} \sum_{q'_i} e^{i\vec{q}'_i \cdot \vec{r}_{\nu}} C_{s,q'_i} \Big|_{|\vec{k}_i|=k_3} + i \frac{3}{8\pi} \oint d\Omega_i [1 - (\hat{k}_i \cdot \hat{d}_i)^2] \times \\
&\quad \int_0^{\infty} d\omega_i \frac{\Gamma_i}{2\pi} \left[ \text{P.V.}(\omega_i - \omega_3)^{-1} + \text{P.V.}(\omega_i + \omega_3)^{-1} \right] \left[ \sum_{\mu} e^{i(\vec{k}_i - \vec{q}_i) \cdot \vec{r}_{\mu}} \sum_{\nu \neq \mu} e^{-i\vec{k}_i \cdot \vec{r}_{\nu}} C_{s,\nu}^{\nu} \right] \\
&= g_s^*(\epsilon_s^* \cdot \hat{d}_s) \sum_{\mu} e^{-i(\vec{k}_s + \vec{q}_i) \cdot \vec{r}_{\mu}} e^{i(\omega_{ks} - \omega_{23} - \Delta_2)t} B_{\mu} - \frac{3}{8\pi} \oint d\Omega_i [1 - (\hat{k}_i \cdot \hat{d}_i)^2] \frac{\Gamma_3}{2} \\
&\quad \times \frac{1}{N} \sum_{\mu} e^{i(\vec{k}_i - \vec{q}_i) \cdot \vec{r}_{\mu}} \sum_{q'_i} \sum_{\nu} e^{i(\vec{q}'_i - \vec{k}_i) \cdot \vec{r}_{\nu}} C_{s,q'_i} \Big|_{|\vec{k}_i|=k_3} + i \frac{3}{8\pi} \oint d\Omega_i [1 - (\hat{k}_i \cdot \hat{d}_i)^2] \\
&\quad \times \int_0^{\infty} d\omega_i \frac{\Gamma_i}{2\pi} \left[ \text{P.V.}(\omega_i - \omega_3)^{-1} + \text{P.V.}(\omega_i + \omega_3)^{-1} \right] \frac{1}{N} \sum_{\mu} e^{i(\vec{k}_i - \vec{q}_i) \cdot \vec{r}_{\mu}} \sum_{q'_i} \\
&\quad \left[ \sum_{\nu} e^{i(\vec{q}'_i - \vec{k}_i) \cdot \vec{r}_{\nu}} - e^{i(\vec{q}'_i - \vec{k}_i) \cdot \vec{r}_{\mu}} \right] C_{s,q'_i}. \tag{A.8}
\end{aligned}$$

Due to the summation of exponential factors from the above, the coupling from the other modes  $q'_i$  is significant only when  $q'_i = k_i = q_i$ , so finally we have

$$\begin{aligned}
\dot{C}_{s,q_i} &= g_s^*(\epsilon_s^* \cdot \hat{d}_s) \sum_{\mu} e^{-i(\vec{k}_s + \vec{q}_i) \cdot \vec{r}_{\mu}} e^{i(\omega_{ks} - \omega_{23} - \Delta_2)t} B_{\mu} - \frac{\Gamma_3}{2} (N\bar{\mu} + 1) C_{s,q_i} \\
&\quad + i\delta\omega_i C_{s,q_i} \tag{A.9}
\end{aligned}$$

where the collective decay rate is [22]

$$\frac{\Gamma_3}{2} (N\bar{\mu} + 1) \equiv \frac{\Gamma_3}{2} \frac{3}{8\pi} \oint d\Omega_i [1 - (\hat{k}_i \cdot \hat{d}_i)^2] \frac{1}{N} \sum_{\mu, \nu} e^{i(\vec{k}_i - \vec{q}_i) \cdot (\vec{r}_{\mu} - \vec{r}_{\nu})}, \tag{A.10}$$

and the collective frequency shift expressed in terms of the continuous integral over a frequency space is

$$\begin{aligned}
\delta\omega_i &\equiv \int_0^\infty d\omega_i \frac{\Gamma_i}{2\pi} \left[ \text{P.V.}(\omega_i - \omega_3)^{-1} + \text{P.V.}(\omega_i + \omega_3)^{-1} \right] N\bar{\mu}(k_i), \\
&= \int_0^\infty d\omega_i \frac{\Gamma_i}{2\pi} \left[ \text{P.V.}(\omega_i - \omega_3)^{-1} + \text{P.V.}(\omega_i + \omega_3)^{-1} \right] \frac{1}{N} \sum_{\mu, \nu \neq \mu} e^{i(\vec{k}_i - \vec{q}_i) \cdot (\vec{r}_\mu - \vec{r}_\nu)}.
\end{aligned} \tag{A.11}$$

The geometrical constant  $\bar{\mu}$  for a cylindrical ensemble (of height  $h$  and radius  $a$ ) is

$$\bar{\mu}(k_3) = \frac{6(N-1)}{NA^2H^2} \int_{-1}^1 \frac{dx(1+x^2)}{(1-x)^2(1-x^2)} \sin^2\left[\frac{1}{2}H(1-x)\right] J_1^2[A(1-x^2)^{1/2}] \tag{A.12}$$

where  $H = k_3h$  and  $A = k_3a$  are dimensionless length scales, and circular polarizations are considered [22].  $J_1$  is the Bessel function of the first kind.

The alternative way to express the collective decay rate and shift is [21]

$$\frac{\Gamma_3^N}{2} = \frac{\Gamma_3}{2} (N\bar{\mu} + 1) \equiv \frac{\Gamma_3}{2} \frac{1}{N} \sum_{\mu, \nu} F_{\mu\nu}(k_3 r_{\mu\nu}) e^{-i\vec{q}_i \cdot (\vec{r}_\mu - \vec{r}_\nu)}, \tag{A.13}$$

$$\begin{aligned}
\delta\omega_i &= -\frac{\Gamma_3}{2} \frac{2}{N} \sum_{\mu, \nu \neq \mu} G_{\mu\nu}(k_3 r_{\mu\nu}) e^{-i\vec{q}_i \cdot (\vec{r}_\mu - \vec{r}_\nu)} \\
&= \frac{\Gamma_3}{Nk_3^3} \text{P.V.} \int_{-\infty}^\infty \frac{dk}{2\pi} \frac{k^3}{k - k_3} \sum_{\mu, \nu \neq \mu} F_{\mu\nu}(k r_{\mu\nu}) e^{-i\vec{q}_i \cdot (\vec{r}_\mu - \vec{r}_\nu)}.
\end{aligned} \tag{A.14}$$

where

$$\begin{aligned}
F_{\alpha\beta}(\xi) &= \frac{3}{2} \{ [1 - (\hat{p} \cdot \hat{r}_{\alpha\beta})^2] \frac{\sin \xi}{\xi} + [1 - 3(\hat{p} \cdot \hat{r}_{\alpha\beta})^2] \left( \frac{\cos \xi}{\xi^2} - \frac{\sin \xi}{\xi^3} \right) \}, \\
G_{\alpha\beta}(\xi) &= \frac{3}{4} \{ -[1 - (\hat{p} \cdot \hat{r}_{\alpha\beta})^2] \frac{\cos \xi}{\xi} + [1 - 3(\hat{p} \cdot \hat{r}_{\alpha\beta})^2] \left( \frac{\sin \xi}{\xi^2} + \frac{\cos \xi}{\xi^3} \right) \},
\end{aligned} \tag{A.15}$$

and note that  $\xi = k_3 r_{\alpha\beta}$ .

## A.2 Adiabatic Approximation

Under the conditions of large detuned laser excitations, we may use the adiabatic approximation to eliminate the laser-excited states and solve for the signal-idler probability amplitude. Before proceeding to the adiabatic approximation, we solve  $C_{s,q_i}$

first and substitute it to solve  $B_\mu$ .

$$C_{s,q_i}(t) = g_s^*(\epsilon_s^* \cdot \hat{d}_s) \sum_\mu e^{-i(\vec{k}_s + \vec{q}_i) \cdot \vec{r}_\mu} \int_0^t dt' e^{i(\omega_s - \omega_{23} - \Delta_2)t'} e^{(-\frac{\Gamma_3^N}{2} + i\delta\omega_i)(t-t')} B_\mu(t'). \quad (\text{A.16})$$

Let  $B_{k_a+k_b} \equiv \sum_\mu e^{-i(\vec{k}_a + \vec{k}_b) \cdot \vec{r}_\mu} B_\mu$  and  $A_{k_a} \equiv \sum_\mu e^{-i\vec{k}_a \cdot \vec{r}_\mu} A_\mu$ , we have

$$\begin{aligned} \dot{B}_{k_a+k_b} &= i\Delta_2 B_{k_a+k_b} + i\frac{\Omega_b}{2} A_{k_a} - \sum_{ks, \lambda_s} |g_s|^2 |\epsilon_{k_s, \lambda_s}^* \cdot \hat{d}_s|^2 \int_0^t dt' e^{i(\omega_{k_s} - \omega_{23} - \Delta_2)(t'-t)} \\ &\quad e^{(-\frac{\Gamma_3^N}{2} + i\delta\omega_i)(t-t')} B_{k_a+k_b}(t') \\ &= i\Delta_2 B_{k_a+k_b} + i\frac{\Omega_b}{2} A_{k_a} - \frac{\Gamma_2}{2} B_{k_a+k_b} + iB_{k_a+k_b} \int_0^\infty d\omega_s \frac{\Gamma_s}{2\pi} \times \\ &\quad \text{P.V.}(\omega_s - \omega_{23} - \Delta_2)^{-1} \end{aligned} \quad (\text{A.17})$$

where the Weisskopf-Wigner approach is used to derive the decay rate for the signal transition, and in conjunction with the result of  $\dot{C}_\mu$ , the Lamb shift is also derived as the difference of level shifts that  $\int_0^\infty d\omega_s \frac{\Gamma_s}{2\pi} [\text{P.V.}(\omega_s - \omega_{23} - \Delta_2)^{-1} - \text{P.V.}(\omega_s + \omega_{23} + \Delta_2)^{-1}]$ . We then renormalize it and apply the adiabatic approximation.

When the detunings are large enough that

$$|\Delta_1|, |\Delta_2| \gg \frac{|\Omega_a|}{2}, \frac{|\Omega_b|}{2}, \frac{\Gamma_2}{2}.$$

We can solve the coupled equations of motion by adiabatically eliminating the intermediate and upper excited states in the excitation process. The adiabatic approximation requires that the driving pulses are smoothly turned on, and we will show under what condition of the pulses that the approximation is valid.

First we use integration by parts to solve the probability amplitudes in the adiabatic approximation (zeroth order) and their first-order correction. Note that we allow time-varying Rabi frequencies.

$$\begin{aligned}
A_{k_a}(t) &= e^{i\Delta_1 t} \left[ \frac{i}{2} \int_{-\infty}^t e^{-i\Delta_1 t'} \Omega_a(t') \mathcal{E}(t') dt' + \frac{i}{2} \int_{-\infty}^t e^{-i\Delta_1 t'} \Omega_b^*(t') B_{k_a+k_b}(t') dt' \right] \\
&\approx -\frac{N\Omega_a(t)\mathcal{E}(t)}{2\Delta_1} - \frac{\Omega_b^*(t)B_{k_a+k_b}(t)}{2\Delta_1} + \frac{i}{2\Delta_1^2} \frac{d}{dt} \left( \Omega_a(t)\mathcal{E}(t) \right) \\
&\quad + \frac{i}{2\Delta_1^2} \frac{d}{dt} \left( \Omega_b^*(t)B_{k_a+k_b}(t) \right), \tag{A.18}
\end{aligned}$$

$$\begin{aligned}
B_{k_a+k_b}(t) &= e^{i(\Delta_2+i\Gamma_2/2)t} \left[ \frac{i}{2} \int_{-\infty}^t e^{-i(\Delta_2+i\Gamma_2/2)t'} \Omega_b(t') A_{k_a}(t') dt' \right] \\
&\approx -\frac{\Omega_b(t)A_{k_a}(t)}{2(\Delta_2+i\Gamma_2/2)} + \frac{i \frac{d}{dt} \left( \Omega_b(t)A_{k_a}(t) \right)}{2(\Delta_2+i\Gamma_2/2)^2} \tag{A.19}
\end{aligned}$$

where higher order terms involving a second derivative of the fields are neglected due to their feature of slow variation. The initial conditions are used in the below,

$$\begin{aligned}
B_{k_a+k_b}(-\infty) &= A_{k_a}(-\infty) = 0, \quad \frac{d}{dt'} \left( \Omega_a(t') \mathcal{E}(t') \right) \Big|_{-\infty} = 0, \\
\frac{d}{dt'} \left( \Omega_b^*(t') B_{k_a+k_b}(t') \right) \Big|_{-\infty} &= \frac{d}{dt'} \left( \Omega_b(t') A_{k_a}(t') \right) \Big|_{-\infty} = 0.
\end{aligned}$$

With conditions in the following (i) to (iii),

$$\text{(i)} \quad \left| \frac{\frac{d}{dt} \left( \Omega_a(t) \mathcal{E}(t) \right)}{\Delta_1 \Omega_a(t) \mathcal{E}(t)} \right| \ll 1, \tag{A.20}$$

$$\text{(ii)} \quad \left| \frac{\frac{d}{dt} \left( \Omega_b^*(t) B_{k_a+k_b}(t) \right)}{\Delta_1 \Omega_b^*(t) B_{k_a+k_b}(t)} \right| \ll 1, \tag{A.21}$$

$$\text{(iii)} \quad \left| \frac{\frac{d}{dt} \left( \Omega_b(t) A_{k_a}(t) \right)}{(\Delta_2 + i\Gamma_2/2) \Omega_b(t) A_{k_a}(t)} \right| \ll 1, \tag{A.22}$$

we can derive  $A_{k_a}(t)$ ,  $B_{k_a+k_b}(t)$ , and  $\mathcal{E}(t)$  in the adiabatic approximation,

$$A_{k_a}(t) = \frac{-\frac{N\Omega_a(t)\mathcal{E}(t)}{2\Delta_1}}{1 - \frac{|\Omega_b(t)|^2}{4\Delta_1(\Delta_2+i\Gamma_2/2)}} \approx -\frac{N\Omega_a(t)}{2\Delta_1} \mathcal{E}(t), \tag{A.23}$$

$$\mathcal{E}(t) = e^{-\frac{iN}{4\Delta_1} \int_{-\infty}^t |\Omega_a(t')|^2 dt'} \approx 1 - \frac{iN}{4\Delta_1} \int_{-\infty}^t |\Omega_a(t')|^2 dt', \tag{A.24}$$

$$B_{k_a+k_b}(t) = \frac{\frac{N\Omega_a(t)\Omega_b(t)}{4\Delta_1\Delta_2} \mathcal{E}(t)}{1 - \frac{|\Omega_b(t)|^2}{4\Delta_1(\Delta_2+i\Gamma_2/2)}} \approx \frac{N\Omega_a(t)\Omega_b(t)}{4\Delta_1\Delta_2} \equiv Nb(t), \tag{A.25}$$

where the probability amplitude of the first excited state follows the first laser field, and the upper excited state follows the products of two laser fields. The AC Stark shift is present in the ground state that can be ignored if  $\Delta_1 \gg N \int_{-\infty}^t |\Omega_a(t')|^2 dt'/4$ . This condition is also required for the assumption of single excitations states we consider.

Finally, we have the probability amplitudes associated with the signal  $C_{s,k_i}(t)$  and signal-idler photons  $D_{s,i}(t)$ ,

$$\begin{aligned}
C_{s,k_i}(t) &= g_s^*(\epsilon_s^* \cdot \hat{d}_s) \int_0^t dt' e^{i(\omega_s - \omega_{23} - \Delta_2)t'} e^{(-\frac{\Gamma_3^N}{2} + i\delta\omega_i)(t-t')} \sum_{\mu} e^{i\Delta\vec{k} \cdot \vec{r}_{\mu}} e^{-i(\vec{k}_a + \vec{k}_b) \cdot \vec{r}_{\mu}} B_{\mu}(t') \\
&= g_s^*(\epsilon_s^* \cdot \hat{d}_s) \frac{1}{N} \sum_{\mu} e^{i\Delta\vec{k} \cdot \vec{r}_{\mu}} \int_0^t dt' e^{i(\omega_s - \omega_{23} - \Delta_2)t'} e^{(-\frac{\Gamma_3^N}{2} + i\delta\omega_i)(t-t')} B_{k_a+k_b}(t'), \quad (\text{A.26})
\end{aligned}$$

$$\begin{aligned}
D_{s,i}(t) &= g_i^* g_s^*(\epsilon_{k_i, \lambda_i}^* \cdot \hat{d}_i)(\epsilon_{k_s, \lambda_s}^* \cdot \hat{d}_s) \sum_{\mu} e^{i\Delta\vec{k} \cdot \vec{r}_{\mu}} \int_0^t \int_0^{t'} dt'' dt' e^{(-\frac{\Gamma_3^N}{2} + i\delta\omega_i)(t'-t'')} \\
&\quad e^{i(\omega_i - \omega_3)t'} e^{i(\omega_s - \omega_{23} - \Delta_2)t''} b(t''). \quad (\text{A.27})
\end{aligned}$$

Note that  $e^{-i(\vec{k}_a + \vec{k}_b) \cdot \vec{r}_{\mu}} B_{\mu}(t')$  does not depend on the atomic index  $\mu$  under the adiabatic approximation, and  $\Delta\vec{k} = \vec{k}_a + \vec{k}_b - \vec{k}_s - \vec{k}_i$  is the phase mismatch.

The above expressions are the main results of this Appendix and we proceed to investigate their properties when Gaussian pump pulses are used in Chapter 3.





## APPENDIX B

### DERIVATION OF A C-NUMBER LANGEVIN EQUATION FOR THE CASCADE EMISSION

In this appendix, we show the details in the derivations of c-number Langevin equations that are the foundation for numerical approaches of the cascade emission in Chapter 4. First we describe how to quantize the free electromagnetic field [29], and we formulate the Fokker-Planck equation for our system using the positive P-representation. We derive the Fokker-Planck equations by characteristic functions [27], and the corresponding c-number Langevin equations are derived. The noise correlations are found from the diffusion coefficients in Fokker-Planck equations.

#### ***B.1 Quantized Electromagnetic Field***

To describe the propagating quantum fields in one dimension, we take the approach of the reference [29]. Before proceeding, we specify the positive frequency of a free propagating field operator in the discrete space,

$$\hat{E}^+(\vec{x}) = i \sum_{k,\lambda} \sqrt{\frac{\hbar\omega_k}{2\epsilon_0 V}} \hat{a}_{k,\lambda} \vec{\epsilon}_{k,\lambda} e^{i\vec{k}\cdot\vec{x}} \quad (\text{B.1})$$

where  $\vec{\epsilon}_{k,\lambda}$  and  $\vec{\epsilon}_\lambda(\vec{k})$  specify polarizations of the field, and the interchange of discrete and continuous space has relation,

$$\sum_k \rightarrow \frac{V}{(2\pi)^3} \int d^3k, \quad \hat{a}_{k,\lambda} \rightarrow \sqrt{\frac{V}{(2\pi)^3}} \int d^3k \hat{a}_\lambda(\vec{k}),$$

where creation and annihilation operators satisfy commutation relations,

$$[\hat{a}_{k,\lambda}, \hat{a}_{k',\lambda'}^\dagger] = \delta_{\lambda,\lambda'} \delta_{k,k'}. \quad (\text{B.2})$$

For the purpose of describing one-dimensional propagating field (paraxial approximation), we discretize the space along the propagation ( $\hat{z}$ ) and denote  $\vec{r}$  as the vectors on the cross section. We then have

$$\hat{E}^+(z, \vec{r}) = i \sum_{n=-M}^M \sqrt{\frac{\hbar\omega_{s,n}}{2\epsilon_0}} e^{i(k_s+k_n)z} \frac{1}{\sqrt{V}} \sum_{\lambda} \sum_{k_{n\perp}} e^{i\vec{k}_{n\perp} \cdot \vec{r}} \vec{\epsilon}_{k_n, \lambda} \hat{a}_{k, \lambda} \quad (\text{B.3})$$

$$k_n = \frac{2\pi n}{L}, \quad \omega_{s,n} = \omega_s + k_n c, \quad \omega_s = k_s c, \quad n = -M, \dots, M$$

where  $L$  is the length of propagation that is equally split into  $2M + 1$  elements, and the center of the interval is  $z = z_m = \frac{mL}{2M+1}$  with  $m = -M, \dots, M$ .  $k_s$  is the central longitudinal mode of the field. Note that the polarization  $\vec{\epsilon}_{k, \lambda}$  with paraxial approximation has  $k \approx k_n$ .

The next step is to characterize the transverse mode of propagating field, and we introduce a set of orthonormal transverse mode functions ( $f_{i, k_{n\perp}}$ ) that  $\sum_{k_{n\perp}} f_{i, k_{n\perp}}^* f_{j, k_{n\perp}} = \delta_{ij}$ . A longitudinal annihilation operator is defined as

$$\hat{c}_{n, i, \lambda} \equiv \sum_{k_{n\perp}} f_{i, k_{n\perp}}^* \hat{a}_{k, \lambda},$$

which also satisfies commutation relations  $[\hat{c}_{n, i, \lambda}, \hat{c}_{n', j, \lambda'}^\dagger] = \delta_{nn'} \delta_{ij} \delta_{\lambda\lambda'}$ . We can substitute  $\hat{a}_{k, \lambda} = \sum_i \hat{c}_{n, i, \lambda} f_{i, k_{n\perp}}$  that

$$\hat{E}^+(z, \vec{r}) = i \sum_{n=-M}^M \sqrt{\frac{\hbar\omega_{s,n}}{2\epsilon_0}} e^{i(k_s+k_n)z} \frac{1}{\sqrt{V}} \sum_{\lambda} \sum_{k_{n\perp}} e^{i\vec{k}_{n\perp} \cdot \vec{r}} \vec{\epsilon}_{k_n, \lambda} f_{i, k_{n\perp}} \hat{c}_{n, i, \lambda}. \quad (\text{B.4})$$

Let the spatial transverse mode function

$$u_i(\vec{r}) \equiv \frac{i}{\sqrt{V}} \sum_{k_{n\perp}} e^{i\vec{k}_{n\perp} \cdot \vec{r}} f_{i, k_{n\perp}}, \quad \text{where} \quad \int d^2r dz u_i^* u_i = 1$$

and we have

$$\hat{E}^+(z, \vec{r}) = \sum_{n=-M}^M \sqrt{\frac{\hbar\omega_{s,n}}{2\epsilon_0}} e^{i(k_s+k_n)z} \sum_{i, \lambda} \vec{\epsilon}_{k_n, \lambda} \hat{c}_{n, i, \lambda} u_i(\vec{r}). \quad (\text{B.5})$$

An approximation of a single transverse mode can be applied if only single mode is collected for the experiment, and a flat transverse mode can be assumed ( $u_i = \frac{1}{\sqrt{V}}$ )

if the collected mode has a narrower spatial bandwidth than the mode function. Finally, we have

$$\hat{E}^+(z, \vec{r}) = \sum_{n=-M}^M \sqrt{\frac{\hbar \omega_{s,n}}{2\epsilon_0 V}} e^{i(k_s+k_n)z} \sum_{\lambda} \vec{\epsilon}_{k_n, \lambda} \hat{c}_{n, \lambda}. \quad (\text{B.6})$$

For a demonstration of deriving an interaction Hamiltonian and Maxwell-Bloch equations, we use a two-state system ( $|0\rangle$  and  $|1\rangle$ ), and the polarization is not concerned here. The free field and interaction Hamiltonian (interacting with atomic ensemble with  $N$  atoms) is

$$H_0 = \sum_n \hbar \omega_{s,n} \hat{c}_n^\dagger \hat{c}_n + \hbar \omega_1 |1\rangle \langle 1|, \quad (\text{B.7})$$

$$V = - \sum_{\mu}^N \vec{d}^{\mu} \cdot \vec{E}(r_{\mu}) = \left[ -\hbar g \sum_{\mu} \sum_{n, m=-M}^M \hat{\sigma}^{\mu, m\dagger} \hat{c}_n e^{i(k_s+k_n)z_m} + h.c. \right]_{\text{RWA}}, \quad (\text{B.8})$$

$$g \equiv \frac{d}{\hbar} \sqrt{\frac{\hbar \omega_s}{2\epsilon_0 V}}, \quad \vec{d}^{\mu} \equiv \hat{\sigma}^{\mu} + \hat{\sigma}^{\mu, \dagger}, \quad \vec{E} \equiv \hat{E}^+ + \hat{E}^- \quad (\text{B.9})$$

where  $\sum_{\mu}$  sums over  $\frac{N}{2M+1}$  atoms in the cross sections and the index  $m$  on raising and lowering atomic operators  $\hat{\sigma}$  characterizes the position of the atoms. The rotating wave approximation (RWA) is made in the interaction Hamiltonian and slowly varying coupling constant  $g$  is taken out of the discrete mode sum and is assigned a central frequency, which is the narrow band assumption for the field.

Now we introduce a new operator

$$\hat{b}_l = \frac{1}{\sqrt{2M+1}} \sum_{n=-M}^M \hat{c}_n e^{ik_n z_l}, \quad l = -M, \dots, M, \quad (\text{B.10})$$

which satisfies commutation relations  $[\hat{b}_l, \hat{b}_{l'}^\dagger] = \delta_{ll'}$ , and the Hamiltonian can be re-expressed as

$$H_0 = \hbar \omega_s \sum_l \hat{b}_l^\dagger \hat{b}_l + \hbar \sum_{l'} \omega_{l'} \hat{b}_l^\dagger \hat{b}_{l'} + \hbar \omega_1 |1\rangle \langle 1|, \quad (\text{B.11})$$

$$V = -\hbar g \sum_{\mu, l} \sqrt{2M+1} \hat{\sigma}^{\mu, l\dagger} \hat{b}_l e^{ik_s z_l} + h.c.. \quad (\text{B.12})$$

The Heisenberg equation of slowly varying field operators ( $\tilde{b}_l \equiv \hat{b}_l e^{i\omega_s t}$ ) is

$$\dot{\tilde{b}}_l = -i \sum_{l'} \omega_{ll'} \tilde{b}_{l'} + ig^* \sum_{\mu} \sqrt{2M+1} \hat{\sigma}^{\mu,l} e^{-ik_s z_l + i\omega_s t}, \quad \omega_{ll'} \equiv \sum_n \frac{k_n c}{2M+1} e^{ik_n(z_l - z_{l'})}, \quad (\text{B.13})$$

and we may use the limit of  $M \rightarrow \infty$  that

$$z_m = \frac{mL}{2M+1} \rightarrow z, \quad \sqrt{2M+1} \tilde{b}_l \rightarrow \tilde{E}_s^+(z, t), \quad -i \sum_{l'} \omega_{ll'} \tilde{b}_{l'} \sqrt{2M+1} \rightarrow -c \frac{d}{dz} \tilde{E}_s^+(z, t) \quad (\text{B.14})$$

where the derivative can be shown from

$$\begin{aligned} -i \sum_{l'} \omega_{ll'} \tilde{b}_{l'} &= -i \sum_{l'} \sum_n \frac{k_n c}{2M+1} e^{ik_n(z_l - z_{l'})} \tilde{b}_{l'} = -\frac{c}{2M+1} \sum_{l'} \sum_n \frac{d}{dz_l} [e^{ik_n(z_l - z_{l'})}] \tilde{b}_{l'} \\ &= -c \sum_{l'} \frac{d}{dz_l} \delta_{ll'} \tilde{b}_{l'} = -c \frac{d}{dz} \tilde{b}_l. \end{aligned} \quad (\text{B.15})$$

In the end, we have

$$\left( \frac{\partial}{\partial t} + c \frac{\partial}{\partial z} \right) \tilde{E}_s^+(z, t) = ig^* \lim_{M \rightarrow \infty} (2M+1) \sum_{\mu} \hat{\sigma}^{\mu,l} e^{-ik_s z_l + i\omega_s t} \Big|_{z_l \rightarrow z}, \quad (\text{B.16})$$

and use the limit,

$$\lim_{M \rightarrow \infty} \frac{2M+1}{L} \delta_{ll'} \rightarrow \delta(z - z'),$$

then we have (define slowly varying atomic operators  $\tilde{\sigma}^{\mu,l} = \hat{\sigma}^{\mu,l} e^{-ik_s z_l + i\omega_s t}$ )

$$\lim_{M \rightarrow \infty} \frac{2M+1}{L} \sum_{\mu=1}^N \tilde{\sigma}^{\mu,l} \delta_{z_{\mu}, z_l} L \Big|_{z_l \rightarrow z} \rightarrow \sum_{\mu=1}^N \tilde{\sigma}^{\mu} \delta(z_{\mu} - z) L = \frac{N}{N_z} \sum_{\mu}^{N_z} \tilde{\sigma}^{\mu}. \quad (\text{B.17})$$

The field propagation equation in Maxwell-Bloch equations becomes

$$\left( \frac{\partial}{\partial t} + c \frac{\partial}{\partial z} \right) \tilde{E}_s^+(z, t) = ig^* \sum_{\mu=1}^N \tilde{\sigma}^{\mu} \delta(z_{\mu} - z) L = ig^* \frac{N}{N_z} \sum_{\mu=1}^{N_z} \tilde{\sigma}^{\mu}. \quad (\text{B.18})$$

## B.2 Positive P-representation

The phase space methods [32] that mainly include P-, Q-, and Wigner (W) representations are techniques of using classical analogues to study quantum systems,

especially harmonic oscillators. The eigenstate of harmonic oscillator is a coherent state that provides the basis expansion to construct various representations. P and Q-representation are associated respectively with evaluations of normal and anti-normal order correlations of creation and destruction operators. W-representation is invented for the purpose of describing symmetrically ordered creation and destruction operators. Since P-representation describes normally ordered quantities that are relevant in experiments, we are interested in investigating one class of generalized P-representations, the positive P-representation that has semi-definite property in the diffusion process, which is important in describing quantum noise systems.

Positive-P representation [35, 94] is an extension to Glauber-Sudarshan P-representation that uses coherent state ( $|\alpha\rangle$ ) as a basis expansion of density operator  $\rho$ . In terms of diagonal coherent states with a quasi-probability distribution,  $P(\alpha, \alpha^*)$ , a density operator in P-representation is

$$\rho = \int_D |\alpha\rangle\langle\alpha| P(\alpha, \alpha^*) d^2\alpha, \quad (\text{B.19})$$

where  $D$  represents the integration domain. The normalization condition of  $\rho$ , which is  $\text{Tr}\{\rho\} = 1$ , indicates the normalization for  $P$  as well,  $\int_D P(\alpha, \alpha^*) d^2\alpha = 1$ .

Positive P-representation uses a non-diagonal coherent state expansion and the density operator can be expressed as

$$\rho = \int_D \Lambda(\alpha, \beta) P(\alpha, \beta) d\mu(\alpha, \beta), \quad (\text{B.20})$$

where

$$d\mu(\alpha, \beta) = d^2\alpha d^2\beta \text{ and } \Lambda(\alpha, \beta) = \frac{|\alpha\rangle\langle\beta^*|}{\langle\beta^*|\alpha\rangle}, \quad (\text{B.21})$$

and  $\langle\beta^*|\alpha\rangle$  in non-diagonal projection operators,  $\Lambda(\alpha, \beta)$ , makes sure of the normalization condition in distribution function,  $P(\alpha, \beta)$ .

Any normally ordered observable can be deduced from the distribution function  $P(\alpha, \beta)$  that

$$\langle (a^\dagger)^m a^n \rangle = \int_D \beta^m \alpha^n P(\alpha, \beta) d\mu(\alpha, \beta). \quad (\text{B.22})$$

A characteristic function  $\chi_p(\lambda_\alpha, \lambda_\beta)$  (Fourier-transformed distribution function in Glauber-Sudarshan P-representation but now is extended into a larger dimension) can help formulate distribution function, which is

$$\chi_p(\lambda_\alpha, \lambda_\beta) = \int_D e^{i\lambda_\alpha \alpha + i\lambda_\beta \beta} P(\alpha, \beta) d\mu(\alpha, \beta). \quad (\text{B.23})$$

It is calculated from a normally ordered exponential operator  $E(\lambda)$ ,

$$\chi_p(\lambda_\alpha, \lambda_\beta) = \text{Tr}\{\rho E(\lambda)\}, \quad E(\lambda) = e^{i\lambda_\beta a^\dagger} e^{i\lambda_\alpha a}. \quad (\text{B.24})$$

Then a Fokker-Planck equation can be derived from the time derivative of characteristic function,

$$\frac{\partial \chi_p}{\partial t} = \frac{\partial}{\partial t} \text{Tr}\{\rho E(\lambda)\} = \text{Tr}\left\{\frac{\partial \rho}{\partial t} E(\lambda)\right\} \quad (\text{B.25})$$

by Liouville equations,

$$\frac{\partial \rho}{\partial t} = \frac{1}{i\hbar} [H, \rho]. \quad (\text{B.26})$$

In laser theory [27], a P-representation method is extended to describe atomic and atom-field interaction systems. When a large number of atoms is considered, which is indeed the case of the actual laser, a macroscopic variable can be defined. Then a generalized Fokker-Planck equation can be derived from characteristic functions by neglecting higher order terms that are proportional to the inverse of number of atoms. It is similar to our case when we solve light-matter interactions in an atomic ensemble that the large number cuts off the higher order terms in characteristic functions, which we will demonstrate in the next subsection.

### B.2.1 Hamiltonian

The Hamiltonian is in Schrödinger picture, and we separate it into two parts where  $H_0$  is the free Hamiltonian of the atomic ensemble and one dimensional counter-propagating signal and idler fields, and  $H_I$  is the interaction Hamiltonian of atoms interacting with two classical fields and two quantum fields (signal and idler). Dipole approximation of  $-\vec{d} \cdot \vec{E}$  and rotating wave approximation (RWA) have been made to these interactions. Similar to the previous Appendix, we have

$$H = H_0 + H_I ,$$

$$H_0 = \sum_{i=1}^3 \sum_{l=-M}^M \hbar \omega_i \tilde{\sigma}_{ii}^l + \hbar \omega_s \sum_{l=-M}^M \hat{a}_{s,l}^\dagger \hat{a}_{s,l} + \hbar \sum_{l,l'} \omega_{l'l} \hat{a}_{s,l}^\dagger \hat{a}_{s,l'} + \hbar \omega_i \sum_{l=-M}^M \hat{a}_{i,l}^\dagger \hat{a}_{i,l} + \hbar \sum_{l,l'} \omega_{ll'} \hat{a}_{i,l}^\dagger \hat{a}_{i,l'} , \quad (\text{B.27})$$

$$H_I = -\hbar \sum_{l=-M}^M \left[ \Omega_a(t) \tilde{\sigma}_{01}^{l\dagger} e^{ik_a z_l - i\omega_a t} + \Omega_b(t) \tilde{\sigma}_{12}^{l\dagger} e^{-ik_b z_l - i\omega_b t} + h.c. \right] \quad (\text{B.28})$$

$$- \hbar \sum_{l=-M}^M \left[ g_s \sqrt{2M+1} \tilde{\sigma}_{32}^{l\dagger} \hat{a}_{s,l} e^{-ik_s z_l} + g_i \sqrt{2M+1} \tilde{\sigma}_{03}^{l\dagger} \hat{a}_{i,l} e^{ik_i z_l} + h.c. \right] \quad (\text{B.29})$$

where  $\tilde{\sigma}_{mn}^l \equiv \sum_{\mu}^{N_z} \hat{\sigma}_{mn}^{\mu,l} = \sum_{\mu}^{N_z} |m\rangle_{\mu} \langle n| \Big|_{r_{\mu}=z_l}$ ,  $\Omega_a(t) \equiv f_a(t) d_{10} \mathcal{E}(k_a) / (2\hbar)$ , and  $f_a$  is slow varying temporal profile without spatial dependence (ensemble scale much less than pulse length).  $g_s \equiv d_{23} \mathcal{E}(k_s) / \hbar$ ,  $\mathcal{E}(k) = \sqrt{\hbar \omega / 2 \epsilon_0 V}$  and  $z_m = \frac{mL}{2M+1}$ ,  $m = -M, \dots, M$ , and  $L$  is the length of propagation. Note that the Rabi frequency is half of the standard definition.

The normally ordered exponential operator is chosen as

$$\begin{aligned}
E(\lambda) &= \prod_l E^l(\lambda), \\
E^l(\lambda) &= e^{i\lambda_{19}^l \tilde{\sigma}_{01}^{l\dagger}} e^{i\lambda_{18}^l \tilde{\sigma}_{12}^{l\dagger}} e^{i\lambda_{17}^l \tilde{\sigma}_{02}^{l\dagger}} e^{i\lambda_{16}^l \tilde{\sigma}_{13}^{l\dagger}} e^{i\lambda_{15}^l \tilde{\sigma}_{03}^{l\dagger}} e^{i\lambda_{14}^l \tilde{\sigma}_{32}^{l\dagger}} e^{i\lambda_{13}^l \tilde{\sigma}_{11}^{l\dagger}} e^{i\lambda_{12}^l \tilde{\sigma}_{22}^{l\dagger}} e^{i\lambda_{11}^l \tilde{\sigma}_{33}^{l\dagger}} e^{i\lambda_{10}^l \tilde{\sigma}_{32}^{l\dagger}} \\
&\quad e^{i\lambda_9^l \tilde{\sigma}_{03}^{l\dagger}} e^{i\lambda_8^l \tilde{\sigma}_{13}^{l\dagger}} e^{i\lambda_7^l \tilde{\sigma}_{02}^{l\dagger}} e^{i\lambda_6^l \tilde{\sigma}_{12}^{l\dagger}} e^{i\lambda_5^l \tilde{\sigma}_{01}^{l\dagger}} e^{i\lambda_4^l \hat{a}_{s,l}^\dagger} e^{i\lambda_3^l \hat{a}_{s,l}} e^{i\lambda_2^l \hat{a}_{i,l}^\dagger} e^{i\lambda_1^l \hat{a}_{i,l}}.
\end{aligned} \tag{B.30}$$

Aside from the atom-field interaction  $\frac{\partial \rho}{\partial t} = \frac{1}{i\hbar} [H, \rho]$ , when dissipation from vacuum is considered (single atomic decay), we can express them in terms of a Lindblad form where we have for the four-level atomic system,

$$\begin{aligned}
\left(\frac{\partial \rho}{\partial t}\right)_{sp} &= \sum_{l=-M}^M \sum_{\mu}^{N_z} \left\{ \frac{\gamma_{01}}{2} [2\hat{\sigma}_{01}^{\mu,l} \rho \hat{\sigma}_{01}^{\mu,l\dagger} - \hat{\sigma}_{01}^{\mu,l\dagger} \hat{\sigma}_{01}^{\mu,l} \rho - \rho \hat{\sigma}_{01}^{\mu,l\dagger} \hat{\sigma}_{01}^{\mu,l}] \right. \\
&\quad + \frac{\gamma_{12}}{2} [2\hat{\sigma}_{12}^{\mu,l} \rho \hat{\sigma}_{12}^{\mu,l\dagger} - \hat{\sigma}_{12}^{\mu,l\dagger} \hat{\sigma}_{12}^{\mu,l} \rho - \rho \hat{\sigma}_{12}^{\mu,l\dagger} \hat{\sigma}_{12}^{\mu,l}] \\
&\quad + \frac{\gamma_{32}}{2} [2\hat{\sigma}_{32}^{\mu,l} \rho \hat{\sigma}_{32}^{\mu,l\dagger} - \hat{\sigma}_{32}^{\mu,l\dagger} \hat{\sigma}_{32}^{\mu,l} \rho - \rho \hat{\sigma}_{32}^{\mu,l\dagger} \hat{\sigma}_{32}^{\mu,l}] \\
&\quad \left. + \frac{\gamma_{03}}{2} [2\hat{\sigma}_{03}^{\mu,l} \rho \hat{\sigma}_{03}^{\mu,l\dagger} - \hat{\sigma}_{03}^{\mu,l\dagger} \hat{\sigma}_{03}^{\mu,l} \rho - \rho \hat{\sigma}_{03}^{\mu,l\dagger} \hat{\sigma}_{03}^{\mu,l}] \right\}.
\end{aligned} \tag{B.31}$$

The characteristic functions can be calculated,

$$\chi = \text{Tr}\{E(\lambda)\rho\}, \tag{B.32}$$

$$\begin{aligned}
\frac{\partial \chi}{\partial t} &= \text{Tr}\{E(\lambda) \frac{\partial \rho}{\partial t}\} = \left(\frac{\partial \chi}{\partial t}\right)_A + \left(\frac{\partial \chi}{\partial t}\right)_L \\
&\quad + \left(\frac{\partial \chi}{\partial t}\right)_{A-L} + \left(\frac{\partial \chi}{\partial t}\right)_{sp},
\end{aligned} \tag{B.33}$$

$$\begin{aligned}
\left(\frac{\partial \chi}{\partial t}\right)_A &= \text{Tr}\{E(\lambda) \frac{1}{i\hbar} [H_A, \rho]\}, \quad \left(\frac{\partial \chi}{\partial t}\right)_L = \text{Tr}\{E(\lambda) \frac{1}{i\hbar} [H_L, \rho]\}, \\
\left(\frac{\partial \chi}{\partial t}\right)_{A-L} &= \text{Tr}\{E(\lambda) \frac{1}{i\hbar} [H_{A-L}, \rho]\}, \quad \left(\frac{\partial \chi}{\partial t}\right)_{sp} = \text{Tr}\{E(\lambda) \left(\frac{\partial \rho}{\partial t}\right)_{sp}\}
\end{aligned} \tag{B.34}$$

where  $H_0 = H_A + H_L$ ,  $H_A$  is the atomic free evolution Hamiltonian,  $H_L$  is the Hamiltonian for laser fields, and  $H_{A-L} = H_I$ . Now we continue to derive the time derivative in each part of characteristic functions.



### B.2.2 Characteristic function - atomic part

The atomic part in characteristic function is deduced from  $(\frac{\partial \rho}{\partial t})_A$

$$\begin{aligned} \left(\frac{\partial \chi}{\partial t}\right)_A &= \text{Tr}\{E(\lambda)\left(\frac{\partial \rho}{\partial t}\right)_A\}, \\ \left(\frac{\partial \rho}{\partial t}\right)_A &= \frac{1}{i\hbar}[H_A, \rho] \\ &= \sum_l \left[ -i\omega_1(\tilde{\sigma}_{11}^l \rho - \rho \tilde{\sigma}_{11}^l) - i\omega_2(\tilde{\sigma}_{22}^l \rho - \rho \tilde{\sigma}_{22}^l) - i\omega_3(\tilde{\sigma}_{33}^l \rho - \rho \tilde{\sigma}_{33}^l) \right] \end{aligned} \quad (\text{B.35})$$

so various components in  $(\frac{\partial \chi}{\partial t})_A$  are

$$\begin{aligned} \text{Tr}\{E(\lambda) \sum_l \tilde{\sigma}_{11}^l \rho\} &= \sum_l \text{Tr}\{E(\lambda) \tilde{\sigma}_{11}^l \rho\} \\ &= \sum_l [i\lambda_5 \frac{\partial}{\partial(i\lambda_5)} - i\lambda_6 \frac{\partial}{\partial(i\lambda_6)} - i\lambda_8 \frac{\partial}{\partial(i\lambda_8)} + \frac{\partial}{\partial(i\lambda_{13})}]_l \chi, \\ \text{Tr}\{E(\lambda) \sum_l \rho \tilde{\sigma}_{11}^l\} &= \sum_l [i\lambda_{19} \frac{\partial}{\partial(i\lambda_{19})} - i\lambda_{18} \frac{\partial}{\partial(i\lambda_{18})} - i\lambda_{16} \frac{\partial}{\partial(i\lambda_{16})} + \frac{\partial}{\partial(i\lambda_{13})}]_l \chi, \\ \text{Tr}\{E(\lambda) \sum_l \tilde{\sigma}_{22}^l \rho\} &= \sum_l [i\lambda_6 \frac{\partial}{\partial(i\lambda_6)} + i\lambda_7 \frac{\partial}{\partial(i\lambda_7)} + i\lambda_{10} \frac{\partial}{\partial(i\lambda_{10})} + \frac{\partial}{\partial(i\lambda_{12})}]_l \chi, \\ \text{Tr}\{E(\lambda) \sum_l \rho \tilde{\sigma}_{22}^l\} &= \sum_l [i\lambda_{18} \frac{\partial}{\partial(i\lambda_{18})} + i\lambda_{17} \frac{\partial}{\partial(i\lambda_{17})} + i\lambda_{14} \frac{\partial}{\partial(i\lambda_{14})} + \frac{\partial}{\partial(i\lambda_{12})}]_l \chi, \\ \text{Tr}\{E(\lambda) \sum_l \tilde{\sigma}_{33}^l \rho\} &= \sum_l [i\lambda_8 \frac{\partial}{\partial(i\lambda_8)} + i\lambda_9 \frac{\partial}{\partial(i\lambda_9)} - i\lambda_{10} \frac{\partial}{\partial(i\lambda_{10})} + \frac{\partial}{\partial(i\lambda_{11})}]_l \chi, \\ \text{Tr}\{E(\lambda) \sum_l \rho \tilde{\sigma}_{33}^l\} &= \sum_l [i\lambda_{16} \frac{\partial}{\partial(i\lambda_{16})} + i\lambda_{15} \frac{\partial}{\partial(i\lambda_{15})} - i\lambda_{14} \frac{\partial}{\partial(i\lambda_{14})} + \frac{\partial}{\partial(i\lambda_{11})}]_l \chi \end{aligned} \quad (\text{B.36})$$

where the subscript  $l$  on the bracket reminds us the derivatives inside the bracket operate on  $l$ th component of the characteristic functions.

### B.2.3 Characteristic function - field part

The field part in characteristic function is deduced from  $(\frac{\partial \rho}{\partial t})_L$

$$\begin{aligned}
\left(\frac{\partial \chi}{\partial t}\right)_L &= \text{Tr}\{E(\lambda)\left(\frac{\partial \rho}{\partial t}\right)_L\}, \\
\left(\frac{\partial \rho}{\partial t}\right)_L &= \frac{1}{i\hbar}[H_L, \rho] = \sum_l \left[ -i\omega_s(\hat{a}_{s,l}^\dagger \hat{a}_{s,l} \rho - \rho \hat{a}_{s,l}^\dagger \hat{a}_{s,l}) - i\omega_i(\hat{a}_{i,l}^\dagger \hat{a}_{i,l} \rho - \rho \hat{a}_{i,l}^\dagger \hat{a}_{i,l}) \right] + \\
&\quad \sum_{l,l'} \left[ -i\omega_{l'l}(\hat{a}_{s,l}^\dagger \hat{a}_{s,l'} \rho - \rho \hat{a}_{s,l}^\dagger \hat{a}_{s,l'}) - i\omega_{l'l'}(\hat{a}_{i,l}^\dagger \hat{a}_{i,l'} \rho - \rho \hat{a}_{i,l}^\dagger \hat{a}_{i,l'}) \right], \tag{B.37}
\end{aligned}$$

and various components in  $\left(\frac{\partial \chi}{\partial t}\right)_L$  are

$$\begin{aligned}
\text{Tr}\{E(\lambda) \sum_l \hat{a}_{s,l}^\dagger \hat{a}_{s,l} \rho\} &= \sum_l \left[ \frac{\partial^2}{\partial(i\lambda_4)\partial(i\lambda_3)} + i\lambda_3 \frac{\partial}{\partial(i\lambda_3)} \right] \chi, \\
\text{Tr}\{E(\lambda) \sum_l \rho \hat{a}_{s,l}^\dagger \hat{a}_{s,l}\} &= \sum_l \left[ \frac{\partial^2}{\partial(i\lambda_4)\partial(i\lambda_3)} + i\lambda_4 \frac{\partial}{\partial(i\lambda_4)} \right] \chi, \\
\text{Tr}\{E(\lambda) \sum_l \hat{a}_{i,l}^\dagger \hat{a}_{i,l} \rho\} &= \sum_l \left[ \frac{\partial^2}{\partial(i\lambda_2)\partial(i\lambda_1)} + i\lambda_1 \frac{\partial}{\partial(i\lambda_1)} \right] \chi, \\
\text{Tr}\{E(\lambda) \sum_l \rho \hat{a}_{i,l}^\dagger \hat{a}_{i,l}\} &= \sum_l \left[ \frac{\partial^2}{\partial(i\lambda_2)\partial(i\lambda_1)} + i\lambda_2 \frac{\partial}{\partial(i\lambda_2)} \right] \chi, \tag{B.38}
\end{aligned}$$

and

$$\begin{aligned}
\text{Tr}\{E(\lambda) \sum_{l,l'} \omega_{l'l} \hat{a}_{s,l}^\dagger \hat{a}_{s,l'} \rho\} &= \sum_{l,l'} \omega_{l'l} \left[ \frac{\partial^2}{\partial(i\lambda_4^l)\partial(i\lambda_3^{l'})} + i\lambda_3^{l'} \frac{\partial}{\partial(i\lambda_3^{l'})} \right] \chi, \\
\text{Tr}\{E(\lambda) \sum_{l,l'} \omega_{l'l} \rho \hat{a}_{s,l}^\dagger \hat{a}_{s,l'}\} &= \sum_{l,l'} \omega_{l'l} \left[ \frac{\partial^2}{\partial(i\lambda_4^l)\partial(i\lambda_3^{l'})} + i\lambda_4^l \frac{\partial}{\partial(i\lambda_4^l)} \right] \chi, \\
\text{Tr}\{E(\lambda) \sum_{l,l'} \omega_{l'l} \hat{a}_{i,l}^\dagger \hat{a}_{i,l'} \rho\} &= \sum_{l,l'} \omega_{l'l} \left[ \frac{\partial^2}{\partial(i\lambda_2^l)\partial(i\lambda_1^{l'})} + i\lambda_1^{l'} \frac{\partial}{\partial(i\lambda_1^{l'})} \right] \chi, \\
\text{Tr}\{E(\lambda) \sum_{l,l'} \omega_{l'l} \rho \hat{a}_{i,l}^\dagger \hat{a}_{i,l'}\} &= \sum_{l,l'} \omega_{l'l} \left[ \frac{\partial^2}{\partial(i\lambda_2^l)\partial(i\lambda_1^{l'})} + i\lambda_2^l \frac{\partial}{\partial(i\lambda_2^l)} \right] \chi. \tag{B.39}
\end{aligned}$$

#### B.2.4 Characteristic function - atom-field part

The atom-field interaction part in characteristic function is deduced from  $\left(\frac{\partial \rho}{\partial t}\right)_{A-L}$ , and we denote part (a) for the classical field interaction.

$$\begin{aligned}
\left(\frac{\partial \chi}{\partial t}\right)_{A-L}^{(a)} &= \text{Tr}\{E(\lambda)\left(\frac{\partial \rho}{\partial t}\right)_{A-L}^{(a)}\}, \\
\left(\frac{\partial \rho}{\partial t}\right)_{A-L}^{(a)} &= \frac{1}{i\hbar} \left[ -\hbar \sum_{l=-M}^M [\Omega_a(t)\tilde{\sigma}_{01}^{l\dagger} e^{ik_a z_l - i\omega_a t} + \Omega_b(t)\tilde{\sigma}_{12}^{l\dagger} e^{-ik_b z_l - i\omega_b t} + h.c.], \rho \right],
\end{aligned}
\tag{B.40}$$

and various components in  $\left(\frac{\partial \chi}{\partial t}\right)_{A-L}^{(a)}$  are

$$\begin{aligned}
&\text{Tr}\{E(\lambda) \sum_l e^{ik_a z_l} \tilde{\sigma}_{01}^{l\dagger} \rho\} = \\
&\sum_l e^{ik_a z_l} \left[ -(i\lambda_5)^2 \frac{\partial}{\partial(i\lambda_5)} + (i\lambda_5)(i\lambda_6) \frac{\partial}{\partial(i\lambda_6)} - (i\lambda_5)(i\lambda_7) \frac{\partial}{\partial(i\lambda_7)} + (i\lambda_5)(i\lambda_8) \frac{\partial}{\partial(i\lambda_8)} \right. \\
&- (i\lambda_5)(i\lambda_9) \frac{\partial}{\partial(i\lambda_9)} - i\lambda_5 \frac{\partial}{\partial(i\lambda_{11})} - i\lambda_5 \frac{\partial}{\partial(i\lambda_{12})} - 2i\lambda_5 \frac{\partial}{\partial(i\lambda_{13})} + i\lambda_5 N_z - i\lambda_7 \frac{\partial}{\partial(i\lambda_6)} \\
&- i\lambda_9 \frac{\partial}{\partial(i\lambda_8)} + i\lambda_{16} e^{i\lambda_{13}} \frac{\partial}{\partial(i\lambda_{15})} + i\lambda_{18} e^{i\lambda_{13}} \frac{\partial}{\partial(i\lambda_{17})} + e^{i\lambda_{13}} \frac{\partial}{\partial(i\lambda_{19})} \Big] \chi, \\
&\text{Tr}\{E(\lambda) \sum_l e^{-ik_a z_l} \tilde{\sigma}_{01}^l \rho\} = \sum_l e^{-ik_a z_l} \left[ \frac{\partial}{\partial(i\lambda_5)} \right]_l \chi, \\
&\text{Tr}\{E(\lambda) \sum_l \rho e^{ik_a z_l} \tilde{\sigma}_{01}^{l\dagger}\} = \sum_l e^{ik_a z_l} \left[ \frac{\partial}{\partial(i\lambda_{19})} \right]_l \chi, \\
&\text{Tr}\{E(\lambda) \sum_l \rho e^{-ik_a z_l} \tilde{\sigma}_{01}^l\} = \text{Tr}\{E(\lambda) \sum_l e^{ik_a z_l} \tilde{\sigma}_{01}^{l\dagger} \rho\}^*_{\substack{\lambda_5^* \leftrightarrow -\lambda_{19}, \lambda_6^* \leftrightarrow -\lambda_{18}, \lambda_7^* \leftrightarrow -\lambda_{17}, \lambda_8^* \leftrightarrow -\lambda_{16}, \\ \lambda_9^* \leftrightarrow -\lambda_{15}, \lambda_{11}^* \leftrightarrow -\lambda_{11}, \lambda_{12}^* \leftrightarrow -\lambda_{12}, \lambda_{13}^* \leftrightarrow -\lambda_{13}}}
\end{aligned}
\tag{B.41}$$

where a correspondence that we denote as  $C$  later is  $\lambda_5^* \leftrightarrow -\lambda_{19}$ ,  $\lambda_6^* \leftrightarrow -\lambda_{18}$ ,  $\lambda_7^* \leftrightarrow -\lambda_{17}$ ,  $\lambda_8^* \leftrightarrow -\lambda_{16}$ ,  $\lambda_9^* \leftrightarrow -\lambda_{15}$ ,  $\lambda_{11}^* \leftrightarrow -\lambda_{11}$ ,  $\lambda_{12}^* \leftrightarrow -\lambda_{12}$ ,  $\lambda_{13}^* \leftrightarrow -\lambda_{13}$ , can be observed to help calculate the characteristic function. Also

$$\begin{aligned}
& \text{Tr}\{E(\lambda) \sum_l e^{-ik_b z_l} \tilde{\sigma}_{12}^{l\dagger} \rho\} = \\
& \sum_l e^{-ik_b z_l} \left[ - (i\lambda_6)^2 \frac{\partial}{\partial(i\lambda_6)} - (i\lambda_6)(i\lambda_8) \frac{\partial}{\partial(i\lambda_8)} - (i\lambda_6)(i\lambda_7) \frac{\partial}{\partial(i\lambda_7)} \right. \\
& - (i\lambda_6)(i\lambda_{10}) \frac{\partial}{\partial(i\lambda_{10})} + (i\lambda_7)(i\lambda_6) \frac{\partial}{\partial(i\lambda_7)} + i\lambda_6 \frac{\partial}{\partial(i\lambda_{13})} - i\lambda_6 \frac{\partial}{\partial(i\lambda_{12})} + i\lambda_7 \frac{\partial}{\partial(i\lambda_5)} \\
& + (i\lambda_8)(i\lambda_{10}) \left( \frac{\partial}{\partial(i\lambda_{12})} - \frac{\partial}{\partial(i\lambda_{11})} \right) - i\lambda_8 (i\lambda_{10})^2 \frac{\partial}{\partial(i\lambda_{10})} - i\lambda_8 e^{i\lambda_{12}-i\lambda_{11}} \frac{\partial}{\partial(i\lambda_{14})} \\
& \left. + i\lambda_{10} e^{i\lambda_{11}-i\lambda_{13}} \frac{\partial}{\partial(i\lambda_{16})} + ((i\lambda_{10})(i\lambda_{14}) e^{i\lambda_{11}-i\lambda_{13}} + e^{i\lambda_{12}-i\lambda_{13}}) \frac{\partial}{\partial(i\lambda_{18})} \right] \chi, \\
& \text{Tr}\{E(\lambda) \sum_l e^{ik_b z_l} \tilde{\sigma}_{12}^l \rho\} = \sum_l e^{ik_b z_l} \left[ \frac{\partial}{\partial(i\lambda_6)} + i\lambda_5 \frac{\partial}{\partial(i\lambda_7)} \right] \chi, \\
& \text{Tr}\{E(\lambda) \sum_l \rho e^{-ik_b z_l} \tilde{\sigma}_{12}^{l\dagger}\} = \text{Tr}\{E(\lambda) \sum_l e^{ik_b z_l} \tilde{\sigma}_{12}^l \rho\}_C^*, \\
& \text{Tr}\{E(\lambda) \sum_l \rho e^{ik_b z_l} \tilde{\sigma}_{12}^l\} = \text{Tr}\{E(\lambda) \sum_l e^{-ik_b z_l} \tilde{\sigma}_{12}^{l\dagger} \rho\}_C^*, \tag{B.42}
\end{aligned}$$

and the atom-field interaction characteristic function for quantum fields, which we denote as part (b), is

$$\begin{aligned}
& \left( \frac{\partial \chi}{\partial t} \right)_{A-L}^{(b)} = \text{Tr}\{E(\lambda) \left( \frac{\partial \rho}{\partial t} \right)_{A-L}^{(b)}\}, \\
& \left( \frac{\partial \rho}{\partial t} \right)_{A-L}^{(b)} = \frac{1}{i\hbar} \left[ -\hbar \sum_{l=-M}^M [g_s \sqrt{2M+1} \tilde{\sigma}_{32}^{l\dagger} \hat{a}_{s,l} e^{-ik_s z_l} \right. \\
& \left. + g_i \sqrt{2M+1} \tilde{\sigma}_{03}^{l\dagger} \hat{a}_{i,l} e^{ik_i z_l} + h.c.], \rho \right]. \tag{B.44}
\end{aligned}$$

For the part of fields only,

$$\begin{aligned}
& \text{Tr}\{E(\lambda) \hat{a}_{s,l} \rho\} = \left[ \frac{\partial}{\partial(i\lambda_3^l)} \right] \chi, \quad \text{Tr}\{E(\lambda) \rho \hat{a}_{s,l}\} = \left[ \frac{\partial}{\partial(i\lambda_3^l)} + i\lambda_4^l \right] \chi, \\
& \text{Tr}\{E(\lambda) \hat{a}_{s,l}^\dagger \rho\} = \left[ \frac{\partial}{\partial(i\lambda_4^l)} + i\lambda_3^l \right] \chi, \quad \text{Tr}\{E(\lambda) \rho \hat{a}_{s,l}^\dagger\} = \left[ \frac{\partial}{\partial(i\lambda_4^l)} \right] \chi, \\
& \text{Tr}\{E(\lambda) \hat{a}_{i,l} \rho\} = \left[ \frac{\partial}{\partial(i\lambda_1^l)} \right] \chi, \quad \text{Tr}\{E(\lambda) \rho \hat{a}_{i,l}\} = \left[ \frac{\partial}{\partial(i\lambda_1^l)} + i\lambda_2^l \right] \chi, \\
& \text{Tr}\{E(\lambda) \hat{a}_{i,l}^\dagger \rho\} = \left[ \frac{\partial}{\partial(i\lambda_2^l)} + i\lambda_1^l \right] \chi, \quad \text{Tr}\{E(\lambda) \rho \hat{a}_{i,l}^\dagger\} = \left[ \frac{\partial}{\partial(i\lambda_2^l)} \right] \chi, \tag{B.45}
\end{aligned}$$

and for the part of atomic operators associated with signal field,

$$\begin{aligned}
\text{Tr}\{E(\lambda)\tilde{\sigma}_{32}^{l\dagger}\rho\} &= \left[ i\lambda_6 \frac{\partial}{\partial(i\lambda_8)} + i\lambda_7 \frac{\partial}{\partial(i\lambda_9)} - (i\lambda_{10})^2 \frac{\partial}{\partial(i\lambda_{10})} \right. \\
&\quad \left. + i\lambda_{10} \left( \frac{\partial}{\partial(i\lambda_{11})} - \frac{\partial}{\partial(i\lambda_{12})} \right) + e^{i\lambda_{12}-i\lambda_{11}} \frac{\partial}{\partial(i\lambda_{14})} \right]_l \chi, \\
\text{Tr}\{E(\lambda)\tilde{\sigma}_{32}^l\rho\} &= \left[ i\lambda_8 \frac{\partial}{\partial(i\lambda_6)} + \frac{\partial}{\partial(i\lambda_{10})} + i\lambda_9 \frac{\partial}{\partial(i\lambda_7)} \right]_l \chi, \\
\text{Tr}\{E(\lambda)\rho\tilde{\sigma}_{32}^{l\dagger}\} &= \text{Tr}\{E(\lambda)\tilde{\sigma}_{32}^l\rho\}_C^*, \\
\text{Tr}\{E(\lambda)\rho\tilde{\sigma}_{32}^l\} &= \text{Tr}\{E(\lambda)\tilde{\sigma}_{32}^{l\dagger}\rho\}_C^*, \tag{B.46}
\end{aligned}$$

and for the part of atomic operators associated with idler field,

$$\begin{aligned}
&\text{Tr}\{E(\lambda)\tilde{\sigma}_{03}^{l\dagger}\rho\} \\
&= \left[ (i\lambda_6)(i\lambda_8)^2 \frac{\partial}{\partial(i\lambda_8)} + (i\lambda_5)(i\lambda_6)(i\lambda_8) \frac{\partial}{\partial(i\lambda_6)} - (i\lambda_5)(i\lambda_8) \left( \frac{\partial}{\partial(i\lambda_{13})} - i\lambda_9 \frac{\partial}{\partial(i\lambda_9)} \right) \right. \\
&\quad + (i\lambda_{10}) \left( \frac{\partial}{\partial(i\lambda_{10})} - \frac{\partial}{\partial(i\lambda_{11})} \right) + (i\lambda_5)(i\lambda_6) \frac{\partial}{\partial(i\lambda_{10})} - i\lambda_5 e^{i\lambda_{11}-i\lambda_{13}} \frac{\partial}{\partial(i\lambda_{16})} \\
&\quad - (i\lambda_5)(i\lambda_{14}) e^{i\lambda_{11}-i\lambda_{13}} \frac{\partial}{\partial(i\lambda_{18})} - (i\lambda_5)(i\lambda_9) \frac{\partial}{\partial(i\lambda_5)} - (i\lambda_7)(i\lambda_8) \frac{\partial}{\partial(i\lambda_6)} - i\lambda_7 \frac{\partial}{\partial(i\lambda_{10})} \\
&\quad - (i\lambda_7)(i\lambda_9) \frac{\partial}{\partial(i\lambda_7)} + i\lambda_9 N_z - (i\lambda_9)^2 \frac{\partial}{\partial(i\lambda_9)} + i\lambda_8 \left[ -(i\lambda_9) \frac{\partial}{\partial(i\lambda_8)} + i\lambda_{16} e^{i\lambda_{13}} \frac{\partial}{\partial(i\lambda_{15})} \right. \\
&\quad \left. + i\lambda_{18} e^{i\lambda_{13}} \frac{\partial}{\partial(i\lambda_{17})} + e^{i\lambda_{13}} \frac{\partial}{\partial(i\lambda_{19})} \right] + e^{i\lambda_{11}} \frac{\partial}{\partial(i\lambda_{15})} + i\lambda_9 \left[ -\frac{\partial}{\partial(i\lambda_{13})} - i\lambda_{10} \frac{\partial}{\partial(i\lambda_{10})} \right. \\
&\quad \left. - \frac{\partial}{\partial(i\lambda_{12})} + 2i\lambda_{10} \frac{\partial}{\partial(i\lambda_{10})} - 2 \frac{\partial}{\partial(i\lambda_{11})} \right] + i\lambda_{14} e^{i\lambda_{11}} \frac{\partial}{\partial(i\lambda_{17})} \Big]_l \chi, \\
&\text{Tr}\{E(\lambda)\tilde{\sigma}_{03}^l\rho\} = \left[ \frac{\partial}{\partial(i\lambda_9)} \right]_l \chi, \\
&\text{Tr}\{E(\lambda)\rho\tilde{\sigma}_{03}^{l\dagger}\} = \text{Tr}\{E(\lambda)\tilde{\sigma}_{03}^l\rho\}_C^*, \\
&\text{Tr}\{E(\lambda)\rho\tilde{\sigma}_{03}^l\} = \text{Tr}\{E(\lambda)\tilde{\sigma}_{03}^{l\dagger}\rho\}_C^*. \tag{B.47}
\end{aligned}$$

### B.2.5 Characteristic function - dissipation part

We calculate the characteristic function from  $\left(\frac{\partial\rho}{\partial t}\right)_{sp}$  up to the second order of various  $\lambda$ 's (where we denote (2)) that account for drift and diffusion terms in Fokker-Planck

equation. Below we drop the summation over spatial slices  $l$ , which we will retrieve later,

$$\begin{aligned}
& \text{Tr}\{E(\lambda)\hat{\sigma}_{01}\rho\hat{\sigma}_{01}^\dagger\}^{(2)} \\
&= \text{Tr}\{[(i\lambda_8)(i\lambda_{10})\hat{\sigma}_{12} + (i\lambda_6)(i\lambda_{14})\hat{\sigma}_{13} + (i\lambda_8)(i\lambda_{15})\hat{\sigma}_{10} + \\
& (i\lambda_8)(i\lambda_{16})\hat{\sigma}_{11} + (i\lambda_6)(i\lambda_{17})\hat{\sigma}_{10} + e^{-i\lambda_{13}}\hat{\sigma}_{11} - i\lambda_{19}e^{-i\lambda_{13}}\hat{\sigma}_{10} \\
& + (i\lambda_6)(i\lambda_{18})\hat{\sigma}_{11} - i\lambda_8e^{-i\lambda_{11}}\hat{\sigma}_{13} - i\lambda_6e^{-i\lambda_{12}}\hat{\sigma}_{12}]E(\lambda)\rho\}^{(2)} \quad (\text{B.48})
\end{aligned}$$

where various properties of tracing can be found in previous sections, and the one we did not have before is (up to first order)

$$\begin{aligned}
& \text{Tr}\{\hat{\sigma}_{13}E(\lambda)\rho\}^{(1)} \\
&= [i\lambda_{15}\frac{\partial}{\partial(i\lambda_{19})} - i\lambda_{16}(\frac{\partial}{\partial(i\lambda_{11})} - \frac{\partial}{\partial(i\lambda_{13})}) - i\lambda_{18}\frac{\partial}{\partial(i\lambda_{14})} \\
& + e^{i\lambda_{11}-i\lambda_{13}}\frac{\partial}{\partial(i\lambda_8)} + i\lambda_{10}\frac{\partial}{\partial(i\lambda_6)}]\chi. \quad (\text{B.49})
\end{aligned}$$

Put everything together, and for the dissipation of first laser transition we have

$$\begin{aligned}
& \gamma_{01}\text{Tr}\{E(\lambda)[\hat{\sigma}_{01}\rho\hat{\sigma}_{01}^\dagger - \frac{1}{2}\hat{\sigma}_{11}\rho - \frac{1}{2}\rho\hat{\sigma}_{11}]\}^{(2)} = \\
& \gamma_{01}[-\frac{i\lambda_5}{2}\frac{\partial}{\partial(i\lambda_5)} - \frac{i\lambda_{19}}{2}\frac{\partial}{\partial(i\lambda_{19})} - \frac{i\lambda_6}{2}\frac{\partial}{\partial(i\lambda_6)} - \frac{i\lambda_{18}}{2}\frac{\partial}{\partial(i\lambda_{18})} - \frac{i\lambda_8}{2}\frac{\partial}{\partial(i\lambda_8)} \\
& - \frac{i\lambda_{16}}{2}\frac{\partial}{\partial(i\lambda_{16})} - i\lambda_{13}\frac{\partial}{\partial(i\lambda_{13})} + (i\lambda_{13})(i\lambda_{18})\frac{\partial}{\partial(i\lambda_{18})} + (i\lambda_{13})(i\lambda_{16})\frac{\partial}{\partial(i\lambda_6)} \\
& + (i\lambda_{13})(i\lambda_{16})\frac{\partial}{\partial(i\lambda_{16})} + (i\lambda_{13})(i\lambda_8)\frac{\partial}{\partial(i\lambda_8)} + (i\lambda_8)(i\lambda_{18})\frac{\partial}{\partial(i\lambda_{14})} + (i\lambda_6)(i\lambda_{16})\frac{\partial}{\partial(i\lambda_{10})} \\
& + (i\lambda_8)(i\lambda_{16})\frac{\partial}{\partial(i\lambda_{11})} + (i\lambda_6)(i\lambda_{18})\frac{\partial}{\partial(i\lambda_{12})} + \frac{(i\lambda_{13})^2}{2}\frac{\partial}{\partial(i\lambda_{13})}]\chi. \quad (\text{B.50})
\end{aligned}$$

And for the second laser,

$$\begin{aligned}
& \text{Tr}\{E(\lambda)\hat{\sigma}_{12}\rho\hat{\sigma}_{12}^\dagger\}^{(2)} = \text{Tr}\left\{\left[(i\lambda_{14})(i\lambda_{15})\hat{\sigma}_{20} + (i\lambda_{16})(i\lambda_{14})\hat{\sigma}_{21} + e^{i\lambda_{13}-i\lambda_{12}}\left(\hat{\sigma}_{22} - i\lambda_{17}\hat{\sigma}_{20} \right. \right. \right. \\
& \left. \left. \left. - i\lambda_{14}\hat{\sigma}_{23} - i\lambda_{18}\hat{\sigma}_{21} + (i\lambda_{19})(i\lambda_{18})\hat{\sigma}_{20}\right)\right]E(\lambda)\rho\right\}^{(2)}. \quad (\text{B.51})
\end{aligned}$$

The above requires

$$\text{Tr}\{\hat{\sigma}_{20}E(\lambda)\rho\} = [\frac{\partial}{\partial(i\lambda_{17})}]\chi.$$

Then we have

$$\begin{aligned} \gamma_{12}\text{Tr}\{E(\lambda)[\hat{\sigma}_{12}\rho\hat{\sigma}_{12}^\dagger - \frac{1}{2}\hat{\sigma}_{22}\rho - \frac{1}{2}\rho\hat{\sigma}_{22}]\}^{(2)} = \\ \gamma_{12}[-\frac{i\lambda_6}{2}\frac{\partial}{\partial(i\lambda_6)} - \frac{i\lambda_{18}}{2}\frac{\partial}{\partial(i\lambda_{18})} - \frac{i\lambda_7}{2}\frac{\partial}{\partial(i\lambda_7)} - \frac{i\lambda_{17}}{2}\frac{\partial}{\partial(i\lambda_{17})} - \frac{i\lambda_{10}}{2}\frac{\partial}{\partial(i\lambda_{10})} \\ - \frac{i\lambda_{14}}{2}\frac{\partial}{\partial(i\lambda_{14})} + (i\lambda_{13} - i\lambda_{12})\frac{\partial}{\partial(i\lambda_{12})} + (i\lambda_5)(i\lambda_{19})\frac{\partial}{\partial(i\lambda_{12})} + \frac{(i\lambda_{13} - i\lambda_{12})^2}{2}\frac{\partial}{\partial(i\lambda_{12})}]\chi. \end{aligned} \quad (\text{B.52})$$

And the dissipation for the signal transition,

$$\begin{aligned} \text{Tr}\{E(\lambda)\hat{\sigma}_{32}\rho\hat{\sigma}_{32}^\dagger\}^{(2)} = \\ \text{Tr}\{[(i\lambda_8)(i\lambda_{16})\hat{\sigma}_{22} + (i\lambda_9)(i\lambda_{15})\hat{\sigma}_{22} + (i\lambda_{14})(i\lambda_{15})\hat{\sigma}_{20} + (i\lambda_{14})(i\lambda_{16})\hat{\sigma}_{21} \\ + e^{i\lambda_{11}-i\lambda_{12}}(-i\lambda_{17}\hat{\sigma}_{20} - i\lambda_{14}\hat{\sigma}_{23} + \hat{\sigma}_{22} - i\lambda_{18}\hat{\sigma}_{21} + (i\lambda_{19})(i\lambda_{18})\hat{\sigma}_{20})]E(\lambda)\rho\}, \end{aligned} \quad (\text{B.53})$$

so we have

$$\begin{aligned} \gamma_{32}\text{Tr}\{E(\lambda)[\hat{\sigma}_{32}\rho\hat{\sigma}_{32}^\dagger - \frac{1}{2}\hat{\sigma}_{22}\rho - \frac{1}{2}\rho\hat{\sigma}_{22}]\}^{(2)} = \\ \gamma_{32}[-\frac{i\lambda_6}{2}\frac{\partial}{\partial(i\lambda_6)} - \frac{i\lambda_{18}}{2}\frac{\partial}{\partial(i\lambda_{18})} - \frac{i\lambda_7}{2}\frac{\partial}{\partial(i\lambda_7)} - \frac{i\lambda_{17}}{2}\frac{\partial}{\partial(i\lambda_{17})} - \frac{i\lambda_{10}}{2}\frac{\partial}{\partial(i\lambda_{10})} \\ - \frac{i\lambda_{14}}{2}\frac{\partial}{\partial(i\lambda_{14})} + (i\lambda_{11} - i\lambda_{12})\frac{\partial}{\partial(i\lambda_{12})} + (i\lambda_5)(i\lambda_{19})\frac{\partial}{\partial(i\lambda_{12})} + (i\lambda_8)(i\lambda_{16})\frac{\partial}{\partial(i\lambda_{12})} \\ + \frac{(i\lambda_{11} - i\lambda_{12})^2}{2}\frac{\partial}{\partial(i\lambda_{12})}]\chi. \end{aligned} \quad (\text{B.54})$$

And for idler transition,

$$\begin{aligned}
& \text{Tr}\{E(\lambda)\hat{\sigma}_{03}\rho\hat{\sigma}_{03}^\dagger\}^{(2)} = \\
& \text{Tr}\{[(i\lambda_{10})(i\lambda_{18})\hat{\sigma}_{31} + (i\lambda_{10})(i\lambda_{14})\hat{\sigma}_{33} + (i\lambda_{10})(i\lambda_{17})\hat{\sigma}_{30} - i\lambda_{10}e^{-i\lambda_{12}}\hat{\sigma}_{32} \\
& e^{-i\lambda_{11}}(\hat{\sigma}_{33} - i\lambda_{16}\hat{\sigma}_{31} + (i\lambda_{16})(i\lambda_{19})\hat{\sigma}_{30} - i\lambda_{15}\hat{\sigma}_{30})E(\lambda)\rho\}^{(2)}. \tag{B.55}
\end{aligned}$$

The above needs

$$\text{Tr}\{\hat{\sigma}_{31}E(\lambda)\rho\} = \left[\frac{\partial}{\partial(i\lambda_{16})} + i\lambda_{19}\frac{\partial}{\partial(i\lambda_{15})}\right]\chi,$$

then we have

$$\begin{aligned}
& \gamma_{03}\text{Tr}\{E(\lambda)[\hat{\sigma}_{03}\rho\hat{\sigma}_{03}^\dagger - \frac{1}{2}\hat{\sigma}_{33}\rho - \frac{1}{2}\rho\hat{\sigma}_{33}]\}^{(2)} \\
& = \gamma_{03}\left[-\frac{i\lambda_8}{2}\frac{\partial}{\partial(i\lambda_8)} - \frac{i\lambda_{16}}{2}\frac{\partial}{\partial(i\lambda_{16})} - \frac{i\lambda_9}{2}\frac{\partial}{\partial(i\lambda_9)} - \frac{i\lambda_{15}}{2}\frac{\partial}{\partial(i\lambda_{15})} - \frac{i\lambda_{10}}{2}\frac{\partial}{\partial(i\lambda_{10})} \right. \\
& \quad - \frac{i\lambda_{14}}{2}\frac{\partial}{\partial(i\lambda_{14})} - i\lambda_{11}\frac{\partial}{\partial(i\lambda_{11})} + (i\lambda_{11})(i\lambda_{14})\frac{\partial}{\partial(i\lambda_{14})} + (i\lambda_{10})(i\lambda_{11})\frac{\partial}{\partial(i\lambda_{10})} \\
& \quad \left. + (i\lambda_{10})(i\lambda_{14})\frac{\partial}{\partial(i\lambda_{12})} + \frac{(i\lambda_{11})^2}{2}\frac{\partial}{\partial(i\lambda_{11})}\right]\chi. \tag{B.56}
\end{aligned}$$

### B.3 Stochastic Differential Equation

A distribution function can be found by Fourier transforming the characteristic functions,

$$f(\vec{\alpha}) = \frac{1}{(2\pi)^n} \int \dots \int e^{-i\vec{\alpha}\cdot\vec{\lambda}} \chi(\vec{\lambda}) d\lambda_1 \dots d\lambda_n, \tag{B.57}$$

then

$$\frac{\partial f}{\partial t} = \frac{1}{(2\pi)^n} \int \dots \int e^{-i\vec{\alpha}\cdot\vec{\lambda}} \frac{\partial \chi}{\partial t} d\lambda_1 \dots d\lambda_n. \tag{B.58}$$

If  $\frac{\partial \chi}{\partial t} = i\lambda_\beta \frac{\partial \chi}{\partial(i\lambda_\gamma)}$ , use integration by parts and neglect the boundary terms, we have  $\frac{\partial f}{\partial t} = -\frac{\partial}{\partial(\alpha_\beta)} \alpha_\gamma f$  where a minus sign is from  $i\lambda_\beta$ . Correspondingly, if  $\frac{\partial \chi}{\partial t} = e^{i\lambda_\beta}$ , we have  $\frac{\partial f}{\partial t} = e^{-\frac{\partial}{\partial(\alpha_\beta)}}$ .



### B.3.1 Fokker-Planck equation

Let

$$\frac{\partial f}{\partial t} = \mathcal{L}f = \sum_{l,l'} [\mathcal{L}_A \delta_{ll'} + \mathcal{L}_L + \mathcal{L}_{A-L}^{(a)} \delta_{ll'} + \mathcal{L}_{A-L}^{(b)} \delta_{ll'} + \mathcal{L}_{sp} \delta_{ll'}] f, \quad (\text{B.59})$$

then we have for the atomic part,

$$\begin{aligned} \mathcal{L}_A = & -i\omega_1 \left[ \frac{\partial}{\partial \alpha_5^l} (-\alpha_5^l) - \frac{\partial}{\partial \alpha_6^l} (-\alpha_6^l) - \frac{\partial}{\partial \alpha_8^l} (-\alpha_8^l) \right] \\ & - i\omega_2 \left[ \frac{\partial}{\partial \alpha_6^l} (-\alpha_6^l) + \frac{\partial}{\partial \alpha_7^l} (-\alpha_7^l) + \frac{\partial}{\partial \alpha_{10}^l} (-\alpha_{10}^l) \right] \\ & - i\omega_3 \left[ \frac{\partial}{\partial \alpha_8^l} (-\alpha_8^l) + \frac{\partial}{\partial \alpha_9^l} (-\alpha_9^l) - \frac{\partial}{\partial \alpha_{10}^l} (-\alpha_{10}^l) \right] + (c.c. \text{ with } C') \end{aligned} \quad (\text{B.60})$$

where  $C'$  is  $\alpha_5^* \leftrightarrow \alpha_{19}$ ,  $\alpha_6^* \leftrightarrow \alpha_{18}$ ,  $\alpha_7^* \leftrightarrow \alpha_{17}$ ,  $\alpha_8^* \leftrightarrow \alpha_{16}$ ,  $\alpha_9^* \leftrightarrow \alpha_{15}$ ,  $\alpha_{10}^* \leftrightarrow \alpha_{14}$ ,  $\alpha_{11}^* \leftrightarrow \alpha_{11}$ ,  $\alpha_{12}^* \leftrightarrow \alpha_{12}$ ,  $\alpha_{13}^* \leftrightarrow \alpha_{13}$ ,  $\alpha_1^* \leftrightarrow \alpha_2$ ,  $\alpha_3^* \leftrightarrow \alpha_4$ , and  $c.c.$  is complex conjugation. Also for the field part,

$$\begin{aligned} \mathcal{L}_L = & [i\omega_s \frac{\partial}{\partial \alpha_3^l} \alpha_3^l - i\omega_s \frac{\partial}{\partial \alpha_4^l} \alpha_4^l + i\omega_i \frac{\partial}{\partial \alpha_1^l} \alpha_1^l - i\omega_i \frac{\partial}{\partial \alpha_2^l} \alpha_2^l] \delta_{ll'} \\ & + i\omega_{l'l} \frac{\partial}{\partial \alpha_3^l} \alpha_3^{l'} - i\omega_{l'l} \frac{\partial}{\partial \alpha_4^l} \alpha_4^{l'} + i\omega_{ll'} \frac{\partial}{\partial \alpha_1^l} \alpha_1^{l'} - i\omega_{ll'} \frac{\partial}{\partial \alpha_2^l} \alpha_2^{l'}. \end{aligned} \quad (\text{B.61})$$

The atom-field interaction part (a) is

$$\begin{aligned}
\mathcal{L}_{A-L}^{(a)} = & i\Omega_a e^{ik_a z_l - i\omega_a t} \left[ -\frac{\partial^2}{\partial \alpha_5^l \partial \alpha_5^l} (\alpha_5^l) + \frac{\partial^2}{\partial \alpha_5^l \partial \alpha_6^l} (\alpha_6^l) - \frac{\partial^2}{\partial \alpha_5^l \partial \alpha_7^l} (\alpha_7^l) + \frac{\partial^2}{\partial \alpha_5^l \partial \alpha_8^l} (\alpha_8^l) \right. \\
& - \frac{\partial^2}{\partial \alpha_5^l \partial \alpha_9^l} (\alpha_9^l) - \frac{\partial}{\partial \alpha_5^l} (-\alpha_{11}^l - \alpha_{12}^l - 2\alpha_{13}^l + N_z) - \frac{\partial}{\partial \alpha_7^l} (-\alpha_6^l) - \frac{\partial}{\partial \alpha_9^l} (-\alpha_8^l) \\
& + \frac{\partial}{\partial \alpha_{16}^l} e^{-\frac{\partial}{\partial \alpha_{13}^l}} (-\alpha_{15}^l) + \frac{\partial}{\partial \alpha_{18}^l} e^{-\frac{\partial}{\partial \alpha_{13}^l}} (-\alpha_{17}^l) + e^{-\frac{\partial}{\partial \alpha_{13}^l}} (\alpha_{19}^l) \left. \right] - i\Omega_a e^{ik_a z_l - i\omega_a t} (\alpha_{19}^l) \\
& + i\Omega_b e^{-ik_b z_l - i\omega_b t} \left[ -\frac{\partial^2}{\partial \alpha_6^l \partial \alpha_6^l} (\alpha_6^l) - \frac{\partial^2}{\partial \alpha_6^l \partial \alpha_8^l} (\alpha_8^l) - \frac{\partial^2}{\partial \alpha_6^l \partial \alpha_{10}^l} (\alpha_{10}^l) \right. \\
& + \frac{\partial}{\partial \alpha_6^l} (-\alpha_{13}^l + \alpha_{12}^l) + \frac{\partial}{\partial \alpha_7^l} (-\alpha_5^l) + \frac{\partial^2}{\partial \alpha_8^l \partial \alpha_{10}^l} (\alpha_{12}^l - \alpha_{11}^l) - \frac{\partial^3}{\partial \alpha_8^l \partial \alpha_{10}^l \partial \alpha_{10}^l} (\alpha_{10}^l) \\
& - \frac{\partial}{\partial \alpha_8^l} e^{-\frac{\partial}{\partial \alpha_{12}^l} + \frac{\partial}{\partial \alpha_{11}^l}} (-\alpha_{14}^l) + \frac{\partial}{\partial \alpha_{10}^l} e^{-\frac{\partial}{\partial \alpha_{11}^l} + \frac{\partial}{\partial \alpha_{13}^l}} (-\alpha_{16}^l) + \left( \frac{\partial^2}{\partial \alpha_{10}^l \partial \alpha_{14}^l} e^{-\frac{\partial}{\partial \alpha_{11}^l} + \frac{\partial}{\partial \alpha_{13}^l}} \right. \\
& \left. \left. + e^{-\frac{\partial}{\partial \alpha_{12}^l} + \frac{\partial}{\partial \alpha_{13}^l}} \right) (\alpha_{18}^l) \right] - i\Omega_b e^{-ik_b z_l - i\omega_b t} \left[ \alpha_{18}^l + \frac{\partial}{\partial \alpha_{19}^l} (-\alpha_{17}^l) \right] + (c.c. \text{ with } C'), \quad (\text{B.62})
\end{aligned}$$

and let  $\mathcal{L}_{A-L}^{(b)} = \mathcal{L}_{A-L,S}^{(b)} + \mathcal{L}_{A-L,I}^{(b)}$ , which are the terms for signal (S) and idler (I) parts,

$$\begin{aligned}
\mathcal{L}_{A-L,S}^{(b)} = & ig_s \sqrt{2M+1} e^{-ik_s z_l} \left[ \frac{\partial}{\partial \alpha_6^l} (-\alpha_8^l) + \frac{\partial}{\partial \alpha_7^l} (-\alpha_9^l) - \frac{\partial^2}{\partial \alpha_{10}^l \partial \alpha_{10}^l} (\alpha_{10}^l) \right. \\
& + \frac{\partial}{\partial \alpha_{10}^l} (-\alpha_{11}^l + \alpha_{12}^l) + e^{-\frac{\partial}{\partial \alpha_{12}^l} + \frac{\partial}{\partial \alpha_{11}^l}} (\alpha_{14}^l) \left. \right] \alpha_3^l + ig_s^* \sqrt{2M+1} e^{ik_s z_l} \\
& \left[ \frac{\partial}{\partial \alpha_8^l} (-\alpha_6^l) + \alpha_{10}^l + \frac{\partial}{\partial \alpha_9^l} (-\alpha_7^l) \right] (\alpha_4^l - \frac{\partial}{\partial \alpha_3^l}) + (c.c. \text{ with } C') \quad (\text{B.63})
\end{aligned}$$

and

$$\begin{aligned}
\mathcal{L}_{A-L,I}^{(b)} = & ig_i \sqrt{2M+1} e^{ik_i z_l} \left[ \frac{\partial^3}{\partial \alpha_5^l \partial \alpha_8^l \partial \alpha_8^l} (-\alpha_8^l) + \frac{\partial^3}{\partial \alpha_5^l \partial \alpha_6^l \partial \alpha_8^l} (-\alpha_6^l) + \frac{\partial^2}{\partial \alpha_5^l \partial \alpha_6^l} (\alpha_{10}^l) \right. \\
& - \frac{\partial^2}{\partial \alpha_5^l \partial \alpha_9^l} (\alpha_5^l) - \frac{\partial^2}{\partial \alpha_5^l \partial \alpha_8^l} (\alpha_{13}^l + \frac{\partial}{\partial \alpha_9^l} \alpha_9^l - \frac{\partial}{\partial \alpha_{10}^l} \alpha_{10}^l - \alpha_{11}^l) \\
& - \frac{\partial}{\partial \alpha_5^l} e^{-\frac{\partial}{\partial \alpha_{11}^l} + \frac{\partial}{\partial \alpha_{13}^l}} (-\alpha_{16}^l) - \frac{\partial^2}{\partial \alpha_5^l \partial \alpha_{14}^l} e^{-\frac{\partial}{\partial \alpha_{11}^l} + \frac{\partial}{\partial \alpha_{13}^l}} (\alpha_{18}^l) - \frac{\partial^2}{\partial \alpha_7^l \partial \alpha_8^l} (\alpha_6^l) \\
& - \frac{\partial}{\partial \alpha_7^l} (-\alpha_{10}^l) - \frac{\partial^2}{\partial \alpha_7^l \partial \alpha_9^l} (\alpha_7^l) - \frac{\partial^2}{\partial \alpha_9^l \partial \alpha_9^l} (\alpha_9^l) - N_z \frac{\partial}{\partial \alpha_9^l} - \frac{\partial}{\partial \alpha_8^l} ( \\
& - \frac{\partial}{\partial \alpha_9^l} (-\alpha_8^l) + \frac{\partial}{\partial \alpha_{16}^l} e^{-\frac{\partial}{\partial \alpha_{13}^l}} (-\alpha_{15}^l) + \frac{\partial}{\partial \alpha_{18}^l} e^{-\frac{\partial}{\partial \alpha_{13}^l}} (-\alpha_{17}^l) + e^{-\frac{\partial}{\partial \alpha_{13}^l}} \alpha_{19}^l) \\
& + e^{-\frac{\partial}{\partial \alpha_{11}^l}} \alpha_{15}^l - \frac{\partial}{\partial \alpha_9^l} (-\alpha_{13}^l + \frac{\partial}{\partial \alpha_{10}^l} (\alpha_{10}^l) - \alpha_{12}^l + 2 \frac{\partial}{\partial \alpha_{10}^l} (-\alpha_{10}^l) \\
& - 2\alpha_{11}^l) + \frac{\partial}{\partial \alpha_{14}^l} e^{-\frac{\partial}{\partial \alpha_{11}^l}} (-\alpha_{17}^l) \alpha_1^l \\
& + ig_i^* \sqrt{2M+1} e^{-ik_i z_l} (\alpha_9^l) (\alpha_2^l - \frac{\partial}{\partial \alpha_1^l}) + (c.c. \text{ with } C'').
\end{aligned} \tag{B.64}$$

The dissipation part  $\mathcal{L}_{sp}$  can be derived accordingly and the above equation, which involves higher order derivatives (third order and higher), is neglected. The validity of truncation to second order is due to the expansion in the small parameter  $1/N_z$ .

If the Fokker-Planck equation is

$$\frac{\partial f}{\partial t} = -\frac{\partial}{\partial \alpha} A_\alpha f - \frac{\partial}{\partial \beta} A_\beta f + \frac{1}{2} \left( \frac{\partial^2}{\partial \alpha \partial \beta} + \frac{\partial^2}{\partial \beta \partial \alpha} \right) D_{\alpha\beta} f \tag{B.65}$$

where  $A$  and  $D$  are drift and diffusion terms then we have a corresponding classical Langevin equation

$$\frac{\partial \alpha}{\partial t} = A_\alpha + \Gamma_\alpha, \quad \frac{\partial \beta}{\partial t} = A_\beta + \Gamma_\beta \tag{B.66}$$

with a correlation function  $\langle \Gamma_\alpha \Gamma_\beta \rangle = \delta(t - t') D_{\alpha\beta}$ . So we have according to various

$\mathcal{L}$ 's,

$$\begin{aligned}
\dot{\alpha}_5^l &= (-i\omega_1 - \frac{\gamma_{01}}{2})\alpha_5^l + i\Omega_a e^{ik_a z_l - i\omega_a t}(\alpha_0^l - \alpha_{13}^l) + i\Omega_b^* e^{ik_b z_l + i\omega_b t}\alpha_7^l \\
&\quad - ig_i \sqrt{2M+1} e^{ik_i z_l} \alpha_{16}^l \alpha_1^l + \Gamma_5^l, \\
\dot{\alpha}_6^l &= i(\omega_1 - \omega_2 + i\frac{\gamma_{01} + \gamma_2}{2})\alpha_6^l - i\Omega_a^* e^{-ik_a z_l + i\omega_a t}\alpha_7^l + i\Omega_b e^{-ik_b z_l - i\omega_b t}(\alpha_{13}^l - \alpha_{12}^l) \\
&\quad + ig_s \sqrt{2M+1} e^{-ik_s z_l} \alpha_8^l \alpha_3^l + \Gamma_6^l, \\
\dot{\alpha}_7^l &= (-i\omega_2 - \frac{\gamma_2}{2})\alpha_7^l - i\Omega_a e^{ik_a z_l - i\omega_a t}\alpha_6^l + i\Omega_b e^{-ik_b z_l - i\omega_b t}\alpha_5^l \\
&\quad + ig_s \sqrt{2M+1} e^{-ik_s z_l} \alpha_9^l \alpha_3^l - ig_i \sqrt{2M+1} e^{ik_i z_l} \alpha_{10}^l \alpha_1^l + \Gamma_7^l, \\
\dot{\alpha}_{13}^l &= -\gamma_{01}\alpha_{13}^l + \gamma_{12}\alpha_{12}^l + i\Omega_a e^{ik_a z_l - i\omega_a t}\alpha_{19}^l - i\Omega_a^* e^{-ik_a z_l + i\omega_a t}\alpha_5^l \\
&\quad - i\Omega_b e^{-ik_b z_l - i\omega_b t}\alpha_{18}^l + i\Omega_b^* e^{ik_b z_l + i\omega_b t}\alpha_6^l + \Gamma_{13}^l, \\
\dot{\alpha}_{12}^l &= -\gamma_2\alpha_{12}^l + i\Omega_b e^{-ik_b z_l - i\omega_b t}\alpha_{18}^l - i\Omega_b^* e^{ik_b z_l + i\omega_b t}\alpha_6^l + ig_s \sqrt{2M+1} e^{-ik_s z_l} \alpha_{14}^l \alpha_3^l \\
&\quad - ig_s^* \sqrt{2M+1} e^{ik_s z_l} \alpha_{10}^l \alpha_4^l + \Gamma_{12}^l, \\
\dot{\alpha}_{11}^l &= -\gamma_{03}\alpha_{11}^l + \gamma_{32}\alpha_{12}^l - ig_s \sqrt{2M+1} e^{-ik_s z_l} \alpha_{14}^l \alpha_3^l + ig_s \sqrt{2M+1} e^{ik_s z_l} \alpha_{10}^l \alpha_4^l \\
&\quad + ig_i \sqrt{2M+1} e^{ik_i z_l} \alpha_{15}^l \alpha_1^l - ig_i^* \sqrt{2M+1} e^{-ik_i z_l} \alpha_9^l \alpha_2^l + \Gamma_{11}^l, \\
\dot{\alpha}_8^l &= i(\omega_1 - \omega_3 + i\frac{\gamma_{01} + \gamma_{03}}{2})\alpha_8^l - i\Omega_a^* e^{-ik_a z_l + i\omega_a t}\alpha_9^l - i\Omega_b e^{-ik_b z_l - i\omega_b t}\alpha_{14}^l \\
&\quad + ig_s^* \sqrt{2M+1} e^{ik_s z_l} \alpha_6^l \alpha_4^l + ig_i \sqrt{2M+1} e^{ik_i z_l} \alpha_{19}^l \alpha_1^l + \Gamma_8^l, \\
\dot{\alpha}_9^l &= (-i\omega_3 - \frac{\gamma_{03}}{2})\alpha_9^l - i\Omega_a e^{ik_a z_l - i\omega_a t}\alpha_8^l + ig_s^* \sqrt{2M+1} e^{ik_s z_l} \alpha_7^l \alpha_4^l \\
&\quad + ig_i \sqrt{2M+1} e^{ik_i z_l} (\alpha_0^l - \alpha_{11}^l) \alpha_1^l + \Gamma_9^l, \\
\dot{\alpha}_{14}^l &= i(\omega_2 - \omega_3 + i\frac{\gamma_{03} + \gamma_2}{2})\alpha_{14}^l - i\Omega_b^* e^{ik_b z_l + i\omega_b t}\alpha_8^l \\
&\quad + ig_s^* \sqrt{2M+1} e^{ik_s z_l} (\alpha_{12}^l - \alpha_{11}^l) \alpha_4^l + ig_i \sqrt{2M+1} e^{ik_i z_l} \alpha_{17}^l \alpha_1^l + \Gamma_{14}^l, \\
\dot{\alpha}_4^l &= i\omega_s \alpha_4^l + i \sum_{l'} \omega_{ll'} \alpha_4^{l'} - ig_s \sqrt{2M+1} e^{-ik_s z_l} \alpha_{14}^l + \Gamma_4^l, \\
\dot{\alpha}_1^l &= -i\omega_i \alpha_1^l - i \sum_{l'} \omega_{ll'} \alpha_1^{l'} + ig_i^* \sqrt{2M+1} e^{-ik_i z_l} \alpha_9^l + \Gamma_1^l, \tag{B.67}
\end{aligned}$$

where  $\gamma_2 = \gamma_{12} + \gamma_{32}$ . We postpone the derivations of diffusion coefficients after the scaling is made in the next section, and note that the complete equations of motion

are found by making complex conjugate of the above with correspondence  $C'$  and changing Langevin noises correspondingly, say  $\Gamma_5^* \rightarrow \Gamma_{19}$ .

### B.3.2 Slowly varying envelopes and scaled equations of motion

Here we introduce the slowly varying envelopes and define our cross-grained collective atomic and field observables, then finally transform the equations in a dimensionless form for later numerical simulations. We note that

$$i \sum_{l'} \omega_{ll'} \alpha_4^{l'} = c \frac{d}{dz_l} \alpha_4^l, \quad -i \sum_{l'} \omega_{ll'} \alpha_1^{l'} = -c \frac{\partial}{\partial z_l} \alpha_1^l, \quad (\text{B.68})$$

and  $\alpha_0^l = N_z - \alpha_{13}^l - \alpha_{12}^l - \alpha_{11}^l$ . Define slow varying observables that

$$\begin{aligned} \tilde{\alpha}_5(z, t) &\equiv \frac{1}{N_z} \alpha_5^l e^{-ik_a z_l + i\omega_a t}, \quad \tilde{\alpha}_6(z, t) \equiv \frac{1}{N_z} \alpha_6^l e^{ik_b z_l + i\omega_b t}, \\ \tilde{\alpha}_7(z, t) &\equiv \frac{1}{N_z} \alpha_7^l e^{-ik_a z_l + ik_b z_l + i\omega_b t + i\omega_a t}, \quad \tilde{\alpha}_8(z, t) \equiv \frac{1}{N_z} \alpha_8^l e^{-i\omega_a t + i\omega_3 t + ik_a z_l - ik_i z_l}, \\ \tilde{\alpha}_9(z, t) &\equiv \frac{1}{N_z} \alpha_9^l e^{-ik_i z_l + i\omega_3 t}, \quad \tilde{\alpha}_{11}(z, t) \equiv \frac{1}{N_z} \alpha_{11}^l, \\ \tilde{\alpha}_{12}(z, t) &\equiv \frac{1}{N_z} \alpha_{12}^l, \quad \tilde{\alpha}_{13}(z, t) \equiv \frac{1}{N_z} \alpha_{13}^l, \\ \tilde{\alpha}_{14}(z, t) &\equiv \frac{1}{N_z} \alpha_{14}^l e^{-i(\omega_{23} + \Delta_2)t} e^{ik_a z_l - ik_b z_l - ik_i z_l} \end{aligned} \quad (\text{B.69})$$

where  $e^{i\Delta k z} = e^{ik_a z_l - ik_b z_l - ik_i z_l + ik_s z_l}$ . Also for the field variables,

$$E_s^-(z, t) \equiv \frac{g_s^*}{d_i/\hbar} \sqrt{2M+1} \alpha_4^l e^{-i\omega_s t}, \quad E_i^+(z, t) \equiv \frac{g_i}{d_i/\hbar} \sqrt{2M+1} \alpha_1^l e^{i\omega_i t}, \quad (\text{B.70})$$

where we use the idler dipole moment in signal field scaling for the purpose of scale-free atomic equation of motions, so we need to keep in mind that in calculating signal intensity or correlation function, an extra factor of  $(d_i/d_s)^2$  needs to be taken care of.

We choose the central frequency of signal and idler as  $\omega_s = \omega_{23} + \Delta_2$ ,  $\omega_i = \omega_3$  where  $\Delta_1 = \omega_a - \omega_1$  and  $\Delta_2 = \omega_a + \omega_b - \omega_2$ . With a scaling of Arecchi-Courtens cooperation length [115], we set up the units of field strength, time, and length in the following,

$$\frac{E_c}{T_c} = \frac{N|g_i|^2}{d_i/\hbar}, \quad L_c = cT_c, \quad \frac{1}{T_c} = \sqrt{\frac{d_i^2 n \omega_i}{2\hbar\epsilon_0}}, \quad E_c = \sqrt{\frac{n\hbar\omega_i}{2\epsilon_0}} = \frac{1}{T_c} \frac{1}{d_i/\hbar}. \quad (\text{B.71})$$

Compared with optical density and superradiant time scale, we have (in terms of single atomic decay rate  $\gamma$ )

$$N|g_i|^2 = \frac{\gamma_N}{L/c}, \quad \gamma_N = N \frac{3}{8\pi} \frac{\lambda^2}{A} \gamma, \quad n = \frac{N}{V}. \quad (\text{B.72})$$

Now the slowly varying and dimensionless equations of motion with Langevin noises in Ito's form are

$$\begin{aligned} \frac{\partial}{\partial t} \tilde{\alpha}_5 &= (i\Delta_1 - \frac{\gamma_{01}}{2}) \tilde{\alpha}_5 + i\Omega_a(\tilde{\alpha}_0 - \tilde{\alpha}_{13}) + i\Omega_b^* \tilde{\alpha}_7 - i\tilde{\alpha}_{16} E_i^+ + \mathcal{F}_5, \\ \frac{\partial}{\partial t} \tilde{\alpha}_6 &= i(\Delta_2 - \Delta_1 + i\frac{\gamma_{01} + \gamma_2}{2}) \tilde{\alpha}_6 - i\Omega_a^* \tilde{\alpha}_7 + i\Omega_b(\tilde{\alpha}_{13} - \tilde{\alpha}_{12}) + i\tilde{\alpha}_8 E_s^+ e^{-i\Delta k z} + \mathcal{F}_6, \\ \frac{\partial}{\partial t} \tilde{\alpha}_7 &= (i\Delta_2 - \frac{\gamma_2}{2}) \tilde{\alpha}_7 - i\Omega_a \tilde{\alpha}_6 + i\Omega_b \tilde{\alpha}_5 + i\tilde{\alpha}_9 E_s^+ e^{-i\Delta k z} - i\tilde{\alpha}_{10} E_i^+ + \mathcal{F}_7, \\ \frac{\partial}{\partial t} \tilde{\alpha}_{13} &= -\gamma_{01} \tilde{\alpha}_{13} + \gamma_{12} \tilde{\alpha}_{12} + i\Omega_a \tilde{\alpha}_{19} - i\Omega_a^* \tilde{\alpha}_5 - i\Omega_b \tilde{\alpha}_{18} + i\Omega_b^* \tilde{\alpha}_6 + \mathcal{F}_{13}, \\ \frac{\partial}{\partial t} \tilde{\alpha}_{12} &= -\gamma_2 \tilde{\alpha}_{12} + i\Omega_b \tilde{\alpha}_{18} - i\Omega_b^* \tilde{\alpha}_6 + i\tilde{\alpha}_{14} E_s^+ e^{-i\Delta k z} - i\tilde{\alpha}_{10} E_s^- e^{i\Delta k z} + \mathcal{F}_{12}, \\ \frac{\partial}{\partial t} \tilde{\alpha}_{11} &= -\gamma_{03} \tilde{\alpha}_{11} + \gamma_{32} \tilde{\alpha}_{12} - i\tilde{\alpha}_{14} E_s^+ e^{-i\Delta k z} + i\tilde{\alpha}_{10} E_s^- e^{i\Delta k z} + i\tilde{\alpha}_{15} E_i^+ - i\tilde{\alpha}_9 E_i^- + \mathcal{F}_{11}, \\ \frac{\partial}{\partial t} \tilde{\alpha}_8 &= -(i\Delta_1 + \frac{\gamma_{01} + \gamma_{03}}{2}) \tilde{\alpha}_8 - i\Omega_a^* \tilde{\alpha}_9 - i\Omega_b \tilde{\alpha}_{14} + i\tilde{\alpha}_6 E_s^- e^{i\Delta k z} + i\tilde{\alpha}_{19} E_i^+ + \mathcal{F}_8, \\ \frac{\partial}{\partial t} \tilde{\alpha}_9 &= -\frac{\gamma_{03}}{2} \tilde{\alpha}_9 - i\Omega_a \tilde{\alpha}_8 + i\tilde{\alpha}_7 E_s^- e^{i\Delta k z} + i(\tilde{\alpha}_0 - \tilde{\alpha}_{11}) E_i^+ + \mathcal{F}_9, \\ \frac{\partial}{\partial t} \tilde{\alpha}_{14} &= -(i\Delta_2 + \frac{\gamma_{03} + \gamma_2}{2}) \tilde{\alpha}_{14} - i\Omega_b^* \tilde{\alpha}_8 + i(\tilde{\alpha}_{12} - \tilde{\alpha}_{11}) E_s^- e^{i\Delta k z} + i\tilde{\alpha}_{17} E_i^+ + \mathcal{F}_{14}, \end{aligned} \quad (\text{B.73})$$

and field propagation equations are

$$\begin{aligned} (\frac{\partial}{\partial t} - \frac{\partial}{\partial z}) E_s^- &= -i\tilde{\alpha}_{14} e^{-i\Delta k z} \frac{|g_s|^2}{|g_i|^2} + \mathcal{F}_4, \\ (\frac{\partial}{\partial t} + \frac{\partial}{\partial z}) E_i^+ &= i\tilde{\alpha}_9 + \mathcal{F}_1, \end{aligned} \quad (\text{B.74})$$

where  $\frac{|g_s|^2}{|g_i|^2}$  is a unit transformation factor from the signal field strength to the idler one. For a recognizable format of the above equations used in the text of Chapter 4, we change the labels in the below,

$$\begin{aligned}
\tilde{\alpha}_5 &\leftrightarrow \pi_{01}, \quad \tilde{\alpha}_6 \leftrightarrow \pi_{12}, \quad \tilde{\alpha}_7 \leftrightarrow \pi_{02}, \quad \tilde{\alpha}_8 \leftrightarrow \pi_{13}, \quad \tilde{\alpha}_9 \leftrightarrow \pi_{03}, \quad \tilde{\alpha}_{10} \leftrightarrow \pi_{32}, \quad \tilde{\alpha}_{11} \leftrightarrow \pi_{33}, \\
\tilde{\alpha}_{12} &\leftrightarrow \pi_{22}, \quad \tilde{\alpha}_{13} \leftrightarrow \pi_{11}, \quad \tilde{\alpha}_{14} \leftrightarrow \pi_{32}^\dagger, \quad \tilde{\alpha}_{15} \leftrightarrow \pi_{03}^\dagger, \quad \tilde{\alpha}_{16} \leftrightarrow \pi_{13}^\dagger, \quad \tilde{\alpha}_{17} \leftrightarrow \pi_{02}^\dagger, \\
\tilde{\alpha}_{18} &\leftrightarrow \pi_{12}^\dagger, \quad \tilde{\alpha}_{19} \leftrightarrow \pi_{01}^\dagger,
\end{aligned} \tag{B.75}$$

where  $\pi_{ij}$  is the stochastic variable that corresponds to the atomic populations of state  $|i\rangle$  when  $i = j$  and to atomic coherence when  $i \neq j$ . Note that the associated c-number Langevin noises are changed accordingly.

The Langevin noises are defined as

$$\begin{aligned}
\mathcal{F}_5(z, t) &= \frac{1}{N_z} \Gamma_5^l e^{-ik_a z_l + i\omega_a t}, \quad \mathcal{F}_6(z, t) = \frac{1}{N_z} \Gamma_6^l e^{ik_b z_l + i\omega_b t}, \\
\mathcal{F}_7(z, t) &= \frac{1}{N_z} \Gamma_7^l e^{-ik_a z_l + ik_b z_l + i\omega_b t + i\omega_a t}, \quad \mathcal{F}_{13}(z, t) = \frac{1}{N_z} \Gamma_{13}^l, \quad \mathcal{F}_{12}(z, t) = \frac{1}{N_z} \Gamma_{12}^l, \\
\mathcal{F}_{11}(z, t) &= \frac{1}{N_z} \Gamma_{11}^l, \quad \mathcal{F}_8(z, t) = \frac{1}{N_z} \Gamma_8^l e^{-i\omega_a t + i\omega_3 t + ik_a z_l - ik_i z_l}, \\
\mathcal{F}_9(z, t) &= \frac{1}{N_z} \Gamma_9^l e^{-ik_i z_l + i\omega_3 t}, \quad \mathcal{F}_{14}(z, t) = \frac{1}{N_z} \Gamma_{14}^l e^{-i(\omega_{23} + \Delta_2)t} e^{ik_a z_l - ik_b z_l - ik_i z_l}, \\
\mathcal{F}_4(z, t) &= \frac{g_s^*}{d_i/\hbar} \sqrt{2M+1} e^{-i\omega_s t} \Gamma_4^l, \quad \mathcal{F}_1(z, t) = \frac{g_i}{d_i/\hbar} \sqrt{2M+1} e^{i\omega_i t} \Gamma_1^l
\end{aligned} \tag{B.76}$$

where other Langevin noises can be found by using the correspondence similar to  $C'$ , for example,  $\mathcal{F}_5^* \leftrightarrow \mathcal{F}_{19}$ .

Before we proceed to formulate the diffusion coefficients, we need to be careful about the scaling factor for the transformation to continuous variables when numerical

simulation is applied. Take  $\langle \mathcal{F}_6 \mathcal{F}_5 \rangle$  for example,

$$\begin{aligned}
& \langle \mathcal{F}_6(z, t) \mathcal{F}_5(z', t') \rangle \\
&= \frac{1}{N_z^2} e^{ik_b z_l + i\omega_b t} e^{-ik_a z_{l'} + i\omega_a t'} \langle \Gamma_6^l \Gamma_5^{l'} \rangle \\
&= \frac{1}{N_z^2} e^{ik_b z_l + i\omega_b t} e^{-ik_a z_{l'} + i\omega_a t'} [i\Omega_a e^{ik_a z_l - i\omega_a t} \alpha_6^l + ig_i \sqrt{2M+1} e^{ik_i z_l} \alpha_{10}^l \alpha_1^l] \delta(t-t') \delta_{ll'} \\
&= \frac{1}{N_z} \left[ i \frac{\Omega_a}{T_c} T_c \tilde{\alpha}_6 + i \frac{d_i}{\hbar} E_c \tilde{\alpha}_{10} \frac{E_i^+}{E_c} \right] \delta(t-t') \delta(z-z') \frac{L}{2M+1} \\
&= [i(\Omega_a T_c) \tilde{\alpha}_6 + i \tilde{\alpha}_{10} (E_i^+ / E_c)] \frac{1}{T_c^2} \delta(t-t') T_c \delta(z-z') L_c \frac{L}{L_c} \frac{N_z}{N} \frac{1}{N_z} \\
&= \frac{1}{N_c} [i(\Omega_a T_c) \tilde{\alpha}_6 + i \tilde{\alpha}_{10} (E_i^+ / E_c)] \frac{1}{T_c^2} \delta(t-t') T_c \delta(z-z') L_c \tag{B.77}
\end{aligned}$$

where we have used  $\lim_{M \rightarrow \infty} \frac{2M+1}{L} \delta_{ll'} = \delta(z-z')$ ,  $2M+1 = \frac{N}{N_z}$ , and  $N_c = \frac{NL_c}{L}$  is the cooperation number. Then we have the dimensionless form of diffusion coefficients.

$$T_c^2 \langle \mathcal{F}_6(z, t) \mathcal{F}_5(z', t') \rangle = \frac{1}{N_c} D_{6,5} \delta(t-t') \delta(z-z') \tag{B.78}$$

$$D_{6,5} = [i\Omega_a \tilde{\alpha}_6 + i \tilde{\alpha}_{10} E_i^+] . \tag{B.79}$$

The dimensionless diffusion coefficients  $D_{ij}$  are



$$\begin{aligned}
& \text{(i)} D_{5,5} = -i2\Omega_a\tilde{\alpha}_5; \quad D_{5,6} = i(\Omega_a\tilde{\alpha}_6 + \tilde{\alpha}_{10}E_i^+); \quad D_{5,7} = -i\Omega_a\tilde{\alpha}_7; \\
& \quad D_{5,8} = i(\Omega_a\tilde{\alpha}_8 + (\tilde{\alpha}_{11} - \tilde{\alpha}_{13})E_i^+); \quad D_{5,9} = -i(\Omega_a\tilde{\alpha}_9 + \tilde{\alpha}_5E_i^+); \\
& \quad D_{5,11} = -i\tilde{\alpha}_{16}E_i^+; \quad D_{5,13} = i\tilde{\alpha}_{16}E_i^+; \quad D_{5,14} = -i\tilde{\alpha}_{18}E_i^+; \quad D_{5,19} = \gamma_{12}\tilde{\alpha}_{12}; \\
& \text{(ii)} D_{6,6} = -i2\Omega_b\tilde{\alpha}_6; \quad D_{6,8} = -i\Omega_b\tilde{\alpha}_8; \quad D_{6,10} = -i\Omega_b\tilde{\alpha}_{10}; \\
& \quad D_{6,13} = -i\Omega_a^*\tilde{\alpha}_7 + \gamma_{01}\tilde{\alpha}_6; \quad D_{6,16} = -i\tilde{\alpha}_7E_i^- + \gamma_{01}\tilde{\alpha}_{10}; \quad D_{6,18} = \gamma_{01}\tilde{\alpha}_{12}; \\
& \text{(iii)} D_{7,8} = -i\tilde{\alpha}_6E_i^+; \quad D_{7,9} = -i\tilde{\alpha}_7E_i^+; \\
& \text{(iv)} D_{8,9} = -i\tilde{\alpha}_8E_i^+; \quad D_{8,10} = i\Omega_b(\tilde{\alpha}_{12} - \tilde{\alpha}_{11}); \quad D_{8,11} = i\Omega_b\tilde{\alpha}_{14}; \\
& \quad D_{8,12} = -i\Omega_b\tilde{\alpha}_{14}; \quad D_{8,13} = -i\Omega_a^*\tilde{\alpha}_9 + i\tilde{\alpha}_{19}E_i^+ + \gamma_{01}\tilde{\alpha}_8; \\
& \quad D_{8,16} = i\tilde{\alpha}_{15}E_i^+ - i\tilde{\alpha}_9E_i^- + \gamma_{01}\tilde{\alpha}_{11} + \gamma_{32}\tilde{\alpha}_{12}; \quad D_{8,18} = i\tilde{\alpha}_{17}E_i^+ + \gamma_{01}\tilde{\alpha}_{14}; \\
& \text{(v)} D_{9,9} = -i2\tilde{\alpha}_9E_i^+; \quad D_{9,10} = i\tilde{\alpha}_{10}E_i^+; \quad D_{9,15} = \gamma_{32}\tilde{\alpha}_{12}; \\
& \text{(vi)} D_{10,10} = -i2\tilde{\alpha}_{10}E_s^+e^{-i\Delta kz}; \quad D_{10,11} = i(\Omega_b\tilde{\alpha}_{16} - \tilde{\alpha}_7E_i^-) + \gamma_{03}\tilde{\alpha}_{10}; \\
& \quad D_{10,13} = -i\Omega_b\tilde{\alpha}_{16}; \quad D_{10,14} = i\Omega_b\tilde{\alpha}_{18} - i\Omega_b^*\tilde{\alpha}_6 + \gamma_{03}\tilde{\alpha}_{12}; \quad D_{10,19} = i\tilde{\alpha}_6E_i^-; \\
& \text{(vii)} D_{11,11} = i\tilde{\alpha}_{14}E_s^+e^{-i\Delta kz} - i\tilde{\alpha}_{10}E_s^-e^{i\Delta kz} + i\tilde{\alpha}_{15}E_i^+ - i\tilde{\alpha}_9E_i^- + \gamma_{32}\tilde{\alpha}_{12} + \gamma_{03}\tilde{\alpha}_{11}; \\
& \quad D_{11,12} = i\tilde{\alpha}_{10}E_s^-e^{i\Delta kz} - i\tilde{\alpha}_{14}E_s^+e^{-i\Delta kz} - \gamma_{32}\tilde{\alpha}_{12}; \\
& \text{(viii)} D_{12,12} = i\Omega_b\tilde{\alpha}_{18} - i\Omega_b^*\tilde{\alpha}_6 - i\tilde{\alpha}_{10}E_s^-e^{i\Delta kz} + i\tilde{\alpha}_{14}E_s^+e^{-i\Delta kz} + \gamma_2\tilde{\alpha}_{12}; \\
& \quad D_{12,13} = -i\Omega_b\tilde{\alpha}_{18} + i\Omega_b^*\tilde{\alpha}_6 - \gamma_{12}\tilde{\alpha}_{12}; \\
& \text{(ix)} D_{13,13} = i\Omega_a\tilde{\alpha}_{19} - i\Omega_a^*\tilde{\alpha}_5 + i\Omega_b\tilde{\alpha}_{18} - i\Omega_b^*\tilde{\alpha}_6 + \gamma_{01}\tilde{\alpha}_{13} + \gamma_{12}\tilde{\alpha}_{12}; \\
& \text{(x)} D_{3,8} = \frac{|g_s|^2}{|g_i|^2}i\tilde{\alpha}_6e^{i\Delta kz}; \quad D_{3,9} = \frac{|g_s|^2}{|g_i|^2}i\tilde{\alpha}_7e^{i\Delta kz}. \tag{B.80}
\end{aligned}$$

### B.3.3 Alternative method to derive diffusion coefficients by Einstein relations

Before going further to set up the stochastic differential equation, we show here how we derive the diffusion coefficients from the Heisenberg-Langevin approach with Einstein relations, and it provides the important check for Fokker-Planck equations.

We note here that a symmetric property of the diffusion coefficients is within Fokker-Planck equation, whereas the quantum diffusion coefficients in quantum Langevin equation do not have symmetric property simply because the quantum operators do not necessarily commute with each other.

The approach involves a quantum-classical correspondence in deriving c-number Langevin equations and requires a chosen normal ordering of quantum operators. We use the same ordering as we use for deriving Fokker-Planck equations in Eq. (B.30),

$$\tilde{\sigma}_{01}^\dagger, \tilde{\sigma}_{12}^\dagger, \tilde{\sigma}_{02}^\dagger, \tilde{\sigma}_{13}^\dagger, \tilde{\sigma}_{03}^\dagger, \tilde{\sigma}_{32}^\dagger, \tilde{\sigma}_{11}, \tilde{\sigma}_{22}, \tilde{\sigma}_{33}, \tilde{\sigma}_{32}, \tilde{\sigma}_{03}, \tilde{\sigma}_{13}, \tilde{\sigma}_{02}, \tilde{\sigma}_{12}, \tilde{\sigma}_{01}, \hat{a}_s^\dagger, \hat{a}_s, \hat{a}_i^\dagger, \hat{a}_i$$

and its classical correspondence is  $\tilde{\alpha}_{19}, \tilde{\alpha}_{18}, \dots, \tilde{\alpha}_1$ .

We take  $D_{8,13} = D_{13,8}$  for a demonstration. We first calculate the quantum diffusion coefficient,  $\hat{\mathcal{D}}_{13,8}$ , using Einstein relations where we attach the hat to it, and then we can find  $\bar{\mathcal{D}}_{13,8}$ , a classical diffusion coefficient, which is reviewed in Chapter 2. Note that in calculating the quantum coefficients, we take advantage of Eq. (B.73) where the drift terms are directly corresponded to quantum Langevin equations. For clarity,  $\hat{\mathcal{D}}_{13,8} = \hat{\mathcal{D}}_{\tilde{\sigma}_{11}, \tilde{\sigma}_{13}}$  with  $\tilde{\alpha}_{13} \rightarrow \tilde{\sigma}_{11}, \tilde{\alpha}_8 \rightarrow \tilde{\sigma}_{13}$  representing a correspondence to quantum Langevin equations. The index in the classical variables  $\tilde{\alpha}$  represents the ordering we choose as defined above, and in various quantum operators  $\tilde{\sigma}$ , the index represents the atomic levels for atomic coherences or populations. We should find  $\bar{\mathcal{D}}_{13,8} = D_{13,8} = D_{8,13}$ , and the proof is illustrated below by the Einstein's relation, Eq. (2.8),

$$\begin{aligned}
\langle \hat{\mathcal{D}}_{13,8} \rangle &= \\
&- \left\langle \left[ -\gamma_{01}\tilde{\sigma}_{11} + \gamma_{12}\tilde{\sigma}_{22} + i\Omega_a\tilde{\sigma}_{01}^\dagger - i\Omega_a^*\tilde{\sigma}_{01} - i\Omega_b\tilde{\sigma}_{12}^\dagger + i\Omega_b^*\tilde{\sigma}_{12} \right] \tilde{\sigma}_{13} \right\rangle \\
&- \left\langle \tilde{\sigma}_{11} \left[ -(i\Delta_1 + \frac{\gamma_{01} + \gamma_{03}}{2})\tilde{\sigma}_{13} - i\Omega_a^*\tilde{\sigma}_{03} - i\Omega_b\tilde{\sigma}_{32}^\dagger + i\tilde{\sigma}_{12}E_s^- e^{i\Delta kz} + i\tilde{\sigma}_{01}^\dagger E_i^+ \right] \right\rangle \\
&+ \frac{\partial}{\partial t} \langle \tilde{\sigma}_{11}\tilde{\sigma}_{13} \rangle \\
&= \langle \gamma_{01}\tilde{\sigma}_{13} \rangle, \tag{B.81}
\end{aligned}$$

where the term  $\frac{\partial}{\partial t} \langle \tilde{\sigma}_{11}\tilde{\sigma}_{13} \rangle = \frac{\partial}{\partial t} \langle \tilde{\sigma}_{13} \rangle$  is the drift term of the quantum Langevin equation that can be found from Eq. (B.73),

$$\frac{\partial}{\partial t} \tilde{\sigma}_{13} = -(i\Delta_1 + \frac{\gamma_{01} + \gamma_{03}}{2})\tilde{\sigma}_{13} - i\Omega_a^*\tilde{\sigma}_{03} - i\Omega_b\tilde{\sigma}_{32}^\dagger + i\tilde{\sigma}_{12}E_s^- e^{i\Delta kz} + i\tilde{\sigma}_{01}^\dagger E_i^+. \tag{B.82}$$

From Eq. (2.15), we have

$$\begin{aligned}
\langle \bar{\mathcal{D}}_{13,8} \rangle &= \\
&\langle \hat{\mathcal{D}}_{13,8} \rangle + \left\{ \left\langle \left[ -\gamma_{01}\tilde{\sigma}_{11} + \gamma_{12}\tilde{\sigma}_{22} + i\Omega_a\tilde{\sigma}_{01}^\dagger - i\Omega_a^*\tilde{\sigma}_{01} - i\Omega_b\tilde{\sigma}_{12}^\dagger + i\Omega_b^*\tilde{\sigma}_{12} \right] \tilde{\sigma}_{13} \right\rangle + \right. \\
&\left\langle \tilde{\sigma}_{11} \left[ -(i\Delta_1 + \frac{\gamma_{01} + \gamma_{03}}{2})\tilde{\sigma}_{13} - i\Omega_a^*\tilde{\sigma}_{03} - i\Omega_b\tilde{\sigma}_{32}^\dagger + i\tilde{\sigma}_{12}E_s^- e^{i\Delta kz} + i\tilde{\sigma}_{01}^\dagger E_i^+ \right] \right\rangle \\
&- \text{classical counterpart} \left. \right\} \\
&= \langle \gamma_{01}\tilde{\alpha}_8 - i\Omega_a^*\tilde{\alpha}_9 + i\tilde{\alpha}_{19}E_i^+ \rangle, \tag{B.83}
\end{aligned}$$

where classical counterpart represents the last two terms of Eq. (2.15). We have used the commutation relations for non-normal correlation functions that

$$\begin{aligned}
[\tilde{\sigma}_{01}, \tilde{\sigma}_{13}] &= \tilde{\sigma}_{03}, \\
[\tilde{\sigma}_{12}, \tilde{\sigma}_{13}] &= 0, \\
[\tilde{\sigma}_{11}, \tilde{\sigma}_{32}^\dagger] &= 0, \\
[\tilde{\sigma}_{11}, \tilde{\sigma}_{01}^\dagger] &= \tilde{\sigma}_{01}^\dagger, \tag{B.84}
\end{aligned}$$

and use the correspondence  $\tilde{\sigma}_{03} \rightarrow \tilde{\alpha}_9$  and  $\tilde{\sigma}_{01}^\dagger \rightarrow \tilde{\alpha}_{19}$  in  $\bar{\mathcal{D}}_{13,8}$ . The rest of the diffusion coefficients are confirmed by the method of Einstein relations illustrated above.

### B.3.4 Ito and Stratonovich stochastic differential equations

The c-number Langevin equations derived from Fokker-Planck equations have a direct correspondence to Ito-type stochastic differential equations. In stochastic simulations, it is important to find the expressions of Langevin noises from diffusion coefficients.

For any symmetric diffusion matrix  $D(\alpha)$ , it can always be factorized into

$$D(\alpha) = B(\alpha)B^T(\alpha) \quad (\text{B.85})$$

where  $B \rightarrow BS$  (an orthogonal matrix  $S$  that  $SS^T = I$ ) preserves the diffusion matrix so  $B$  is not unique. The matrix  $B$  is in terms of the Langevin noises where  $\xi_i dt = dW_t^i$  (Wiener process) and  $\langle \xi_i(t)\xi_j(t') \rangle = \delta_{ij}\delta(t-t')$  and the  $\xi_i$  below is just a random number in Gaussian distribution with zero mean and unit variance.

In numerical simulation, we use the semi-implicit algorithm that guarantees the stability and convergence in the integration of stochastic differential equations. So a transformation from Ito to Stratonovich-type stochastic differential equation is necessary,

$$dx_t^i = A_i(t, \vec{x}_t)dt + \sum_j B_{ij}(t, \vec{x}_t)dW_t^j \quad (\text{Ito}) \quad (\text{B.86})$$

$$\begin{aligned} dx_t^i = & [A_i(t, \vec{x}_t) - \frac{1}{2} \sum_j \sum_k B_{jk}(t, \vec{x}_t) \frac{\partial}{\partial x^j} B_{ik}(t, \vec{x}_t)]dt \\ & + \sum_j B_{ij}(t, \vec{x}_t)dW_t^j \quad (\text{Stratonovich}) \end{aligned} \quad (\text{B.87})$$

where a correction in drift term appears due to the transformation.

Here we have the full equations with 19 variables in the positive-P representation, 64 diffusion matrix elements, and 117 noise terms (random number generators). A

correction in drift term is underlined and we have (S for Stratonovich)

$$\begin{aligned}
\frac{\partial}{\partial \tau} \tilde{\alpha}_5 &= \underbrace{\left(\frac{i\Omega_a}{2}\right)} + (i\Delta_1 - \frac{\gamma_{01}}{2})\tilde{\alpha}_5 + i\Omega_a(\tilde{\alpha}_0 - \tilde{\alpha}_{13}) + i\Omega_b^* \tilde{\alpha}_7 - i\tilde{\alpha}_{16} E_i^+ + \mathcal{F}_5, \quad (\text{S}) \\
\frac{\partial}{\partial \tau} \tilde{\alpha}_{19} &= \underbrace{\left(\frac{-i\Omega_a^*}{2}\right)} + (-i\Delta_1 - \frac{\gamma_{01}}{2})\tilde{\alpha}_{19} - i\Omega_a^*(\tilde{\alpha}_0 - \tilde{\alpha}_{13}) - i\Omega_b \tilde{\alpha}_{17} + i\tilde{\alpha}_8 E_i^- + \mathcal{F}_{19}, \\
\frac{\partial}{\partial \tau} \tilde{\alpha}_6 &= \underbrace{(i\Omega_b)} + i(\Delta_2 - \Delta_1 + i\frac{\gamma_{01} + \gamma_2}{2})\tilde{\alpha}_6 - i\Omega_a^* \tilde{\alpha}_7 + i\Omega_b(\tilde{\alpha}_{13} - \tilde{\alpha}_{12}) \\
&\quad + i\tilde{\alpha}_8 E_s^+ e^{-i\Delta k z} + \mathcal{F}_6, \\
\frac{\partial}{\partial \tau} \tilde{\alpha}_{18} &= \underbrace{(-i\Omega_b^*)} - i(\Delta_2 - \Delta_1 - i\frac{\gamma_{01} + \gamma_2}{2})\tilde{\alpha}_{18} + i\Omega_a \tilde{\alpha}_{17} - i\Omega_b^*(\tilde{\alpha}_{13} - \tilde{\alpha}_{12}) \\
&\quad - i\tilde{\alpha}_{16} E_s^- e^{i\Delta k z} + \mathcal{F}_{18}, \\
\frac{\partial}{\partial \tau} \tilde{\alpha}_7 &= (i\Delta_2 - \frac{\gamma_2}{2})\tilde{\alpha}_7 - i\Omega_a \tilde{\alpha}_6 + i\Omega_b \tilde{\alpha}_5 + i\tilde{\alpha}_9 E_s^+ e^{-i\Delta k z} - i\tilde{\alpha}_{10} E_i^+ + \mathcal{F}_7, \\
\frac{\partial}{\partial \tau} \tilde{\alpha}_{17} &= (-i\Delta_2 - \frac{\gamma_2}{2})\tilde{\alpha}_{17} + i\Omega_a^* \tilde{\alpha}_{18} - i\Omega_b^* \tilde{\alpha}_{19} - i\tilde{\alpha}_{15} E_s^- e^{i\Delta k z} + i\tilde{\alpha}_{14} E_i^- + \mathcal{F}_{17}, \\
\frac{\partial}{\partial \tau} \tilde{\alpha}_8 &= (-i\Delta_1 - \frac{\gamma_{01} + \gamma_{03}}{2})\tilde{\alpha}_8 - i\Omega_a^* \tilde{\alpha}_9 - i\Omega_b \tilde{\alpha}_{14} + i\tilde{\alpha}_6 E_s^- e^{i\Delta k z} + i\tilde{\alpha}_{19} E_i^+ + \mathcal{F}_8, \\
\frac{\partial}{\partial \tau} \tilde{\alpha}_{16} &= (i\Delta_1 - \frac{\gamma_{01} + \gamma_{03}}{2})\tilde{\alpha}_{16} + i\Omega_a \tilde{\alpha}_{15} + i\Omega_b^* \tilde{\alpha}_{10} - i\tilde{\alpha}_{18} E_s^+ e^{-i\Delta k z} - i\tilde{\alpha}_5 E_i^- + \mathcal{F}_{16}, \\
\frac{\partial}{\partial \tau} \tilde{\alpha}_9 &= \underbrace{(iE_i^+)} - \frac{\gamma_{03}}{2}\tilde{\alpha}_9 - i\Omega_a \tilde{\alpha}_8 + i\tilde{\alpha}_7 E_s^- + i(\tilde{\alpha}_0 - \tilde{\alpha}_{11})E_i^+ + \mathcal{F}_9, \\
\frac{\partial}{\partial \tau} \tilde{\alpha}_{15} &= \underbrace{(-iE_i^-)} - \frac{\gamma_{03}}{2}\tilde{\alpha}_{15} + i\Omega_a^* \tilde{\alpha}_{16} - i\tilde{\alpha}_{17} E_s^+ - i(\tilde{\alpha}_0 - \tilde{\alpha}_{11})E_i^- + \mathcal{F}_{15}, \\
\frac{\partial}{\partial \tau} \tilde{\alpha}_{10} &= \underbrace{(\frac{i}{2}E_s^+)} + (i\Delta_2 - \frac{\gamma_{03} + \gamma_2}{2})\tilde{\alpha}_{10} + i\Omega_b \tilde{\alpha}_{16} - i(\tilde{\alpha}_{12} - \tilde{\alpha}_{11})E_s^+ e^{-i\Delta k z} \\
&\quad - i\tilde{\alpha}_7 E_i^- + \mathcal{F}_{10}, \\
\frac{\partial}{\partial \tau} \tilde{\alpha}_{14} &= \underbrace{(-\frac{i}{2}E_s^-)} + (-i\Delta_2 - \frac{\gamma_{03} + \gamma_2}{2})\tilde{\alpha}_{14} - i\Omega_b^* \tilde{\alpha}_8 + i(\tilde{\alpha}_{12} - \tilde{\alpha}_{11})E_s^- e^{i\Delta k z} \\
&\quad + i\tilde{\alpha}_{17} E_i^+ + \mathcal{F}_{14}, \\
\frac{\partial}{\partial \tau} \tilde{\alpha}_{13} &= \underbrace{\frac{-5\gamma_{01} + \gamma_{12}}{4}} - \gamma_{01}\tilde{\alpha}_{13} + \gamma_{12}\tilde{\alpha}_{12} + i\Omega_a \tilde{\alpha}_{19} - i\Omega_a^* \tilde{\alpha}_5 - i\Omega_b \tilde{\alpha}_{18} \\
&\quad + i\Omega_b^* \tilde{\alpha}_6 + \mathcal{F}_{13}, \\
\frac{\partial}{\partial \tau} \tilde{\alpha}_{12} &= \underbrace{-\frac{\gamma_2}{4}} - \gamma_2\tilde{\alpha}_{12} + i\Omega_b \tilde{\alpha}_{18} - i\Omega_b^* \tilde{\alpha}_6 + i\tilde{\alpha}_{14} E_s^+ e^{-i\Delta k z} - i\tilde{\alpha}_{10} E_s^- e^{i\Delta k z} + \mathcal{F}_{12}, \\
\frac{\partial}{\partial \tau} \tilde{\alpha}_{11} &= \underbrace{\frac{-3\gamma_{03} + \gamma_{32}}{4}} - \gamma_{03}\tilde{\alpha}_{11} + \gamma_{32}\tilde{\alpha}_{12} - i\tilde{\alpha}_{14} E_s^+ e^{-i\Delta k z} + i\tilde{\alpha}_{10} E_s^- e^{i\Delta k z} + i\tilde{\alpha}_{15} E_i^+ \\
&\quad - i\tilde{\alpha}_9 E_i^- + \mathcal{F}_{11},
\end{aligned}$$

$$\begin{aligned}
-\frac{\partial}{\partial z} E_s^+ &= i\tilde{\alpha}_{10} \frac{|g_s|^2}{|g_i|^2} + \mathcal{F}_3, \\
-\frac{\partial}{\partial z} E_s^- &= -i\tilde{\alpha}_{14} \frac{|g_s|^2}{|g_i|^2} + \mathcal{F}_4, \\
\frac{\partial}{\partial z} E_i^+ &= i\tilde{\alpha}_9 + \mathcal{F}_1, \\
\frac{\partial}{\partial z} E_i^- &= -i\tilde{\alpha}_{15} + \mathcal{F}_2.
\end{aligned} \tag{B.88}$$

The Langevin noises are formulated as a non-square form [35, 84]

$$\mathcal{F}_1 = \mathcal{F}_2 = 0;$$

$$\begin{aligned}
\mathcal{F}_5 &= \sqrt{D_{5,5}}\xi_1 + \sqrt{\frac{D_{5,19}}{2}}(\xi_{12} + i\xi_{13}) + \sqrt{\frac{D_{5,6}}{2}}(\xi_{14} + i\xi_{15}) + \sqrt{\frac{D_{5,7}}{2}}(\xi_{16} + i\xi_{17}) \\
&+ \sqrt{\frac{D_{5,8}}{2}}(\xi_{18} + i\xi_{19}) + \sqrt{\frac{D_{5,9}}{2}}(\xi_{20} + i\xi_{21}) + \sqrt{\frac{D_{5,14}}{2}}(\xi_{22} + i\xi_{23}) \\
&+ \sqrt{\frac{D_{5,13}}{2}}(\xi_{24} + i\xi_{25}) + \sqrt{\frac{D_{5,11}}{2}}(\xi_{26} + i\xi_{27}); \\
\mathcal{F}_{19} &= \sqrt{\frac{D_{5,19}}{2}}(\xi_{12} - i\xi_{13}) + \sqrt{D_{19,19}}\xi_2 + \sqrt{\frac{D_{19,18}}{2}}(\xi_{28} + i\xi_{29}) + \sqrt{\frac{D_{19,17}}{2}}(\xi_{30} + i\xi_{31}) \\
&+ \sqrt{\frac{D_{19,16}}{2}}(\xi_{32} + i\xi_{33}) + \sqrt{\frac{D_{19,15}}{2}}(\xi_{34} + i\xi_{35}) + \sqrt{\frac{D_{19,10}}{2}}(\xi_{36} + i\xi_{37}) \\
&+ \sqrt{\frac{D_{19,13}}{2}}(\xi_{38} + i\xi_{39}) + \sqrt{\frac{D_{19,11}}{2}}(\xi_{40} + i\xi_{41});
\end{aligned}$$

$$\begin{aligned}
\mathcal{F}_6 &= \sqrt{\frac{D_{5,6}}{2}}(\xi_{14} - i\xi_{15}) + \sqrt{D_{6,6}}\xi_3 + \sqrt{\frac{D_{6,18}}{2}}(\xi_{42} + i\xi_{43}) + \sqrt{\frac{D_{6,8}}{2}}(\xi_{44} + i\xi_{45}) \\
&+ \sqrt{\frac{D_{6,16}}{2}}(\xi_{46} + i\xi_{47}) + \sqrt{\frac{D_{6,10}}{2}}(\xi_{48} + i\xi_{49}) + \sqrt{\frac{D_{6,13}}{2}}(\xi_{50} + i\xi_{51}); \\
\mathcal{F}_{18} &= \sqrt{\frac{D_{19,18}}{2}}(\xi_{28} - i\xi_{29}) + \sqrt{\frac{D_{6,18}}{2}}(\xi_{42} - i\xi_{43}) + \sqrt{D_{18,18}}\xi_4 + \sqrt{\frac{D_{18,8}}{2}}(\xi_{52} + i\xi_{53}) \\
&+ \sqrt{\frac{D_{18,16}}{2}}(\xi_{54} + i\xi_{55}) + \sqrt{\frac{D_{18,14}}{2}}(\xi_{56} + i\xi_{57}) + \sqrt{\frac{D_{18,13}}{2}}(\xi_{58} + i\xi_{59}); \\
\mathcal{F}_7 &= \sqrt{\frac{D_{5,7}}{2}}(\xi_{16} - i\xi_{17}) + \sqrt{\frac{D_{7,8}}{2}}(\xi_{60} + i\xi_{61}) + \sqrt{\frac{D_{7,9}}{2}}(\xi_{62} + i\xi_{63}); \\
\mathcal{F}_{17} &= \sqrt{\frac{D_{19,17}}{2}}(\xi_{30} - i\xi_{31}) + \sqrt{\frac{D_{17,16}}{2}}(\xi_{64} + i\xi_{65}) + \sqrt{\frac{D_{17,15}}{2}}(\xi_{66} + i\xi_{67});
\end{aligned}$$

$$\begin{aligned}
\mathcal{F}_8 &= \sqrt{\frac{D_{5,8}}{2}}(\xi_{18} - i\xi_{19}) + \sqrt{\frac{D_{6,8}}{2}}(\xi_{44} - i\xi_{45}) + \sqrt{\frac{D_{18,8}}{2}}(\xi_{52} - i\xi_{53}) \\
&+ \sqrt{\frac{D_{7,8}}{2}}(\xi_{60} - i\xi_{61}) + \sqrt{\frac{D_{8,16}}{2}}(\xi_{68} + i\xi_{69}) + \sqrt{\frac{D_{8,9}}{2}}(\xi_{70} + i\xi_{71}) \\
&+ \sqrt{\frac{D_{8,10}}{2}}(\xi_{72} + i\xi_{73}) + \sqrt{\frac{D_{8,13}}{2}}(\xi_{74} + i\xi_{75}) + \sqrt{\frac{D_{8,12}}{2}}(\xi_{76} + i\xi_{77}) \\
&+ \sqrt{\frac{D_{8,11}}{2}}(\xi_{78} + i\xi_{79}) + \sqrt{\frac{D_{8,3}}{2}}(\xi_{80} + i\xi_{81}); \\
\mathcal{F}_{16} &= \sqrt{\frac{D_{19,16}}{2}}(\xi_{32} - i\xi_{33}) + \sqrt{\frac{D_{6,16}}{2}}(\xi_{46} - i\xi_{47}) + \sqrt{\frac{D_{18,16}}{2}}(\xi_{54} - i\xi_{55}) \\
&+ \sqrt{\frac{D_{17,16}}{2}}(\xi_{64} - i\xi_{65}) + \sqrt{\frac{D_{8,16}}{2}}(\xi_{68} - i\xi_{69}) + \sqrt{\frac{D_{16,15}}{2}}(\xi_{82} + i\xi_{83}) \\
&+ \sqrt{\frac{D_{16,14}}{2}}(\xi_{84} + i\xi_{85}) + \sqrt{\frac{D_{16,13}}{2}}(\xi_{86} + i\xi_{87}) + \sqrt{\frac{D_{16,12}}{2}}(\xi_{88} + i\xi_{89}) \\
&+ \sqrt{\frac{D_{16,11}}{2}}(\xi_{90} + i\xi_{91}) + \sqrt{\frac{D_{16,4}}{2}}(\xi_{92} + i\xi_{93}); \\
\mathcal{F}_9 &= \sqrt{\frac{D_{5,9}}{2}}(\xi_{20} - i\xi_{21}) + \sqrt{\frac{D_{7,9}}{2}}(\xi_{62} - i\xi_{63}) + \sqrt{\frac{D_{8,9}}{2}}(\xi_{70} - i\xi_{71}) \\
&+ \sqrt{D_{9,9}}\xi_5 + \sqrt{\frac{D_{9,15}}{2}}(\xi_{94} + i\xi_{95}) + \sqrt{\frac{D_{9,10}}{2}}(\xi_{96} + i\xi_{97}) + \sqrt{\frac{D_{9,3}}{2}}(\xi_{98} + i\xi_{99}); \\
\mathcal{F}_{15} &= \sqrt{\frac{D_{19,15}}{2}}(\xi_{34} - i\xi_{35}) + \sqrt{\frac{D_{17,15}}{2}}(\xi_{66} - i\xi_{67}) + \sqrt{\frac{D_{16,15}}{2}}(\xi_{82} - i\xi_{83}) \\
&+ \sqrt{\frac{D_{9,15}}{2}}(\xi_{94} - i\xi_{95}) + \sqrt{D_{15,15}}\xi_6 + \sqrt{\frac{D_{15,14}}{2}}(\xi_{100} + i\xi_{101}) \\
&+ \sqrt{\frac{D_{15,4}}{2}}(\xi_{102} + i\xi_{103});
\end{aligned}$$

$$\begin{aligned}
\mathcal{F}_{10} &= \sqrt{\frac{D_{19,10}}{2}}(\xi_{36} - i\xi_{37}) + \sqrt{\frac{D_{6,10}}{2}}(\xi_{48} - i\xi_{49}) + \sqrt{\frac{D_{8,10}}{2}}(\xi_{72} - i\xi_{73}) \\
&+ \sqrt{\frac{D_{9,10}}{2}}(\xi_{96} - i\xi_{97}) + \sqrt{D_{10,10}}\xi_7 + \sqrt{\frac{D_{10,14}}{2}}(\xi_{104} + i\xi_{105}) \\
&+ \sqrt{\frac{D_{10,13}}{2}}(\xi_{106} + i\xi_{107}) + \sqrt{\frac{D_{10,11}}{2}}(\xi_{108} + i\xi_{109}); \\
\mathcal{F}_{14} &= \sqrt{\frac{D_{5,14}}{2}}(\xi_{22} - i\xi_{23}) + \sqrt{\frac{D_{18,14}}{2}}(\xi_{56} - i\xi_{57}) + \sqrt{\frac{D_{16,14}}{2}}(\xi_{84} - i\xi_{85}) \\
&+ \sqrt{\frac{D_{15,14}}{2}}(\xi_{100} - i\xi_{101}) + \sqrt{\frac{D_{10,14}}{2}}(\xi_{104} - i\xi_{105}) + \sqrt{D_{14,14}}\xi_8 \\
&+ \sqrt{\frac{D_{14,13}}{2}}(\xi_{110} + i\xi_{111}) + \sqrt{\frac{D_{14,11}}{2}}(\xi_{112} + i\xi_{113}); \\
\mathcal{F}_{13} &= \sqrt{\frac{D_{5,13}}{2}}(\xi_{24} - i\xi_{25}) + \sqrt{\frac{D_{19,13}}{2}}(\xi_{38} - i\xi_{39}) + \sqrt{\frac{D_{6,13}}{2}}(\xi_{50} - i\xi_{51}) \\
&+ \sqrt{\frac{D_{18,13}}{2}}(\xi_{58} - i\xi_{59}) + \sqrt{\frac{D_{8,13}}{2}}(\xi_{74} - i\xi_{75}) + \sqrt{\frac{D_{16,13}}{2}}(\xi_{86} - i\xi_{87}) \\
&+ \sqrt{\frac{D_{10,13}}{2}}(\xi_{106} - i\xi_{107}) + \sqrt{\frac{D_{14,13}}{2}}(\xi_{110} - i\xi_{111}) + \sqrt{D_{13,13}}\xi_9 \\
&+ \sqrt{\frac{D_{12,13}}{2}}(\xi_{114} + i\xi_{115}); \\
\mathcal{F}_{12} &= \sqrt{\frac{D_{8,12}}{2}}(\xi_{76} - i\xi_{77}) + \sqrt{\frac{D_{16,12}}{2}}(\xi_{88} - i\xi_{89}) + \sqrt{\frac{D_{12,13}}{2}}(\xi_{114} - i\xi_{115}) \\
&+ \sqrt{D_{12,12}}\xi_{10} + \sqrt{\frac{D_{11,12}}{2}}(\xi_{116} + i\xi_{117}); \\
\mathcal{F}_{11} &= \sqrt{\frac{D_{5,11}}{2}}(\xi_{26} - i\xi_{27}) + \sqrt{\frac{D_{19,11}}{2}}(\xi_{40} - i\xi_{41}) + \sqrt{\frac{D_{8,11}}{2}}(\xi_{78} - i\xi_{79}) \\
&+ \sqrt{\frac{D_{16,11}}{2}}(\xi_{90} - i\xi_{91}) + \sqrt{\frac{D_{10,11}}{2}}(\xi_{108} - i\xi_{109}) + \sqrt{\frac{D_{14,11}}{2}}(\xi_{112} - i\xi_{113}) \\
&+ \sqrt{\frac{D_{11,12}}{2}}(\xi_{116} - i\xi_{117}) + \sqrt{D_{11,11}}\xi_{11}; \\
\mathcal{F}_3 &= \sqrt{\frac{D_{8,3}}{2}}(\xi_{80} - i\xi_{81}) + \sqrt{\frac{D_{9,3}}{2}}(\xi_{98} - i\xi_{99}); \\
\mathcal{F}_4 &= \sqrt{\frac{D_{16,4}}{2}}(\xi_{92} - i\xi_{93}) + \sqrt{\frac{D_{15,4}}{2}}(\xi_{102} - i\xi_{103}). \tag{B.89}
\end{aligned}$$

In numerical simulations, we have a factor  $\frac{1}{\sqrt{N_c \Delta t \Delta z}}$  for Langevin noises  $\mathcal{F}$  and  $\frac{1}{N_c \Delta t \Delta z}$  for correction terms.



# APPENDIX C

## MULTIMODE DESCRIPTION OF CORRELATED TWO-PHOTON STATE

In this Appendix, we introduce a general model for quantum detection efficiency for multimode analysis in various quantum communication scheme. Based on this detection model with the spectral description of correlated two-photon state, we derive the effective density matrix conditioning on the detection events of entanglement swapping, polarization maximally entangled (PME) state projection, and quantum teleportation.

### *C.1 Quantum Efficiency of Detector*

To account for quantum efficiency of detector and the affect of its own spectrum filtering, we introduce an extra beam splitter (B.S.) with a transmissivity  $\eta(\omega, \omega_0)$  [117] before the detection event.  $\eta$  models the quantum efficiency of the detectors in the microscopic level (response at frequency  $\omega_0$ ) and the macroscopic level (time-integrated detection). One example of conditioning on the single click of the detector, the output density operator becomes

$$\hat{\rho}_{out} = \int_{-\infty}^{\infty} d\omega_0 \hat{\Pi}_1 \text{Tr}_{ref} [\hat{U}_{BS} \hat{\rho}_{in} \hat{U}_{BS}^\dagger] \hat{\Pi}_1 \quad (\text{C.1})$$

$$\hat{\Pi}_1 \equiv \int_{-\infty}^{\infty} d\omega |\omega\rangle \langle \omega| \quad (\text{C.2})$$

$$\hat{U}_{BS} \equiv \begin{pmatrix} \sqrt{1-\eta} & \sqrt{\eta} \\ \sqrt{\eta} & -\sqrt{1-\eta} \end{pmatrix} \quad (\text{C.3})$$

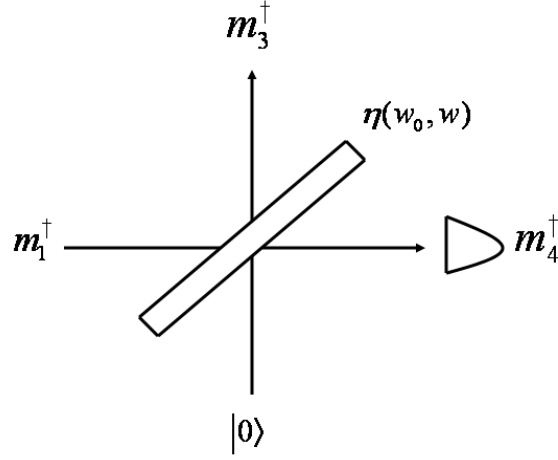


**Figure C.1:** Model of quantum efficiency of detector.

where  $\text{Tr}_{ref}$  is the trace over the reflected modes  $m_3^\dagger$ , and the flat spectrum projection operator  $\hat{\Pi}_1$  (only photon number is projected and no frequency resolution) is considered in the measurement process [76]. In Figure C.1,  $m_1^\dagger$  is the incoming photon operator before the detection,  $m_3^\dagger$  is the reflected mode, and  $m_4^\dagger$  is now the detection mode with a modelling of spectral quantum efficiency and an effective quantum efficiency is defined as

$$\int_{-\infty}^{\infty} \eta(\omega, \omega_0) d\omega_0 = \eta_{eff}(\omega). \quad (\text{C.4})$$

## ***C.2 Multimode Description of Entanglement Swapping***

From Eq. (5.4), we use single mode  $\Phi(\omega)$  for Raman photon and a multimode description  $f(\omega_s, \omega_i)$  for cascade photons and rewrite the effective state. Note that a symmetric setup is considered so the mode description is the same for both sides A and B in the scheme of entanglement swapping.

$$\begin{aligned}
|\Psi\rangle_{eff} = & \eta_1(1 - \eta_2) \times \\
& \int f(\omega_s, \omega_i) \hat{a}_s^{\dagger,A}(\omega_s) \hat{a}_i^{\dagger,A}(\omega_i) d\omega_s d\omega_i \int f(\omega'_s, \omega'_i) \hat{a}_s^{\dagger,B}(\omega'_s) \hat{a}_i^{\dagger,B}(\omega'_i) d\omega'_s d\omega'_i |0\rangle + \\
& \eta_2(1 - \eta_1) \int \Phi(\omega) d\omega \hat{a}_r^{\dagger,A}(\omega) \hat{S}_A^\dagger \int \Phi(\omega') d\omega' \hat{a}_r^{\dagger,B}(\omega') \hat{S}_B^\dagger |0\rangle + \sqrt{\eta_1(1 - \eta_1)} \times \\
& \sqrt{\eta_2(1 - \eta_2)} \int f(\omega_s, \omega_i) d\omega_s d\omega_i \times \hat{a}_s^{\dagger,A}(\omega_s) \hat{a}_i^{\dagger,A}(\omega_i) \int \Phi(\omega') d\omega' \hat{a}_r^{\dagger,B}(\omega') \hat{S}_B^\dagger |0\rangle + \\
& \sqrt{\eta_1\eta_2(1 - \eta_1)(1 - \eta_2)} \int \Phi(\omega) d\omega \hat{a}_r^{\dagger,A}(\omega) \hat{S}_A^\dagger \int f(\omega'_s, \omega'_i) \hat{a}_s^{\dagger,B}(\omega'_s) \hat{a}_i^{\dagger,B}(\omega'_i) d\omega'_s d\omega'_i |0\rangle.
\end{aligned} \tag{C.5}$$

With the B.S., we have  $\hat{a}_i^{\dagger,A} = \frac{\hat{m}_1^\dagger + \hat{m}_2^\dagger}{\sqrt{2}}$ ,  $\hat{a}_i^{\dagger,B} = \frac{\hat{n}_1^\dagger + \hat{n}_2^\dagger}{\sqrt{2}}$ ,  $\hat{a}_r^{\dagger,A} = \frac{\hat{m}_1^\dagger - \hat{m}_2^\dagger}{\sqrt{2}}$ ,  $\hat{a}_r^{\dagger,B} = \frac{\hat{n}_1^\dagger - \hat{n}_2^\dagger}{\sqrt{2}}$ , where  $\hat{a}_i^\dagger$  is the creation operator for idler photon and  $\hat{a}_r^\dagger$  is for Raman photon. The input density operator is  $\hat{\rho}_{in} = |\Psi\rangle_{eff}\langle\Psi|$  and conditioning on the pair of single click  $(\hat{m}_{1,2}^\dagger, \hat{n}_{1,2}^\dagger)$ , we are able to generate maximally entangled singlet or triplet state  $|\Psi\rangle_{DLCZ} = \frac{\hat{S}_A^\dagger \pm \hat{S}_B^\dagger}{\sqrt{2}} |0\rangle_{A,B}$ . Without loss of generality, we consider a triplet state along with a pair of clicks  $(\hat{m}_1^\dagger, \hat{n}_1^\dagger)$  and use the model of quantum efficiency in Eq. (C.1) with tracing over the detection modes  $(\hat{m}_4^\dagger, \hat{n}_4^\dagger)$ . Note that  $\hat{m}_1^\dagger = \sqrt{1 - \eta} \hat{m}_3^\dagger + \sqrt{\eta} \hat{m}_4^\dagger$  and  $\hat{n}_1^\dagger = \sqrt{1 - \eta} \hat{n}_3^\dagger + \sqrt{\eta} \hat{n}_4^\dagger$  as we model the quantum efficiency in the previous Section.

$$\hat{\rho}_{out} = \int_{-\infty}^{\infty} d\omega_0 \text{Tr}_{m4,n4} \{ \text{Tr}_{m3,n3} [\hat{U}_{BS}^B \hat{U}_{BS}^A \hat{\rho}_{in} \hat{U}_{BS}^{\dagger,A} \hat{U}_{BS}^{\dagger,B}] \hat{M}_{4,4} \} \tag{C.6}$$

$$\hat{M}_{4,4} \equiv (\hat{I}_{m4}^\dagger - |0\rangle_{m4}\langle 0|) \otimes |0\rangle_{m2}\langle 0| \otimes (\hat{I}_{n4}^\dagger - |0\rangle_{n4}\langle 0|) \otimes |0\rangle_{n2}\langle 0| \tag{C.7}$$

where the unitary B.S. operator is denoted by both sides (A and B) and NRPD projection operators are used [99]. These operators project the state with single click of the detected mode without resolving the number of photons.  $\hat{I}$  is identity operator. The un-normalized output density operator after tracing out these modes becomes

$$\begin{aligned}
\hat{\rho}_{out} = & \frac{\eta_1^2(1-\eta_2)^2}{4} \times \\
& \int d\omega_i d\omega'_i \eta_{eff}(\omega_i) \eta_{eff}(\omega'_i) \left[ \int f(\omega_s, \omega_i) \hat{a}_s^{\dagger, A}(\omega_s) d\omega_s \int f(\omega'_s, \omega'_i) \hat{a}_s^{\dagger, B}(\omega'_s) d\omega'_s \right] \\
& |0\rangle\langle 0| \left[ \int f^*(\omega''_s, \omega_i) \hat{a}_s^A(\omega''_s) d\omega''_s \int f^*(\omega'''_s, \omega'_i) \hat{a}_s^B(\omega'''_s) d\omega'''_s \right] \\
& + \frac{\eta_1 \eta_2 (1-\eta_1)(1-\eta_2)}{4} \left\{ \int d\omega_i \eta_{eff}(\omega_i) \left[ \int f(\omega_s, \omega_i) d\omega_s \int f^*(\omega'_s, \omega_i) d\omega'_s \right. \right. \\
& \int |\Phi(\omega)|^2 \eta_{eff}(\omega) d\omega \left. \right] \left( \hat{a}_s^{\dagger, A}(\omega_s) \hat{S}_B^\dagger |0\rangle\langle 0| \hat{S}_B \hat{a}_s^A(\omega'_s) + \right. \\
& \hat{a}_s^{\dagger, B}(\omega_s) \hat{S}_A^\dagger |0\rangle\langle 0| \hat{S}_A \hat{a}_s^B(\omega'_s) \left. \right) + \int \int f(\omega_s, \omega_i) d\omega_s \Phi^*(\omega_i) \eta_{eff}(\omega_i) d\omega_i \times \\
& \int \int f^*(\omega'_s, \omega'_i) d\omega'_s \Phi(\omega'_i) \eta_{eff}(\omega'_i) d\omega'_i \left( \hat{a}_s^{\dagger, A}(\omega_s) \hat{S}_B^\dagger |0\rangle\langle 0| \hat{S}_A \hat{a}_s^B(\omega'_s) + \right. \\
& \left. \left. \hat{a}_s^{\dagger, B}(\omega_s) \hat{S}_A^\dagger |0\rangle\langle 0| \hat{S}_B \hat{a}_s^A(\omega'_s) \right) \right\} + \hat{\rho}'_{out} \tag{C.8}
\end{aligned}$$

where  $\eta_{eff}(\omega)$  is introduced after integration of  $\omega_0$ , and we denote it as an effective quantum efficiency for idler field  $\omega_i$  or Raman photon at frequency  $\omega$  (wavelength 780 nm for D2 line of Rb atom).  $\hat{\rho}'_{out}$  includes the terms that won't survive after the interference of telecom photons in the middle B.S. (conditioning on a single click of detector). They involve operators like  $\hat{a}_s^{\dagger, A} \hat{a}_s^{\dagger, B} |0\rangle\langle 0| \hat{a}_s^A \hat{S}_B$ ,  $\hat{a}_s^{\dagger, A} \hat{a}_s^{\dagger, B} |0\rangle\langle 0| \hat{S}_A \hat{S}_B$  and  $\hat{S}_A^{\dagger, A} \hat{S}_B^{\dagger, B} |0\rangle\langle 0| \hat{S}_A \hat{S}_B$ .

The normalization factor is derived by tracing over the atomic degree of freedom.

$$\begin{aligned}
\text{Tr}(\hat{\rho}_{out}) \equiv \mathcal{N} = & \frac{\eta_1^2(1-\eta_2)^2}{4} \int d\omega_s d\omega_i \eta_{eff}(\omega_i) |f(\omega_s, \omega_i)|^2 \int d\omega'_s d\omega'_i \eta_{eff}(\omega'_i) |f(\omega'_s, \omega'_i)|^2 + \\
& \frac{\eta_1 \eta_2 (1-\eta_1)(1-\eta_2)}{2} \int d\omega_s d\omega_i \eta_{eff}(\omega_i) |f(\omega_s, \omega_i)|^2 \int |\Phi|^2(\omega) \eta_{eff}(\omega) d\omega + \\
& \frac{\eta_2^2(1-\eta_1)^2}{4} \int |\Phi|^2(\omega) \eta_{eff}(\omega) d\omega \int |\Phi|^2(\omega') \eta_{eff}(\omega') d\omega' \tag{C.9}
\end{aligned}$$

which will be put back when we calculate the heralding and success probabilities.

Next we interfere telecom photons with B.S. that  $\hat{a}_s^{\dagger, A} = \frac{\hat{c}_1^\dagger + \hat{c}_2^\dagger}{\sqrt{2}}$ ,  $\hat{a}_s^{\dagger, B} = \frac{\hat{c}_1^\dagger - \hat{c}_2^\dagger}{\sqrt{2}}$ , and again a quantum efficiency  $\eta(\omega, \omega_0)$  for telecom photon is introduced. Use

$\hat{c}_1^\dagger = \sqrt{1-\eta}\hat{c}_3^\dagger + \sqrt{\eta}\hat{c}_4^\dagger$  and trace over the reflected mode  $\hat{c}_3^\dagger$  conditioning on the click of  $\hat{c}_4^\dagger$  from NRPD. The effective density matrix becomes

$$\begin{aligned}\hat{\rho}_{out}^{(2)} &= \int_{-\infty}^{\infty} d\omega_0 \text{Tr}_{c4} \{ \text{Tr}_{c3} [\hat{U}_{BS}^C \hat{\rho}_{in} \hat{U}_{BS}^{\dagger,C}] \hat{M}_4 \} \\ &\equiv \int_{-\infty}^{\infty} d\omega_0 \hat{\rho}_{out}^{(2)}(\omega_0),\end{aligned}\tag{C.10}$$

$$\hat{\rho}_{out}^{(2)}(\omega_0) \equiv \text{Tr}_{c4} \{ \hat{\rho}_{in}^{(2)}(\omega_0) \}\tag{C.11}$$

$$\hat{M}_4 \equiv (\hat{I}_{c4}^\dagger - |0\rangle_{c4}\langle 0|) \otimes |0\rangle_{c2}\langle 0|,\tag{C.12}$$

$$\begin{aligned}\hat{\rho}_{in}^{(2)}(\omega_0) &= \frac{\eta_1^2(1-\eta_2)^2}{16} \int d\omega_i d\omega'_i \eta_{eff}(\omega_i) \eta_{eff}(\omega'_i) \left\{ \right. \\ &\quad \int d\omega_s (1-\eta(\omega_s)) f(s, i) f^*(s, i') \int d\omega'_s f(s', i') \sqrt{\eta(\omega'_s)} \hat{c}_4^\dagger(\omega'_s) |0\rangle\langle 0| \times \\ &\quad \int d\omega''_s \hat{c}_4(\omega''_s) \sqrt{\eta(\omega''_s)} f^*(s'', i) + \int d\omega_s (1-\eta(\omega_s)) f(s, i) f^*(s, i) \times \\ &\quad \int d\omega'_s f(s', i') \sqrt{\eta(\omega'_s)} \hat{c}_4^\dagger(\omega'_s) |0\rangle\langle 0| \int d\omega'''_s \hat{c}_4(\omega'''_s) \sqrt{\eta(\omega'''_s)} f^*(s''', i') + \\ &\quad \int d\omega'_s (1-\eta(\omega'_s)) f(s', i') f^*(s', i') \int d\omega_s f(s, i) \sqrt{\eta(\omega_s)} \hat{c}_4^\dagger(\omega_s) |0\rangle\langle 0| \times \\ &\quad \int d\omega''_s \hat{c}_4(\omega''_s) \sqrt{\eta(\omega''_s)} f^*(s'', i) + \int d\omega'_s (1-\eta(\omega'_s)) f(s', i') f^*(s', i) \times \\ &\quad \int d\omega_s f(s, i) \sqrt{\eta(\omega_s)} \hat{c}_4^\dagger(\omega_s) |0\rangle\langle 0| \int d\omega'''_s \hat{c}_4(\omega'''_s) \sqrt{\eta(\omega'''_s)} f^*(s''', i') + \\ &\quad \int d\omega'_s \sqrt{\eta(\omega'_s)} f(s', i') \int d\omega_s \sqrt{\eta(\omega_s)} f(s, i) \hat{c}_4^\dagger(\omega_s) \hat{c}_4^\dagger(\omega'_s) |0\rangle\langle 0| \times \\ &\quad \left. \int d\omega''_s \sqrt{\eta(\omega''_s)} f^*(s'', i) \int d\omega'''_s \sqrt{\eta(\omega'''_s)} f^*(s''', i') \hat{c}_4(\omega''_s) \hat{c}_4(\omega'''_s) \right\} + \\ &\quad \frac{\eta_1 \eta_2 (1-\eta_1)(1-\eta_2)}{8} \left\{ \int d\omega_i \eta_{eff}(\omega_i) \int f(s, i) d\omega_s \int f^*(s', i) d\omega'_s \times \right. \\ &\quad \int d\omega |\Phi(\omega)|^2 \eta_{eff}(\omega) \sqrt{\eta(\omega_s)} \hat{c}_4^\dagger(\omega_s) \left( \hat{S}_B^\dagger |0\rangle\langle 0| \hat{S}_B + \hat{S}_A^\dagger |0\rangle\langle 0| \hat{S}_A \right) \times \\ &\quad \hat{c}_4(\omega'_s) \sqrt{\eta(\omega'_s)} \int \int f(s, i) d\omega_s \Phi^*(\omega_i) \eta_{eff}(\omega_i) d\omega_i \times \\ &\quad \int \int f^*(s', i') d\omega'_s \Phi(\omega'_i) \eta_{eff}(\omega'_i) d\omega'_i \sqrt{\eta(\omega_s)} \hat{c}_4^\dagger(\omega_s) \times \\ &\quad \left. \left( \hat{S}_B^\dagger |0\rangle\langle 0| \hat{S}_A + \hat{S}_A^\dagger |0\rangle\langle 0| \hat{S}_B \right) \hat{c}_4(\omega'_s) \sqrt{\eta(\omega'_s)} \right\}\end{aligned}\tag{C.13}$$

where a brief notation for spectrum  $f(s, i) \equiv f(\omega_s, \omega_i)$  and quantum efficiency  $\eta(\omega) \equiv \eta(\omega, \omega_0)$ . This quantum efficiency refers to the telecom photon. We proceed to trace over the detected modes and the density matrix can be simplified by interchange of variables in integration.

$$\begin{aligned}
\hat{\rho}_{out}^{(2)}(\omega_0) = & \frac{\eta_1^2(1-\eta_2)^2}{8} \int d\omega_i d\omega'_i \eta_{eff}(\omega_i) \eta_{eff}(\omega'_i) \left\{ \right. \\
& \int d\omega_s (1-\eta(\omega_s, \omega_0)) f(\omega_s, \omega_i) f^*(\omega_s, \omega'_i) \int d\omega'_s f(\omega'_s, \omega'_i) f^*(\omega'_s, \omega_i) \eta(\omega'_s, \omega_0) + \\
& \int d\omega_s (1-\eta(\omega_s, \omega_0)) |f(\omega_s, \omega_i)|^2 \int d\omega'_s |f(\omega'_s, \omega'_i)|^2 \eta(\omega'_s, \omega_0) + \\
& \frac{1}{2} \int d\omega'_s \eta(\omega'_s, \omega_0) |f(\omega'_s, \omega'_i)|^2 \int d\omega_s \eta(\omega_s, \omega_0) |f(\omega_s, \omega_i)|^2 + \frac{1}{2} \times \\
& \left. \int d\omega'_s \eta(\omega'_s, \omega_0) f(\omega'_s, \omega'_i) f^*(\omega'_s, \omega_i) \int d\omega_s \eta(\omega_s, \omega_0) f(\omega_s, \omega_i) f^*(\omega_s, \omega'_i) \right\} |0\rangle\langle 0| \\
& + \frac{\eta_1 \eta_2 (1-\eta_1)(1-\eta_2)}{8} \left\{ \int d\omega_i \eta_{eff}(\omega_i) \int \eta(\omega_s, \omega_0) |f(\omega_s, \omega_i)|^2 d\omega_s \times \right. \\
& \int d\omega |\Phi(\omega)|^2 \eta_{eff}(\omega) \left( \hat{S}_B^\dagger |0\rangle\langle 0| \hat{S}_B + \hat{S}_A^\dagger |0\rangle\langle 0| \hat{S}_A \right) + \\
& \int \int \eta(\omega_s, \omega_0) f(\omega_s, \omega_i) d\omega_s \Phi^*(\omega_i) \eta_{eff}(\omega_i) d\omega_i \int f^*(\omega_s, \omega'_i) \Phi(\omega'_i) \eta_{eff}(\omega'_i) d\omega'_i \times \\
& \left. \left( \hat{S}_B^\dagger |0\rangle\langle 0| \hat{S}_A + \hat{S}_A^\dagger |0\rangle\langle 0| \hat{S}_B \right) \right\} \quad (C.14)
\end{aligned}$$

where the trace over two photon states requires the commutation relation of photon operators.

$$\begin{aligned}
& \text{Tr}[\hat{m}_4^\dagger(\omega_s) \hat{m}_4^\dagger(\omega'_s) |0\rangle\langle 0| \hat{m}_4(\omega''_s) \hat{m}_4(\omega'''_s)] \\
& = \langle 0| \hat{m}_4(\omega''_s) [\delta(\omega_s, \omega'''_s) + \hat{m}_4^\dagger(\omega_s) \hat{m}_4(\omega'''_s)] \hat{m}_4^\dagger(\omega'_s) |0\rangle \\
& = \delta(\omega_s, \omega'''_s) \delta(\omega''_s, \omega'_s) + \delta(\omega_s, \omega''_s) \delta(\omega'_s, \omega'''_s). \quad (C.15)
\end{aligned}$$

The above is the general formulation for the un-normalized density matrix conditioning on three clicks of NRPD's. We've included spectral quantum efficiency of the detector either for near-infrared ( $\eta_{eff}$ ) or telecom wavelength ( $\eta_t \equiv \int_{-\infty}^{\infty} \eta(\omega, \omega_0) d\omega_0$ )

To proceed, we assume a flat and finite spectrum response ( $\eta_{eff}(\omega) = \eta_{eff}$ ,  $\eta_t(\omega) = \eta_t$ ) with the range  $\omega_0 \in [\Omega - \Delta, \Omega + \Delta]$  centered at  $\Omega$  (near-infrared or telecom) and  $\omega \in [\omega_0 - \delta, \omega_0 + \delta]$ . The widths  $2\Delta$  and  $2\delta$  are large enough compared to our source bandwidth so these detection events do not give us any information of spectrum for our source. A perfect efficiency also means no photon loss during detection. Note that the integral involves multiplication of two telecom photon efficiency  $\int_{-\infty}^{\infty} \eta(\omega, \omega_0) \eta(\omega', \omega_0) d\omega_0 = \eta_t^2(\omega)$  that is valid if the source bandwidth is smaller than detector's.

After the integration of  $\omega_0$ , we have

$$\begin{aligned}
\hat{\rho}_{out}^{(2)} = & \frac{\eta_1^2(1-\eta_2)^2}{8} \eta_{eff}^2 \int d\omega_i d\omega'_i \left\{ (1-\eta_t) \eta_t \int d\omega_s f(\omega_s, \omega_i) f^*(\omega_s, \omega'_i) \times \right. \\
& \int d\omega'_s f(\omega'_s, \omega'_i) f^*(\omega'_s, \omega_i) + (1-\eta_t) \eta_t \int d\omega_s |f(\omega_s, \omega_i)|^2 \int d\omega'_s |f(\omega'_s, \omega'_i)|^2 + \\
& \frac{\eta_t^2}{2} \int d\omega'_s |f(\omega'_s, \omega'_i)|^2 \int d\omega_s |f(\omega_s, \omega_i)|^2 + \frac{\eta_t^2}{2} \int d\omega'_s f(\omega'_s, \omega'_i) f^*(\omega'_s, \omega_i) \times \\
& \left. \int d\omega_s f(\omega_s, \omega_i) f^*(\omega_s, \omega'_i) \right\} |0\rangle\langle 0| + \frac{\eta_1 \eta_2 (1-\eta_1)(1-\eta_2)}{8} \eta_t \eta_{eff}^2 \times \\
& \left\{ \int d\omega_i \int |f(\omega_s, \omega_i)|^2 d\omega_s \int d\omega |\Phi(\omega)|^2 \left( \hat{S}_B^\dagger |0\rangle\langle 0| \hat{S}_B + \hat{S}_A^\dagger |0\rangle\langle 0| \hat{S}_A \right) + \right. \\
& \int \int f(\omega_s, \omega_i) d\omega_s \Phi^*(\omega_i) d\omega_i \int f^*(\omega_s, \omega'_i) \Phi(\omega'_i) d\omega'_i \\
& \left. \left( \hat{S}_B^\dagger |0\rangle\langle 0| \hat{S}_A + \hat{S}_A^\dagger |0\rangle\langle 0| \hat{S}_B \right) \right\}. \tag{C.16}
\end{aligned}$$

### C.3 Density Matrix of PME Projection and Quantum Teleportation

In Chapter 5.4, we have the normalized density operator  $\hat{\rho}_{out,n}^{(2),AB}$  of the DLCZ entangled state through entanglement swapping. With another pair of DLCZ entangled state,  $\hat{\rho}_{out,n}^{(2),CD}$ , the joint density operator for these two pairs constructs the polarization maximally entangled state (PME) projection and is interpreted as

$$\begin{aligned}
& \hat{\rho}_{out,n}^{(2),AB} \otimes \hat{\rho}_{out,n}^{(2),CD} = \\
& \frac{1}{(a+b)^2} \left\{ a^2 |0\rangle\langle 0| + \frac{ab}{2} \left[ |0\rangle_{AB}\langle 0| \left( \hat{S}_C^\dagger |0\rangle\langle 0| \hat{S}_C + \hat{S}_D^\dagger |0\rangle\langle 0| \hat{S}_D \right. \right. \right. \\
& + \lambda_1 \hat{S}_C^\dagger |0\rangle\langle 0| \hat{S}_D + \lambda_1 \hat{S}_D^\dagger |0\rangle\langle 0| \hat{S}_C \left. \left. \left. + |0\rangle_{CD}\langle 0| \left( \hat{S}_B^\dagger |0\rangle\langle 0| \hat{S}_B + \hat{S}_A^\dagger |0\rangle\langle 0| \hat{S}_A \right. \right. \right. \right. \\
& + \lambda_1 \hat{S}_B^\dagger |0\rangle\langle 0| \hat{S}_A + \lambda_1 \hat{S}_A^\dagger |0\rangle\langle 0| \hat{S}_B \left. \left. \left. \right] + \frac{b^2}{4} \left( \hat{S}_C^\dagger |0\rangle\langle 0| \hat{S}_C + \hat{S}_D^\dagger |0\rangle\langle 0| \hat{S}_D \right. \right. \\
& + \lambda_1 \hat{S}_C^\dagger |0\rangle\langle 0| \hat{S}_D + \lambda_1 \hat{S}_D^\dagger |0\rangle\langle 0| \hat{S}_C \left. \left. \otimes \left( \hat{S}_B^\dagger |0\rangle\langle 0| \hat{S}_B + \hat{S}_A^\dagger |0\rangle\langle 0| \hat{S}_A \right. \right. \right. \\
& \left. \left. \left. + \lambda_1 \hat{S}_B^\dagger |0\rangle\langle 0| \hat{S}_A + \lambda_1 \hat{S}_A^\dagger |0\rangle\langle 0| \hat{S}_B \right) \right\}, \tag{C.17}
\end{aligned}$$

which is used to calculate the success probability after post measurement [a click from each side, the side of (A or C) and (B or D)].  $a = \eta_r(2 - \eta) \left( 1 + \sum_j \lambda_j^2 \right)$ ,  $b = 4$ , and  $\eta_r = \eta_1/\eta_2$ ,  $\eta = \eta_t$ ,  $\lambda_j$  is Schmidt number that is used to decompose the two-photon source from the cascade transition.

In DLCZ protocol, quantum teleportation uses the similar setup in PME projection and combines with the desired teleported state,  $|\Phi\rangle = (d_0 \hat{S}_{I_1}^\dagger + d_1 \hat{S}_{I_2}^\dagger) |0\rangle$ , which is represented by two other atomic ensembles  $I_1$  and  $I_2$ . The requirement of normalization of the state is  $|d_0|^2 + |d_1|^2 = 1$ , and the density operator of quantum teleportation is  $\hat{\rho}_{QT} = |\Phi\rangle\langle\Phi| \otimes \hat{\rho}_{out,n}^{(2),AB} \otimes \hat{\rho}_{out,n}^{(2),CD}$ . Conditioning on clicks of  $\hat{D}_{I_1}$  and  $\hat{D}_{I_2}$ , the effective density matrix for quantum teleportation is (using  $\hat{S}_{I_1}^\dagger = (\hat{D}_{I_1} + \hat{D}_A)/\sqrt{2}$ ,  $\hat{S}_{I_2}^\dagger = (\hat{D}_{I_2} + \hat{D}_C)/\sqrt{2}$  for the effect of beam splitter)



$$\begin{aligned}
\hat{\rho}_{QT,eff} = & \left[ \frac{|d_0|^2}{2} (\hat{D}_{I_1}^\dagger |0\rangle\langle 0| \hat{D}_{I_1}) + \frac{|d_1|^2}{2} (\hat{D}_{I_2}^\dagger |0\rangle\langle 0| \hat{D}_{I_2}) + \frac{d_0 d_1^*}{2} (\hat{D}_{I_1}^\dagger |0\rangle\langle 0| \hat{D}_{I_2}) \right. \\
& + \left. \frac{d_0^* d_1}{2} (\hat{D}_{I_2}^\dagger |0\rangle\langle 0| \hat{D}_{I_1}) \right] \otimes \frac{1}{(a+b)^2} \left\{ a^2 |0\rangle\langle 0| + \frac{ab}{2} \left[ |0\rangle_{AB} \langle 0| \right. \right. \\
& \left( \frac{\hat{D}_{I_2}^\dagger |0\rangle\langle 0| \hat{D}_{I_2}}{2} + \hat{S}_D^\dagger |0\rangle\langle 0| \hat{S}_D + \lambda_1 \frac{\hat{D}_{I_2}^\dagger}{\sqrt{2}} |0\rangle\langle 0| \hat{S}_D + \lambda_1 \hat{S}_D^\dagger |0\rangle\langle 0| \frac{\hat{D}_{I_2}}{\sqrt{2}} \right) \\
& + |0\rangle_{CD} \langle 0| \left( \hat{S}_B^\dagger |0\rangle\langle 0| \hat{S}_B + \frac{\hat{D}_{I_1}^\dagger |0\rangle\langle 0| \hat{D}_{I_1}}{2} + \lambda_1 \hat{S}_B^\dagger |0\rangle\langle 0| \frac{\hat{D}_{I_1}}{\sqrt{2}} + \lambda_1 \frac{\hat{D}_{I_2}^\dagger}{\sqrt{2}} |0\rangle\langle 0| \hat{S}_B \right) \Big] \\
& + \frac{b^2}{4} \left( \frac{\hat{D}_{I_2}^\dagger |0\rangle\langle 0| \hat{D}_{I_2}}{2} + \hat{S}_D^\dagger |0\rangle\langle 0| \hat{S}_D + \lambda_1 \frac{\hat{D}_{I_2}^\dagger}{\sqrt{2}} |0\rangle\langle 0| \hat{S}_D + \lambda_1 \hat{S}_D^\dagger |0\rangle\langle 0| \frac{\hat{D}_{I_2}}{\sqrt{2}} \right) \otimes \\
& \left. \left( \hat{S}_B^\dagger |0\rangle\langle 0| \hat{S}_B + \frac{\hat{D}_{I_1}^\dagger |0\rangle\langle 0| \hat{D}_{I_1}}{2} + \lambda_1 \hat{S}_B^\dagger |0\rangle\langle 0| \frac{\hat{D}_{I_1}}{\sqrt{2}} + \lambda_1 \frac{\hat{D}_{I_2}^\dagger}{\sqrt{2}} |0\rangle\langle 0| \hat{S}_B \right) \right\}, \quad (C.18)
\end{aligned}$$

which is used to calculate the success probability for teleported state.



## APPENDIX D

# HAMILTONIAN AND EQUATION OF MOTION FOR FREQUENCY CONVERSION IN A DIAMOND TYPE ATOMIC ENSEMBLE

In this appendix, we derive the Hamiltonian and the Maxwell-Bloch equation for frequency conversion in ladder-type transition. The steady state solutions for atoms are solved, and the solution to the field equations are discussed in Chapter 6. Similar to the derivation in Appendix B where the cascade emissions are investigated, the conversion scheme here also involves four-wave mixing with two classical driving lasers and two quantum fields, signal and idler. The driving lasers are applied in a way that signal or idler is converted only when an idler or signal is put into interaction with the atoms (see Figure 6.1). We will use the same quantization procedure for electromagnetic fields as discussed in Appendix B.2.1.

### *D.1 Hamiltonian and Maxwell-Bloch Equation*

To derive the coupled Maxwell-Bloch equations it is convenient to employ a quantized description of the electromagnetic field [29] and use Heisenberg-Langevin equation methods, and then invoke a standard semiclassical factorization assumption. The propagation length  $L$  is discretized into  $2M+1$  elements. The positive frequency component of the electric field operator is given by  $\hat{E}^+(z) = \sum_{n=-M}^M \sqrt{\frac{\hbar\omega_{s,n}}{2\epsilon_0 V}} e^{i(k_s+k_n)z} \hat{c}_n$  where  $[\hat{c}_n, \hat{c}_{n'}^\dagger] = \delta_{nn'}$ ,  $k_n = \frac{2\pi n}{L}$ ,  $\omega_{s,n} = \omega_s + k_n c$ ,  $n = -M, \dots, M$  and  $\omega_s = k_s c$  is the central frequency. Define the local boson operators  $\hat{a}_l = \frac{1}{\sqrt{2M+1}} \sum_{n=-M}^M \hat{c}_n e^{ik_n z_l}$  where  $[\hat{a}_l, \hat{a}_{l'}^\dagger] = \delta_{ll'}$ . Similar definitions hold for the signal, s, and idler field,  $i$ , which

carry an additional index in the following.

The Hamiltonian for the interacting system,  $\hat{H}_I = -\vec{d} \cdot \vec{E}$ , depicted in Figure 6.1 is given by, (we ignore the interactions responsible for atomic spontaneous emission for the moment)

$$\hat{H} = \hat{H}_0 + \hat{H}_I, \quad (\text{D.1})$$

where

$$\begin{aligned} \hat{H}_0 = & \sum_{i=1}^3 \sum_{l=-M}^M \hbar \omega_i \hat{\sigma}_{ii}^l + \hbar \omega_s \sum_{l=-M}^M \hat{a}_{s,l}^\dagger \hat{a}_{s,l} + \hbar \sum_{l,l'} \omega_{ll'} \hat{a}_{s,l}^\dagger \hat{a}_{s,l'} \\ & + \hbar \omega_i \sum_{l=-M}^M \hat{a}_{i,l}^\dagger \hat{a}_{i,l} + \hbar \sum_{l,l'} \omega_{ll'} \hat{a}_{i,l}^\dagger \hat{a}_{i,l'}, \end{aligned} \quad (\text{D.2})$$

and

$$\begin{aligned} \hat{H}_I = & -\hbar \sum_{l=-M}^M \left\{ \Omega_a(t) \hat{\sigma}_{01}^{l\dagger} e^{ik_a z_l - i\omega_a t} + \Omega_b(t) \hat{\sigma}_{32}^{l\dagger} e^{-ik_b z_l - i\omega_b t} \right. \\ & \left. + g_s \sqrt{2M+1} \hat{\sigma}_{12}^{l\dagger} \hat{a}_{s,l} e^{-ik_s z_l} + g_i \sqrt{2M+1} \hat{\sigma}_{03}^{l\dagger} \hat{a}_{i,l} e^{ik_i z_l} + h.c. \right\} \end{aligned} \quad (\text{D.3})$$

where  $\hat{\sigma}_{mn}^l \equiv \sum_{\mu}^{N_z} \hat{\sigma}_{mn}^{\mu,l} = \sum_{\mu}^{N_z} |m\rangle_{\mu} \langle n| \Big|_{r_{\mu}=z_l}$ , the Rabi frequencies  $\Omega_{a,(b)}(t) = f_{a,(b)}(t) d_{10,(23)} \mathcal{E}(k_{a,(b)}) / (2\hbar)$  is half the standard definition, and  $f_{a,(b)}$  is a slowly varying temporal profile without spatial dependence (ensemble scale much less than pulse length). The dipole matrix element  $d_{mn} \equiv \langle m | \hat{d} | n \rangle$ , coupling strength  $g_{s,(i)} \equiv d_{21,(30)} \mathcal{E}(k_{s,(i)}) / \hbar$ ,  $\mathcal{E}(k) = \sqrt{\hbar \omega / 2 \epsilon_0 V}$ , and  $z_p = \frac{pL}{2M+1}$ ,  $p = -M, \dots, M$ . The matrix  $\omega_{ll'} \equiv \sum_{n=-M}^M k_n e^{ik_n(z_l - z_{l'})} / (2M+1)$  accounts for field propagation by coupling the local mode operators.

The dynamical equations including dissipation due to spontaneous emission may be treated by standard Langevin-Heisenberg equation methods [30], and we define  $\gamma_{ij}$  as the natural transition rate from  $|j\rangle \rightarrow |i\rangle$ . Since we are interested in a semiclassical

description, we replace the field operators by c-numbers in the Langevin equations, and drop the zero-mean Langevin noise sources. All atomic spin operators are also replaced by their expectation values. Finally, in the co-moving frame coordinates  $z$  and  $\tau = t - z/c$  the atomic equations are

$$\begin{aligned}
\frac{\partial}{\partial \tau} \tilde{\sigma}_{01} &= (i\Delta_1 - \frac{\gamma_{01}}{2})\tilde{\sigma}_{01} + i\Omega_a(\tilde{\sigma}_{00} - \tilde{\sigma}_{11}) + ig_s^* \tilde{\sigma}_{02} E_s^- - ig_i \tilde{\sigma}_{13}^\dagger E_i^+, \\
\frac{\partial}{\partial \tau} \tilde{\sigma}_{12} &= (i\Delta\omega_s - \frac{\gamma_{01} + \gamma_2}{2})\tilde{\sigma}_{12} - i\Omega_a^* \tilde{\sigma}_{02} + ig_s(\tilde{\sigma}_{11} - \tilde{\sigma}_{22})E_s^+ + iP^* \Omega_b \tilde{\sigma}_{13}, \\
\frac{\partial}{\partial \tau} \tilde{\sigma}_{02} &= (i\Delta_2 - \frac{\gamma_2}{2})\tilde{\sigma}_{02} - i\tilde{\sigma}_{12} \Omega_a + ig_s \tilde{\sigma}_{01} E_s^+ + iP^* \tilde{\sigma}_{03} \Omega_b - iP^* g_i \tilde{\sigma}_{32} E_i^+, \\
\frac{\partial}{\partial \tau} \tilde{\sigma}_{11} &= -\gamma_{01} \tilde{\sigma}_{11} + \gamma_{12} \tilde{\sigma}_{22} + i\Omega_a \tilde{\sigma}_{01}^\dagger - i\Omega_a^* \tilde{\sigma}_{01} - ig_s \tilde{\sigma}_{12}^\dagger E_s^+ + ig_s^* \tilde{\sigma}_{12} E_s^-, \\
\frac{\partial}{\partial \tau} \tilde{\sigma}_{22} &= -\gamma_2 \tilde{\sigma}_{22} + ig_s \tilde{\sigma}_{12}^\dagger E_s^+ - ig_s^* \tilde{\sigma}_{12} E_s^- + i\Omega_b \tilde{\sigma}_{32}^\dagger - i\Omega_b^* \tilde{\sigma}_{32}, \\
\frac{\partial}{\partial \tau} \tilde{\sigma}_{33} &= -\gamma_{03} \tilde{\sigma}_{33} + \gamma_{32} \tilde{\sigma}_{22} - i\Omega_b \tilde{\sigma}_{32}^\dagger + i\Omega_b^* \tilde{\sigma}_{32} + ig_i \tilde{\sigma}_{03}^\dagger E_i^+ - ig_i^* \tilde{\sigma}_{03} E_i^-, \\
\frac{\partial}{\partial \tau} \tilde{\sigma}_{13} &= (i\Delta\omega_i - i\Delta_1 - \frac{\gamma_{01} + \gamma_{03}}{2})\tilde{\sigma}_{13} - i\Omega_a^* \tilde{\sigma}_{03} - iP g_s \tilde{\sigma}_{32}^\dagger E_s^+ + iP \Omega_b^* \tilde{\sigma}_{12} \\
&\quad + ig_i \tilde{\sigma}_{01}^\dagger E_i^+, \\
\frac{\partial}{\partial \tau} \tilde{\sigma}_{03} &= (i\Delta\omega_i - \frac{\gamma_{03}}{2})\tilde{\sigma}_{03} - i\Omega_a \tilde{\sigma}_{13} + iP \Omega_b^* \tilde{\sigma}_{02} + ig_i(\tilde{\sigma}_{00} - \tilde{\sigma}_{33})E_i^+, \\
\frac{\partial}{\partial \tau} \tilde{\sigma}_{32}^\dagger &= (-i\Delta_b - \frac{\gamma_{03} + \gamma_2}{2})\tilde{\sigma}_{32}^\dagger - iP^* g_s^* \tilde{\sigma}_{13} E_s^- + i\Omega_b^*(\tilde{\sigma}_{22} - \tilde{\sigma}_{33}) + iP^* g_i \tilde{\sigma}_{02}^\dagger E_i^+
\end{aligned} \tag{D.4}$$

where  $\gamma_2 = \gamma_{12} + \gamma_{32}$ ,  $P \equiv e^{i\Delta k z - i\Delta\omega t}$ , the four-wave mixing mismatch wavevector  $\Delta k = k_a - k_s + k_b - k_i$ , the frequency mismatch  $\Delta\omega = \omega_a + \omega_s - \omega_b - \omega_i = \Delta_1 - \Delta_b + \Delta\omega_s - \Delta\omega_i$ , and various detunings are defined as  $\Delta\omega_i = \omega_i - \omega_3$ ,  $\Delta\omega_s = \omega_s - \omega_{12}$ ,  $\Delta_1 = \omega_a - \omega_1$ ,  $\Delta_2 = \omega_a + \omega_s - \omega_2 = \Delta_1 + \Delta\omega_s$ ,  $\Delta_b = \omega_b - \omega_{23}$ . The slow-varying atomic operators are defined

$$\begin{aligned}
\tilde{\sigma}_{01} &\equiv \frac{1}{N_z} \sigma_{01}^l e^{-ik_a z_l + i\omega_a t}, \quad \tilde{\sigma}_{12} \equiv \frac{1}{N_z} \sigma_{12}^l e^{ik_s z_l + i\omega_s t}, \quad \tilde{\sigma}_{02} \equiv \frac{1}{N_z} \sigma_{02}^l e^{-ik_a z_l + ik_s z_l + i\omega_s t + i\omega_a t}, \\
\tilde{\sigma}_{13} &\equiv \frac{1}{N_z} \sigma_{13}^l e^{-i\omega_a t + i\omega_i t + ik_a z_l - ik_i z_l}, \quad \tilde{\sigma}_{03} \equiv \frac{1}{N_z} \sigma_{03}^l e^{-ik_i z_l + i\omega_i t}, \quad \tilde{\sigma}_{32}^\dagger \equiv \frac{1}{N_z} \sigma_{32}^{l\dagger} e^{-i\omega_b t} e^{-ik_b z_l}, \\
\tilde{\sigma}_{22} &\equiv \frac{1}{N_z} \tilde{\sigma}_{22}^l, \quad \tilde{\sigma}_{33} \equiv \frac{1}{N_z} \tilde{\sigma}_{33}^l, \quad \tilde{\sigma}_{11} \equiv \frac{1}{N_z} \tilde{\sigma}_{11}^l
\end{aligned} \tag{D.5}$$

where  $N_z(2M+1) = N$ .

The field equations are

$$\frac{\partial}{\partial z} E_s^+ = \frac{iNg_s^*}{c} \tilde{\sigma}_{12}, \tag{D.6}$$

$$\frac{\partial}{\partial z} E_i^+ = \frac{iNg_i^*}{c} \tilde{\sigma}_{03} \tag{D.7}$$

where the field operators are defined as

$$E_s^-(z, t) \equiv \sqrt{2M+1} \hat{a}_{s,l}^\dagger e^{-i\omega_s t}, \quad E_i^+(z, t) \equiv \sqrt{2M+1} \hat{a}_{i,l} e^{i\omega_i t}. \tag{D.8}$$

Langevin noises are not concerned here for we are interested in the normally-ordered quantity, frequency conversion efficiency, of input field and additional quantum noise corrections vanish as the  $|2\rangle \rightarrow |3\rangle$  transition driven by pump laser b has vanishing populations and atomic coherence. For energy and momentum conservation ( $P = 1$ ), and in the weak field limit, we solve atomic operators in steady state after linearizing with respect to the probe fields

$$\begin{aligned}
T_{01} \tilde{\sigma}_{01} &= i\Omega_a (1 - 2\tilde{\sigma}_{11} - \tilde{\sigma}_{22} - \tilde{\sigma}_{33}), \\
T_{32}^* \tilde{\sigma}_{32}^\dagger &= i\Omega_b^* (\tilde{\sigma}_{22} - \tilde{\sigma}_{33}), \\
T_{02} \tilde{\sigma}_{02} &= -i\Omega_a \tilde{\sigma}_{12} + ig_s \tilde{\sigma}_{01} E_s^+ + i\Omega_b \tilde{\sigma}_{03} - ig_i \tilde{\sigma}_{32} E_i^+, \\
T_{13} \tilde{\sigma}_{13} &= -i\Omega_a^* \tilde{\sigma}_{03} - ig_s \tilde{\sigma}_{32}^\dagger E_s^+ + i\Omega_b^* \tilde{\sigma}_{12} + ig_i \tilde{\sigma}_{01}^\dagger E_i^+, \\
T_{12} \tilde{\sigma}_{12} &= -i\Omega_a^* \tilde{\sigma}_{02} + ig_s (\tilde{\sigma}_{11} - \tilde{\sigma}_{22}) E_s^+ + i\tilde{\sigma}_{13} \Omega_b, \\
T_{03} \tilde{\sigma}_{03} &= -i\Omega_a \tilde{\sigma}_{13} + i\tilde{\sigma}_{02} \Omega_b^* + ig_i (\tilde{\sigma}_{00} - \tilde{\sigma}_{33}) E_i^+
\end{aligned} \tag{D.9}$$

where  $T_{01} = \frac{\gamma_{01}}{2} - i\Delta_1$ ,  $T_{32}^* = \frac{\gamma_{03} + \gamma_2}{2} + i\Delta_b$ ,  $T_{02} = \frac{\gamma_2}{2} - i\Delta_2$ ,  $T_{13} = \frac{\gamma_{01} + \gamma_{03}}{2} + i\Delta_1 - i\Delta\omega_i$ ,  $T_{12} = \frac{\gamma_{01} + \gamma_2}{2} - i\Delta\omega_s$ ,  $T_{03} = \frac{\gamma_{03}}{2} - i\Delta\omega_i$ , and note that  $\tilde{\sigma}_{02}$ ,  $\tilde{\sigma}_{13}$ ,  $\tilde{\sigma}_{12}$ ,  $\tilde{\sigma}_{03}$  are expressed in first order of fields and  $\tilde{\sigma}_{01}$ ,  $\tilde{\sigma}_{32}^\dagger$  in zeroth order. For population operators, we solve them in the zeroth order of fields and the nonzero steady states of population and coherence operator are (s denotes steady state solution)

$$\tilde{\sigma}_{11,s} = \frac{|\Omega_a|^2}{\Delta_1^2 + \frac{\gamma_{01}^2}{4} + 2|\Omega_a|^2}, \quad \tilde{\sigma}_{00,s} = 1 - \tilde{\sigma}_{11,s}, \quad \tilde{\sigma}_{01,s} = \frac{i\Omega_a}{\frac{\gamma_{01}}{2} - i\Delta_1} (1 - 2\tilde{\sigma}_{11,s}). \quad (\text{D.10})$$

Substitute the above back into Eq. (D.9) and solve for  $\tilde{\sigma}_{12}$  and  $\tilde{\sigma}_{03}$ . The parametric coupling equations for the signal and idler fields become

$$\begin{aligned} \frac{\partial}{\partial z} E_s^+ &= \beta_s E_s^+ + \kappa_s E_i^+ \\ \frac{\partial}{\partial z} E_i^+ &= \kappa_i E_s^+ + \alpha_i E_i^+ \end{aligned} \quad (\text{D.11})$$

where

$$\beta_s = \frac{-N|g_s|^2}{cD} [\tilde{\sigma}_{11,s}(T_{03} + \frac{|\Omega_a|^2}{T_{13}} + \frac{|\Omega_b|^2}{T_{02}}) - \frac{i\Omega_a^* \tilde{\sigma}_{01,s}}{T_{02}} (T_{03} + \frac{|\Omega_a|^2 - |\Omega_b|^2}{T_{13}})], \quad (\text{D.12})$$

$$\kappa_s = \frac{-Ng_i g_s^*}{cD} [\tilde{\sigma}_{00,s}(\frac{\Omega_a^* \Omega_b}{T_{02}} + \frac{\Omega_a^* \Omega_b}{T_{13}}) + \frac{i\Omega_b \tilde{\sigma}_{01,s}^\dagger}{T_{13}} (T_{03} + \frac{|\Omega_b|^2 - |\Omega_a|^2}{T_{02}})], \quad (\text{D.13})$$

$$\kappa_i = \frac{-Ng_s g_i^*}{cD} [\tilde{\sigma}_{11,s}(\frac{\Omega_a \Omega_b^*}{T_{02}} + \frac{\Omega_a \Omega_b^*}{T_{13}}) + \frac{i\Omega_b^* \tilde{\sigma}_{01,s}}{T_{02}} (T_{12} + \frac{|\Omega_b|^2 - |\Omega_a|^2}{T_{13}})], \quad (\text{D.14})$$

$$\alpha_i = \frac{-N|g_i|^2}{cD} [\tilde{\sigma}_{00,s}(T_{12} + \frac{|\Omega_a|^2}{T_{02}} + \frac{|\Omega_b|^2}{T_{13}}) - \frac{i\Omega_a \tilde{\sigma}_{01,s}^\dagger}{T_{13}} (T_{12} + \frac{|\Omega_a|^2 - |\Omega_b|^2}{T_{02}})], \quad (\text{D.15})$$

$$D \equiv T_{12}T_{03} + T_{12}(\frac{|\Omega_a|^2}{T_{13}} + \frac{|\Omega_b|^2}{T_{02}}) + T_{03}(\frac{|\Omega_a|^2}{T_{02}} + \frac{|\Omega_b|^2}{T_{13}}) + \frac{(|\Omega_a|^2 - |\Omega_b|^2)^2}{T_{02}T_{13}}. \quad (\text{D.16})$$

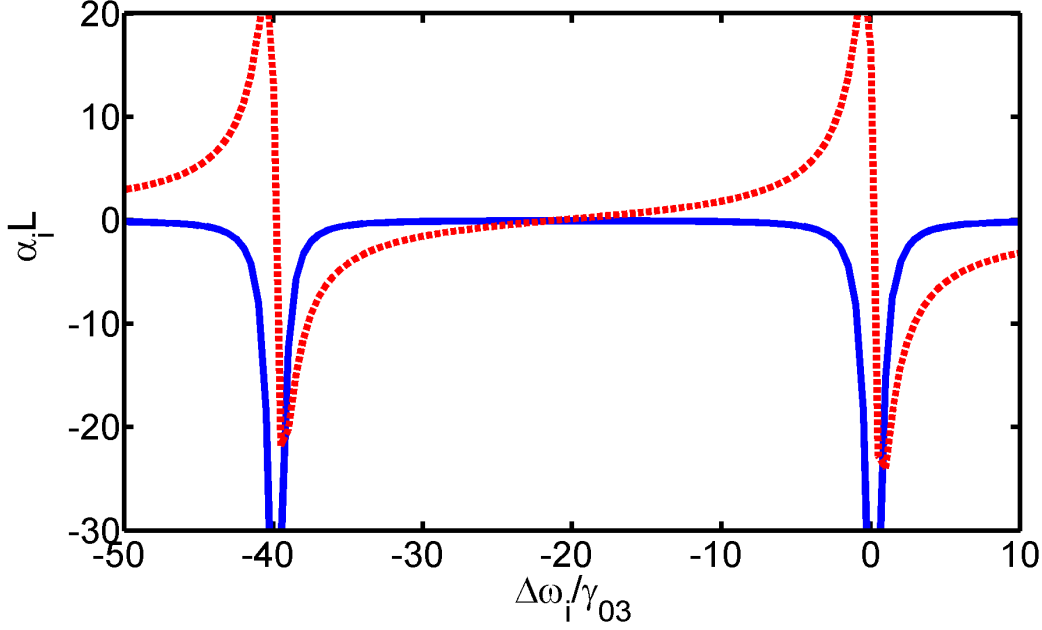


**Figure D.1:** Self-coupling coefficient  $\alpha_i$ . A dimensionless quantity  $\alpha_i L$  is plotted with real (solid blue) and imaginary (dashed red) parts as a dependence of idler detuning  $\Delta\omega_i$  showing a normal dispersion inside the EIT window.

The absorption coefficient for idler field is the real part of  $(-\alpha_i)$  and phase velocity  $v_p = \omega/k(\omega) = c/n(\omega)$  that  $k(\omega) = n(\omega)\omega/c$ . The wavevector is related to coefficient  $\alpha_i$  that  $k(\omega) = \text{Im}(\alpha_i) + \omega/c$  so  $n(\omega) = 1 + \text{Im}(\alpha_i)/(\omega/c)$ . The group velocity is  $v_g = d\omega/dk(\omega) = c/(n + \omega dn/d\omega)$  where  $n \approx 1$ , and it is this steep slope of refractive index that makes a large group delay ( $dn/d\omega > 0$  inside EIT window). As an example in Figure D.1, we demonstrate the real and imaginary parts of self-coupling coefficient  $\alpha_i$  with the optical depth (opd)  $\rho\sigma L = 150$  (see Chapter 6 for more details on other parameters). The dispersion curve ( $\text{Im}(\alpha_i L)$ ) inside the left parametric coupling window bounded by two absorption peaks ( $\text{Re}(\alpha_i L)$ ) shows a normal dispersion indicating a group delay at the center of the window (see Figure 6.3 for complete parametric coupling windows). Note that we plot out unitless  $\alpha_i L$  where  $L$  is in the order of millimeter for regular cold atomic ensemble, and see Sec. II and III for detail discussion of various coupling coefficients in Eq. (D.11) and



efficiency dependence on optical depth.



# REFERENCES

- [1] M. A. Nielsen and I. L. Chuang, *Quantum Computation and Quantum Information* (Cambridge University Press, 2000)
- [2] A. K. Ekert, “Quantum Cryptography Based on Bell’s Theorem,” *Phys. Rev. Lett.* 67, 661 (1991)
- [3] D. Bouwmeester, A. K. Ekert, and A. Zeilinger, *The Physics of Quantum Information: quantum cryptography, quantum teleportation, quantum computation* (Springer-Verlag Berlin, 2000)
- [4] H.-J. Briegel, W. Dür, J. I. Cirac, and P. Zoller, “Quantum Repeaters: The Role of Imperfect Local Operations in Quantum Communication,” *Phys. Rev. Lett.* 81, 5932 (1998)
- [5] W. Dür, H.-J. Briegel, J. I. Cirac, and P. Zoller, “Quantum Repeaters Based on Entanglement Purification,” *Phys. Rev. A* 59, 169 (1999)
- [6] L.-M. Duan, M. D. Lukin, J. I. Cirac, and P. Zoller, “Long-Distance Quantum Communication with Atomic Ensembles and Linear Optics,” *Nature* 414, 413 (2001)
- [7] D. N. Matsukevich and A. Kuzmich, “Quantum State Transfer Between Matter and Light,” *Science* 306, 663 (2004)
- [8] C. W. Chou, S. V. Polyakov, A. Kuzmich, and H. J. Kimble, “Single-Photon Generation from Stored Excitation in an Atomic Ensemble,” *Phys. Rev. Lett.* 92, 213601 (2004)
- [9] A. T. Black, J. K. Thompson, and V. Vuletić, “On-Demand Superradiant Conversion of Atomic Spin Gratings into Single Photons with High Efficiency,” *Phys. Rev. Lett.*, 95, 133601 (2005)
- [10] D. N. Matsukevich, T. Chanelière, M. Bhattacharya, S.-Y. Lan, S. D. Jenkins, T. A. B. Kennedy, and A. Kuzmich, “Entanglement of a Photon and a Collective Atomic Excitation,” *Phys. Rev. Lett.* 95, 040405 (2005)
- [11] T. Chanelière, D. N. Matsukevich, S. D. Jenkins, S.-Y. Lan, T. A. B. Kennedy, and A. Kuzmich, “Storage and Retrieval of Single Photons Transmitted Between Remote Quantum Memories,” *Nature* 438, 833 (2005)
- [12] D. N. Matsukevich, T. Chanelière, S. D. Jenkins, S.-Y. Lan, T. A. B. Kennedy, and A. Kuzmich, “Entanglement of Remote Atomic Qubits,” *Phys. Rev. Lett.* 96, 030405 (2006)

- [13] D. N. Matsukevich, T. Chanelière, S. D. Jenkins, S.-Y. Lan, T.A.B. Kennedy, and A. Kuzmich, “Observation of Dark State Polariton Collapses and Revivals,” *Phys. Rev. Lett.* 97, 013601 (2006)
- [14] S. Chen, Y-A Chen, T. Strassel, Z-S Yuan, B Zhao, J. Schmiedmayer, and J.-W. Pan, “Deterministic and Storable Single-Photon Source Based on a Quantum Memory,” *Phys. Rev. Lett.* 97, 173004 (2006)
- [15] J. Laurat, H. de Riedmatten, D. Felinto, C.-W. Chou, E. W. Schomburg, and H. J. Kimble, “Efficient Retrieval of a Single Excitation Stored in an Atomic Ensemble,” *Opt. Exp.* 14, 6912 (2006)
- [16] T. Chanèliere, D. N. Matsukevich, S. D. Jenkins, S.-Y. Lan, R. Zhao, T. A. B. Kennedy, and A. Kuzmich, “Quantum Telecommunication Based on Atomic Cascade Transitions,” *Phys. Rev. Lett.* 97, 093604 (2006)
- [17] J. J. McClelland and J. L. Hanssen, “Laser Cooling without Repumping: A Magneto-Optical Trap for Erbium Atoms,” *Phys. Rev. Lett.* 96, 143005 (2006)
- [18] M. Lu, S. H. Youn, and B. L. Lev, “Trapping Ultracold Dysprosium: A Highly Magnetic Gas for Dipolar Physics,” *Phys. Rev. Lett.* 104, 063001 (2010)
- [19] B. Lauritzen, J. Minář, H. de Riedmatten, M. Afzelius, N. Sangouard, C. Simon, and N. Gisin, “Telecommunication-Wavelength Solid-State Memory at the Single Photon Level,” *Phys. Rev. Lett.* 104, 080502 (2010)
- [20] M. J. Stephen, “First-Order Dispersion Forces,” *J. Chem. Phys.* 40, 669 (1964)
- [21] R. H. Lehmberg, “Radiation from an N-Atom System. I. General Formalism,” *Phys. Rev. A* 2, 883 (1970)
- [22] N. E. Rehler and J. H. Eberly, “Superradiance,” *Phys. Rev. A* 3, 1735 (1971)
- [23] R. H. Dicke, “Coherence in Spontaneous Radiation Processes,” *Phys. Rev.* 93, 99 (1954)
- [24] L. Mandel and E. Wolf, *Optical Coherence and Quantum Optics*, (Cambridge University Press, 1995)
- [25] A. G. Radnaev, Y. O. Dudin, R. Zhao, H. H. Jen, S. D. Jenkins, A. Kuzmich, and T. A. B. Kennedy, “A Quantum Memory with Telecom-Wavelength Conversion,” doi:10.1038/nphys1773, *Nature Physics* (2010)
- [26] W. H. Louisell, *Quantum Statistical Properties of Radiation* (Wiley, New York, 1973)
- [27] H. Haken, *Laser Theory* (Springer-Verlag Berlin, 1970)
- [28] C. W. Gardiner, *Handbook of Stochastic Methods: for Physics, Chemistry and the Natural Sciences* (Springer-Verlag Berlin, 2004)

- [29] P. D. Drummond and S. J. Carter, “Quantum-Field Theory of Squeezing in Solitons,” *J. Opt. Soc. Am. B*, Vol. 4, 1565 (1987)
- [30] M. O. Scully and M. S. Zubairy, *Quantum Optics* (Cambridge University Press, 1997)
- [31] M. Sargent, M. O. Scully and W. E. Lamb, Jr., *Laser Physics* (Addison-Wesley Publishing Company, Inc. 1974)
- [32] C. W. Gardiner and P. Zoller, *Quantum Noise: A Handbook of Markovian and Non-Markovian Quantum Stochastic Methods with Applications to Quantum Optics*, 2nd ed. (Springer-Verlag Berlin, 2000)
- [33] M. Fleischhauer and M. O. Scully, “Quantum Sensitivity Limits of an Optical Magnetometer Based on Atomic Phase Coherence,” *Phys. Rev. A* 49, 1973 (1994)
- [34] H. J. Carmichael, *Statistical Methods in Quantum Optics 1* (Springer-Verlag Berlin, 1999)
- [35] D. F. Walls and G. J. Milburn, *Quantum Optics* (Springer-Verlag Berlin, 1994)
- [36] P. D. Drummond and I. K. Mortimer, “Computer Simulations of Multiplicative Stochastic Differential Equations,” *J. Comp. Phys.* 93, 144 (1991)
- [37] G. R. Collocutt, P. Cochrane, J. Hope, and P. D. Drummond, <http://www.xmds.org/index.html>
- [38] V. Ernst and P. Stehle, “Emission of Radiation from a System of Many Excited Atoms,” *Phys. Rev.* 176, 1456 (1968)
- [39] E. Ressayre and A. Tallet, “Quantum Theory for Superradiance,” *Phys. Rev. A* 15, 2410 (1977)
- [40] G. S. Agarwal, “Master-Equation Approach to Spontaneous Emission,” *Phys. Rev. A* 2, 2038 (1970)
- [41] R. Bonifacio, P. Schwendimann, and F. Haake, “Quantum Statistical Theory of Superradiance. I,” *Phys. Rev. A* 4, 302 (1971)
- [42] R. Bonifacio, P. Schwendimann, and F. Haake, “Quantum Statistical Theory of Superradiance. II,” *Phys. Rev. A* 4, 854 (1971)
- [43] R. Bonifacio and L. A. Lugiato, “Cooperative Radiation Processes in Two-Level Systems: Superfluorescence,” *Phys. Rev. A* 11, 1507 (1975)
- [44] J. C. MacGillivray and M. S. Feld, “Theory of Superradiance in an Extended, Optically Thick Medium,” *Phys. Rev. A* 14, 1169 (1976)

- [45] M. Gross and S. Haroche, “Superradiance: An Essay on the Theory of Collective Spontaneous Emission,” *Phys. Rep.* 93, 301 (1982)
- [46] L. I. Men’shikov, “Superradiance and Related Phenomena,” *Phys. Uspekhi* 42, 107 (1999)
- [47] H. J. Carmichael and Kisik Kim, “A Quantum Trajectory Unraveling of the Superradiance Master Equation,” *Opt. Commun.* 179, 417 (2000)
- [48] J. P. Clemens, L. Horvath, B. C. Sanders, and H. J. Carmichael, “Collective Spontaneous Emission from a Line of Atoms,” *Phys. Rev. A* 68, 023809 (2003)
- [49] M. Fleischhauer and S. F. Yelin, “Radiative Atom-Atom Interactions in Optically Dense Media: Quantum Corrections to the Lorentz-Lorenz Formula,” *Phys. Rev. A* 59, 2427 (1999)
- [50] J. H. Eberly, “Emission of One Photon in an Electric Dipole Transition of One Among N Atoms,” *J. Phys. B: At. Mol. Opt. Phys.* 39, S599 (2006)
- [51] M. O. Scully, Edward S. Fry, C. H. Raymond Ooi, and Krzysztof Wódkiewicz, “Directed Spontaneous Emission from an Extended Ensemble of N Atoms: Timing Is Everything,” *Phys. Rev. Lett.* 96, 010501 (2006)
- [52] I. E. Mazets and G. Kurizki, “Multiatom Cooperative Emission Following Single-Photon Absorption: Dicke-State Dynamics,” *J. Phys. B: At. Mol. Opt. Phys.* 40, F 105 (2007)
- [53] A. A. Svidzinsky, Jun-Tao Chang, and M. O. Scully, “Dynamical Evolution of Correlated Spontaneous Emission of a Single Photon from a Uniformly Excited Cloud of N Atoms,” *Phys. Rev. Lett.* 100, 160504 (2008)
- [54] A. A. Svidzinsky and Jun-Tao Chang, “Cooperative Spontaneous Emission as a Many-Body Eigenvalue Problem,” *Phys. Rev. A* 77, 043833 (2008)
- [55] R. Friedberg and J. T. Manassah, “Effects of Including the Counterrotating Term and Virtual Photons on the Eigenfunctions and Eigenvalues of a Scalar Photon Collective Emission Theory,” *Phys. Lett. A* 372, 2514 (2008)
- [56] A. Svidzinsky and J.-T. Chang, “Comment on: ‘Effects of including the counterrotating term and virtual photons on the eigenfunctions and eigenvalues of a scalar photon collective emission theory’ [*Phys. Lett. A* 372 (2008) 2514],” *Phys. Lett. A* 372, 5732 (2008)
- [57] R. Friedberg and J. T. Manassah, “Reply to: ‘Comment on: ‘Effects of including the counterrotating term and virtual photons on the eigenfunctions and eigenvalues of a scalar photon collective emission theory’ [*Phys. Lett. A* 372 (2008) 2514]’ [*Phys. Lett. A* 372 (2008) 5732],” *Phys. Lett. A* 372, 5734 (2008)

- [58] R. Friedberg and J. T. Manassah, “Time-Dependent directionality of Cooperative Emission After Short Pulse Excitation,” *Optics Comm.* 281, 4391 (2008)
- [59] F. T. Arecchi and D. M. Kim, “Line Shifts in Cooperative Spontaneous Emission,” *Opt. Commun.* 2, 324 (1970)
- [60] H. Morawitz, “Superradiant Level Shift and Its Possible Detection in a Transient Optical Experiment,” *Phys. Rev. A* 7, 1148 (1973)
- [61] M. O. Scully, “Collective Lamb Shift in Single Photon Dicke Superradiance,” *Phys. Rev. Lett.* 102, 143601 (2009)
- [62] R. Röhlsberger, K. Schlage, B. Sahoo, S. Couet, and R. Ruffer, “Collective Lamb Shift in Single-Photon Superradiance,” *Science* 328, 1248 (2010)
- [63] S. M. Tan, “A Computational Toolbox for Quantum and Atomic Optics,” *J. Opt. B* 1, 424, (1999)
- [64] R. Loudon, *The Quantum Theory of Light* (Oxford University Press, 2000)
- [65] T. E. Keller and M. H. Rubin, “Theory of Two-Photon Entanglement for Spontaneous Parametric Down-Conversion Driven by a Narrow Pump Pulse,” *Phys. Rev. A* 56, 1534 (1997)
- [66] W. P. Grice and I. A. Walmsley, “Spectral Information and Distinguishability in Type-II Down-Conversion with a Broadband Pump,” *Phys. Rev. A* 56, 1627 (1997)
- [67] D. Branning, W. P. Grice, R. Erdmann, and I. A. Walmsley, “Engineering the Indistinguishability and Entanglement of Two Photons,” *Phys. Rev. Lett.* 83, 955 (1999)
- [68] C. K. Law and I. A. Walmsley, and J. H. Eberly, “Continuous Frequency Entanglement: Effective Finite Hilbert Space and Entropy Control,” *Phys. Rev. Lett.* 84, 5304 (2000)
- [69] S. Parker, S. Bose, and M. B. Plenio, “Entanglement Quantification and Purification in Continuous-Variable Systems,” *Phys. Rev. A* 61, 032305 (2000)
- [70] W. P. Grice, A. B. U'Ren, and I. A. Walmsley, “Eliminating Frequency and Space-Time Correlations in Multiphoton States,” *Phys. Rev. A* 64, 063815 (2001)
- [71] E. Knill, R. Laflamme and G. J. Milburn, “A Scheme for Efficient Quantum Computation with Linear Optics,” *Nature* 409, 46 (2001)
- [72] A. B. U'Ren, C. Silberhorn, R. Erdmann, K. Banaszek, W. P. Grice, I. A. Walmsley, and M. G. Raymer, “Generation of Pure-State Single-Photon Wavepackets by Conditional Preparation Based on Spontaneous Parametric Down Conversion,” *Laser Phys.* 15, 146 (2005)

- [73] C. K. Law and J. H. Eberly, “Analysis and Interpretation of High Transverse Entanglement in Optical Parametric Down Conversion,” *Phys. Rev. Lett.* 92, 127903 (2004)
- [74] M. G. Raymer, J. Noh, K. Banaszek, and I. A. Walmsley, “Pure-State Single-Photon Wave-Packet Generation by Parametric Down-Conversion in a Distributed Microcavity,” *Phys. Rev. A* 72, 023825 (2005)
- [75] K. Garay-Palmett, H. J. McGuinness, O. Cohen, J. S. Lundeen, R. Rangel-Rojo, A. B. U’Ren, M. G. Raymer, C. J. McKinstrie, S. Radic, and I. A. Walmsley, “Photon Pair-State Preparation with Tailored Spectral Properties by Spontaneous Four-Wave Mixing in Photonic-Crystal Fiber,” *Opt. Express* 22, 14870 (2007)
- [76] T. S. Humble and W. P. Grice, “Spectral Effects in Quantum Teleportation,” *Phys. Rev. A* 75, 022307 (2007)
- [77] F. Haake, H. King, G. Schroder, J. Haus, R. Glauber, and F. Hopf, “Macroscopic Quantum Fluctuations in Superfluorescence,” *Phys. Rev. Lett.* 42, 1740 (1979)
- [78] F. Haake, H. King, G. Schroder, J. Haus, and R. Glauber, “Fluctuations in Superfluorescence,” *Phys. Rev. A* 20, 2047 (1979)
- [79] D. Polder, M. F. H. Schuurmans, and Q. H. F. Vreken, “Superfluorescence: Quantum-Mechanical Derivation of Maxwell-Bloch Description with Fluctuating Field Source,” *Phys. Rev. A* 19, 1192 (1979)
- [80] E. L. Bolda, R. Y. Chiao, and J. C. Garrison, “Superfluorescence in a Continuously Pumped Medium,” *Phys. Rev. A* 52, 3308 (1995)
- [81] J. C. Garrison, H. Nathel, and R. Y. Chiao, “Quantum Theory of Amplified Spontaneous Emission: Scaling Properties,” *J. Opt. Soc. Am. B*, Vol. 5, 1528 (1988)
- [82] J. J. Maki, M. S. Malcuit, M. G. Raymer, R. W. Boyd, and P. D. Drummond, “Influence of Collisional Dephasing Processes on Superfluorescence,” *Phys. Rev. A* 40, 5135 (1989)
- [83] A. M. Smith and C. W. Gardiner, “Phase-Space Method without Large-N Scaling for the Laser and Optical Bistability,” *Phys. Rev. A* 38, 4073 (1988)
- [84] A. M. Smith and C. W. Gardiner, “Three-Level Atom Laser Model with Results and Applications,” *Phys. Rev. A* 41, 2730 (1990)
- [85] A. M. Smith and C. W. Gardiner, “Simulations of Nonlinear Quantum Damping Using the Positive P Representation,” *Phys. Rev. A* 39, 3511 (1989)



- [86] P. D. Drummond and M. G. Raymer, “Quantum Theory of Propagation of Nonclassical Radiation in a Near-Resonant Medium,” *Phys. Rev. A* 44, 2072 (1991)
- [87] H. J. Carmichael, J. S. Satchell and S. Sarkar, “Nonlinear Analysis of Quantum Fluctuations in Absorptive Optical Bistability,” *Phys. Rev. A* 34, 3166 (1986)
- [88] W. H. Press, S.A. Teukolsky, W. T. Vetterling and B. P. Flannery, *Numerical Recipes in C*, Second Edition (Cambridge University Press, 1992)
- [89] P. Deuar and P. D. Drummond, “Gauge P Representations for Quantum-Dynamical Problems: Removal of Boundary Terms,” *Phys. Rev. A* 66, 033812 (2002)
- [90] P. Deuar and P. D. Drummond, “Stochastic Gauges in Quantum Dynamics for Many-Body Simulations,” *Comp. Phys. Comm.* 142, 442 (2001)
- [91] L. I. Plimak, M. K. Olsen, and M. J. Collett, “Optimization of the Positive-P Representation for the Anharmonic Oscillator,” *Phys. Rev. A* 64, 025801 (2001)
- [92] J. F. Corney and P. D. Drummond, “Gaussian Quantum Operator Representation for Bosons,” *Phys. Rev. A* 68, 063822 (2003)
- [93] J. F. Corney and P. D. Drummond, “Gaussian Phase-Space Representations for Fermions,” *Phys. Rev. B* 73, 125112 (2006)
- [94] P. D. Drummond and C. W. Gardiner, “Generalised P-Representations in Quantum Optics,” *J. Phys. A* 13, 2353 (1980)
- [95] P. D. Drummond, “Central Partial Difference Propagation Algorithms,” *Comp. Phys. Comm.* 29, 211 (1983)
- [96] P. E. Kloeden and E. Platen, *Numerical Solution of Stochastic Differential Equation* (Springer-Verlag Berlin, 1992)
- [97] O. S. Heavens, “Radiative Transition Probabilities of the Lower Excited States of the Alkali Metals,” *J. Opt. Soc. Am.*, Vol. 51, 1058 (1961)
- [98] S. J. van Enk, “Single-Particle Entanglement,” *Phys. Rev. A* 72, 064306 (2005)
- [99] M. Razavi and J. H. Shapiro, “Long-Distance Quantum Communication with Neutral Atoms,” *Phys. Rev. A* 73, 042303 (2006)
- [100] H. H. Jen and T. A. B. Kennedy, “Efficiency of Light-Frequency Conversion in an Atomic Ensemble,” *Phys. Rev. A* 82, 023815 (2010)
- [101] S. E. Harris, “Electromagnetically Induced Transparency,” *Phys. Today* 50, No. 7, 36 (1997)

- [102] M. Fleischhauer and M. D. Lukin, “Dark-State Polaritons in Electromagnetically Induced Transparency,” *Phys. Rev. Lett.* 84, 5094 (2000)
- [103] S. D. Jenkins, D. N. Matsukevich, T. Chanelière, A. Kuzmich, and T. A. B. Kennedy, “Theory of Dark-State Polariton Collapses and Revivals,” *Phys. Rev. A* 73, 021803(R) (2006)
- [104] D. L. Moehring, P. Maunz, S. Olmschenk, K. C. Younge, D. N. Matsukevich, L-M. Duan, and C. Monroe, “Entanglement of Single-Atom Quantum Bits at a Distance,” *Nature* 449, 68 (2007)
- [105] D. N. Matsukevich, P. Maunz, D. L. Moehring, S. Olmschenk, and C. Monroe, “Bell Inequality Violation with Two Remote Atomic Qubits,” *Phys. Rev. Lett.* 100, 150404 (2008)
- [106] R. Zhao, Y. O. Dudin, S. D. Jenkins, C. J. Campbell, D. N. Matsukevich, T. A. B. Kennedy, and A. Kuzmich, “Long-Lived Quantum Memory,” *Nature Phys.* 5, 100 (2009)
- [107] F. E. Becerra, R. T. Willis, S. L. Rolston, and L. A. Orozco, “Nondegenerate Four-Wave Mixing in Rubidium Vapor: The Diamond Configuration,” *Phys. Rev. A* 78, 013834 (2008)
- [108] A. V. Gorshkov, A. André, M. D. Lukin, and A. S. Sørensen, “Photon Storage in  $\Lambda$ -type Optically Dense Atomic Media. I. Cavity Model,” *Phys. Rev. A* 76, 033804 (2007)
- [109] K. Hammerer, A. S. Sørensen, and E. S. Polzik, “Quantum Interface Between Light and Atomic Ensembles,” *Rev. Mod. Phys.* 82, 1041 (2010)
- [110] D. A. Braje, V. Balić, S. Goda, G. Y. Yin, and S. E. Harris, “Frequency Mixing Using Electromagnetically Induced Transparency in Cold Atoms,” *Phys. Rev. Lett.* 93, 183601 (2004)
- [111] M. D. Lukin, A. B. Matsko, M. Fleischhauer, and M. O. Scully, “Quantum Noise and Correlations in Resonantly Enhanced Wave Mixing Based on Atomic Coherence,” *Phys. Rev. Lett.* 82, 1847 (1999)
- [112] A. Gogyan and Yu. Malakyan, “Entanglement-Preserving Frequency Conversion in Cold Atoms,” *Phys. Rev. A* 77, 033822 (2008)
- [113] A. Gogyan, “Qubit Transfer Between Photons at Telecom and Visible Wavelengths in a Slow-Light Atomic Medium,” *Phys. Rev. A* 81, 024304 (2010)
- [114] P. Kumar, “Quantum Frequency Conversion,” *Optics Lett.*, Vol. 15, 1476 (1990)
- [115] F. T. Arecchi and E. Courtens, “Cooperative Phenomena in Resonant Electromagnetic Propagation,” *Phys. Rev. A* 2, 1730 (1970)

- [116] V. Weisskopf and E. Wigner, “Berechnung der nat uralichen Linienbreite auf Grund der Diracschen Lichttheorie,” *Z. Phys.* 63, 54 (1930)
- [117] P. P. Rohde and T. C. Ralph, “Modelling Photo-Detectors in Quantum Optics,” *J. of Modern Optics* 53, 1589 (2006)